AD NUMBER

ADB031555

NEW LIMITATION CHANGE

TO

Approved for public release, distribution unlimited

FROM

Distribution authorized to U.S. Gov't. agencies only; Test and Evaluation; 10 Jul 1978. Other requests shall be referred to Air Force Flight Dynamics Laboratory, Attn: AFFDL/FXB, Wright-Patterson AFB, OH 45433.

AUTHORITY

AFWL ltr, 11 Feb 1980

AFFDL-TR-78-91
Volume IV

LEVEL II

RAPID EVALUATION OF PROPULSION SYSTEM EFFECTS
Volume IV—Library of Configurations and Performance Maps

W.H. Ball

BOEING AEROSPACE COMPANY
SEATTLE, WASHINGTON 98124

JULY 1978

TECHNICAL REPORT AFFDL-TR-78-91, VOLUME IV
Final Report for Period July 1977—July 1978

AIR FORCE FLIGHT DYNAMICS LABORATORY
AIR FORCE WRIGHT AERONAUTICAL LABORATORIES
AIR FORCE SYSTEMS COMMAND
WRIGHT-PATTERSON AIR FORCE BASE, OHIO 45433

NOTICE

When Government drawings, specifications, or other data are used for any purpose other than in connection with a definitely related Government procurement operation, the United States Government thereby incurs no responsibility nor any obligation whatsoever; and the fact that the government may have formulated, furnished, or in any way supplied the said drawings, specifications, or other data, is not to be regarded by implication or otherwise as in any manner licensing the holder or any other person or corporation, or conveying any rights or permission to manufacture, use, or sell any patented invention that may in any way be related thereto.

This technical report has been reviewed and is approved for publication.

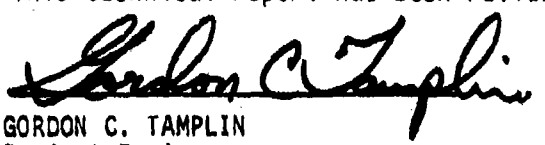

GORDON C. TAMPLIN
Project Engineer
Vehicle Synthesis Branch

RAYMOND L. HAAS
Chief, Vehicle Synthesis Branch
AF Flight Dynamics Laboratory

FOR THE COMMANDER

MELVIN L. BUCK
Acting Chief
Aeromechanics Division

"If your address has changed, if you wish to be removed from our mailing list, or if the addressee is no longer employed by your organization, please notify AFFDL/FXB, W-PAFB, OH 45433 to help us maintain a current mailing list."

Copies of this report should not be returned unless return is required by security considerations, contractual obligations, or notice on a specific document.

Unclassified

SECURITY CLASSIFICATION OF THIS PAGE (When Data Entered)

REPORT DOCUMENTATION PAGE	READ INSTRUCTIONS BEFORE COMPLETING FORM
1. REPORT NUMBER: AFFDL-TR-78-91 Vol IV	2. GOVT ACCESSION NO. / 3. RECIPIENT'S CATALOG NUMBER
4. TITLE (and Subtitle): RAPID EVALUATION OF PROPULSION SYSTEM EFFECTS. VOLUME IV, LIBRARY OF CONFIGURATIONS AND PERFORMANCE MAPS.	5. TYPE OF REPORT & PERIOD COVERED: FINAL, JUL [redacted] 77 - JUL [redacted] 78
	6. PERFORMING ORG. REPORT NUMBER
7. AUTHOR(s): W. H. Ball	8. CONTRACT OR GRANT NUMBER(s): F33615-77-C-3085
9. PERFORMING ORGANIZATION NAME AND ADDRESS: Boeing Aerospace Company, A Division of The Boeing Company, Seattle, Washington 98124	10. PROGRAM ELEMENT, PROJECT, TASK AREA & WORK UNIT NUMBERS: 24040121 / 01
11. CONTROLLING OFFICE NAME AND ADDRESS: Vehicle Synthesis Branch (AFFDL/FXB), Air Force Flight Dynamics Laboratory, Wright-Patterson AFB, Ohio 45433	12. REPORT DATE: Jul [redacted] 78 / 13. NUMBER OF PAGES: 188
14. MONITORING AGENCY NAME & ADDRESS (if different from Controlling Office)	15. SECURITY CLASS. (of this report): Unclassified / 15a. DECLASSIFICATION/DOWNGRADING SCHEDULE

16. DISTRIBUTION STATEMENT (of this Report)

Distribution limited to U.S. Government Agencies only; Test and Evaluation; Statement applied 10 July 1978. Other requests for this document must be referred to Air Force Flight Dynamics Laboratory (AFFDL/FXB) Wright-Patterson Air Force Base, Ohio 45433

17. DISTRIBUTION STATEMENT (of the abstract entered in Block 20, if different from Report)

18. SUPPLEMENTARY NOTES

19. KEY WORDS (Continue on reverse side if necessary and identify by block number)

Installed engine performance
Inlet performance
Nozzle performance

20. ABSTRACT (Continue on reverse side if necessary and identify by block number)

This report presents the results of a research program to develop computerized preliminary analysis procedures for calculating propulsion system installation losses. These losses include inlet and nozzle internal losses and external drag losses for a wide variety of subsonic and supersonic aircraft configurations up to Mach 3.5. The calculation procedures used in the computer programs, which were largely developed from existing engineering procedures and experimental data, are suitable for preliminary studies of advanced aircraft configurations. Two interactive computer programs were developed during the contract:

DD FORM 1 JAN 73 1473 EDITION OF 1 NOV 65 IS OBSOLETE

Unclassified

SECURITY CLASSIFICATION OF THIS PAGE (When Data Entered)

(1) A propulsion installation effects program that calculates installed performance, using input maps of inlet and nozzle/aftbody characteristics for specific configurations, and (2) A derivative program that allows the user to generate new sets of input maps by perturbations to the geometries of the basic input maps. The work accomplished during the contract is documented in four separate volumes. Volume I is a Final Report discussing the analysis methods and data used to develop the programs, and major technical observations from the study. Volume II is a PIPSI Users Manual, containing documentation of the interactive propulsion installation program. Volume III is the Derivative Procedure Users Manual, documenting the methods and usage of the derivative procedure. Volume IV is a library of inlet and nozzle/aftbody configurations and input data.

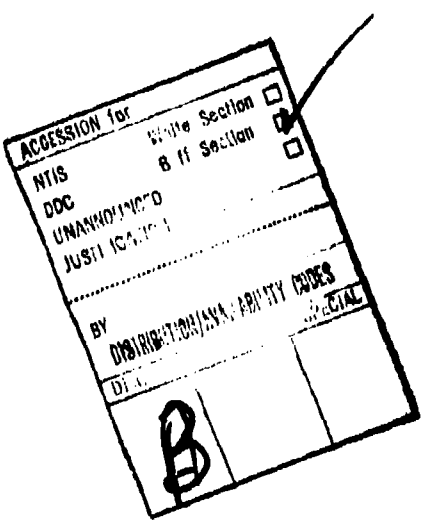

FOREWORD

This report documents the work accomplished during USAF Contract No. F33615-77-C-3085. The work consisted of developing an interactive PIPSI computer program, developing an interactive derivative computer program, and developing and documenting supporting data libraries. The work was accomplished in three phases. As part of the work accomplished in Phase I of the contract, the interactive PIPSI program was completed and delivered to the Air Force. As part of Phase II work, derivative parameters were selected and development work was completed on the derivative program. During Phase III a library of inlet and nozzle/aftbody characteristics was prepared, test cases were completed, documentation was accomplished, and final programs were delivered to the Air Force. The program was conducted under the direction of the Vehicle Synthesis Branch, Air Force Flight Dynamics Laboratory, Air Force Systems Command. Mr. Gordon Tamplin was the Air Force Program Monitor.

The program was initiated on 17 July 1977 and draft copies of the final reports were submitted for approval on 15 May 1978.

Mr. W. H. Ball was Program Manager for The Boeing Company. The following individuals contributed significantly to the work accomplished during this contract: R. A. Atkins, Jr., computer programming; T. E. Hickcox, inlet derivative procedure development; E. J. Kowalski, inlet configurations and performance; and J. E. Petit and R. M. Trayler, nozzle/aftbody procedure and configurations.

TABLE OF CONTENTS

LIST OF ILLUSTRATIONS

LIST OF FIGURES (cont.)

LIST OF ILLUSTRATIONS (concluded)

LIST OF NOMENCLATURE AND SYMBOLS

A^*	Sonic area, in^2
A	Area, in^2
A_c	Inlet capture area, in^2
A_o	Local stream tube area ahead of the inlet, in^2
A_{o_I}	Free-stream tube area of air entering the inlet, in^2
AR	Aspect ratio, W_c/H_c for inlets, W_9/H_9 for nozzles, dimensionless
C_D	Drag coefficient, $\frac{D}{q A_{ref.}}$, dimensionless
C	Sonic velocity; ft/sec.
C-D	Convergent-divergent
$C_{D_{ADD}}$	Additive drag coefficient, $C_{D_{ADD}} = \frac{D_{ADD}}{q A_c}$, dimensionless
$C_{D_{A10}}$	Afterbody drag coefficient, $\frac{DRAG}{q A_{10}}$, dimensionless
$C_{D_{Base}}$	Base drag coefficient $\frac{(P_b - P_\infty) A_{base}}{q A_{10}}$, dimensionless
$C_{D_{A10-A9}}$, $C_{D_{PAP}}$	Drag coefficient, $\frac{D}{q_o (A_{10} - A_9)}$, based on projected area, dimensionless
C_{D_S}	Scrubbing drag coefficient, $\frac{DRAG}{q A_{10}}$, dimensionless
C_{f_G}	Thrust coefficient, $\frac{F_g}{\frac{W}{g}(V_{cp})}$ dimensionless
C_V	Nozzle velocity coefficient, dimensionless
Conv.	Convergent

D	Drag, lb.; Hydraulic Diameter, $\frac{4A}{P}$, in., diameter, in.
F	Thrust, lb.
F_N	Net thrust, lb.
F_{N_A}	Installed net thrust, lb.
F_{g_i}	Ideal gross thrust (fully expanded), lb.
f/a	Fuel/air ratio, dimensionless
g	Gravitational constant, ft/sec^2
h	Enthalpy per unit mass, BTU/lb.; height, in.
h_{fan}	Enthalpy of fan discharge flow, BTU/lb
h_{pri}	Enthalpy of primary exhaust flow after heat addition, BTU/lb
h_t	Throat height, in^2
IMS_T	Integral mean slope parameter, truncated $$IMS_T = -\frac{1}{(1 - A_9/A_{10})} \int_{A_9/A_{10}}^{1.0} \frac{d(A/A_{10})}{d(L/D_{eq})} \, d(A/A_{10})$$
L	Length, in.
M	Mach number, dimensionless
P	Static pressure, lb/in^2, perimeter, in.
P_r	Relative pressure,; the ratio of the pressures p_a and p_b corresponding to the temperatures T_a and T_b, respectivaly, along a given isentrope, dimensionless
P.S.	Power setting
P_T	Total pressure, lb/in2
Q	Effective heating value of fuel, BTU/lb.

q	Dynamic pressure, lb/in^2
R	Gas constant
R, r	Radius, in.
R_F	Total pressure recovery
SFC	Specific fuel consumption
SFC_A	Installed specific fuel consumption
T	Temperature, $^{\circ}R$
V	Velocity, ft/sec
W	Mass flow, lb/sec
W_{BX}	Bleed air removed from engine, lb/sec.
W_C,	Corrected airflow, lb/sec. $\frac{W\sqrt{\theta}}{\delta}$
W_f	Weight flow rate of fuel, lb/sec.
W_2	Weight flow rate of air, primary plus secondary, lb/sec.
W_8	Primary nozzle airflow rate, lb/sec.
x	Length, in.
α	Angle of attack; convergence angle of nozzle, degrees
γ	Ratio of specific heats, dimensionless
δ_{T_2}	Pressure correction factor, $P_{T_2}/P_{STD.}$
ϵ	Diffuser loss coefficient, $\frac{\Delta P_T}{q}$, dimensionless
θ_{T_2}	Temperature correction factor, $T_{T_2}/T_{STD.}$

θ_N	2-D Nozzle wedge half-angle
θ_P	Round Plug nozzle half-angle
η_B	Burner efficiency, dimensionless
ν	Kinematic viscosity, $ft^2/sec.$
ρ	Density, lb/ft^3

SUBSCRIPTS

amb	Ambient
AB	Afterbody
B	Burner
B_X	Bleed airflow extracted from the engine
b, base	Base flow region
BP	Bypass
BLC	Boundary layer bleed
btail	Boattail

SECTION I
INTRODUCTION

An essential element of the PIPSI and DERIVP computer procedures is the use of maps of standardized format to represent the inlet and nozzle/aftbody performance characteristics. This volume of the contract documents contains the existing library of performance characteristics for inlets and nozzle/aftbodies. It also contains descriptions of the configurations and the baseline derivative parameters.

The plotted data maps and derivative parameters contained in this document represent the data that are converted (in the form of data tables) into computer disk files for rapid use by the calculation procedures of the PIPSI and DERIVP computer programs.

SECTION II
INLET CONFIGURATIONS AND PERFORMANCE MAPS

This section contains descriptions of the geometric characteristics of the eighteen inlet configurations in the inlet library and their performance characteristics. The performance characteristics are presented in the form of plotted data in the standardized format required as input to the PIPSI and DERIVP computer programs. For the exact card format to use in converting the plotted data in this document (and other data which the user may wish to use) into data tables for use by either of the computer programs, the user should refer to Volume II (PIPSI Program) and Volume III (DERIVP Program).

A summary of the inlet types that are included in the inlet library is presented in Figure 1. The design Mach number for each inlet is also shown in Figure 1. A brief description of the sources used to obtain the inlet configurations and data is presented in Figure 2.

The derivative parameters for each of the inlet configurations are summarized in Figure 3.

2.1 INLET DESCRIPTIONS AND PLOTTED DATA

This section contains sketches of each inlet geometry and the plotted performance data for each inlet. In a general case, the performance characteristics for each inlet are defined by a series of fourteen plots. For some inlets, however, not all the performance plots are required because (for example) some of the inlet designs do not require bypass or bleed. In such cases, where tables would be zeroed out, those plots have been omitted from this document. In several cases, the input data plots for each configuration representing the variation of local inlet Mach number as a function of free-stream Mach have also been omitted because the free-stream Mach number is equal to the free-stream Mach number for these configurations.

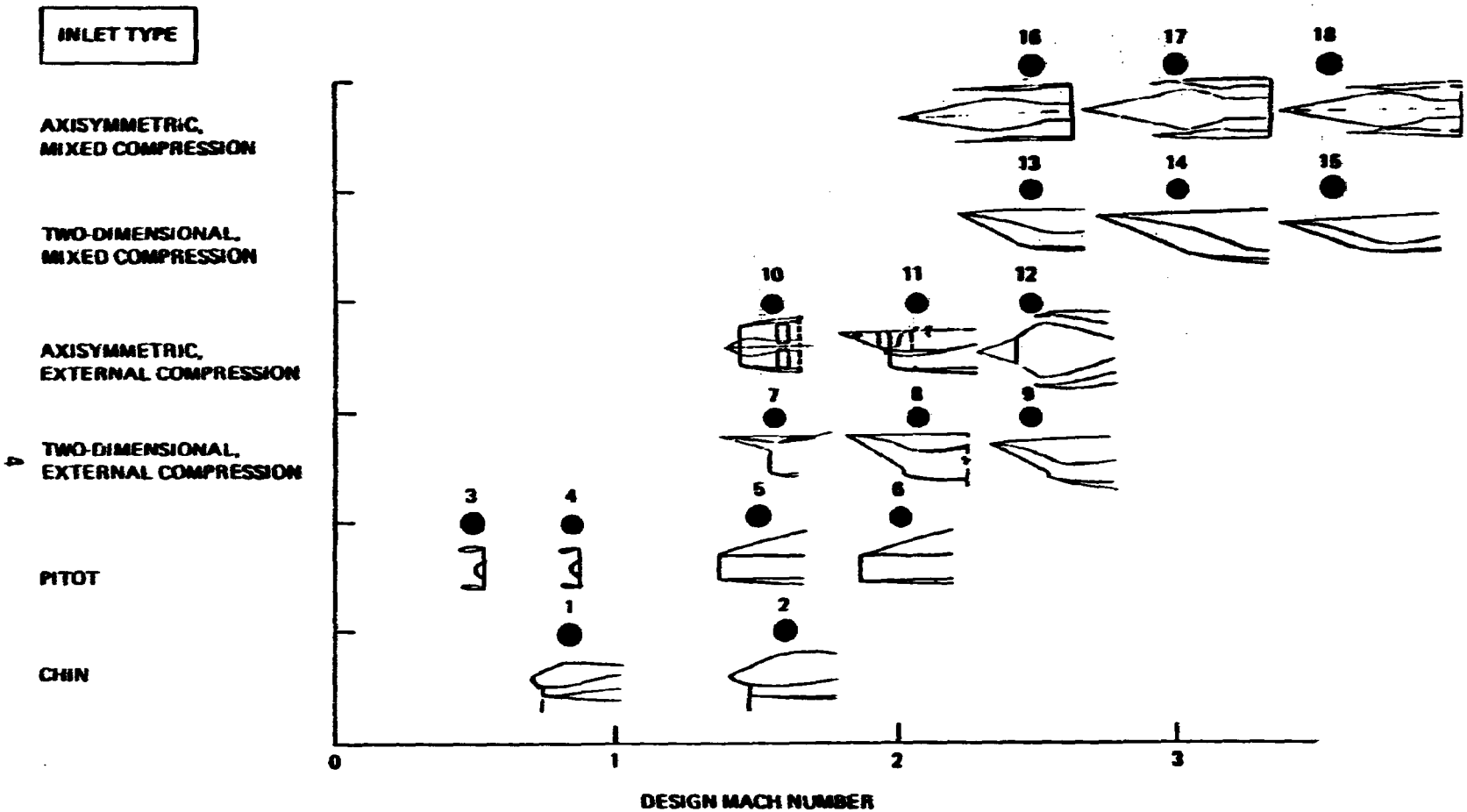

Figure 1 Matrix of Inlet Maps

Inlet No.	INLET CONFIGURATIONS AND SOURCES OF DATA USED TO DEVELOP THE INLET MAPS
1	A-7 type inlet; developed from published A-7 data and engineering analysis
2	F-8 type inlet; developed from published F-8 inlet data and analysis
3	Subsonic inlet type; based on data and methods from Boeing subsonic inlet (i.e., 707, 727, etc.)
4	Subsonic inlet type; based on data and methods used to develop Boeing 747-type inlets
5	Normal shock inlet; based on data from Rockwell tests of F-100 airplane inlet
6	Normal shock-type inlet; based on data from Rockwell F-100 inlet, Boeing LWF inlet tests, and GD LWF inlet data
7	Fixed-Geometry, 2-shock inlet; based on data from Boeing LWF inlet tests
8	Four-shock, variable ramp inlet; throretical design based on analysis, optimized for Mo = 2.0
9	Four-shock, variable ramp inlet; based on data from NR inlet tests of IPS model
10	Fixed-geometry, single cone inlet; based on analytical design for a Mo = 1.6 VTOL
11	3-Shock, half-round inlet with variable-diameter centerbody; analytical design for a supersonic Navy VTOL configuration
12	3-Shock , half-round inlet with variable second cone angle; GD tailor-mate tests
13	Mixed-compression; analytical design documented in AFFDL-TR-72-147-vol IV
14	Mixed compression; based on XB-70 type configuration and data
15	Mixed compression; based on NASA AMES configuration and tests of a mach 3.5, 2-D inlet
16	Mixed compression axisymmetric; based on a Boeing analytical study of an AST inlet for NASA AMES
17	Mixed compression axisymmetric; based on data from NASA AMES tests of M_{oo} = 3.0 inlet
18	Mixed compression axisymmetric; based on results of Boeing analytical studies for a NASA AMES mach 3.5 inlet

Figure 2 Sources of Data for Inlet Maps

	DERIVATIVE PARAMETERS	DEFINITION	CONFIGURATION NUMBERS 1	2	3	4	5	6	7	8	9	10	11	12	13	14	15	16	17	18
1	Inlet Aspect Ratio	W_C/h_C	N/A	N/A	N/A	N/A	N/A	N/A	2.0	1.0	1.0	N/A	N/A	N/A	1.0	1.0	1.0	N/A	N/A	N/A
2	Sideplate Cutback	A_{CB}/A_{sp}	N/A	N/A	N/A	N/A	N/A	N/A	.75	.20	.25	N/A	N/A	N/A	0.0	0.0	0.0	N/A	N/A	N/A
3	First Ramp Angle	Deg.	N/A	N/A	N/A	N/A	N/A	N/A	7.0	7.3	6.0	25.0	22.0	18.0	7.0	7.0	7.0	10.4	10.0	10.0
4	Design Mach Number	~	.80	1.60	.50	.88	1.50	1.60	1.60	2.0	2.5	1.60	2.0	2.5	2.5	3.0	3.5	2.35	3.0	3.5
5	Cowl Lip Bluntness	R_{lip}/h_C	.03	.02	.030	.022	.022	0.	.012	.012	.006	.02	.015	015	0.	0.	0.	0.	0.	0.
6	Takeoff Door Area	A_{to}/A_C	0.0	0.0	N/A	.026	.18	.22	.235	.20	.11	.462	.46	.25	.12	.50	.20	.20	.20	20
7	External Cowl Angle	Deg.	4.5	2.5	12.	17.	5.0	5.9	13.0	17.5	17.0	18.	19.	12.	12.	12.	15.0	1.0	0.0	3.0
8	Bleed Exit Nozzle Type	Conv. or C-D	N/A	N/A	N/A	N/A	N/A	N/A	Conv.	Conv.	Conv.	N/A	Conv.	Conv.	Conv.	Conv.	Conv.	Conv.	Conv.	Conv.
9	Bleed Exit Nozzle Angle	Deg.	N/A	N/A	N/A	N/A	N/A	N/A	20.0	15.0	20.0	N/A	20.0	15.	20.0	0.0	15.	15.	15.	10
10	Bleed Exit Flap Aspect Ratio	W_f/h_f	N/A	N/A	N/A	N/A	N/A	N/A	1.0	2.0	.90	N/A	1.0	1.0	.90	N/A	1.0	1.0	1.0	1.0
11	Bleed Exit Flap Area	A_f/A_C	N/A	N/A	N/A	N/A	N/A	N/A	.10	.10	.50	N/A	.10	.10	.20	N/A	.20	.20	.20	20
12	Bypass Exit Nozzle Type	Conv. or C-D	N/A	N/A	N/A	N/A	N/A	N/A	N/A	Conv.	C-D	N/A	Conv.	Conv.	C-D	C-D	C-D	C-D	C-D	C-D
13	Bypass Exit Nozzle Angle	Deg.	N/A	N/A	N/A	N/A	N/A	N/A	N/A	15.0	20.	N/A	20.	15.	20.	15.	15.	15.	15.	10
14	Bypass Exit Flap Aspect Ratio	W_f/h_f	N/A	N/A	N/A	N/A	N/A	N/A	N/A	2.0	.67	N/A	1.0	1.0	1.0	2.0	1.0	1.0	1.0	1.0
15	Bypass Exit Flap Area	A_f/A_C	N/A	N/A	N/A	N/A	N/A	N/A	N/A	.20	.268	N/A	.20	.20	.20	.20	.20	.20	.20	20
16	Subsonic Diffuser Area Ratio	A_2/A_1	1.40	1.40	1.25	1.25	1.305	1.305	1.373	1.50	1.89	1.44	1.83	2.0	1.40	2.8	4.7	1.57	2.1	4.97
17	Diffuser Total Wall Angle	Deg.	2.5	3.5	12.0	12.0	4.0	4.0	5.0	10.0	8.5	6.0	9.0	15.0	9.0	12.0	11.5	7.0	12.0	9.0
18	Subsonic Diffuser Loss Coefficient	ϵ	.12	.12	.015	.015	.12	.12	.12	.12	.16	.08	.12	.14	.14	.12	.14	.06	.12	.12
19	Throat/Capture Area Ratio	A_T/A_C	N/A	N/A	.80	.90	.96	1.00	N/A	N/A	N/A	N/A	N/A	N/A	N/A	N/A	N/A	N/A	N/A	N/A
	INLET TYPE		Chin	Chin	Pitot	Pitot	Pitot (N.S.)	Pitot (N.S.)	E.C. 2-D	E.C. 2-D	E.C. 2-D	E.C. AXI	E.C. AXI	E.C AXI	M.C. 2-D	M.C. 2-D	M.C. 2-D	M.C. AXI	M.C. AXI	M.C AXI
	FILE NAME		A7	F8	M5SUB	M5SUB	NS	NS2	LWF	ATS2	ASF	VSTOL	NVSTO	TM183	FB	INT	M352D	AST	NASA3	BCAC35

Figure 3. Summary of Baseline Inlet Configurations

2.1.1 Inlet Configuration #1 - Subsonic, Chin Inlet

This inlet is a subsonic, scoop-type inlet mounted under the nose of the forebody. No boundary layer bleed or bypass are employed, and the configuration is characterized by a rather long subsonic diffuser. A reasonably blunt cowl lip is used and angle-of-attack shielding is provided by the presence of the fuselage forebody. This configuration is similar to the A-7 aircraft inlet. Available inlet test data from similar configurations were supplemented by engineering analyses (such as the calculation procedures in Reference 1) to develop the maps of inlet performance. A sketch of the inlet configuration is shown in Figure 4. The performance characteristics of the inlet are presented in Figure 5.

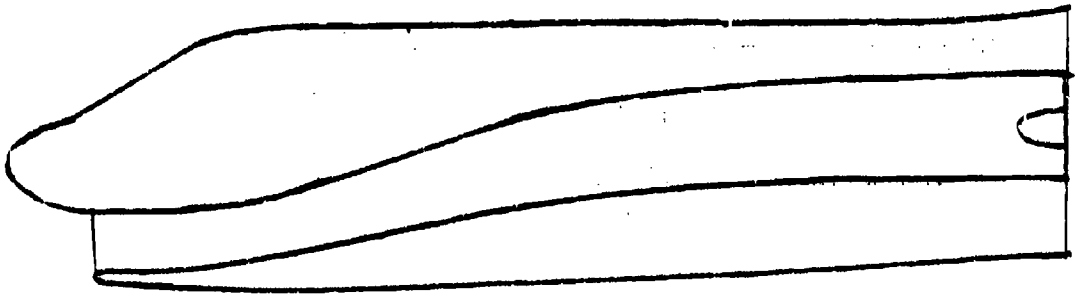

Figure 4. Subsonic Chin Inlet

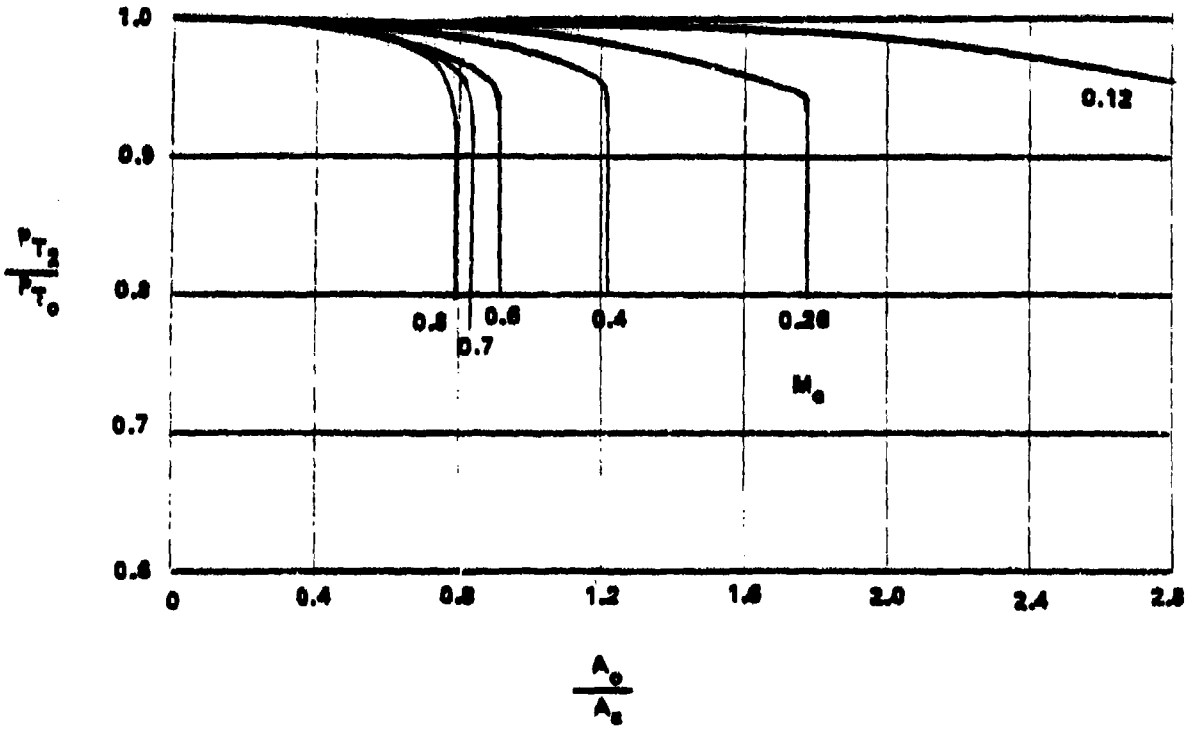

Figure 5. Performance Characteristics for Inlet Configuration #1

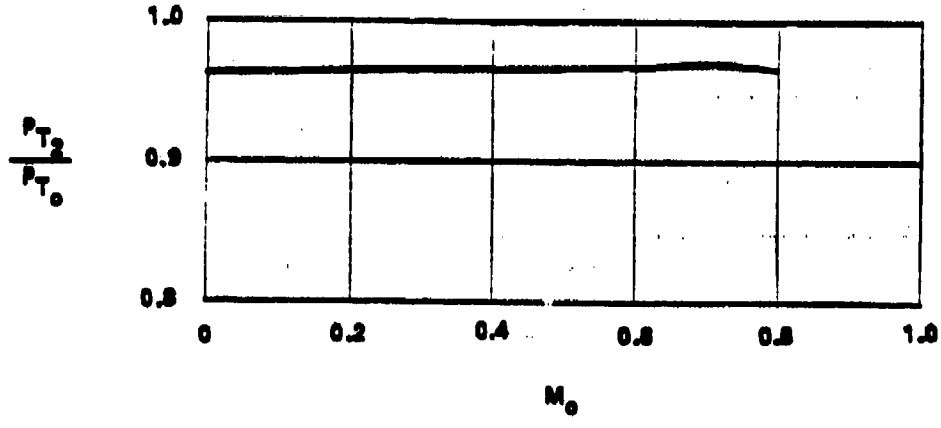

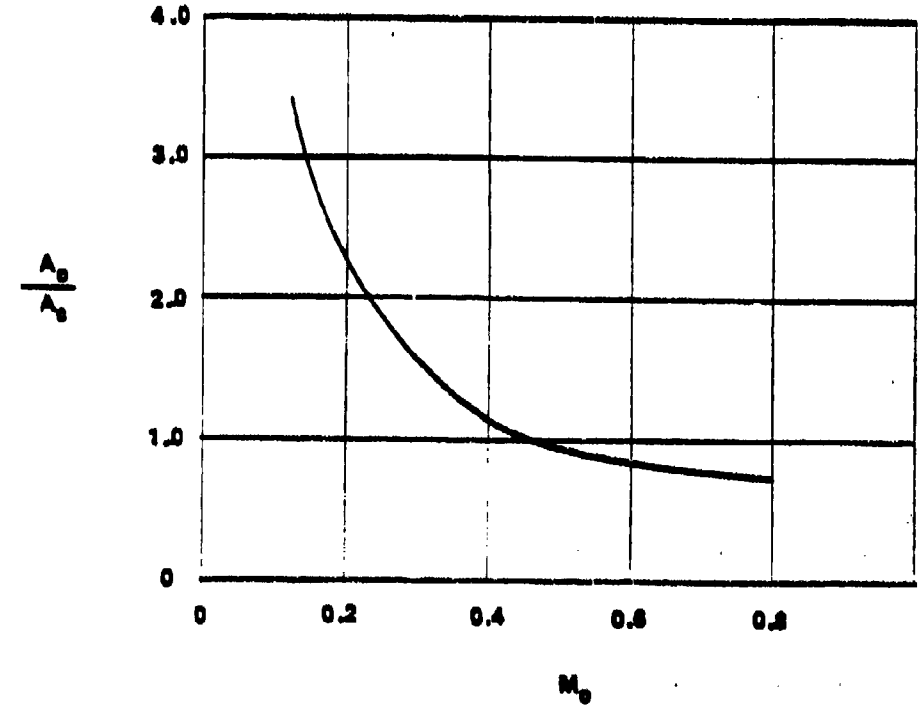

Figure 5. Performance Characteristics for Inlet Configuration #1 (continued)

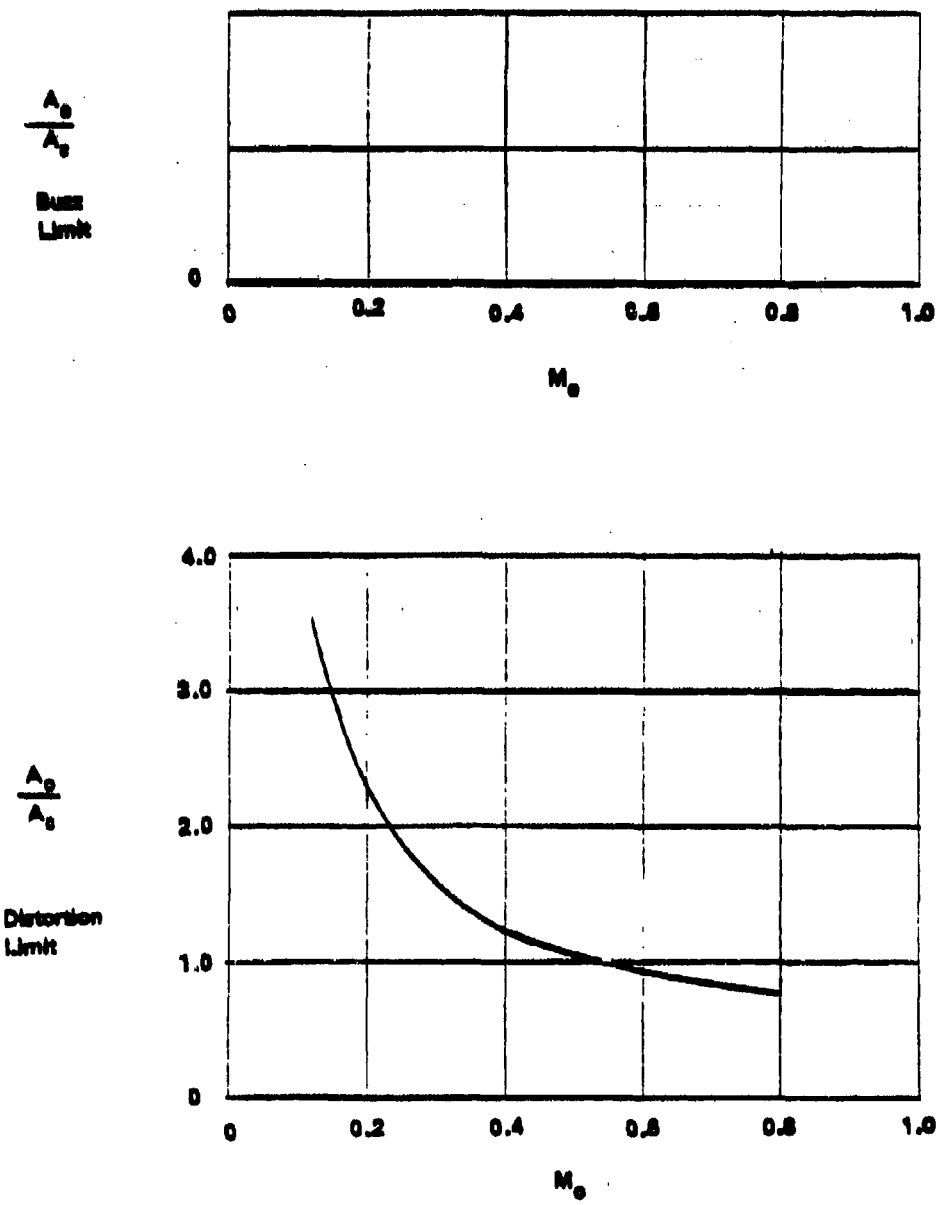

Figure 5. Performance Characteristics for Inlet Configuration #1 (continued)

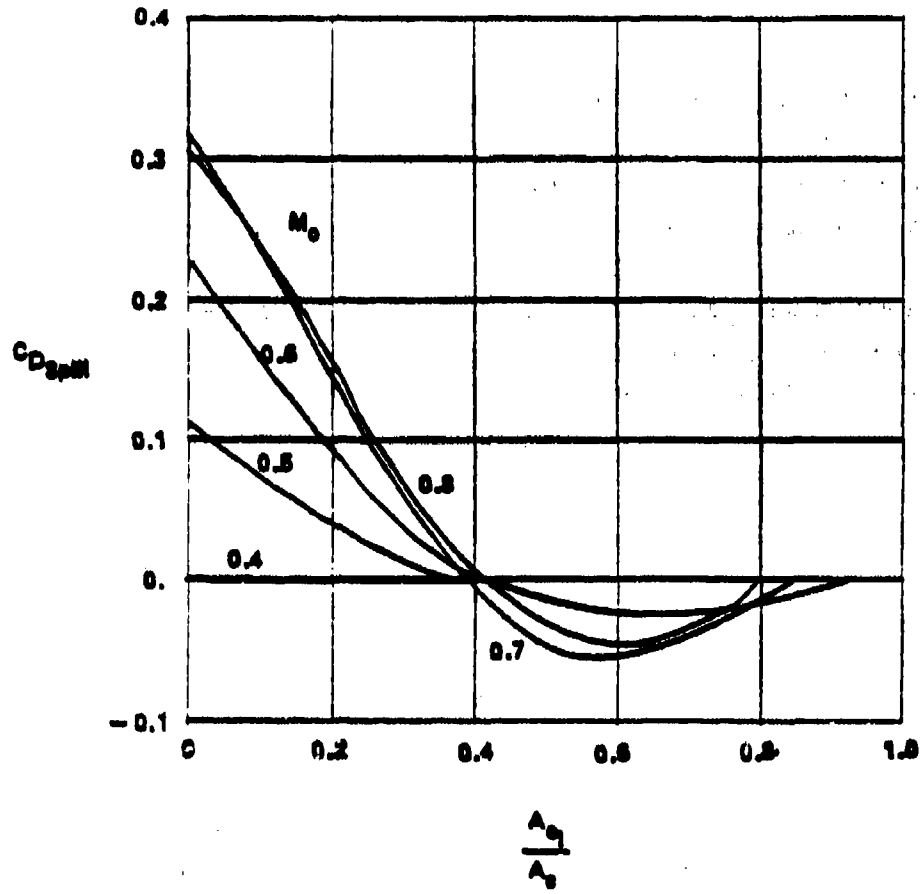

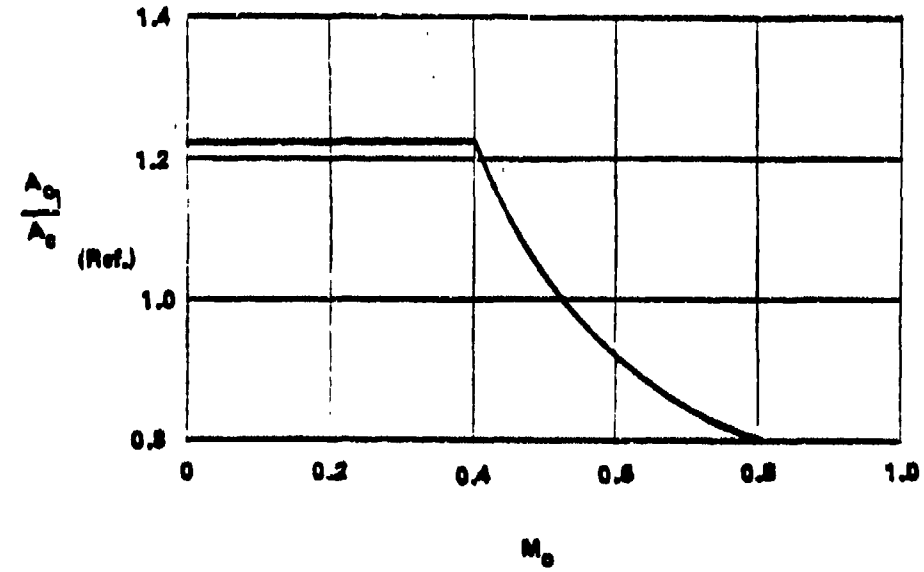

Figure 5. Performance Characteristics for Inlet Configuration #1 (concluded)

2.1.2 Inlet Configuration #2 - Supersonic, Chin Inlet

This inlet is a fixed geometry, nose-mounted cone-scoop configuration. The inlet has no boundary layer control bleed system or bypass system. It is designed for a maximum Mach number of 1.60. The cowl lip is relatively sharp, and the subsonic diffuser is relatively long. The inlet performance characteristics for this inlet were developed from the data published in Reference 2 and analyses methods described in Reference 1. A sketch of the inlet geometry is presented in Figure 6. The performance characteristics of the inlet are presented in Figure 7.

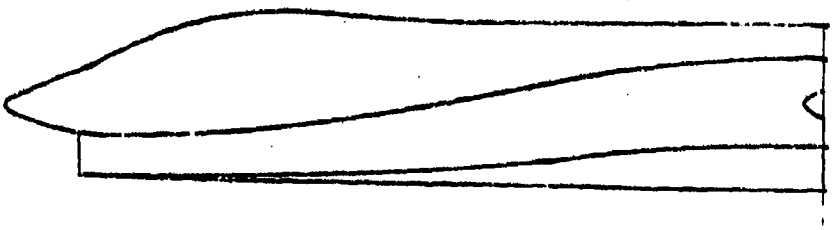

Figure 6. Supersonic Chin Inlet

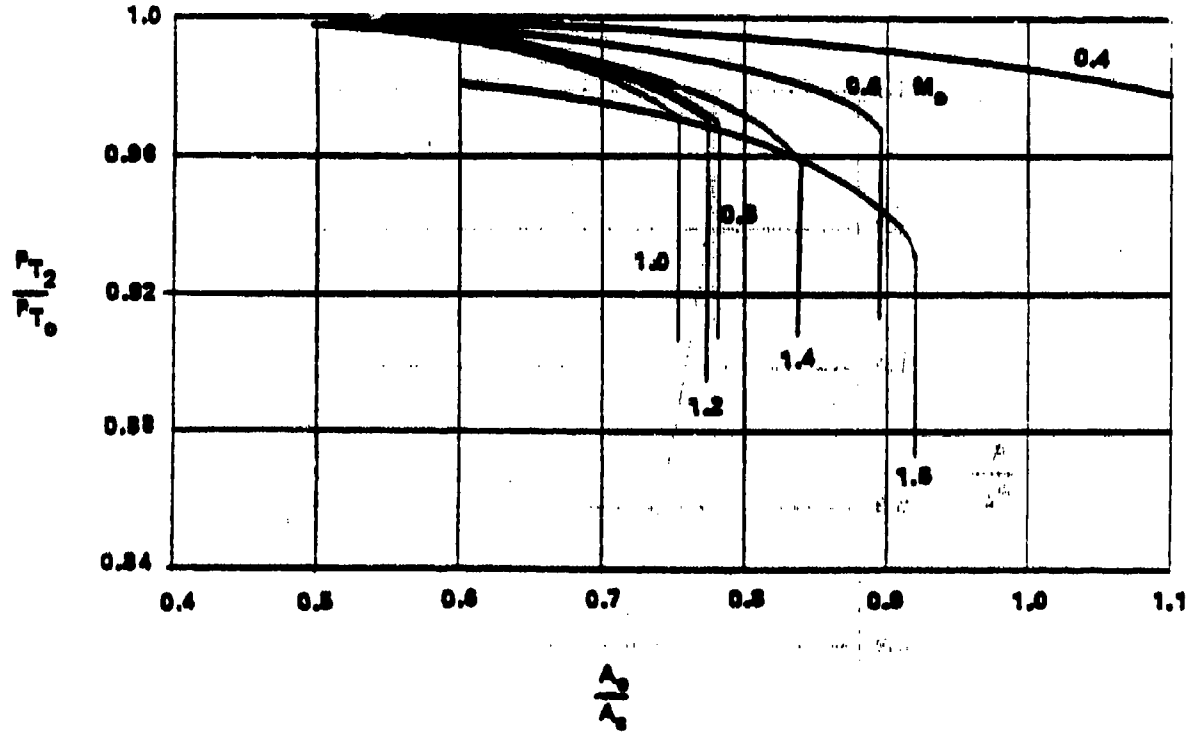

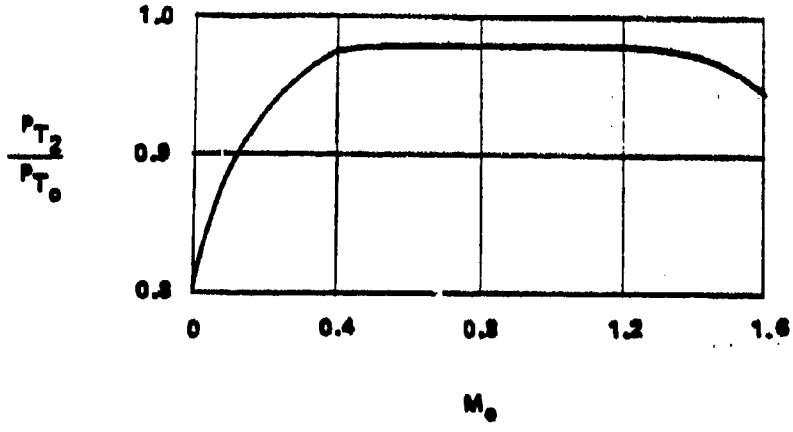

Figure 7. Performance Characteristics for Inlet Configuration #2

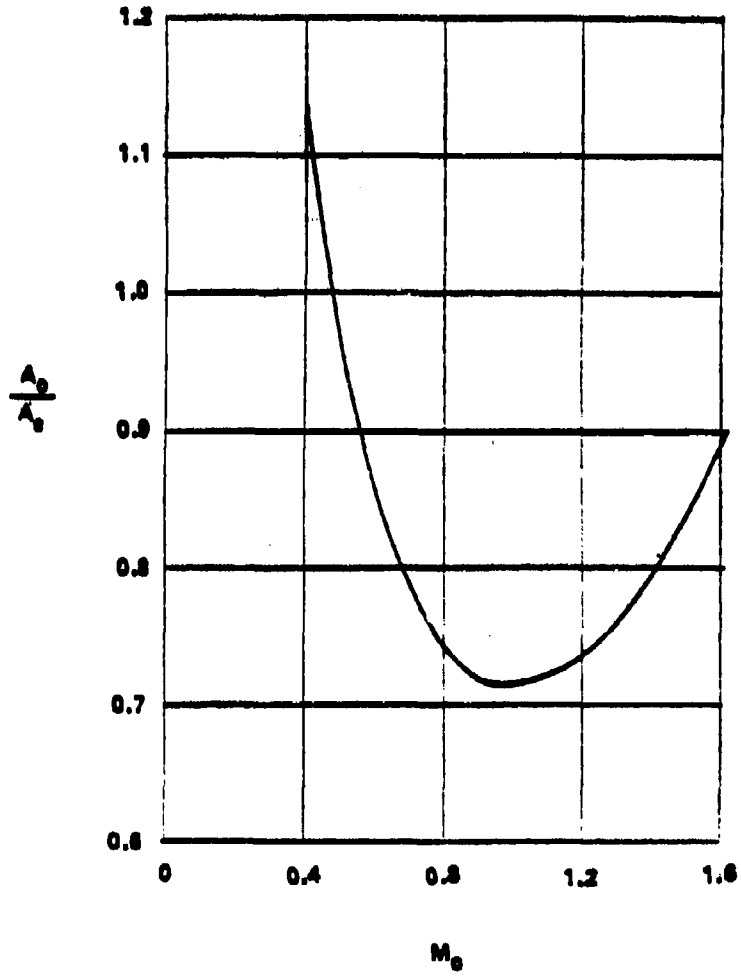

Figure 7. Performance Characteristics for Inlet Configuration #2 (continued)

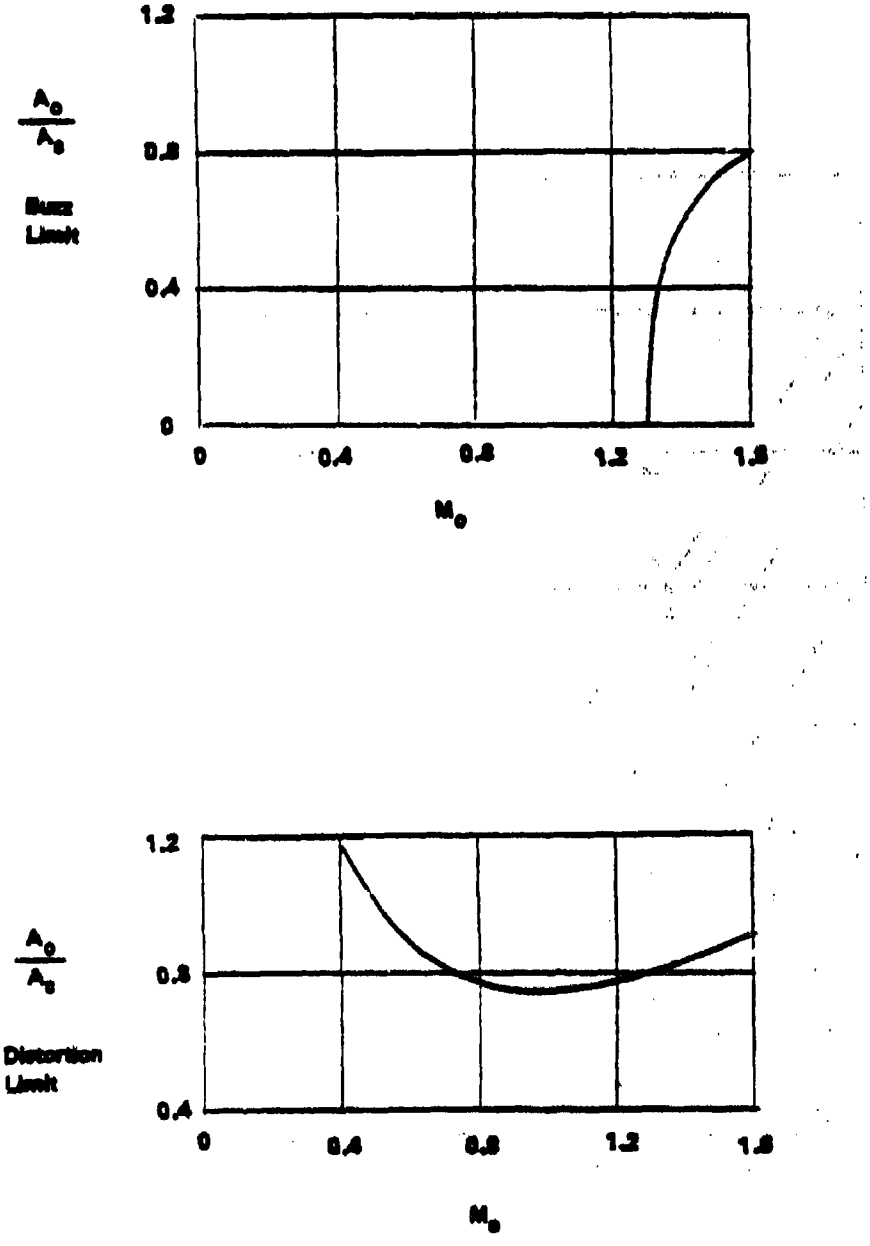

Figure 7. Performance Characteristics for Inlet Configuration #2 (continued)

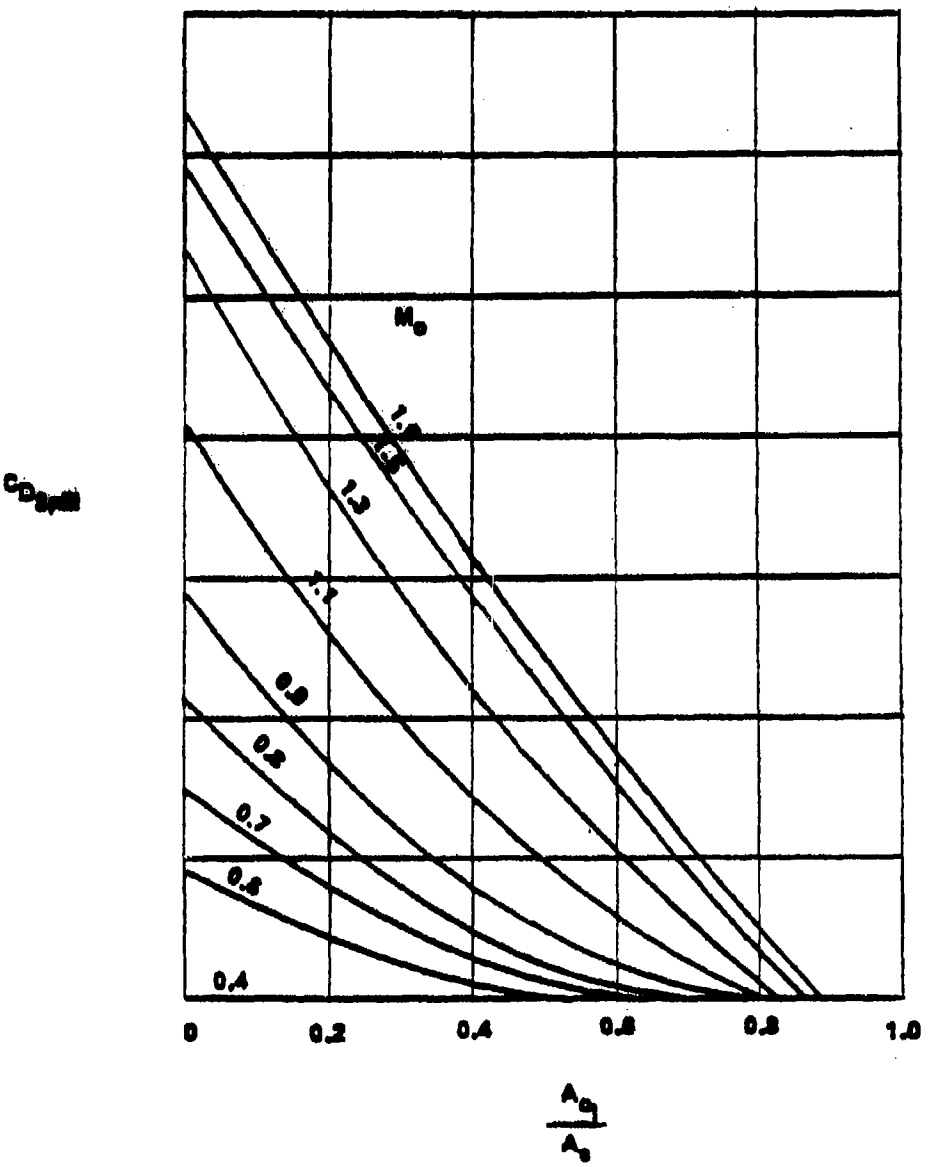

Figure 7. Performance Characteristics for Inlet Configuration #2 (continued)

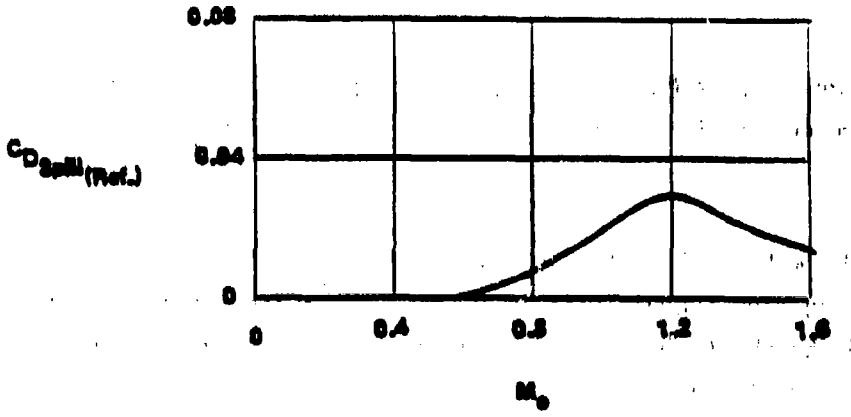

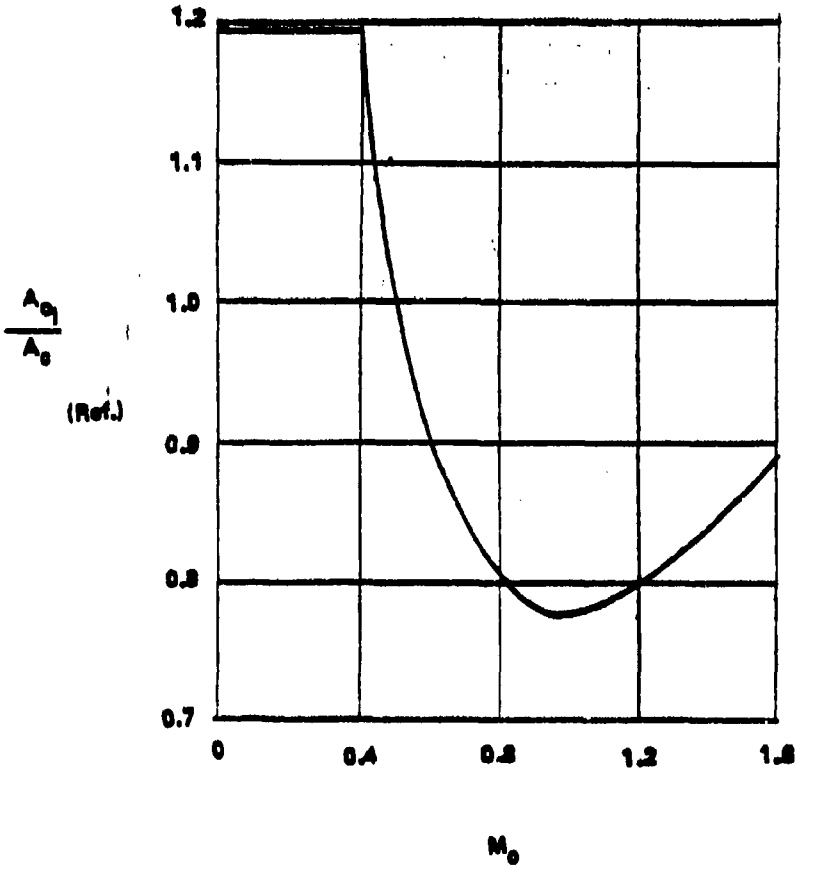

Figure 7. Performance Characteristics for Inlet Configuration #2 (concluded)

2.1.3 Inlet Configuration #3 - Subsonic, Pitot Inlet

This inlet is designed for a Mach number of 0.5. It has a very blunt lip; no bleed or bypass systems are used and the subsonic diffuser is short.

The performance characteristics of this inlet were generated from test data obtained during wind tunnel tests to develop the 747 fixed-lip inlet (Reference 3). A sketch of the inlet is presented in Figure 8 and the inlet performance characteristics are presented in Figure 9.

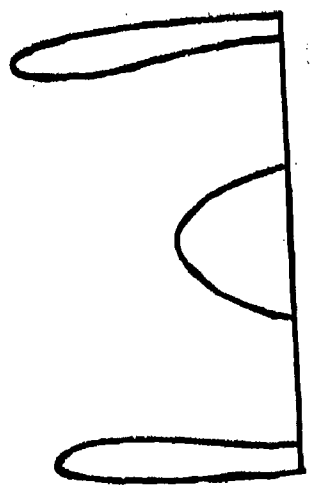

Figure 8. Subsonic Fixed Lip Inlet

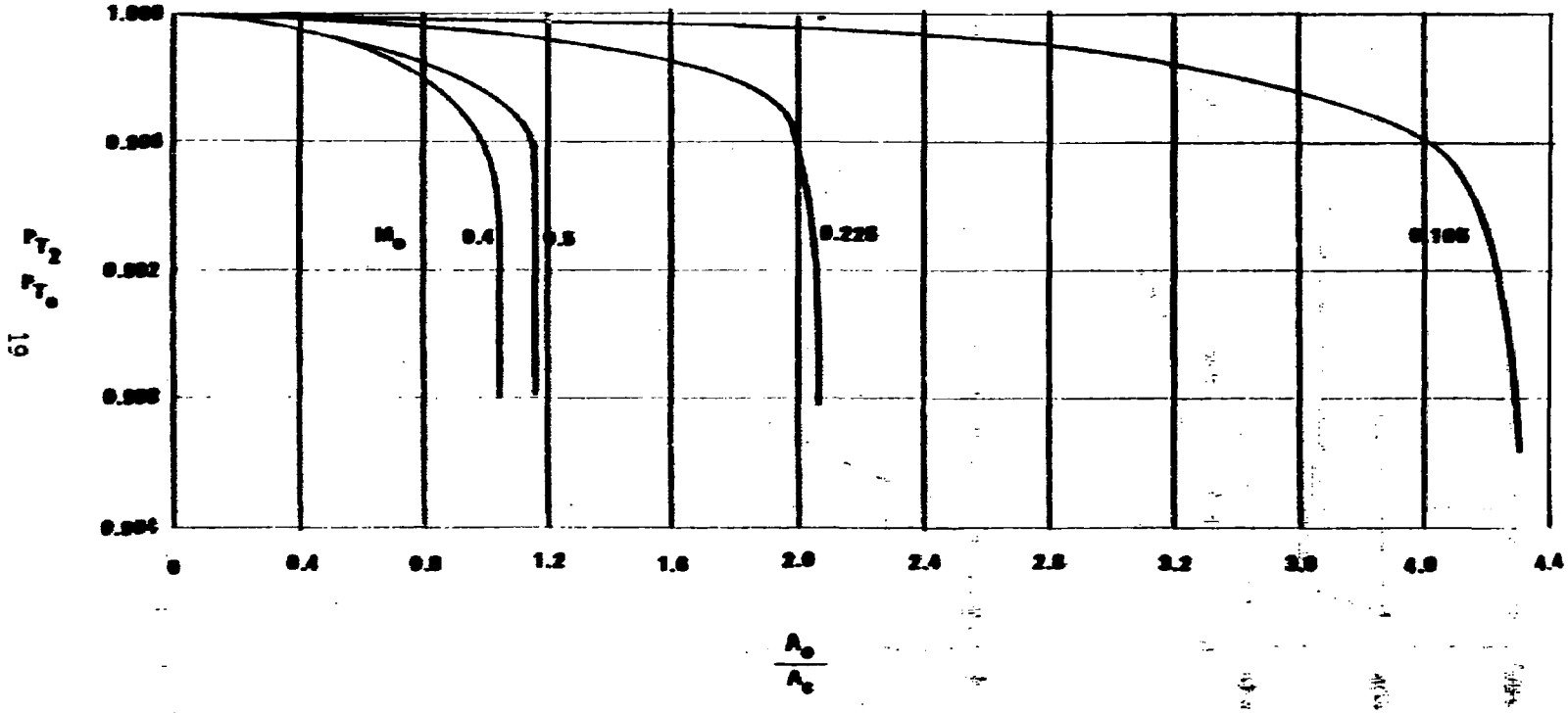

Figure 9. Performance Characteristics for Inlet Configuration #3

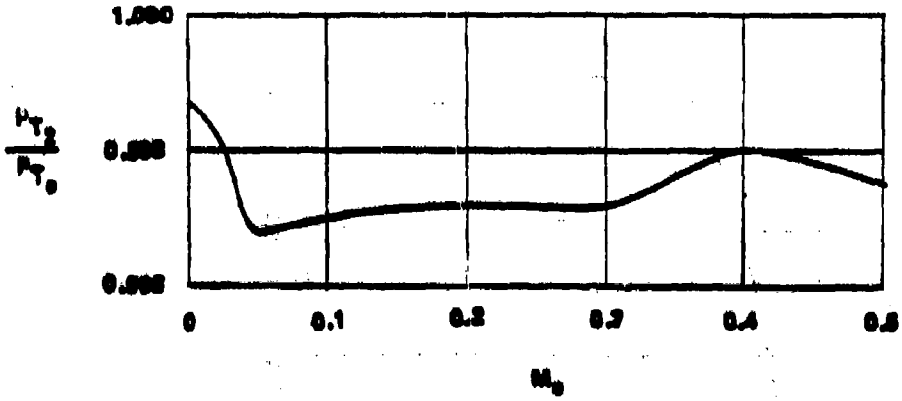

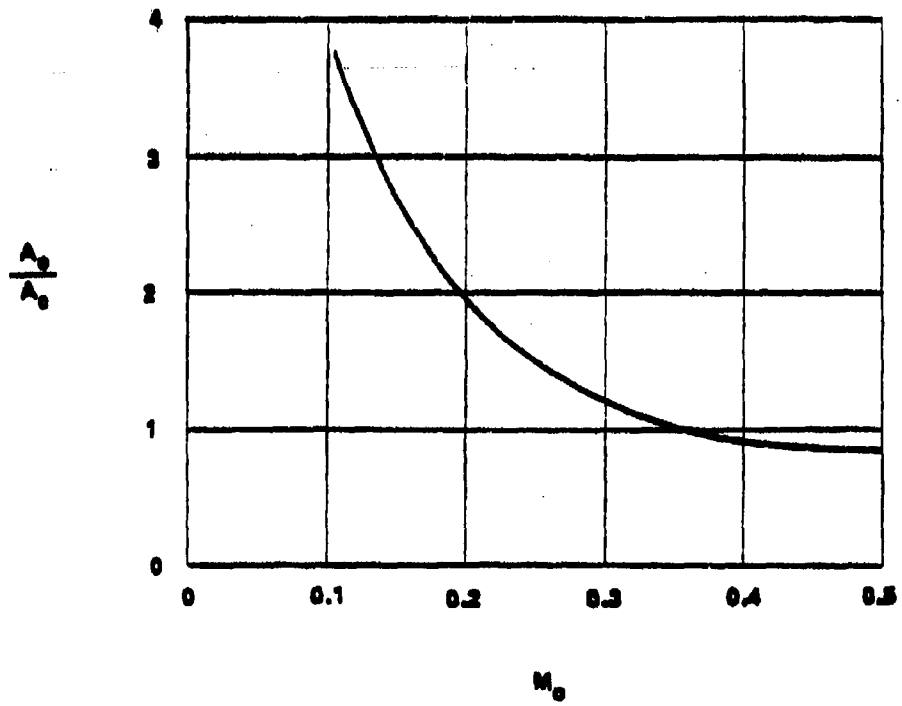

Figure 9. Performance Characteristics for Inlet Configuration #3 (continued)

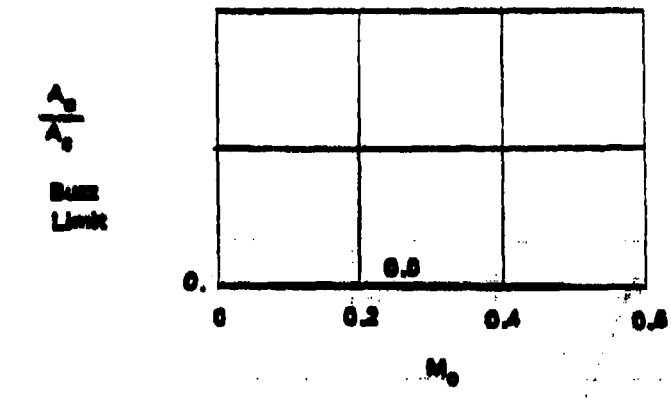

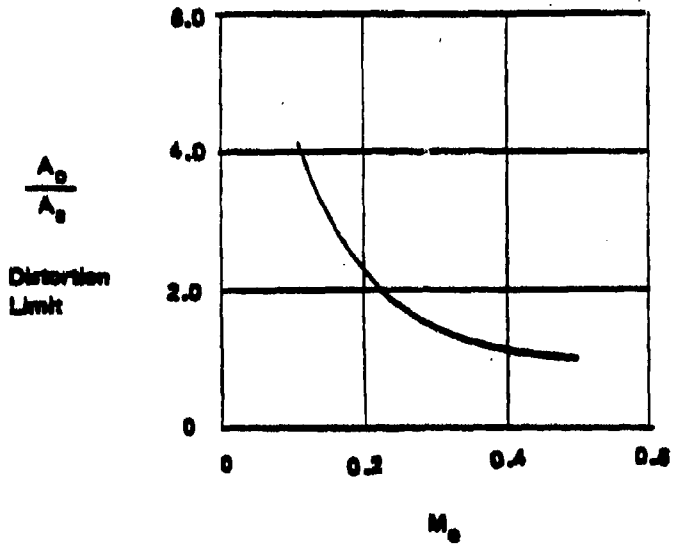

Figure 9. Performance Characteristics for Inlet Configuration #3 (continued)

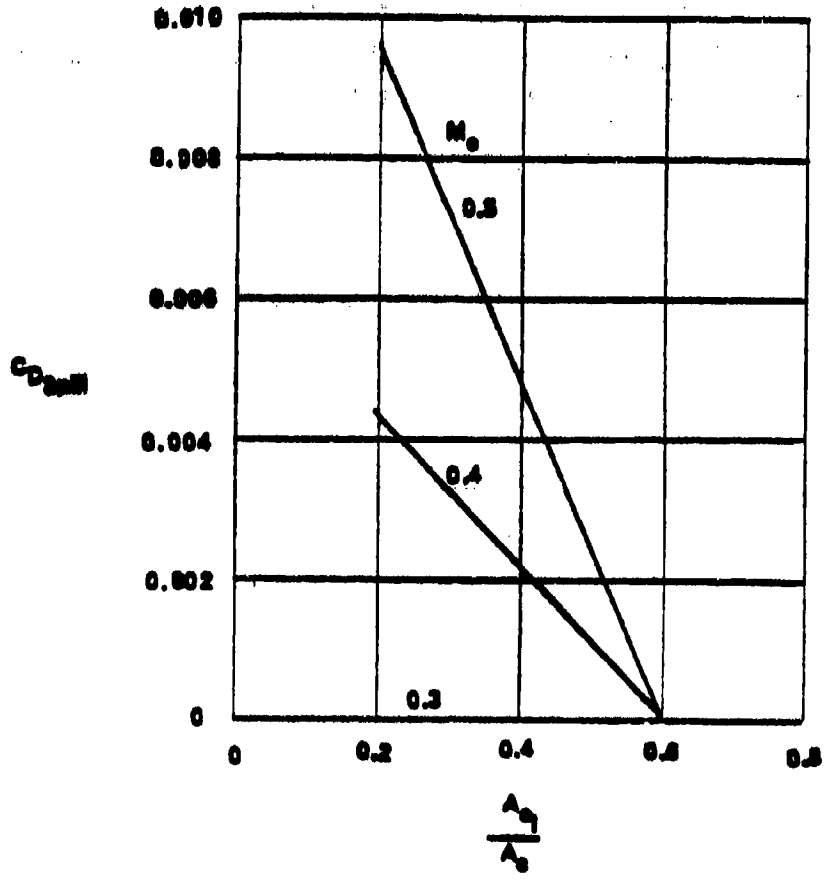

Figure 9. Performance Characteristics for Inlet Configuration #3 (continued)

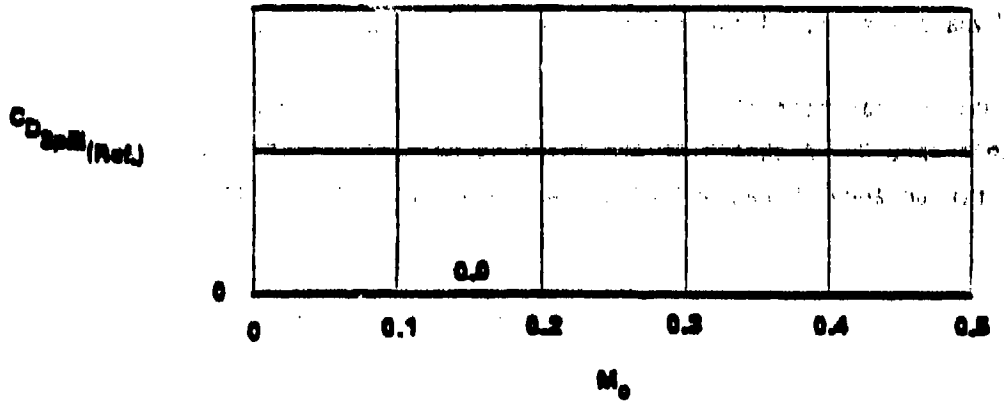

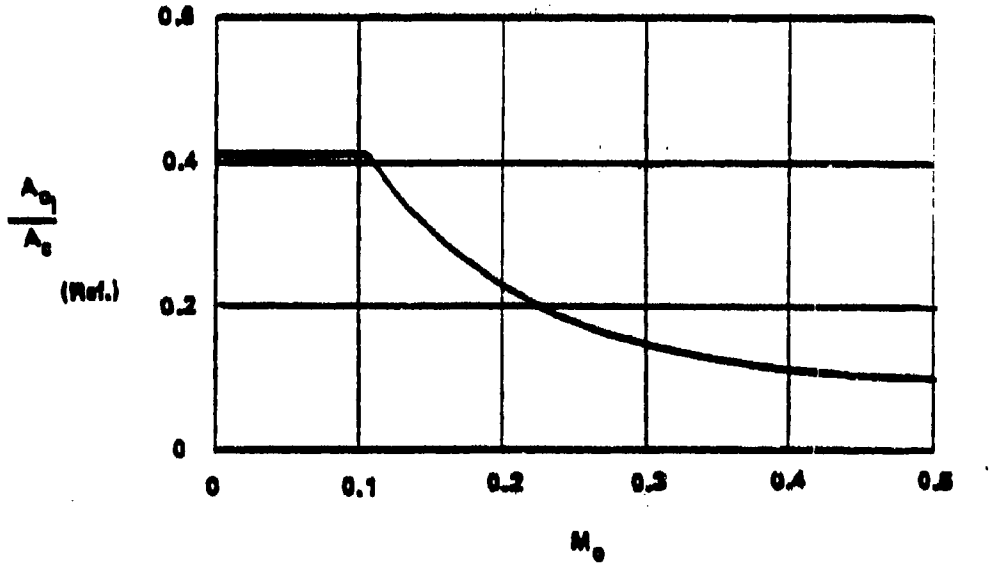

Figure 9. Performance Characteristics for Inlet Configuration #3 (concluded)

2.1.4 Inlet Configuration #4 - Subsonic, Pitot-Type Inlet

This subsonic inlet is designed for a Mach number of 0.8. It has a relatively thin lip (for a subsonic inlet) and has no boundary layer bleed or bypass system. Blow-in doors are used at takeoff and low speed.

The performance characteristics of this inlet were developed from the data of Reference 3. A sketch of the inlet is presented in Figure 10 and the inlet performance characteristics are presented in Figure 11.

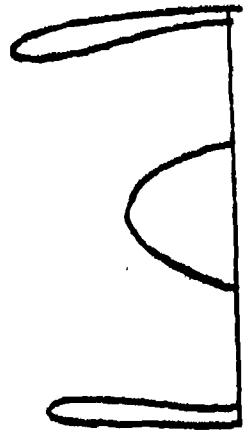

Figure 10. Subsonic Blow-In Door Inlet

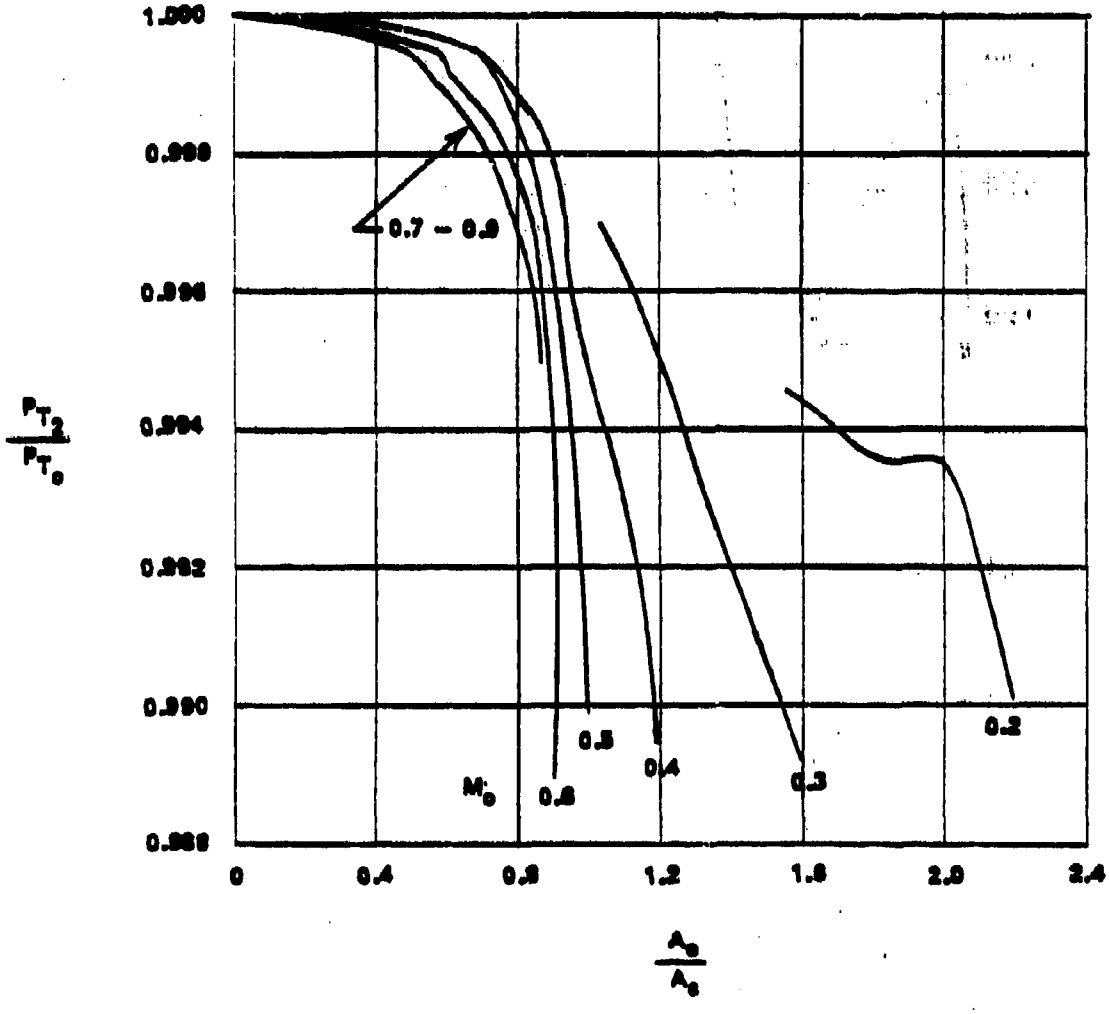

Figure 11. Performance Characteristics for Inlet Configuration #4

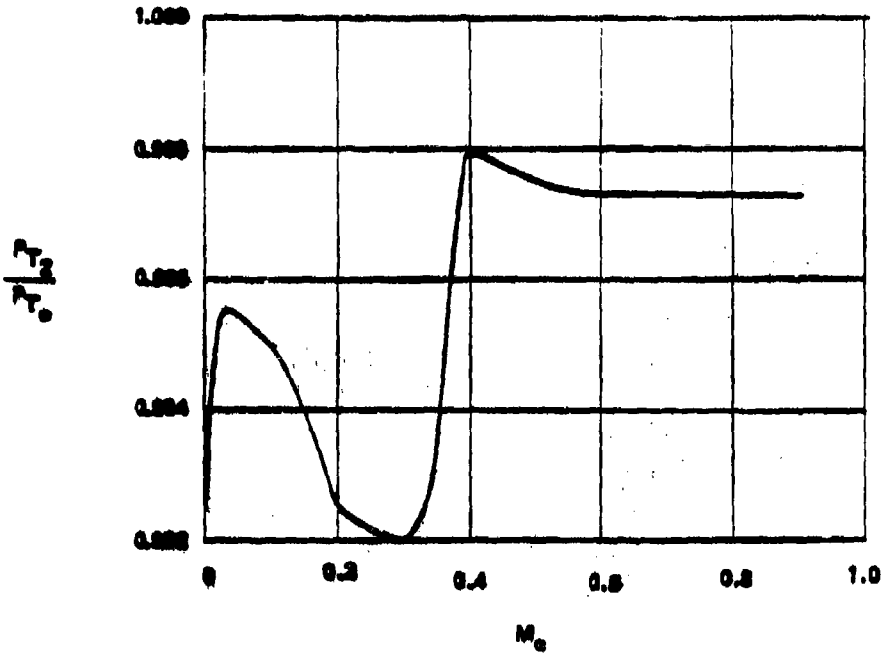

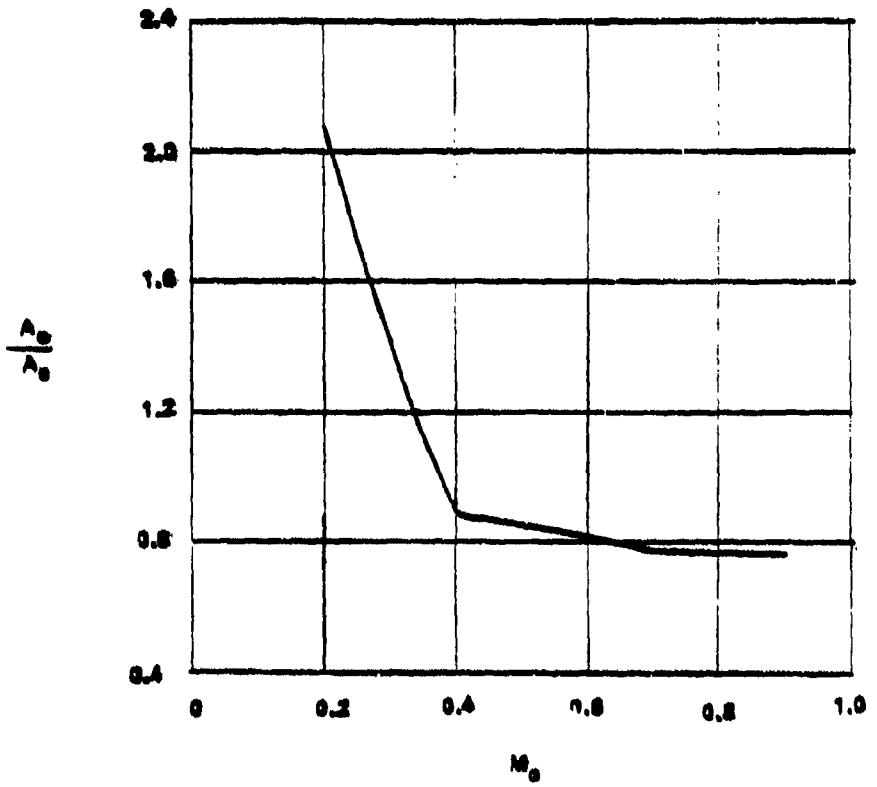

Figure 11. Performance Characteristics for Inlet Configuration #4 (continued)

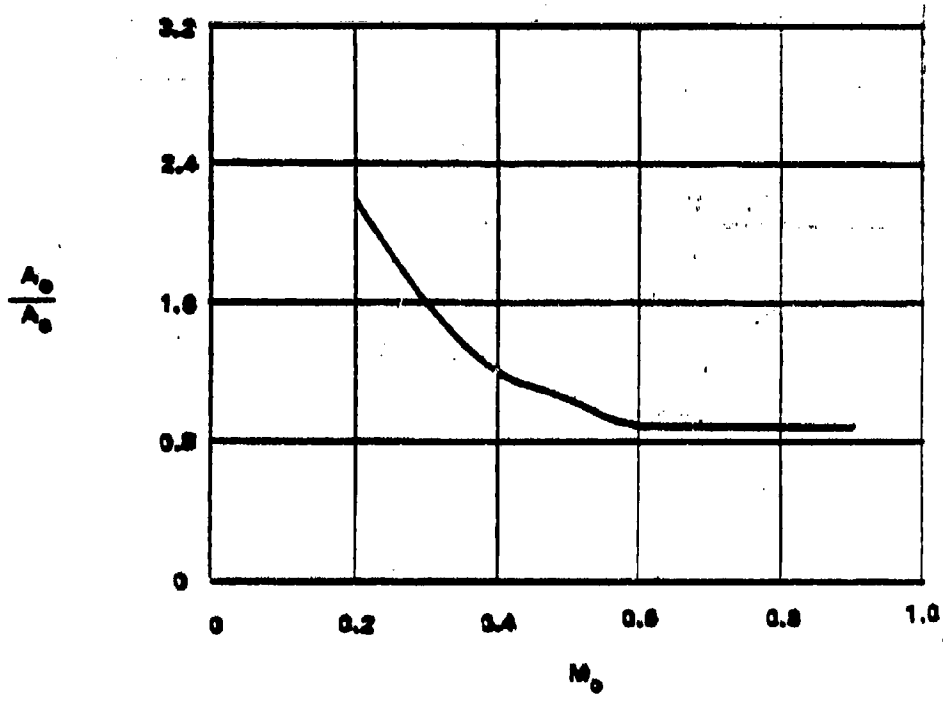

Figure 11. Performance Characteristics for Inlet Configuration #4 (continued)

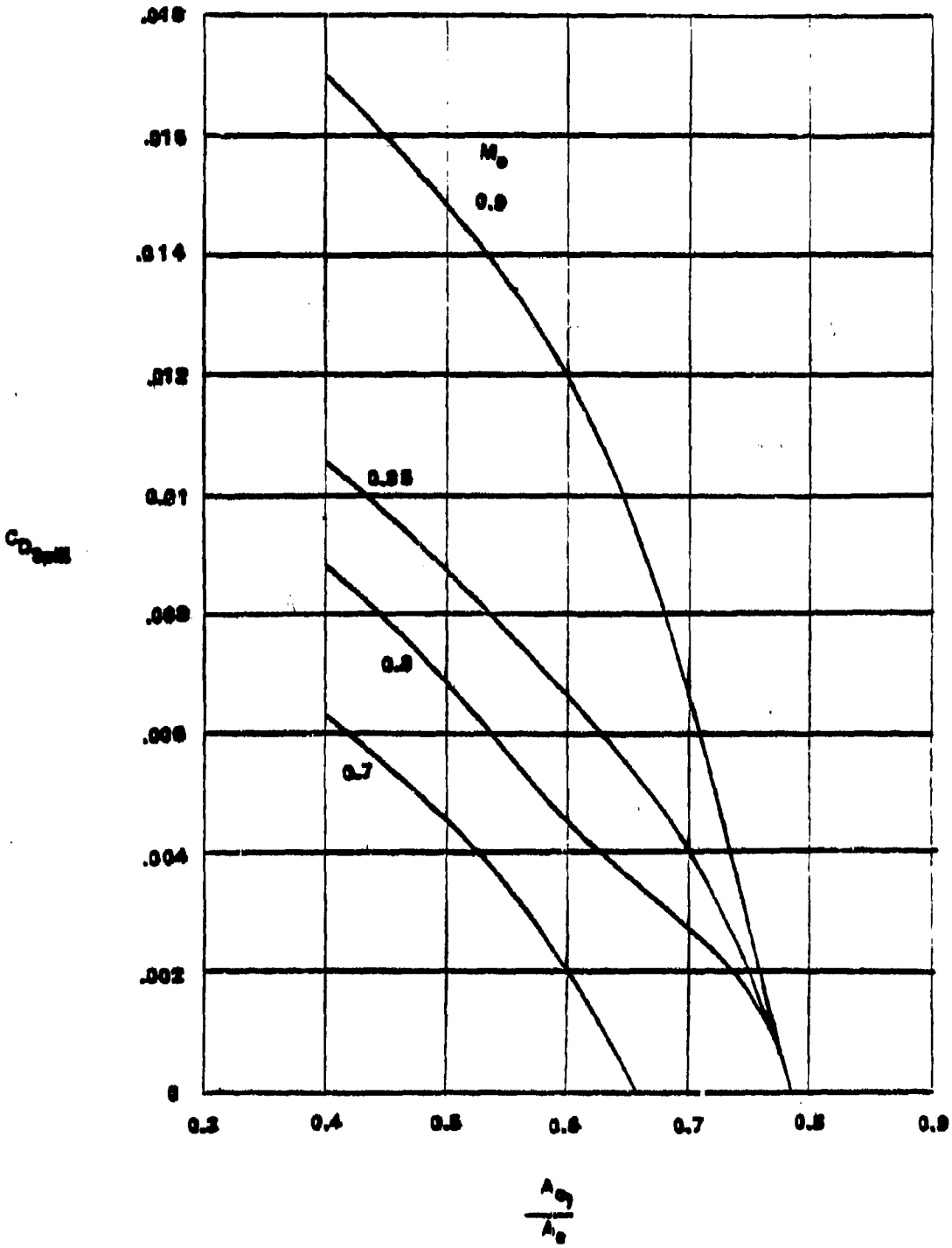

Figure 11. Performance Characteristics for Inlet Configuration #4 (concluded)

2.1.5 Inlet Configuration #5 - Supersonic, Normal Shock Inlet

This inlet is designed for a Mach number of 1.50. It has no bleed or bypass system. The subsonic diffuser is relatively long and the cowl lip is relatively sharp, for reduced drag at supersonic speeds.

The inlet performance characteristics are based on the test data contained in Reference 4. The inlet geometry is shown in Figue 12 and the inlet performance characteristics are presented in Figure 13.

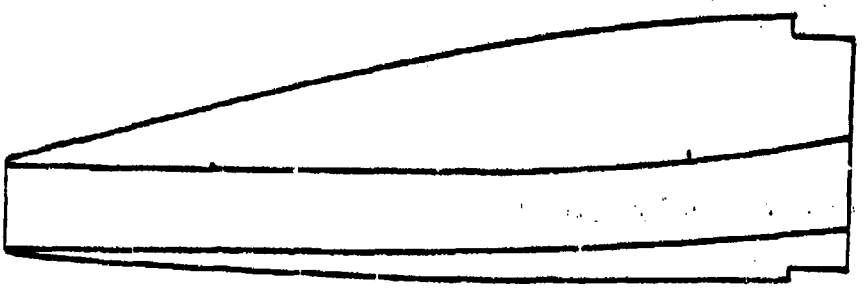

Figure 12. Supersonic Normal Shock Inlet (First Version)

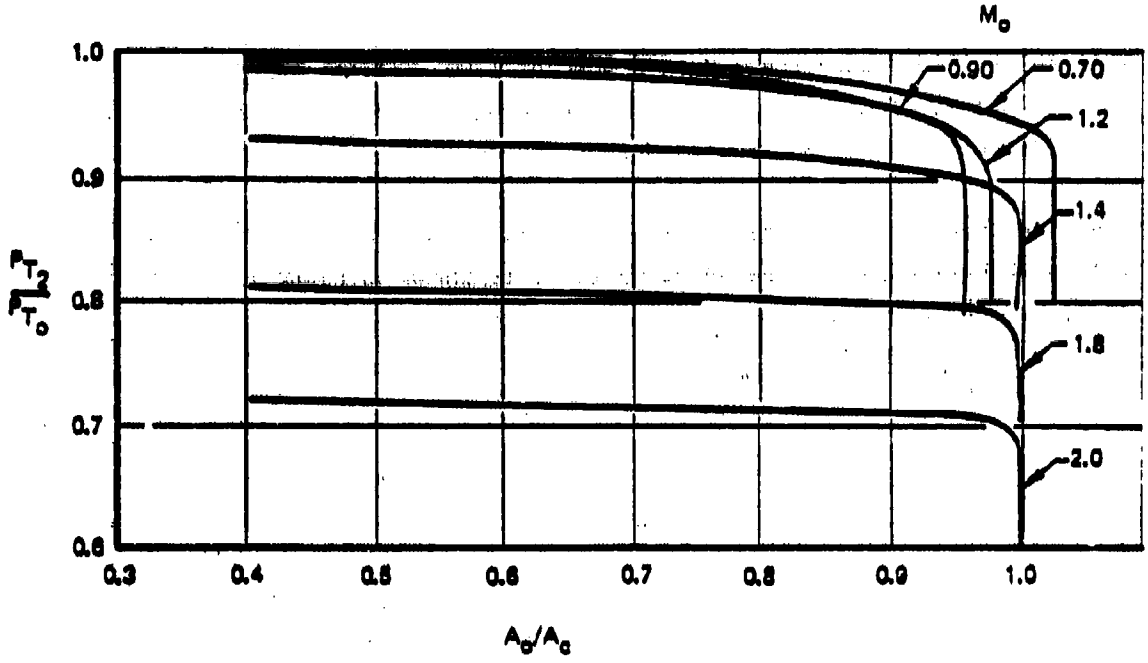

Figure I3. Performance Characteristics for Inlet Configuration #5

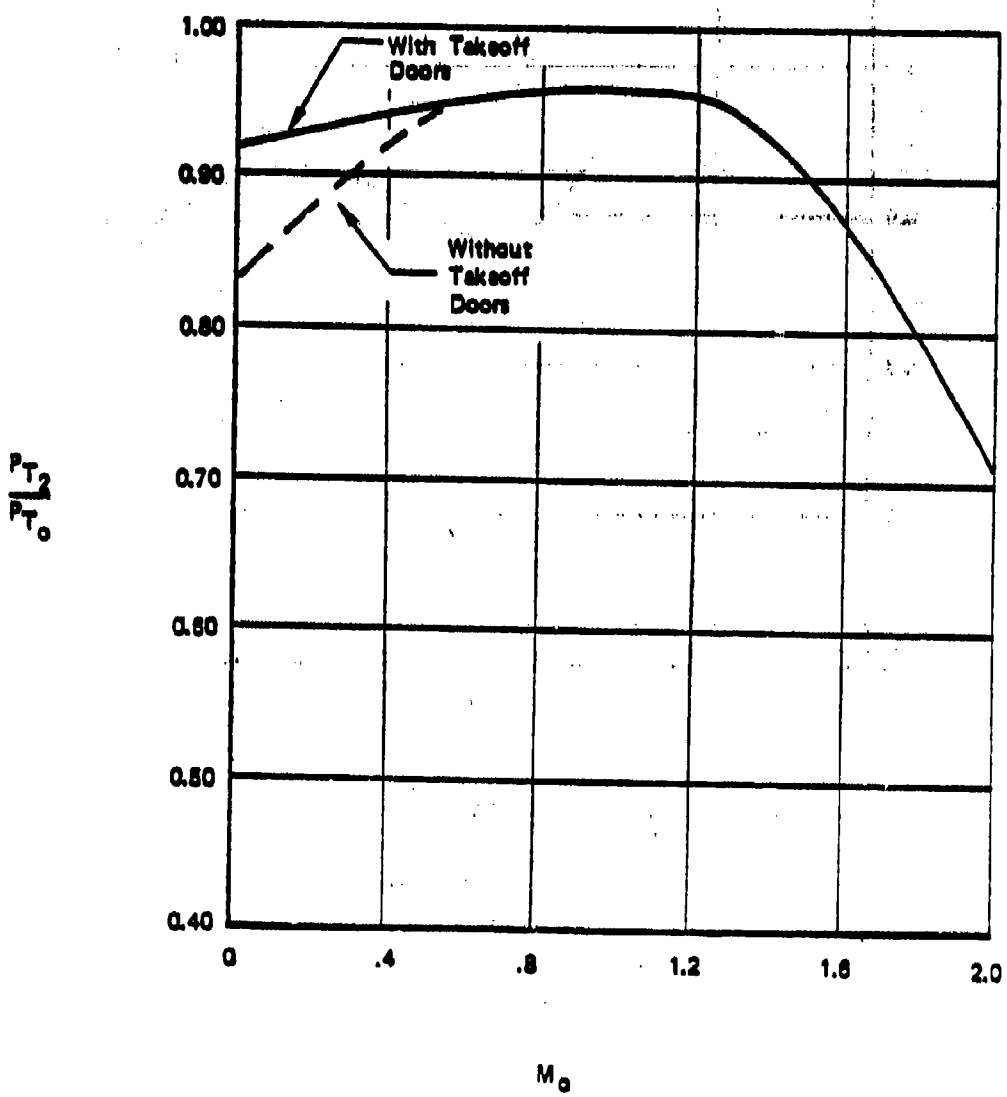

Figure 13. Performance Characteristics for Inlet Configuration #5 (continued)

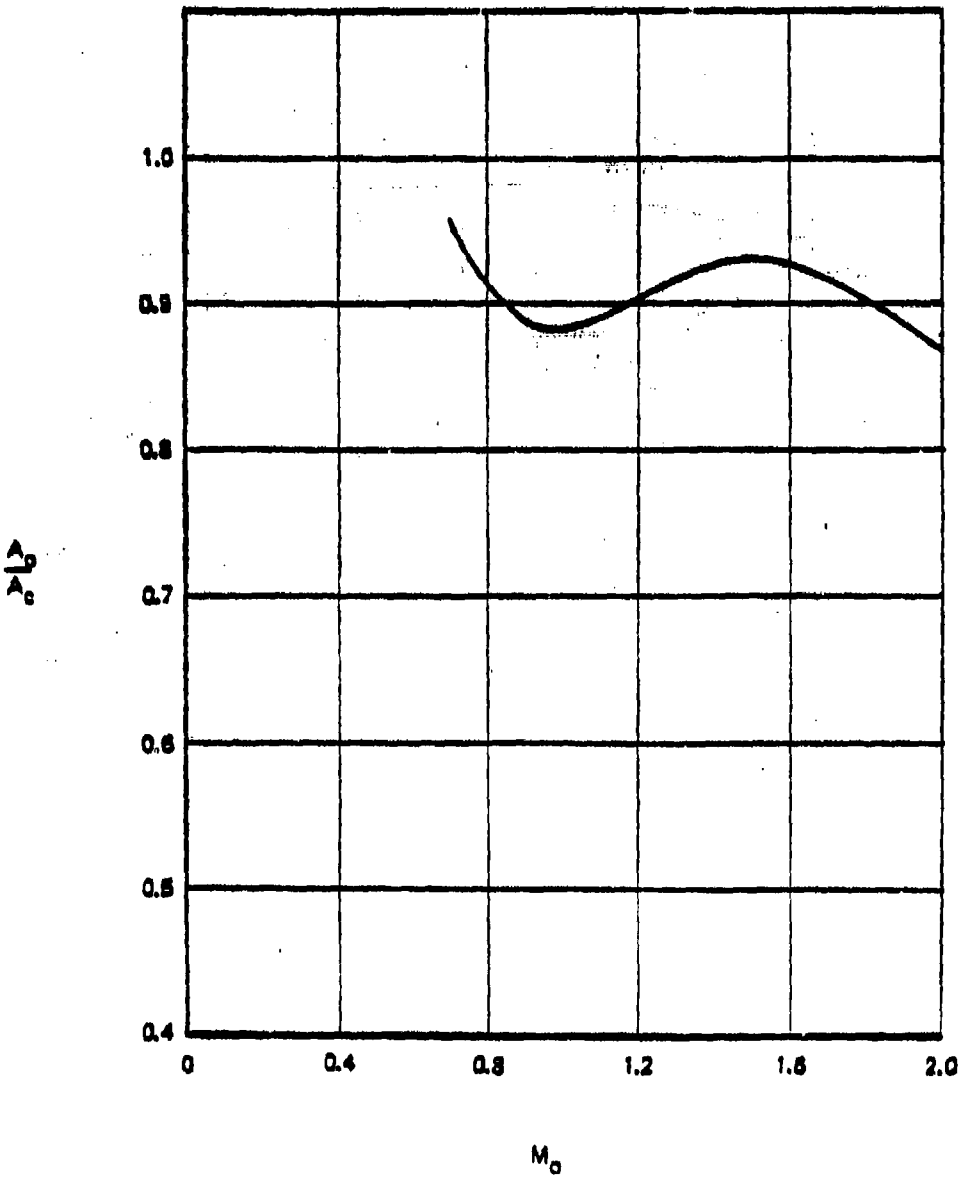

Figure 13. Performance Characteristics for Inlet Configuration #5 (continued)

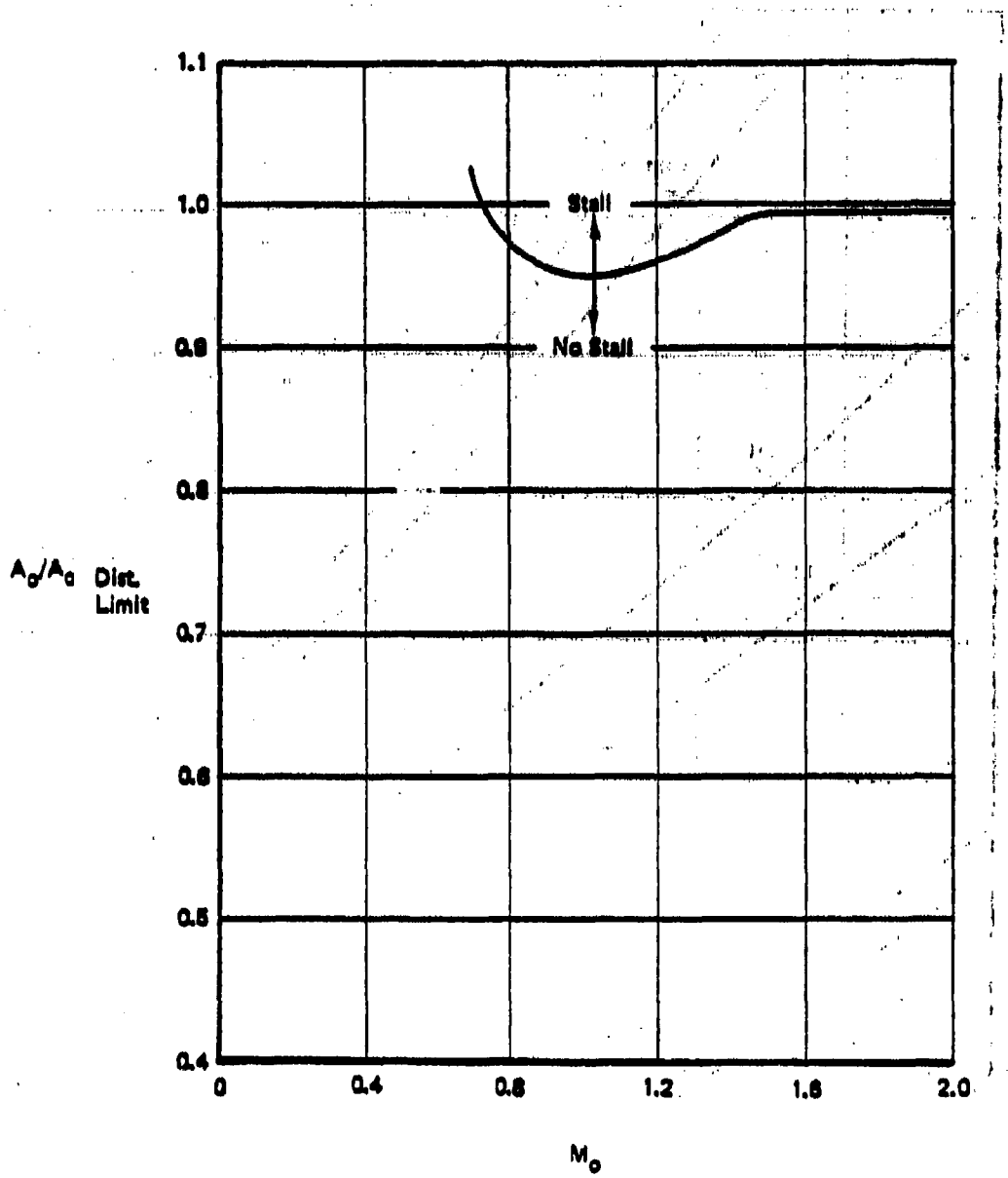

Figure 13. Performance Characteristics for Inlet Configuration #5 (continued)

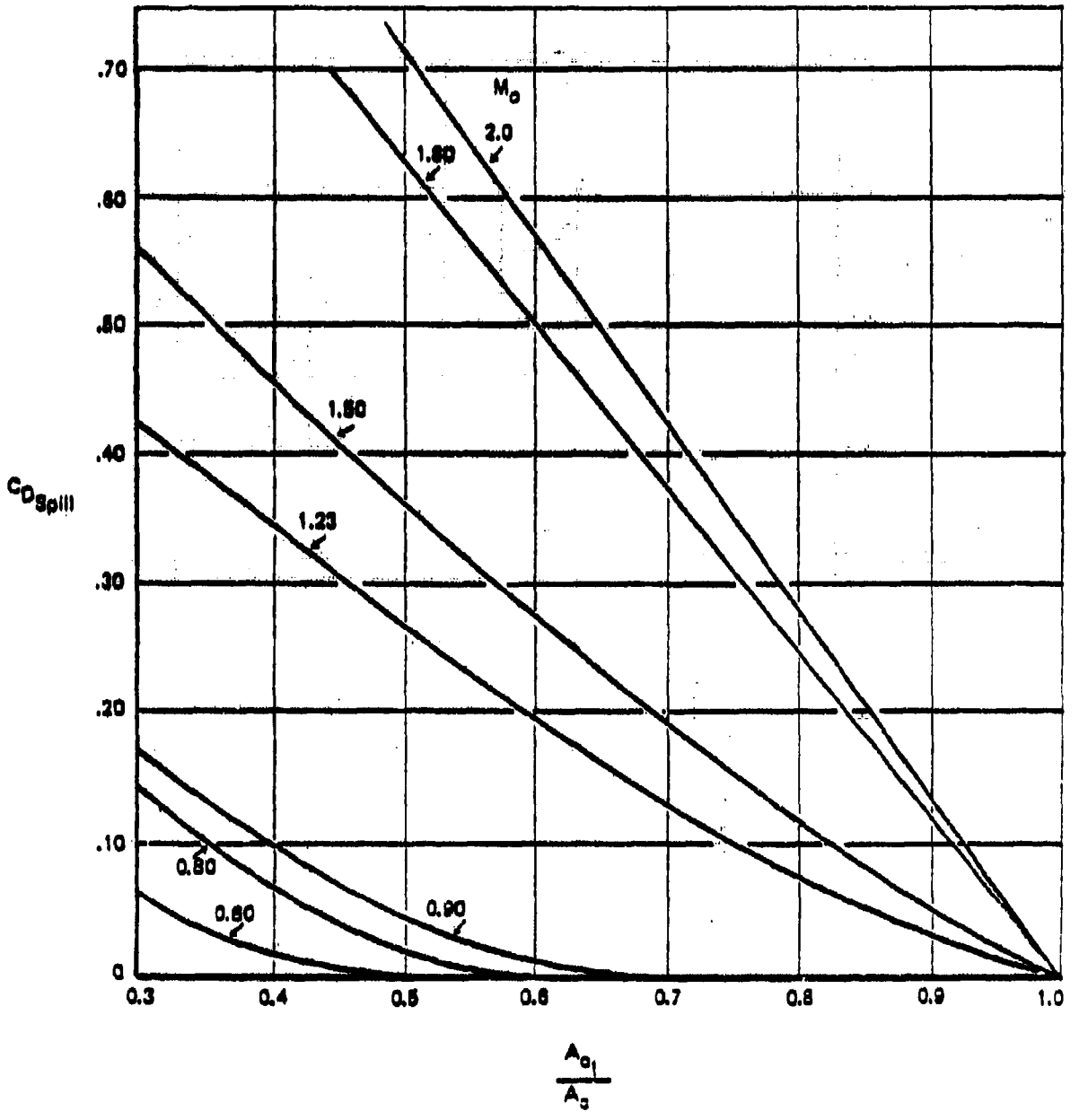

Figure 13. Performance Characteristics for Inlet Configuration #5 (concluded)

2.1.6 Inlet Configuration #6 - Supersonic, Normal Shock Inlet

This inlet has no boundary layer bleed or bypass system. Cowl lips are sharp, for reduced drag at higher supersonic Mach numbers.

The inlet performance characteristics are based on the test data from Reference 4 up to Mach 1.5. Above Mach 1.5 inlet performance is calculated from normal shock total pressure losses and subsonic diffuser losses for a duct loss coefficient, $\zeta = .12$. Unpublished test data were also available for a normal shock inlet up to Mach 2.0 from Boeing Lightweight Fighter inlet development tests. These data were used to substantiate the recovery predictions. The inlet geometry is shown in Figure 14, and the inlet performance characteristics are presented in Figure 15.

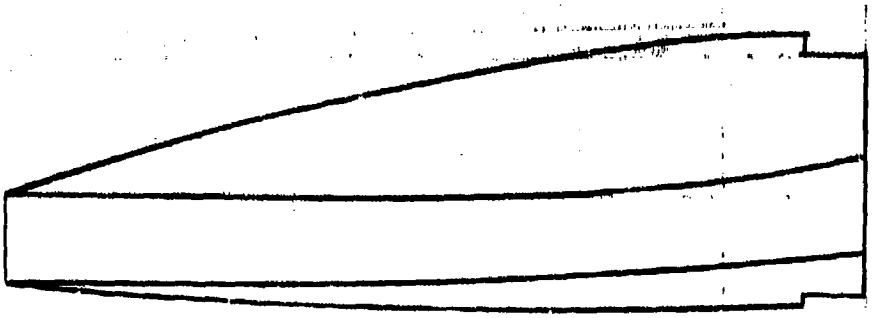

Figure 14. Supersonic Normal Shock Inlet (Second Version)

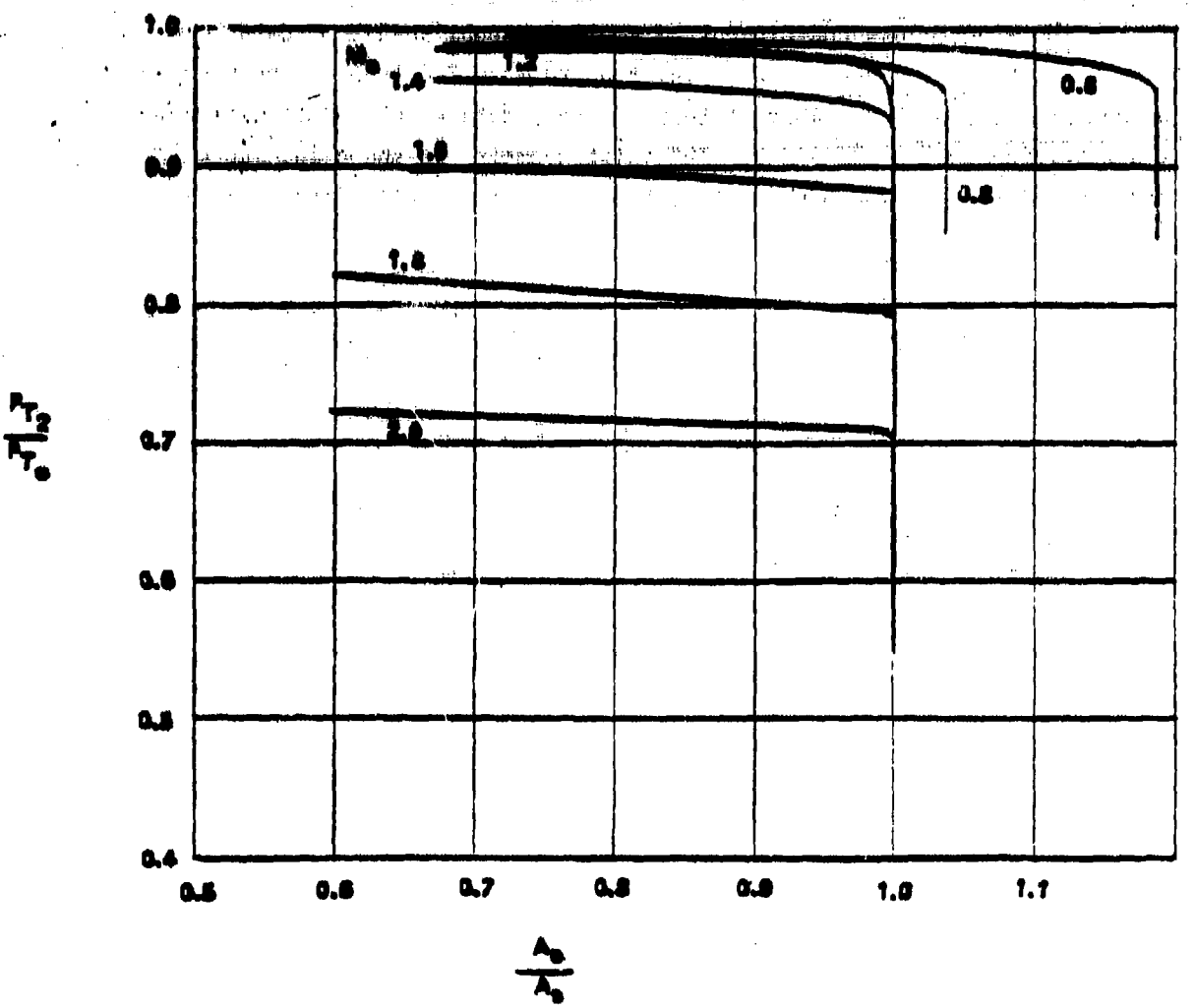

Figure 15. Performance Characteristics for Inlet Configuration #6

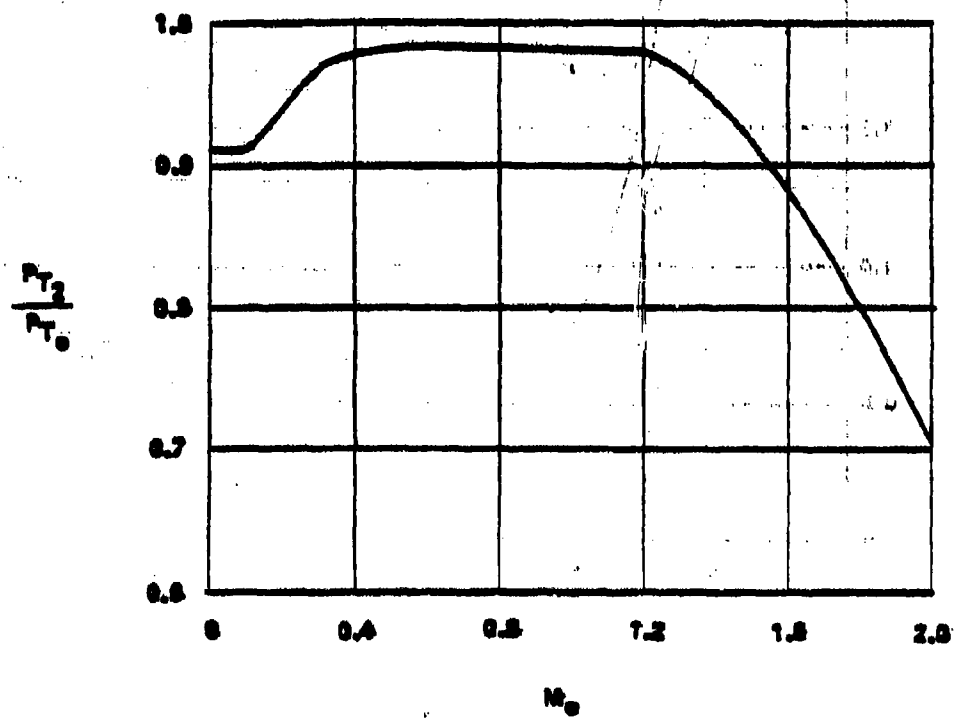

Figure 15. Performance Characteristics for Inlet Configuration 46 (continued)

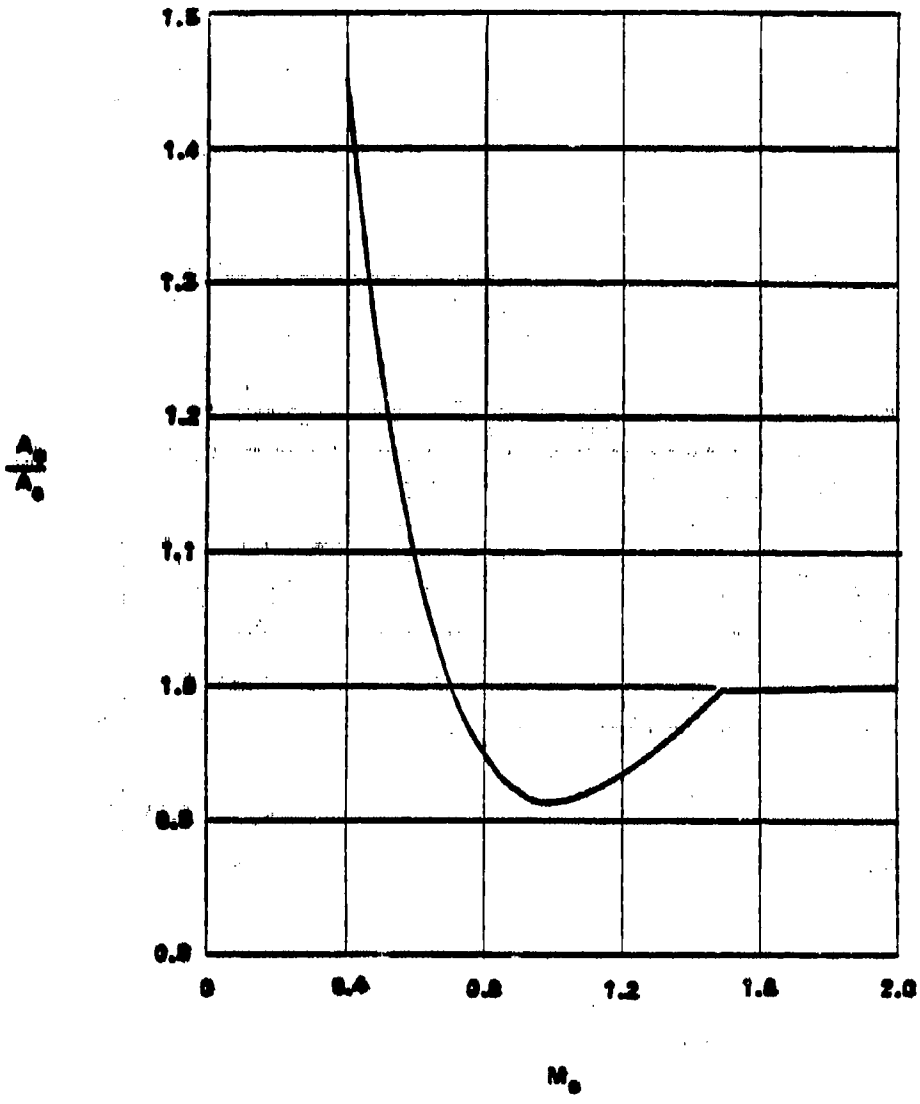

Figure 15. Performance Characteristics for Inlet Configuration #6 (continued)

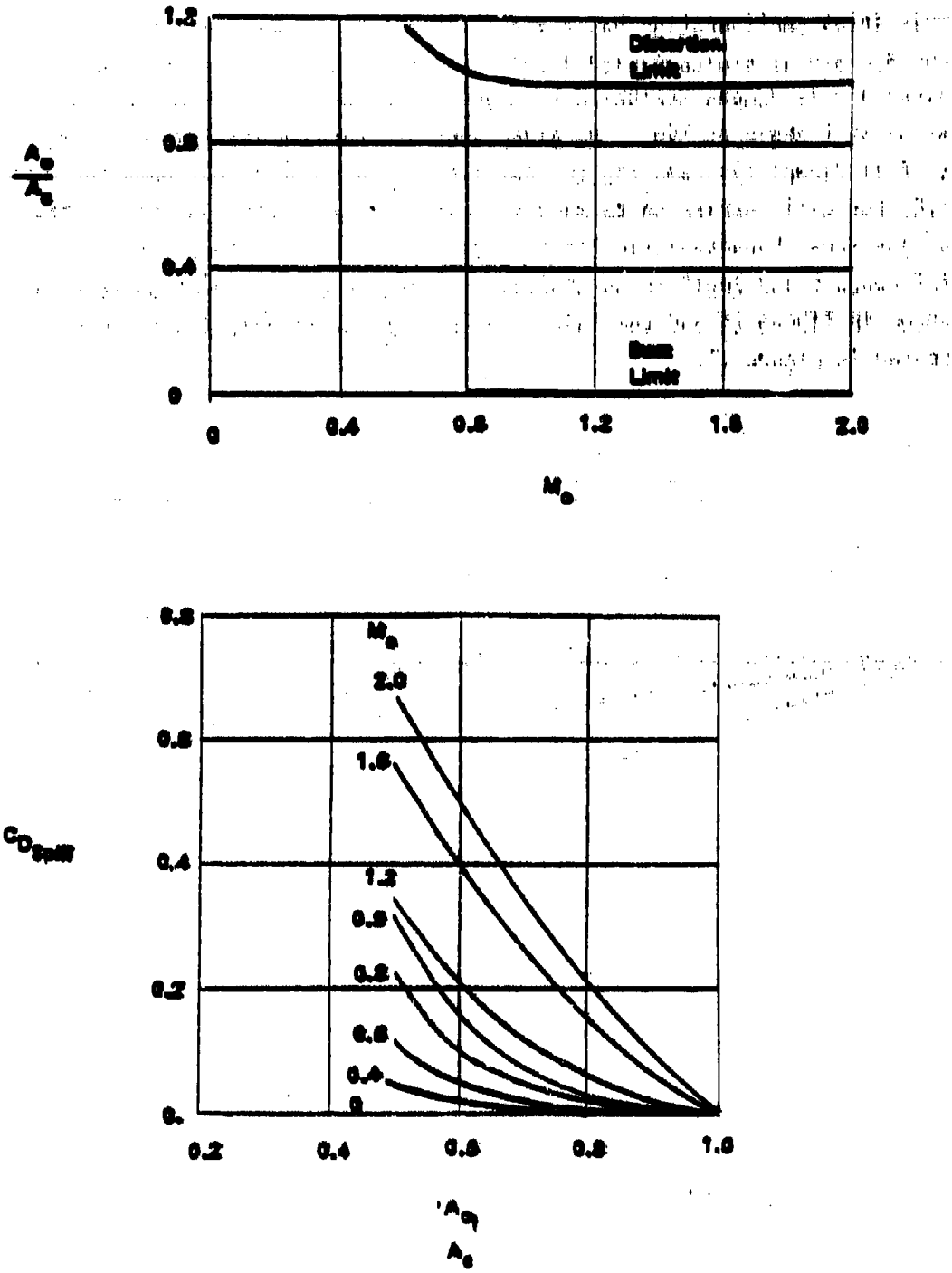

Figure 15. Performance Characteristics for Inlet Configuration #6 (concluded)

2.1.7 Inlet Configuration #7 - Fixed Geometry, Two-Shock Inlet

This inlet configuration has a single 7° external ramp compression surface and is equipped with a throat slot for boundary layer bleed. Bleed air is dumped overboard through a fixed geometry convergent nozzle at an exit angle of 15°. The sideplates are cutback 75% (as compared to full sideplates-ramp tip to cowl lip). The inlet is designed for Mach 1.6, but will operate up to Mach 2.0 without ramp shock ingestion. The performance characteristics of this inlet are based on test data from Reference 5 and engineering analysis. A sketch of the inlet geometry is shown in Figure 16 and the inlet performance characteristics are presented in Figure 17.

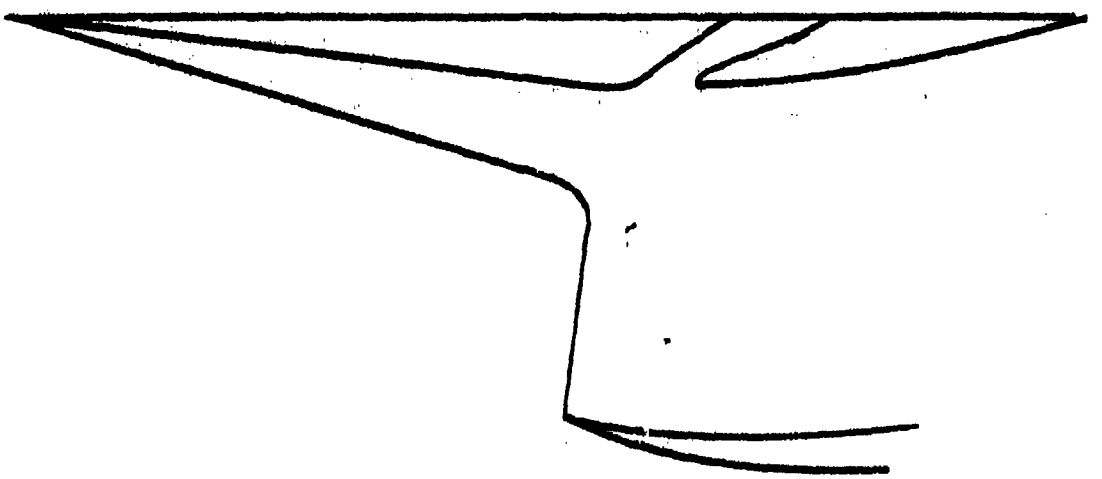

Figure 16. Fixed-Geometry Two-Shock Inlet Design for Mach 1.60

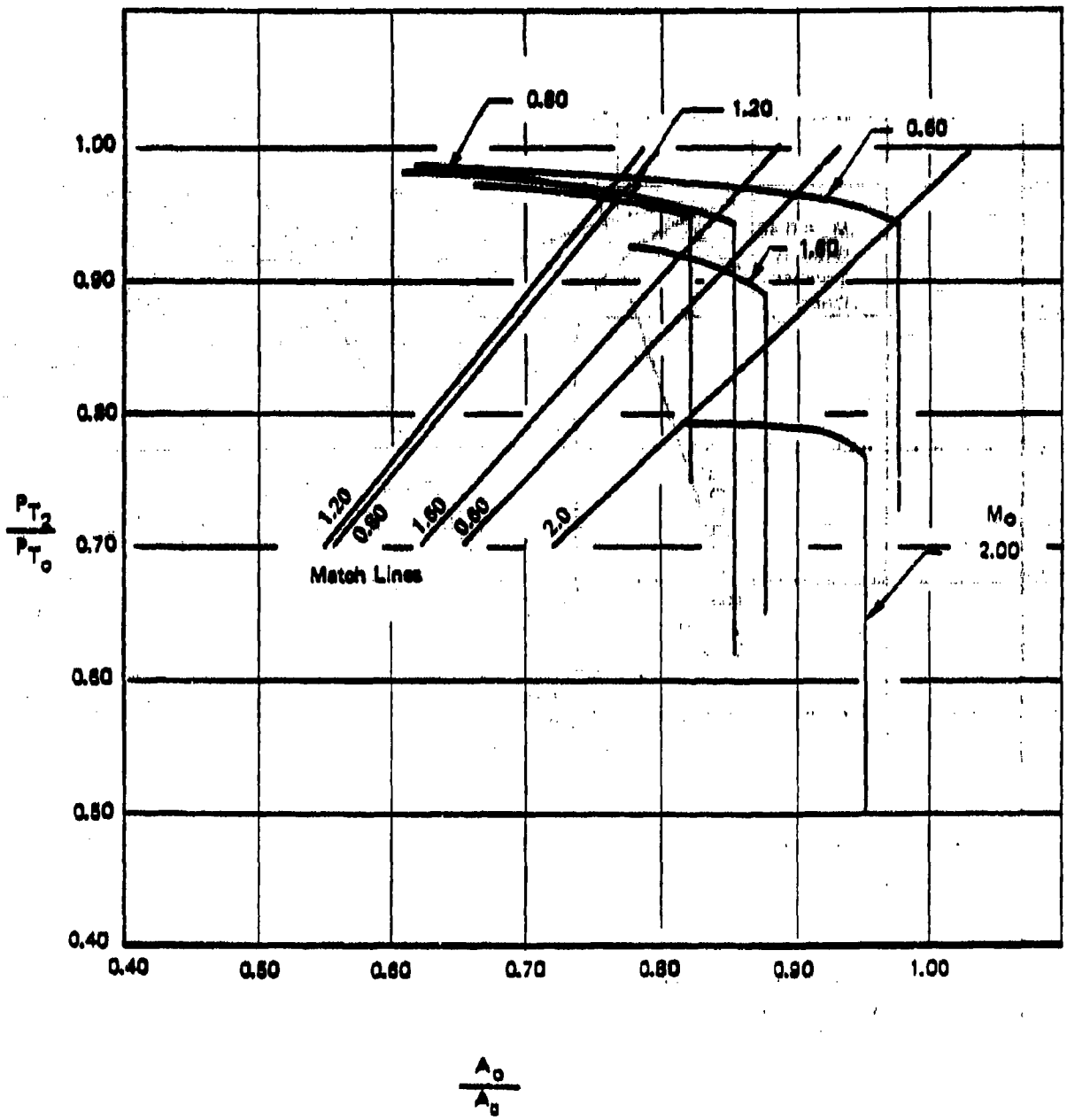

Figure 17. Performance Characteristics for Inlet Configuration #7

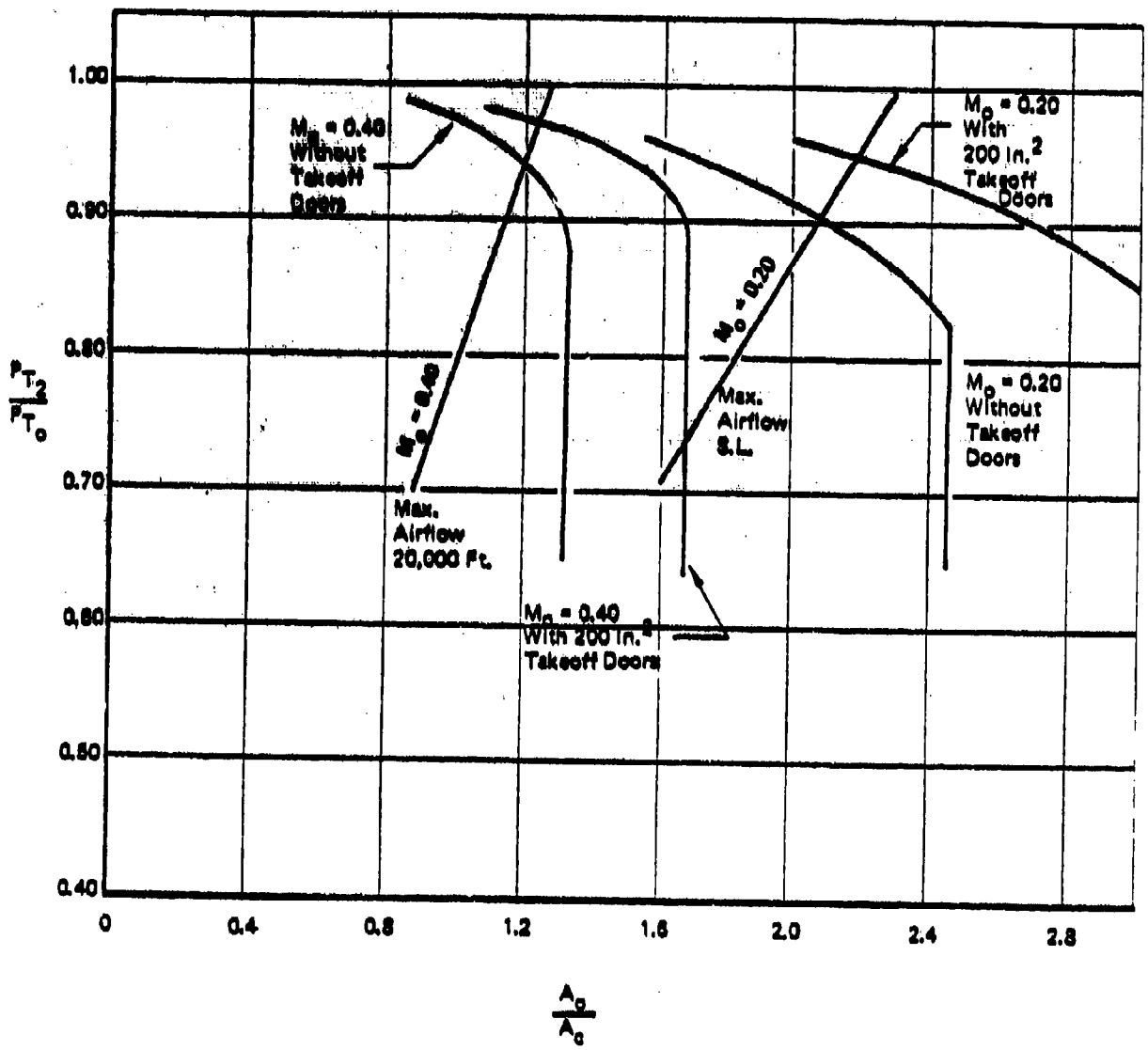

Figure 17. Performance Characteristics for Inlet Configuration #7 (continued)

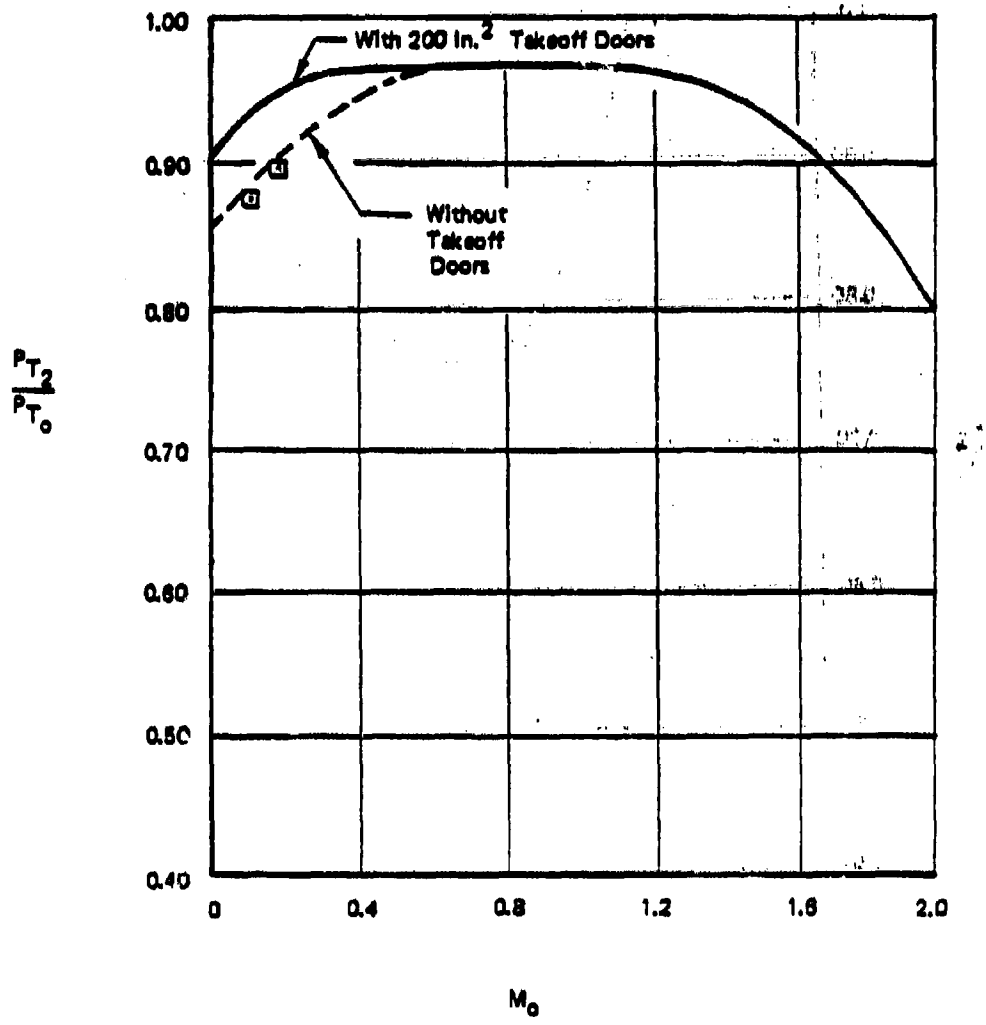

Figure 17. Performance Characteristics for Inlet Configuration #7 (continued)

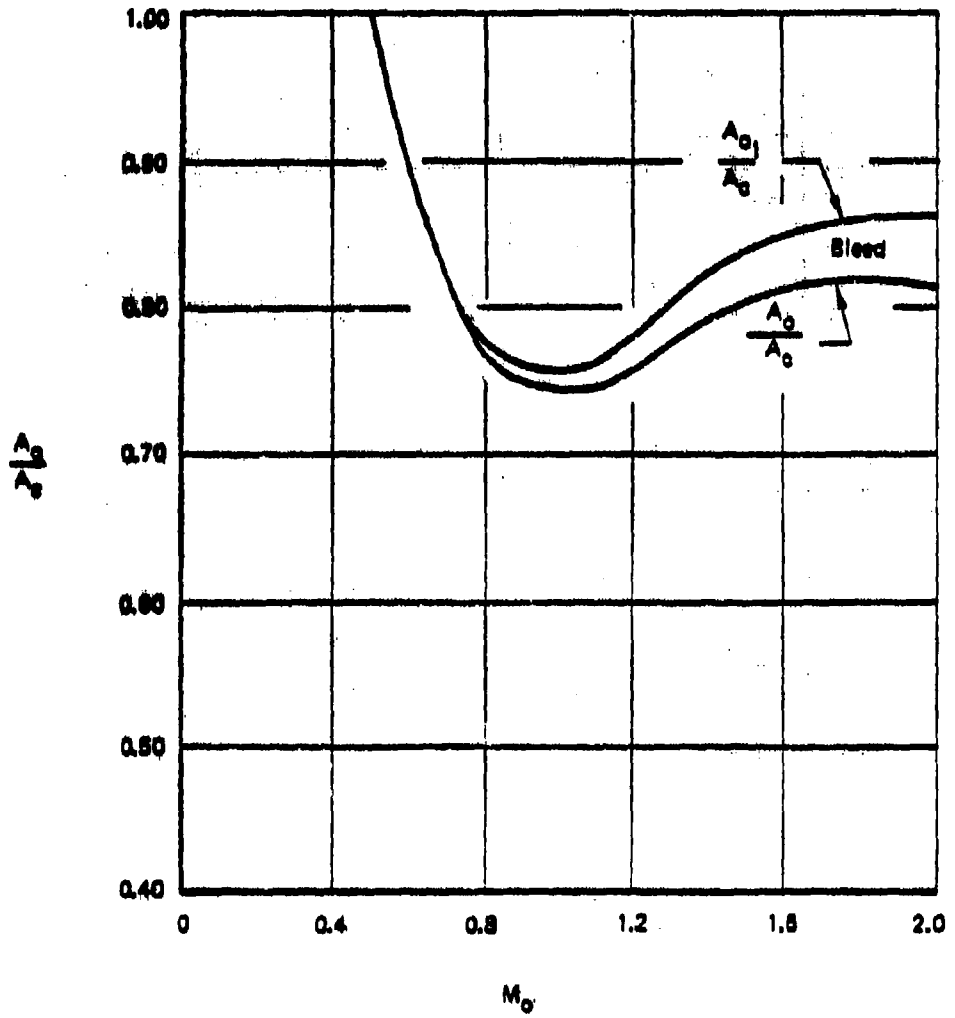

Figure 17. Performance Characteristics for Inlet Configuration #7 (continued)

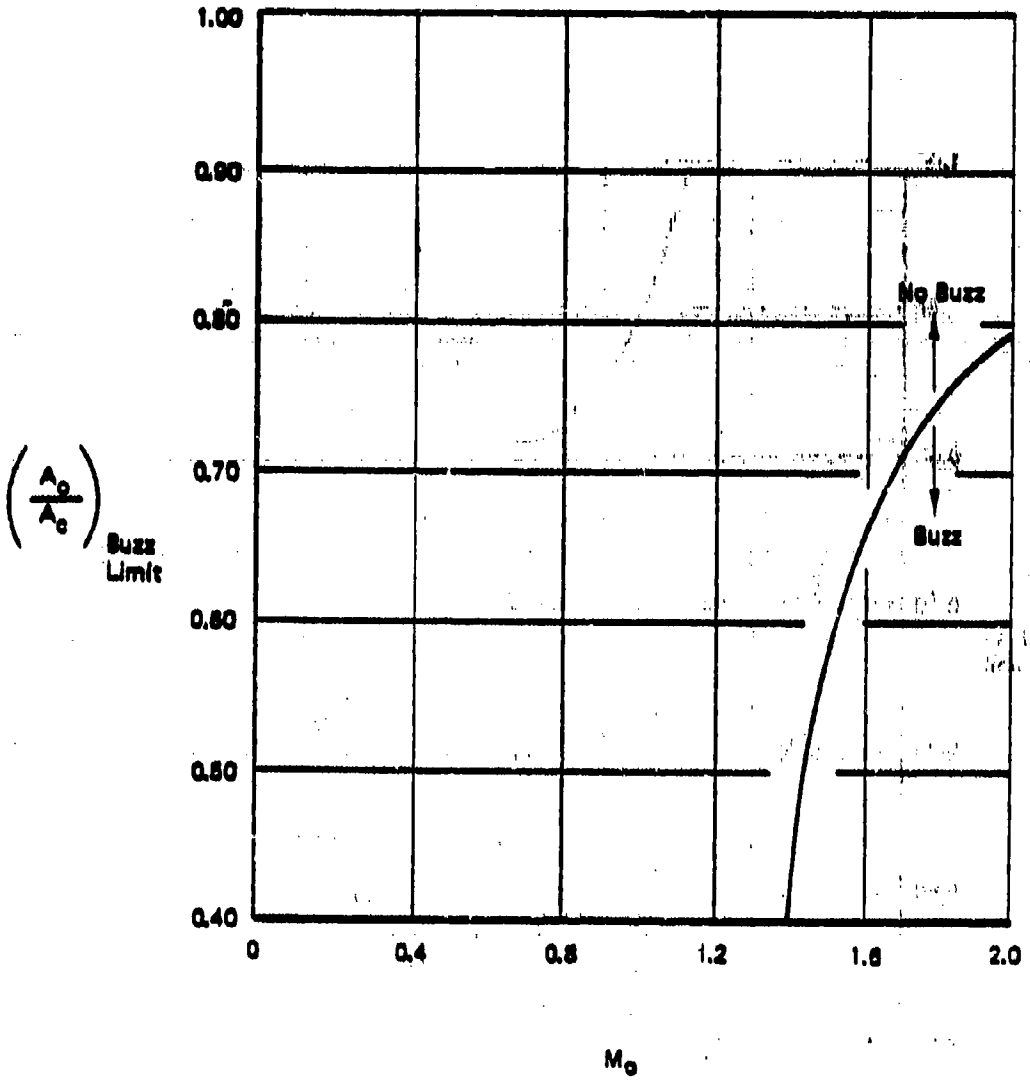

Figure I7. Performance Characteristics for Inlet Configuration #7 (continued)

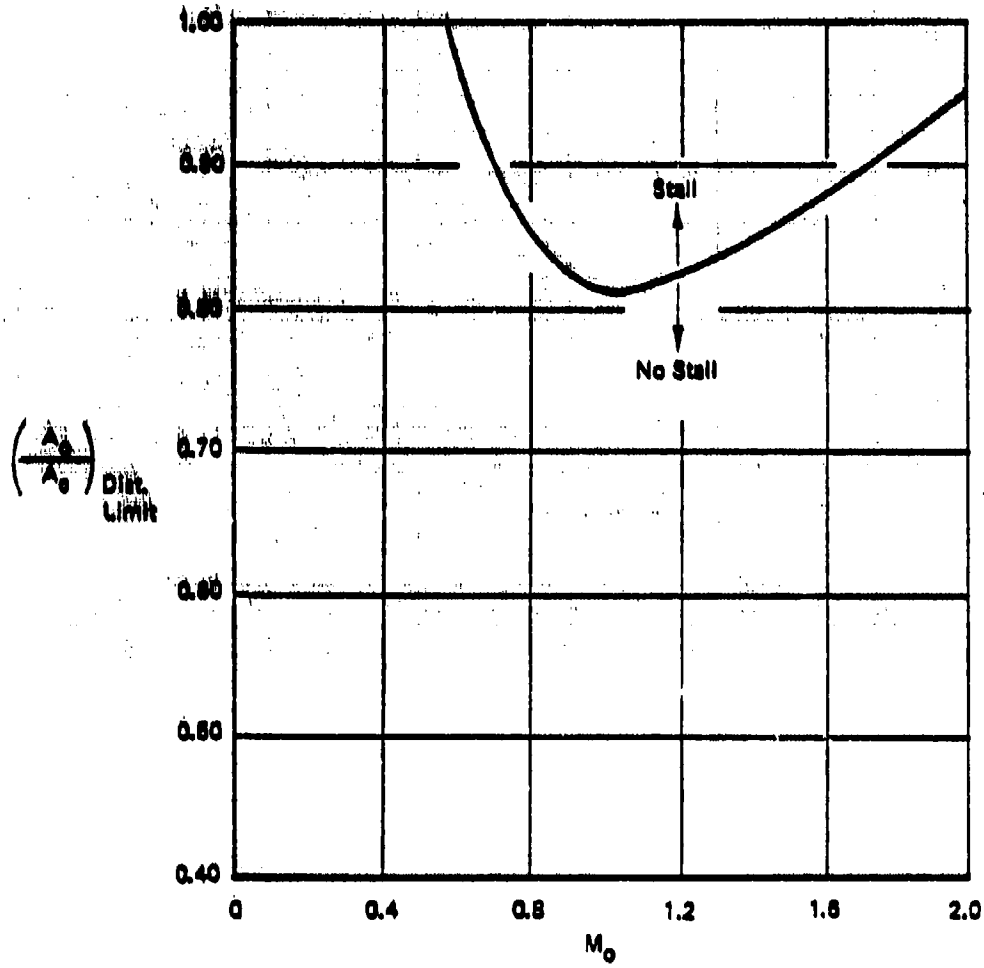

Figure 17. Performance Characteristics for Inlet Configuration #7 (continued)

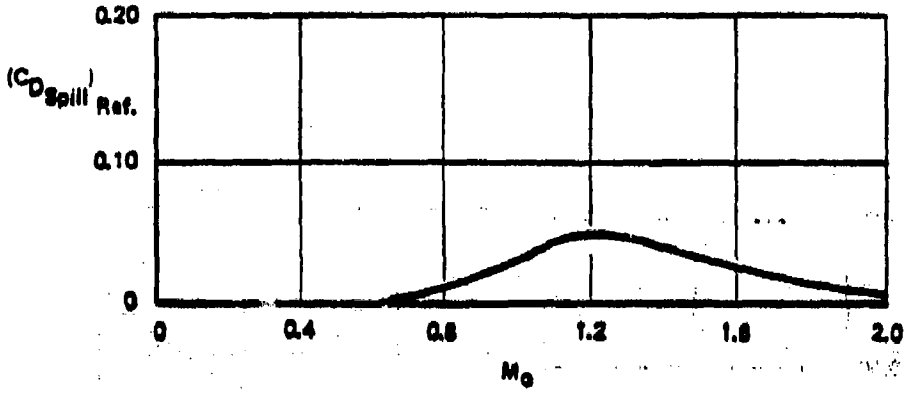

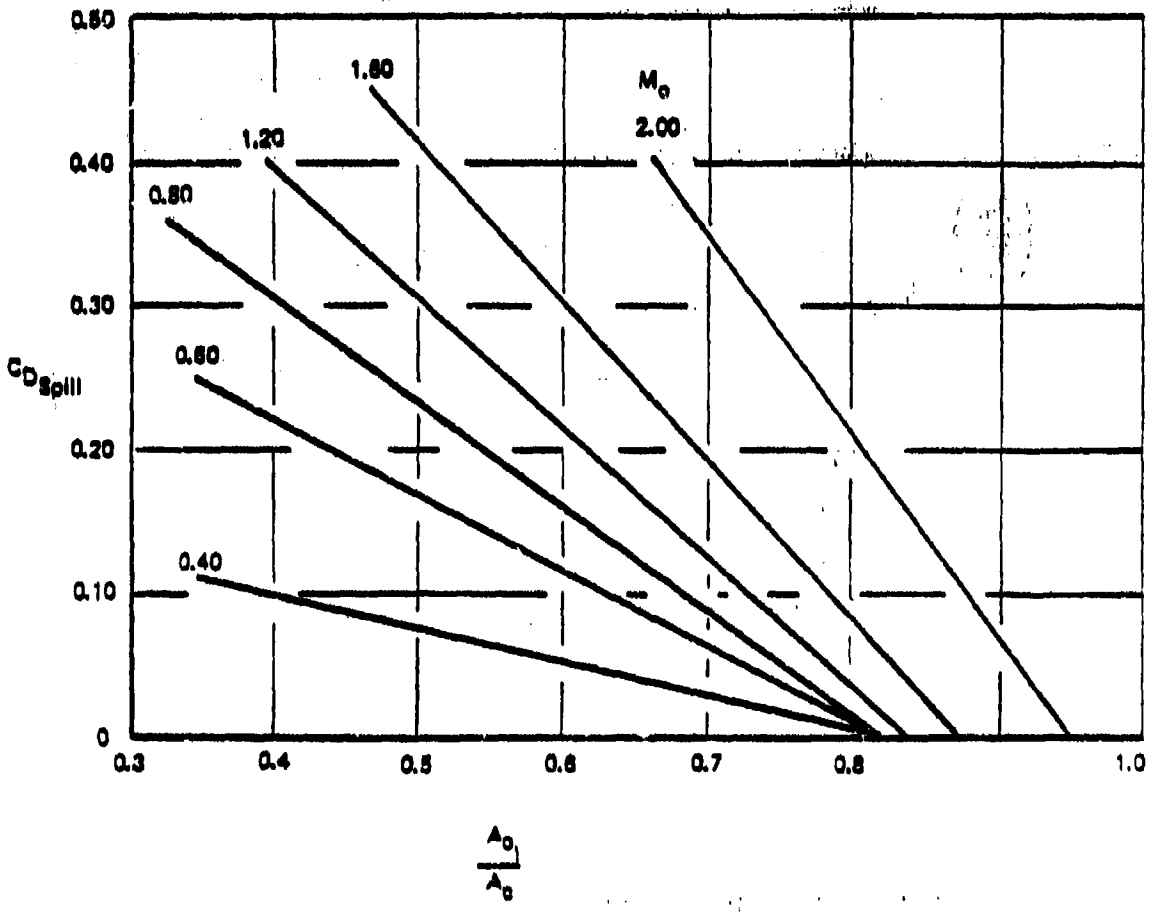

Figure 17. Performance Characteristics for Inlet Configuration #7 (continued)

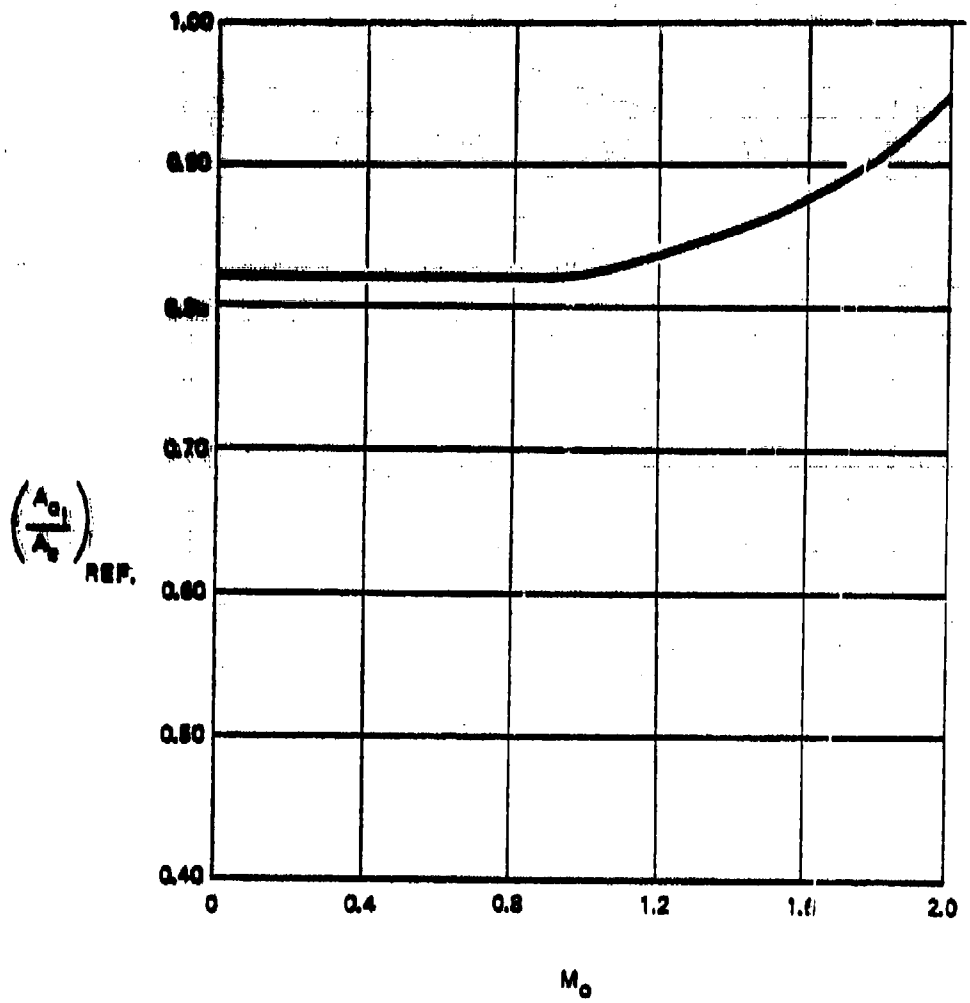

Figure 17. Performance Characteristics for Inlet Configuration #7 (continued)

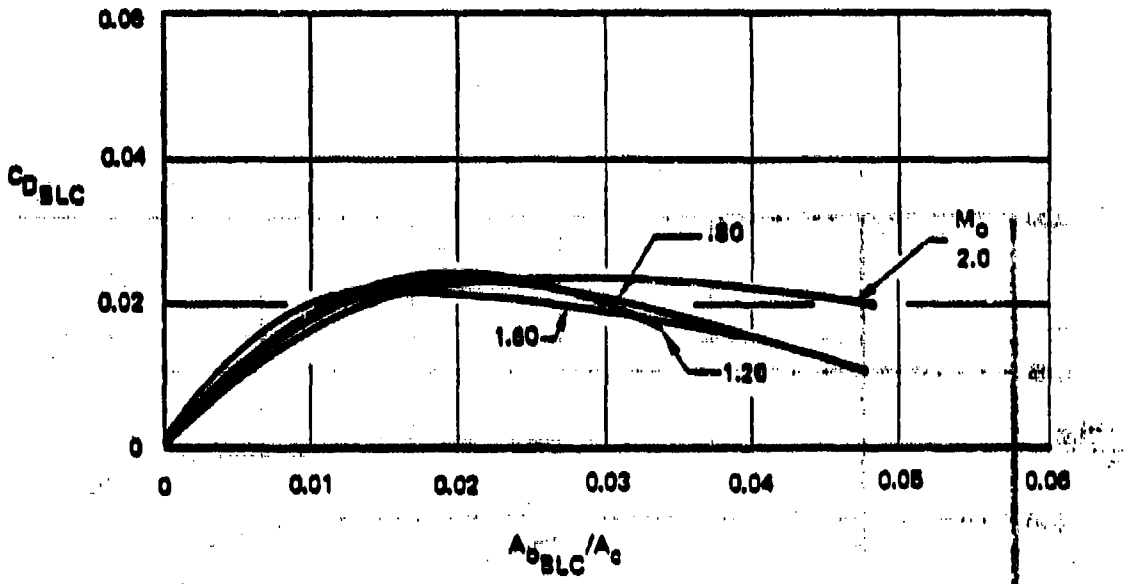

Figure 103: BOUNDARY LAYER BLEED DRAG

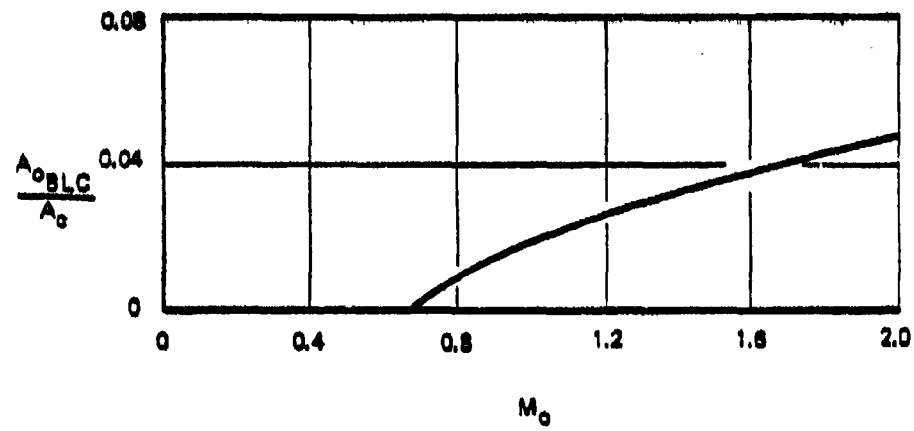

Figure 17. Performance Characteristics for Inlet Configuration #2 (continued)

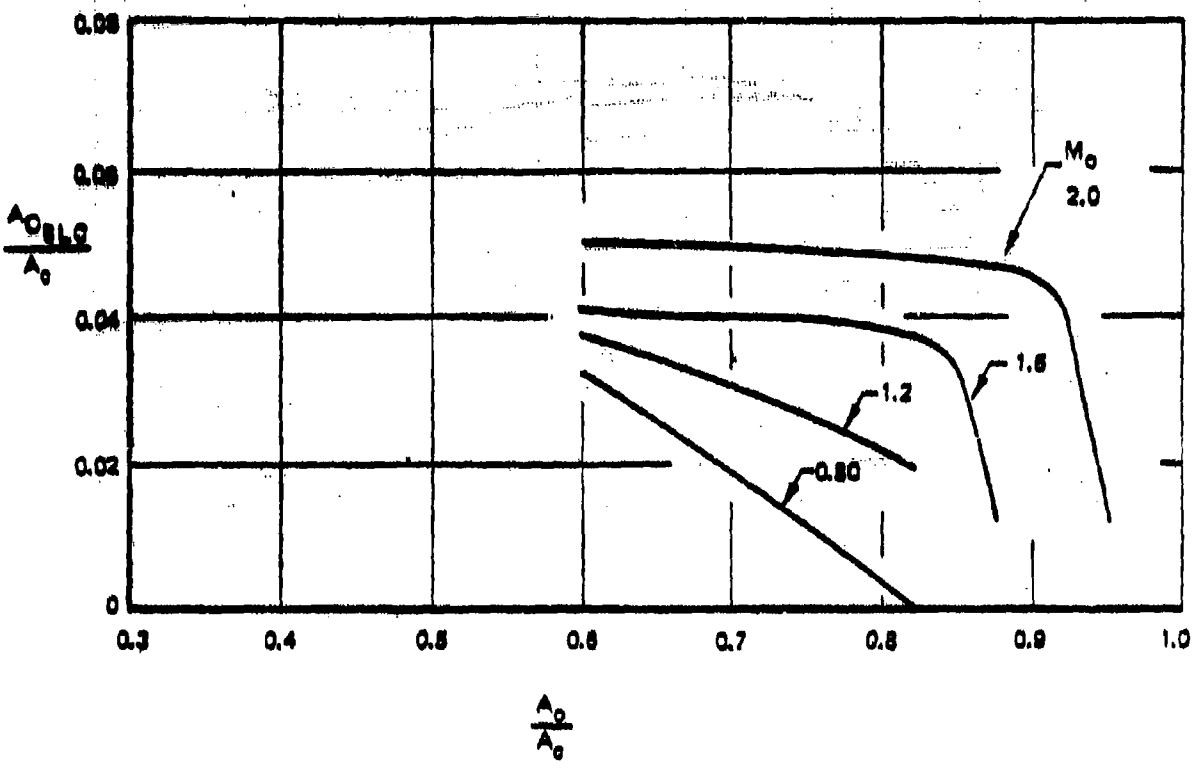

Figure 17. Performance Characteristics for Inlet Configuration #7 (concluded)

2.1.8 Inlet Configuration #8 - Variable Ramp, Four-Shock, Two-Dimensional, External Compression Inlet

This inlet has two movable external ramps, a 7.3^{0} initial ramp angle, a boundary layer control bleed system consisting of perous bleed on the second and third ramp surfaces, sideplates, and a throat bleed slot located aft of the normal shock. The throat slot also acts as a bypass to remove excess inlet airflow for matching engine airflow demand with inlet supply.

The inlet performance characteristics were build up from engineering analyses and available data from similar configurations and components. The inlet geometry is shown in Figure 18 and the inlet performance characteristics are presented in Figure 19.

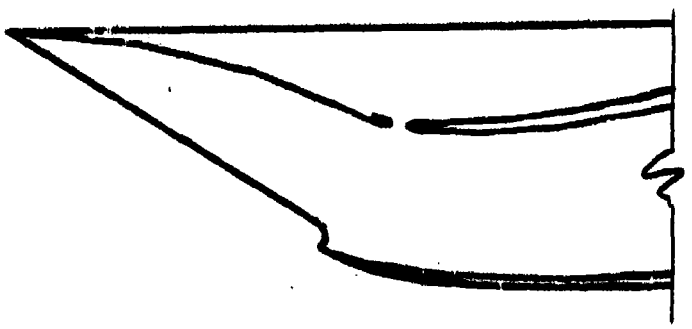

Figure 18. Mach 2.0 Four-Shock Variable-Geometry Inlet

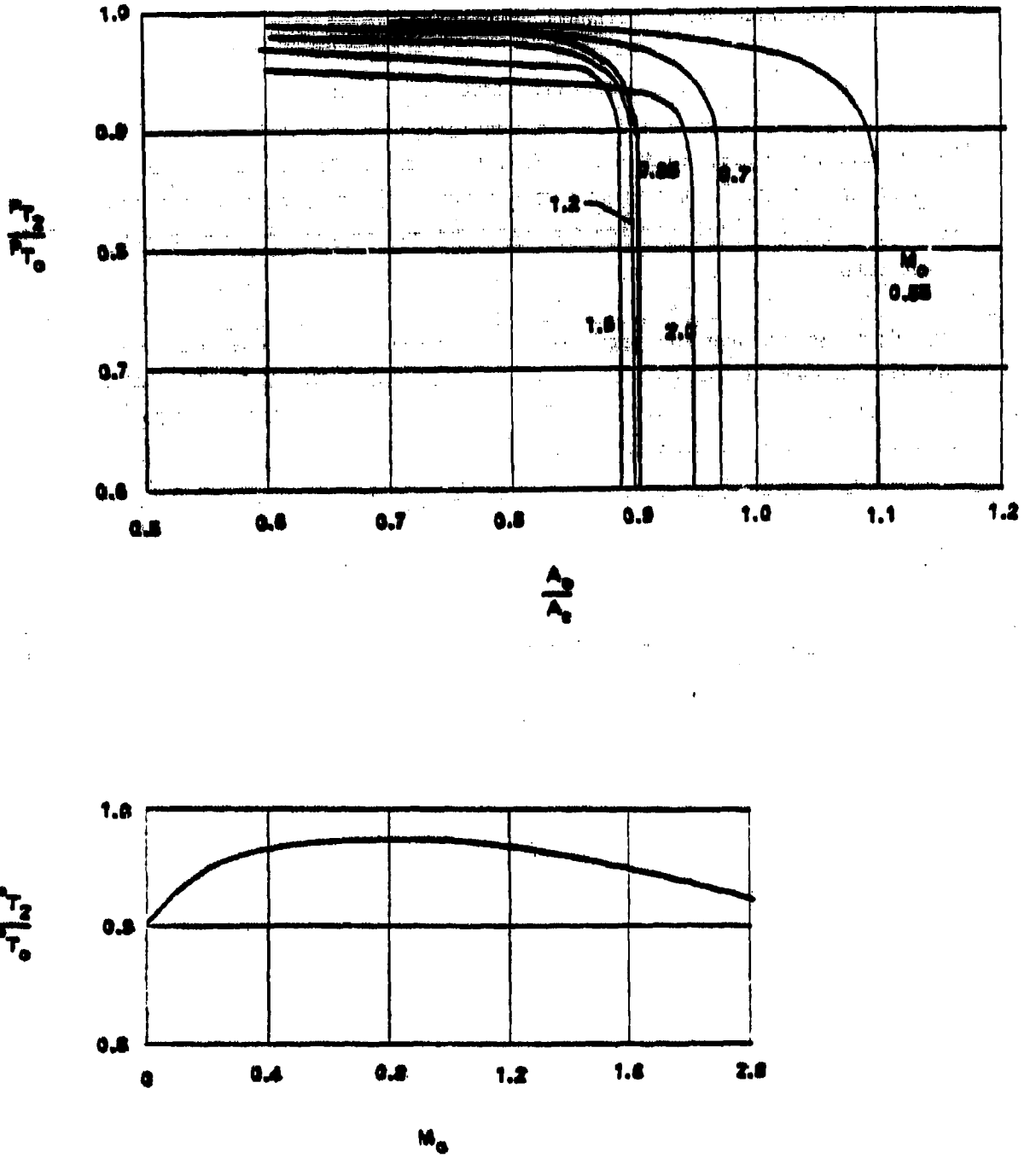

Figure 19. Performance Characteristics for Inlet Configuration #8

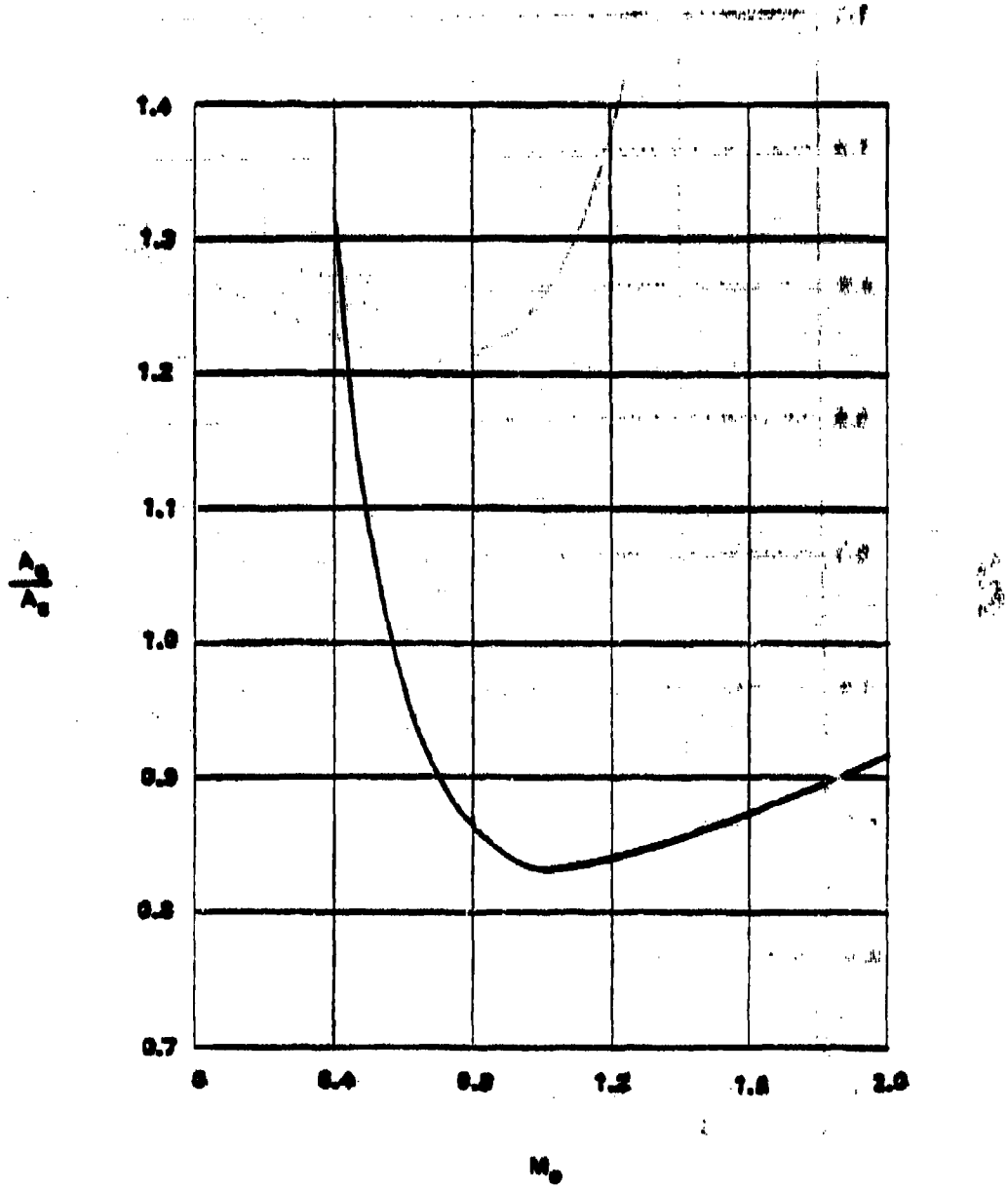

Figure 19. Performance Characteristics for Inlet Configuration #8 (continued)

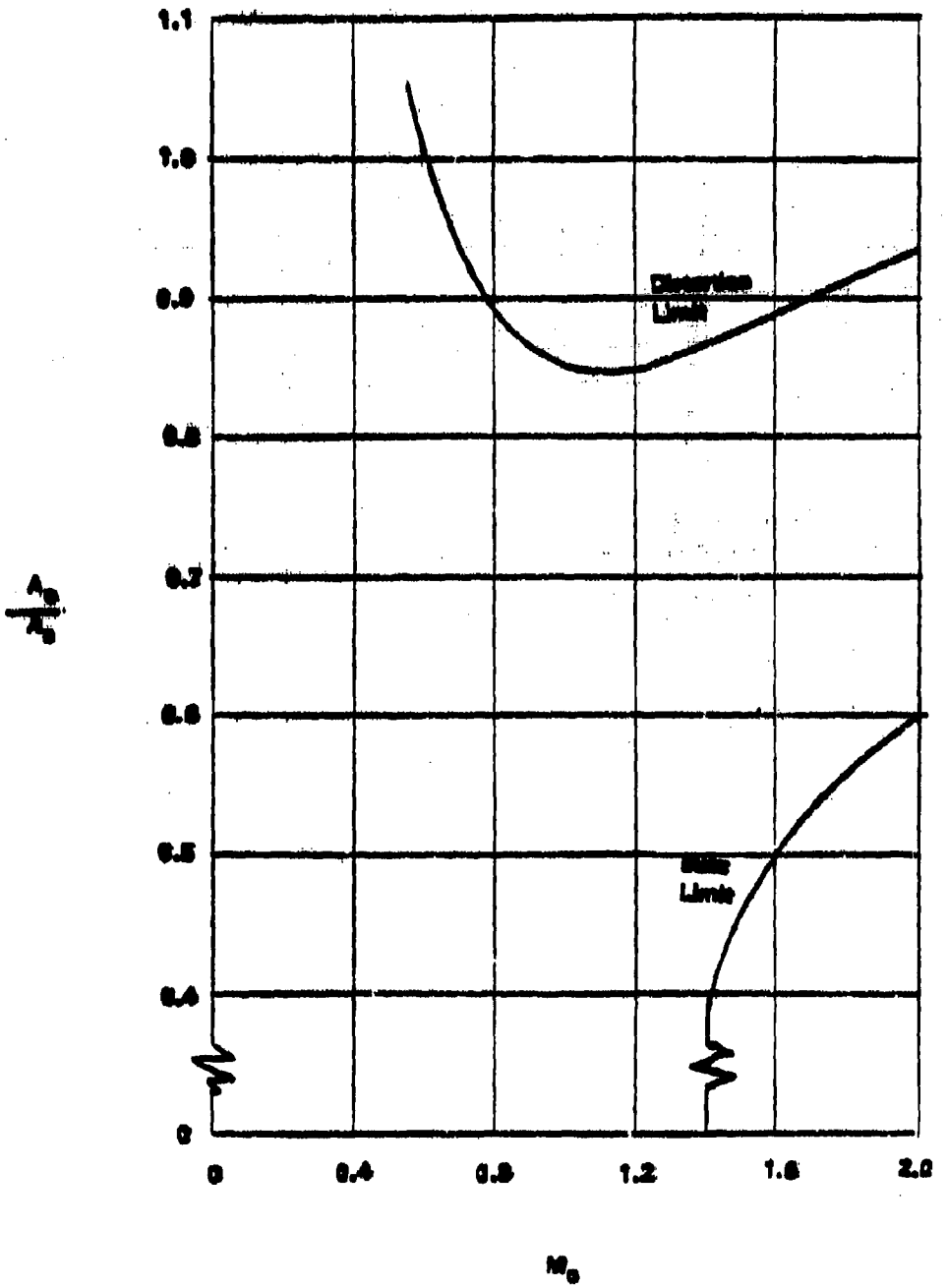

Figure 19. Performance Characteristics for Inlet Configuration #8 (continued)

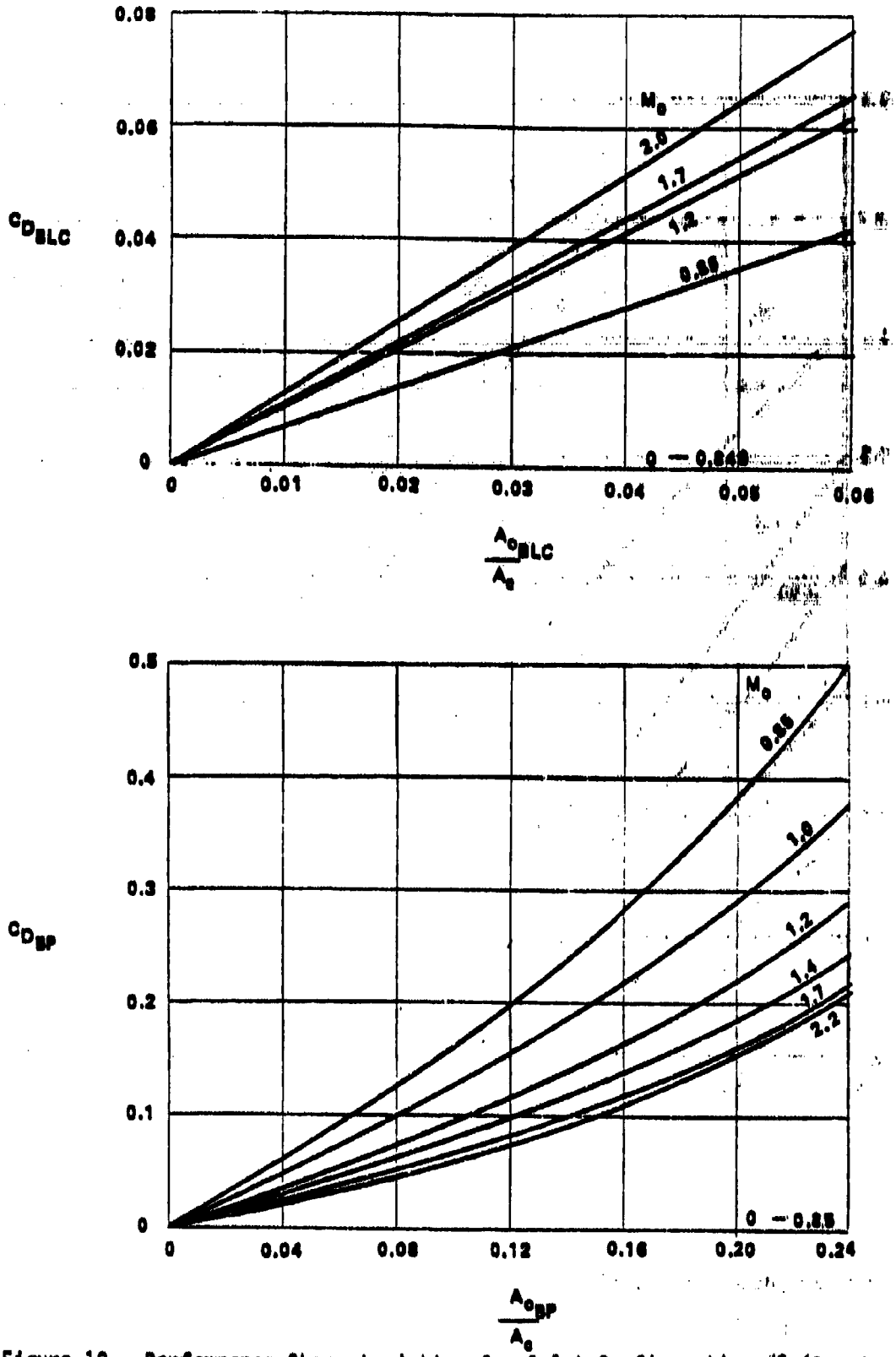

Figure 19. Performance Characteristics for Inlet Configuration #8 (Continued)

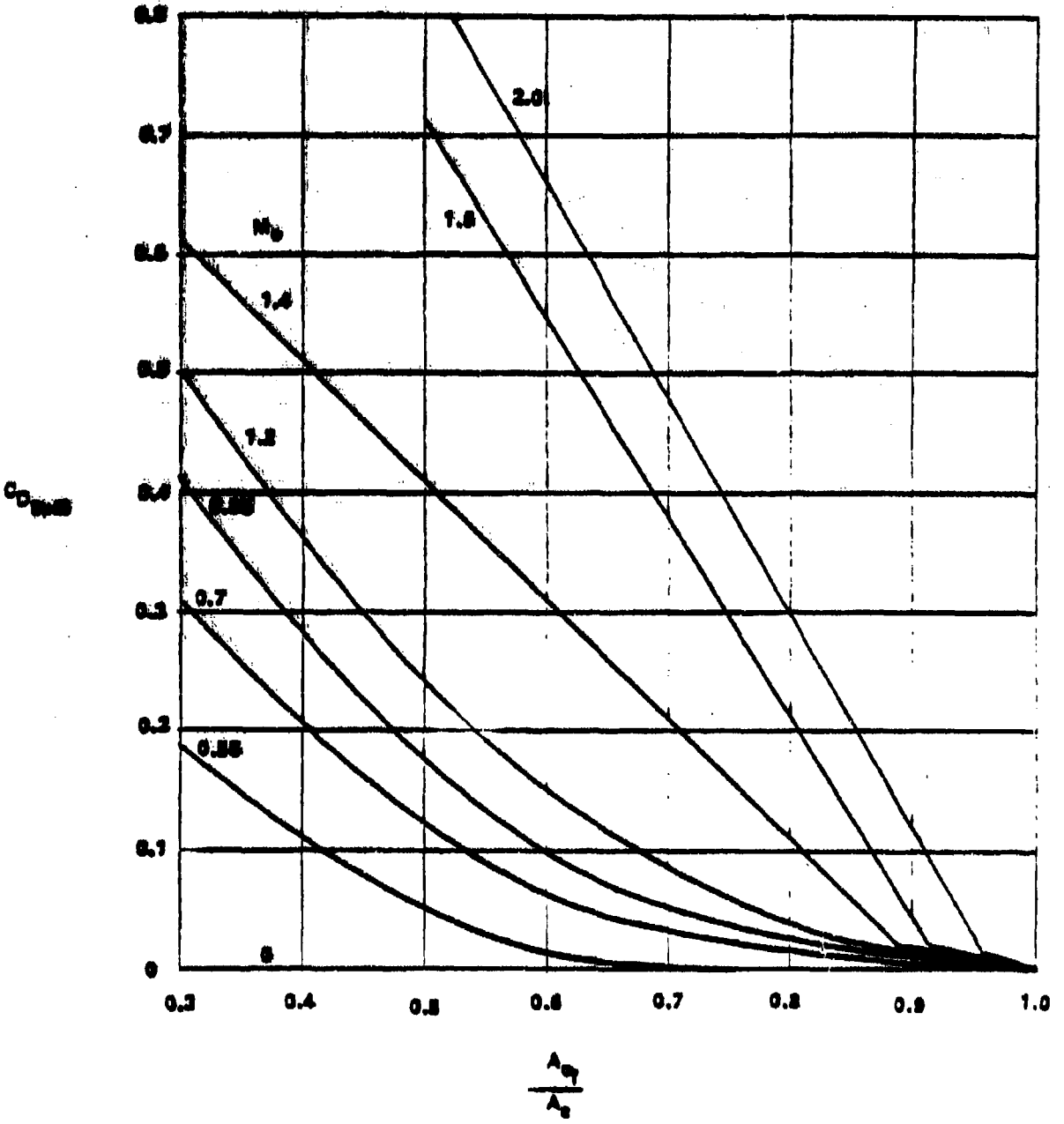

Figure 19. Performance Characteristics for Inlet Configuration 48 (continued)

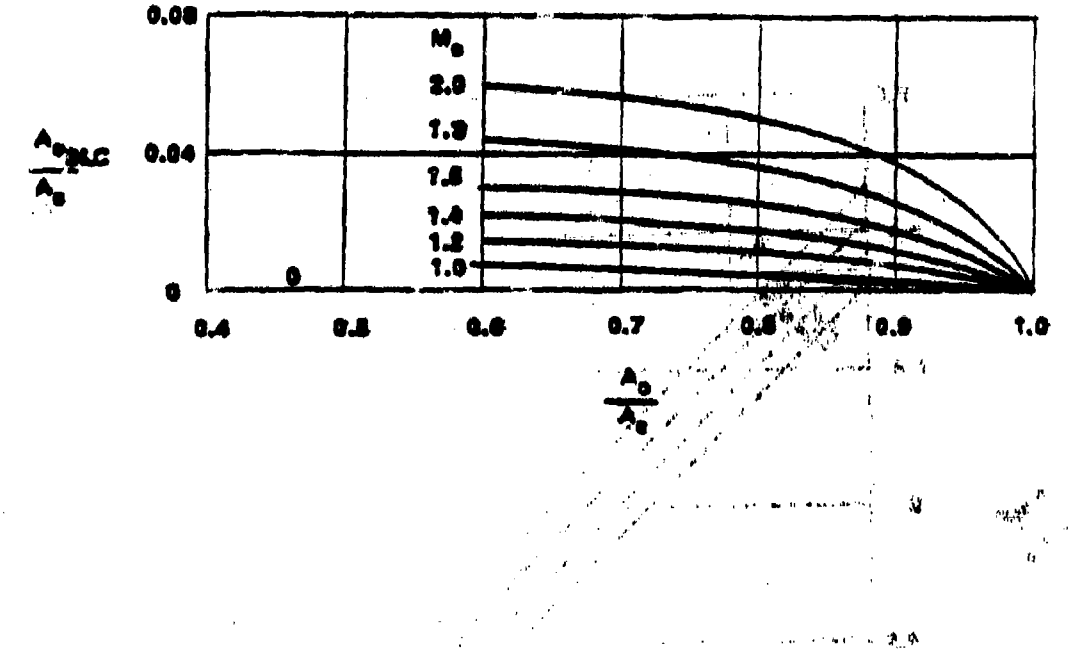

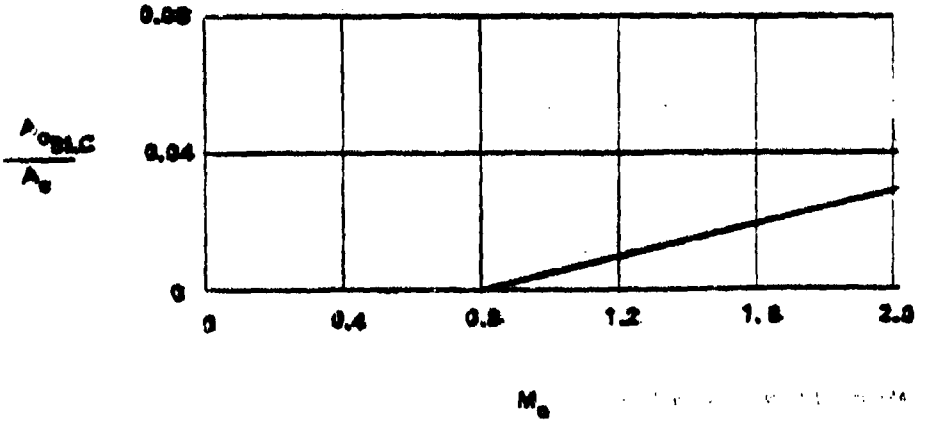

Figure 19. Performance Characteristics for Inlet Configuration #8 (continued)

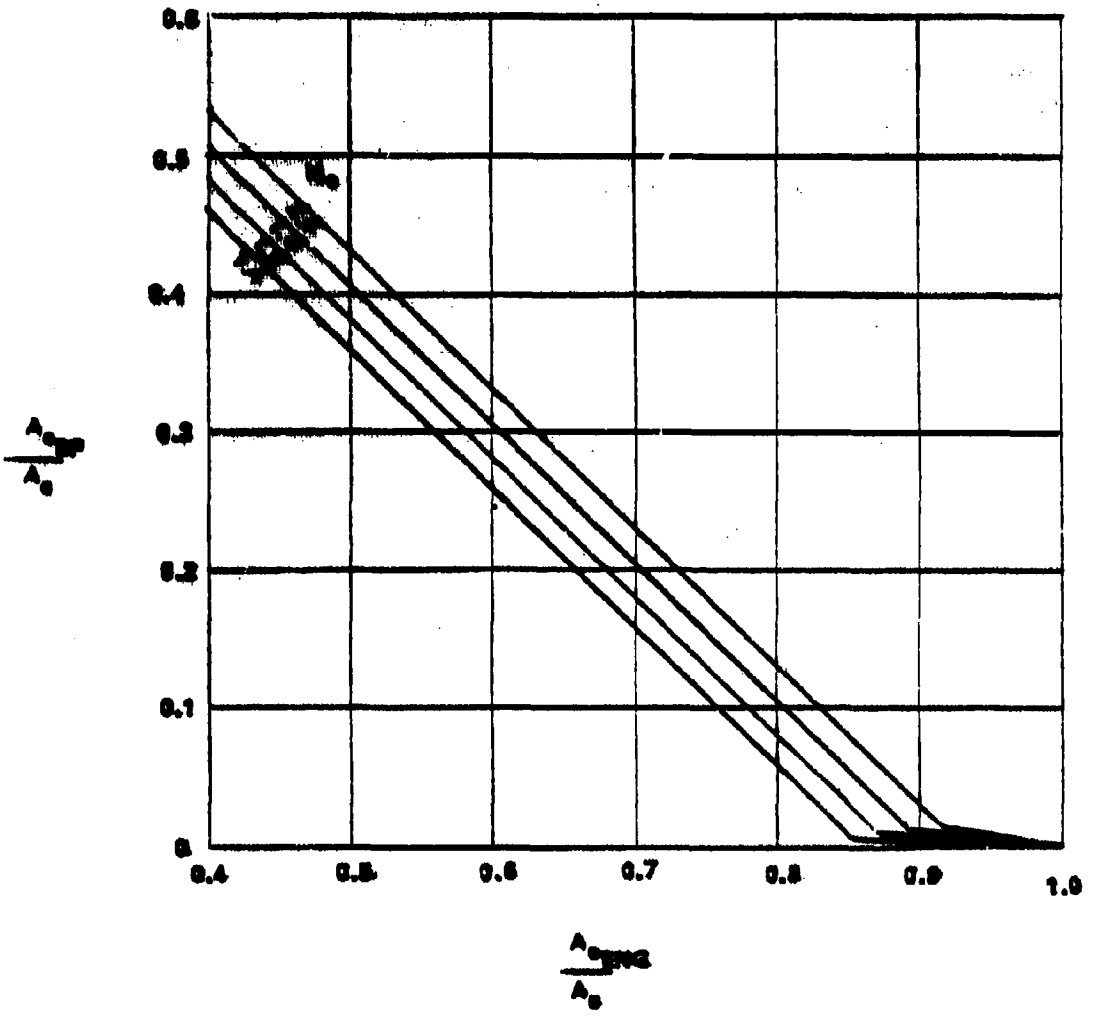

Figure 19. Performance Characteristics for Inlet Configuration #8 (concluded)

2.1.9 Inlet Configuration #9 - Four-Shock, Variable-Geometry, External Compression, Two-Dimensional Inlet

This inlet is designed to have shock-on-lip at Mach 2.5. The inlet is an external compression, horizontal ramp design. It has internal boundary layer bleed through a porous third ramp panel and a throat panel. The bleed from each of these panels is collected in separate, divided plenum compartments and then is exited overboard through convergent nozzles provided by exit louvers. The bleed flow is exited at an angle of 20 degrees relative to the fuselage reference line. The inlet is oriented down at an angle of 2 degrees relative to the F.R.P. so that the initial fixed ramp angle of 4 degrees (relative to the F.R.P.) will provide 6 degrees of compression at the +2 degrees angle of attack flight attitude.

The first two ramps are fixed, but the third ramp and throat panel are movable. This provides capability to vary shock geometry and throat area. The maximum throat area corresponds to $A_{throat}/A_c = .70$. This is obtainable by collapsing the third ramp to the 6-degree position.

A bypass system is provided forward of the engine entrance to dump excess inlet air overboard. The bypass doors are convergent-divergent nozzles provided by movable doors. The bypass air is collected through porous material into a plenum chamber surrounding the duct, then is exited through the doors.

To achieve high performance at takeoff (M = .20), either the maximum throat area would have to be increased or takeoff doors may be added.

This inlet configuration is based on the model configuration and data of Reference 6. The inlet configuration in shown in Figure 20, and the inlet performance characteristics are presented in Figure 21.

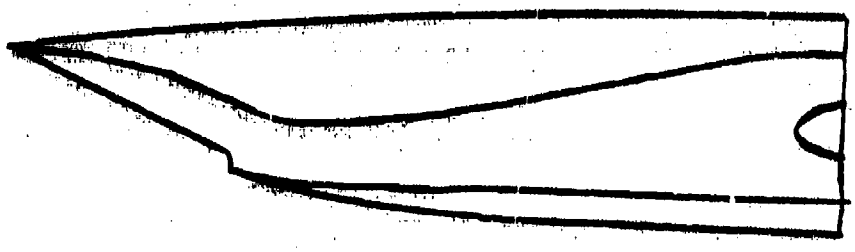

Figure 20. Mach 2.5 External Compression Inlet

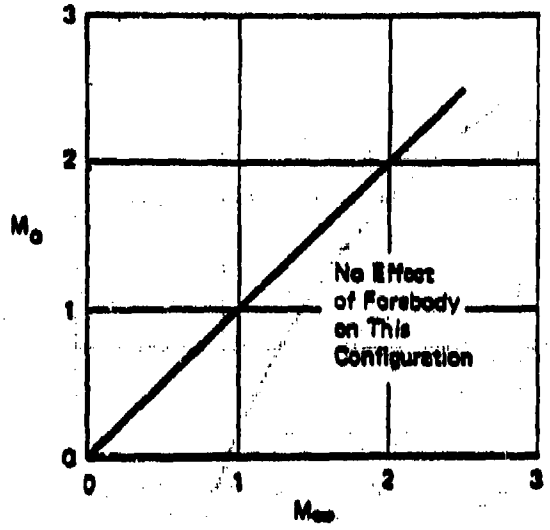

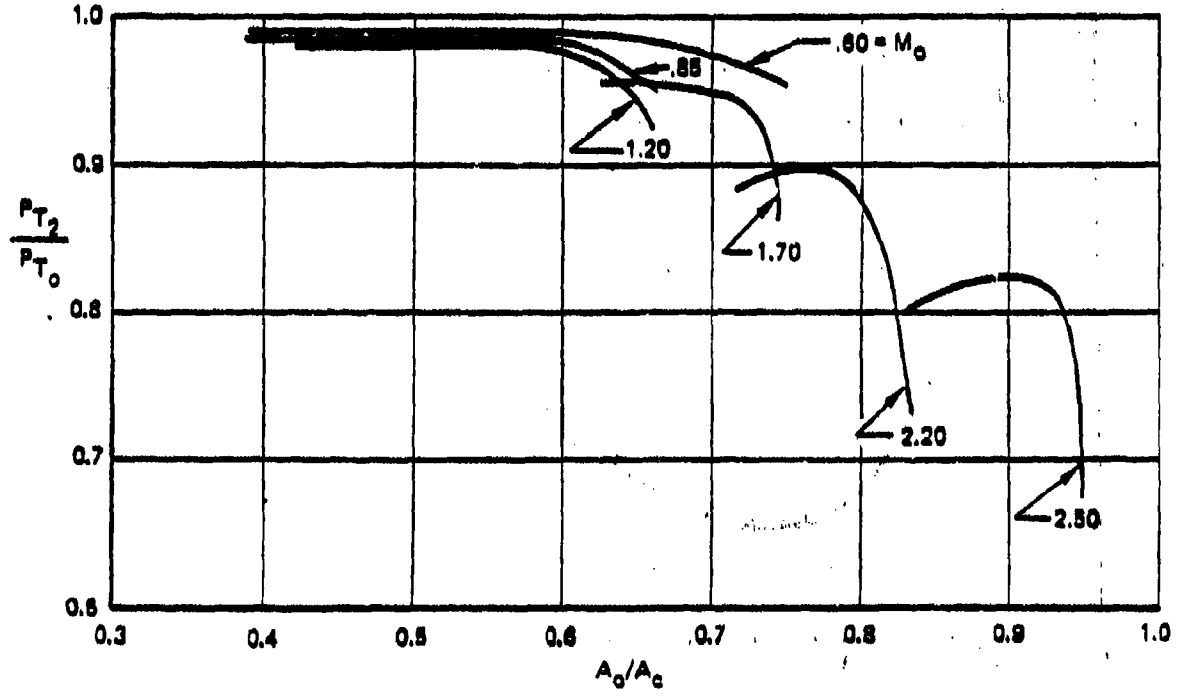

Figure 21. Performance Characteristics for Inlet Configuration #9

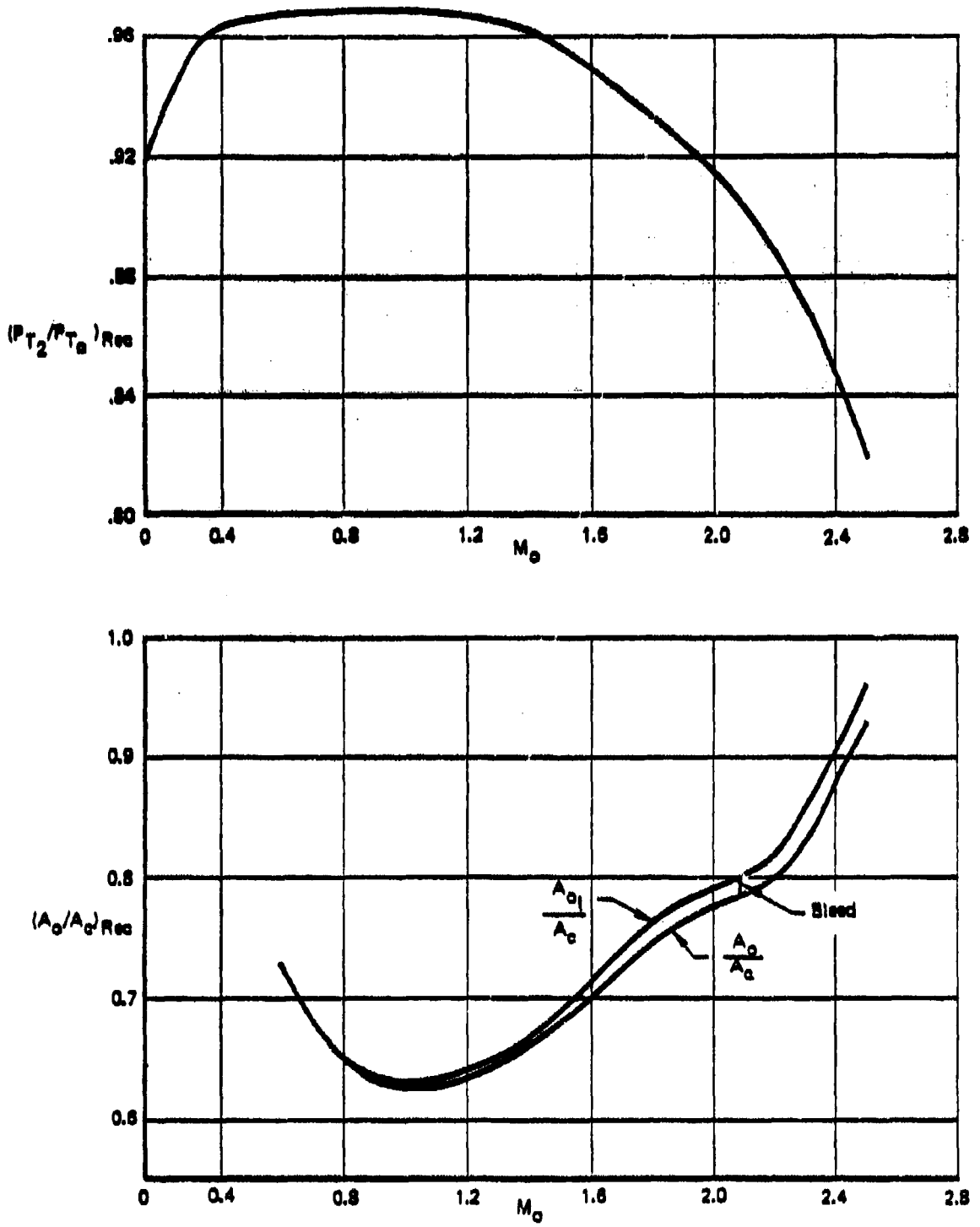

Figure 21. Performance Characteristics for Inlet Configuration #9 (continued)

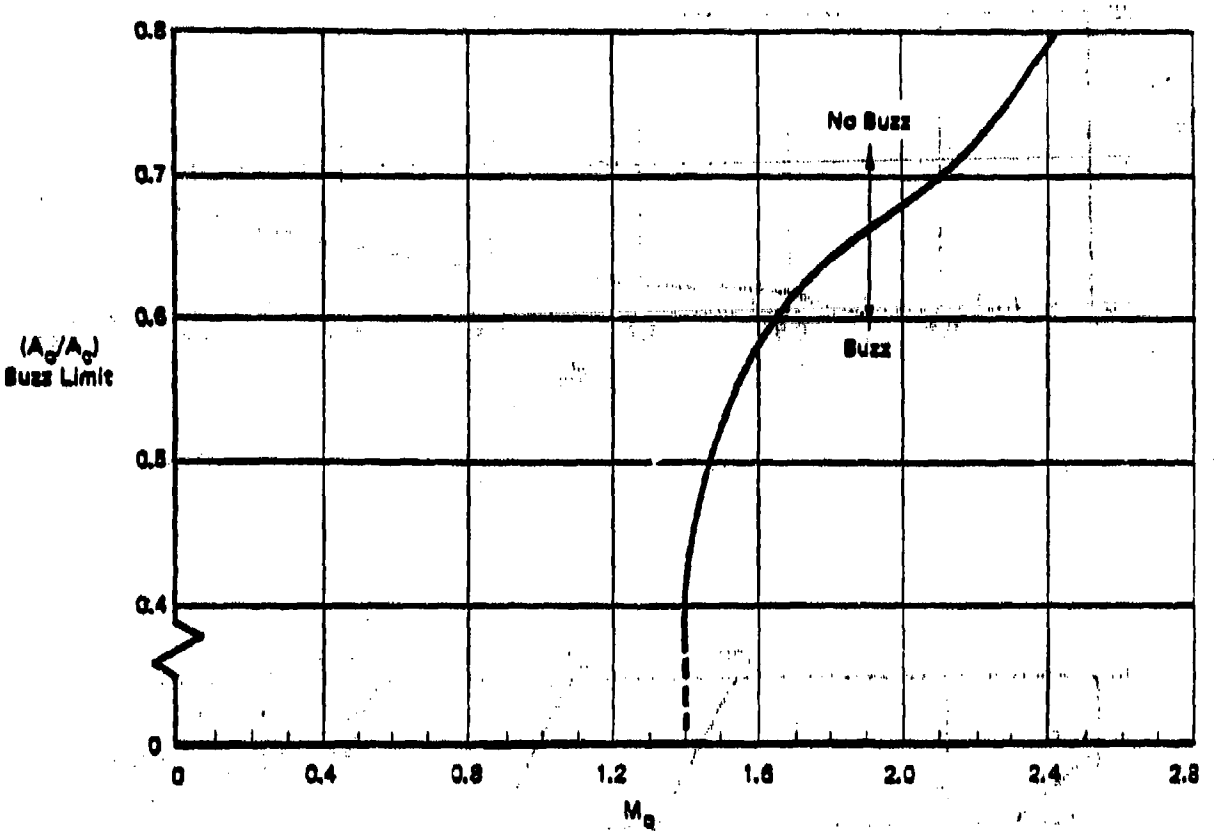

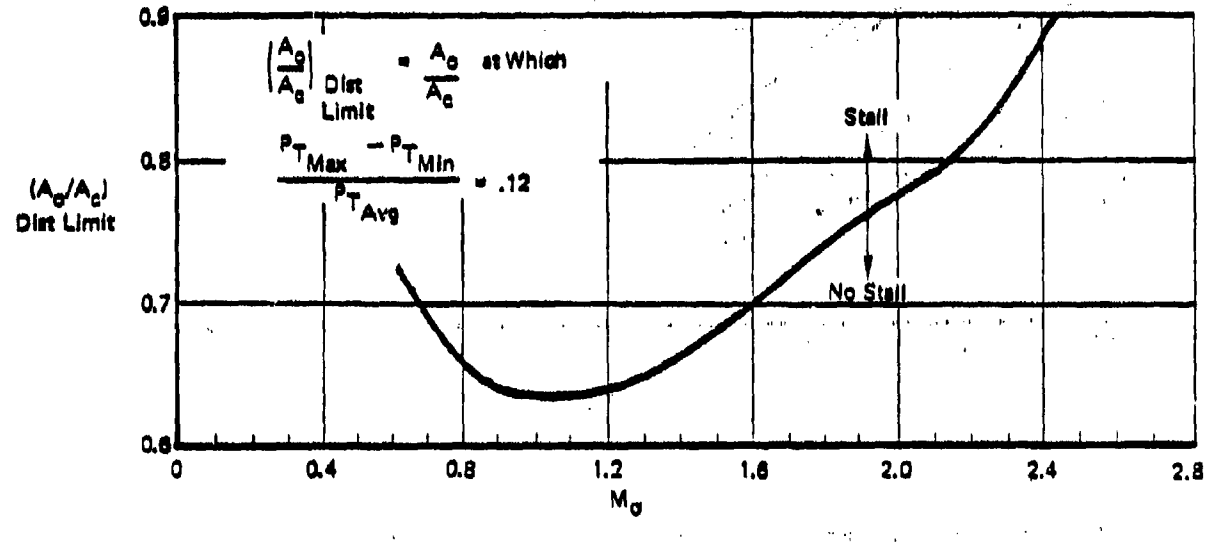

Figure 21. Performance Characteristics for Inlet Configuration #9 (continued)

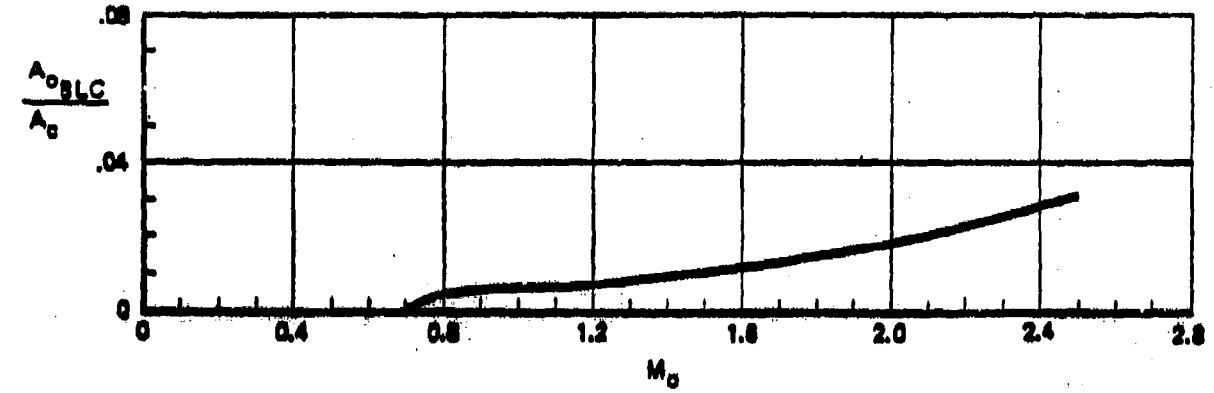

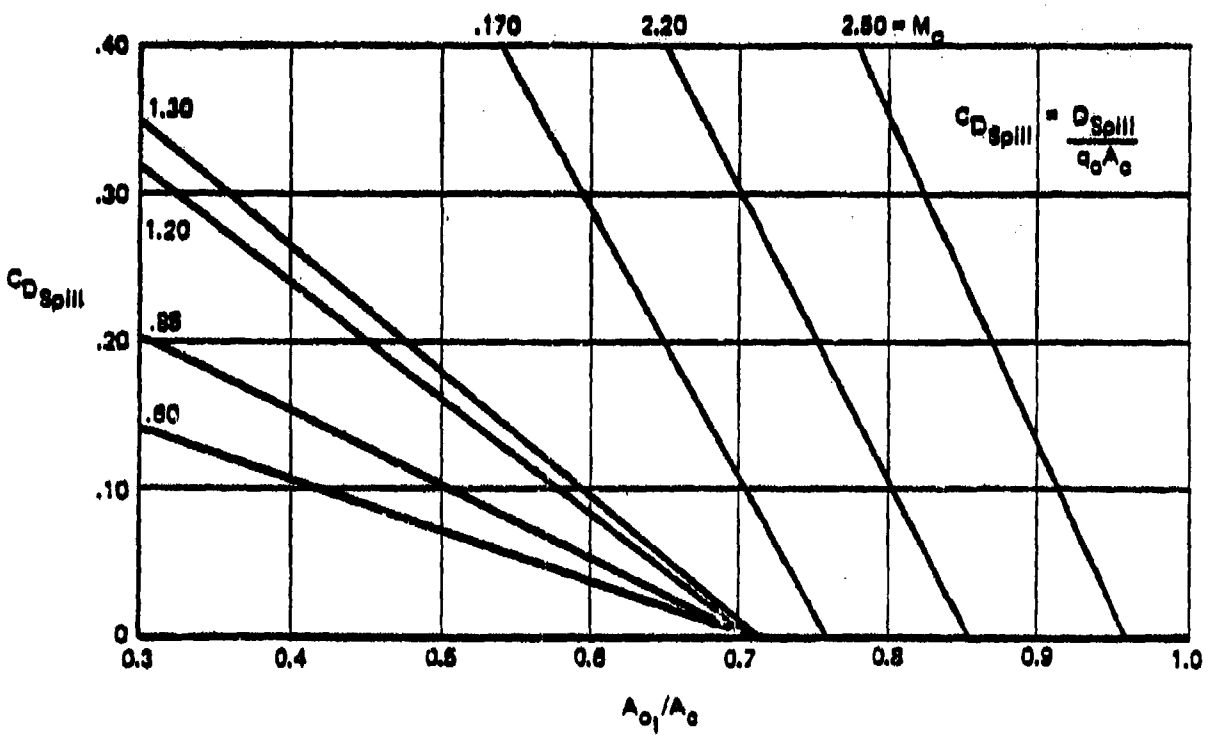

Figure 21. Performance Characteristics for Inlet Configuration #9 (continued)

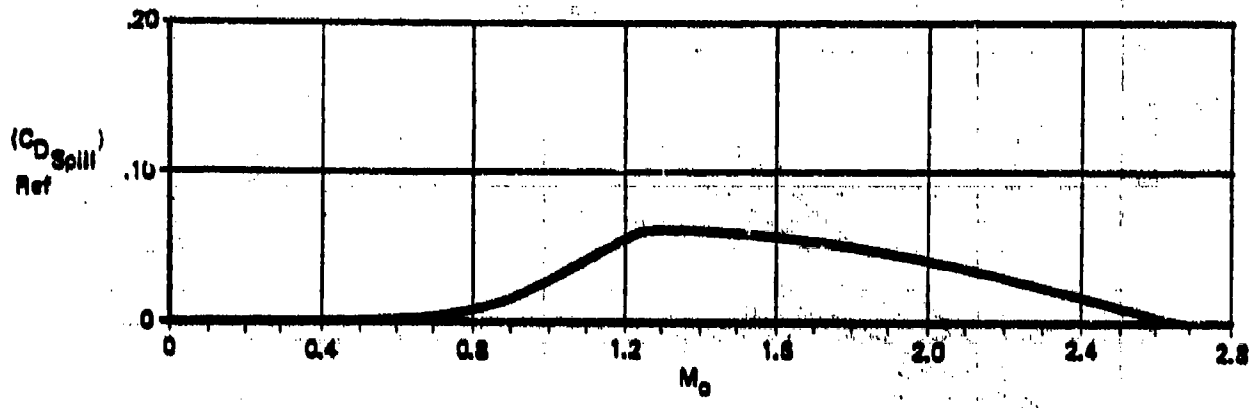

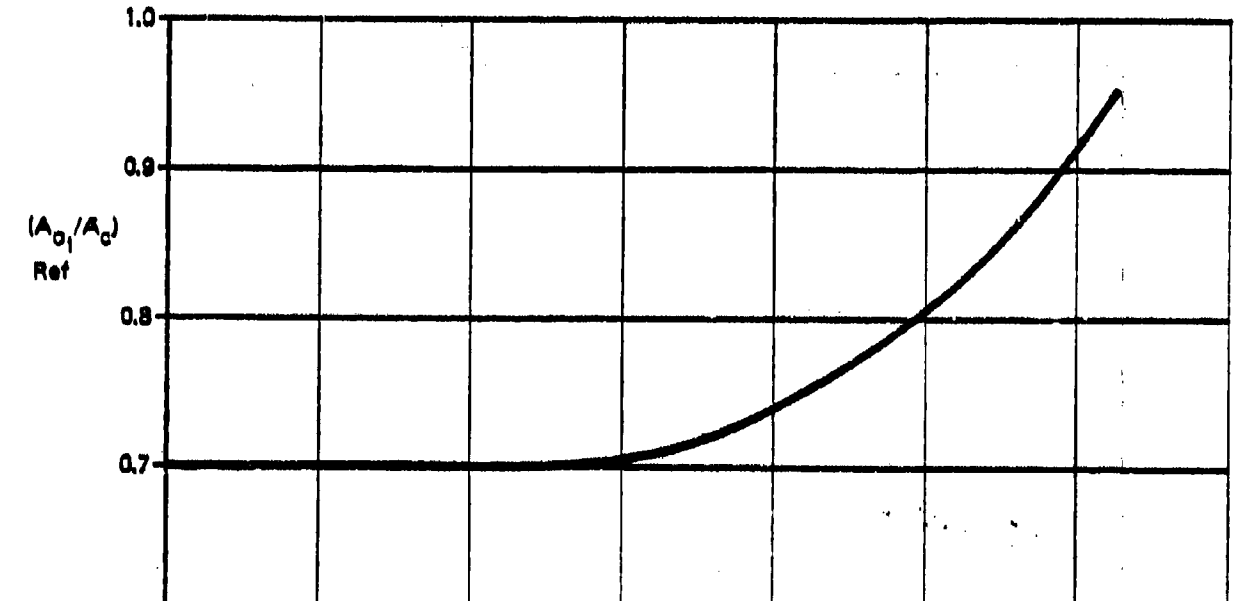

Figure 21. Performance Characteristics for Inlet Configuration #9 (continued)

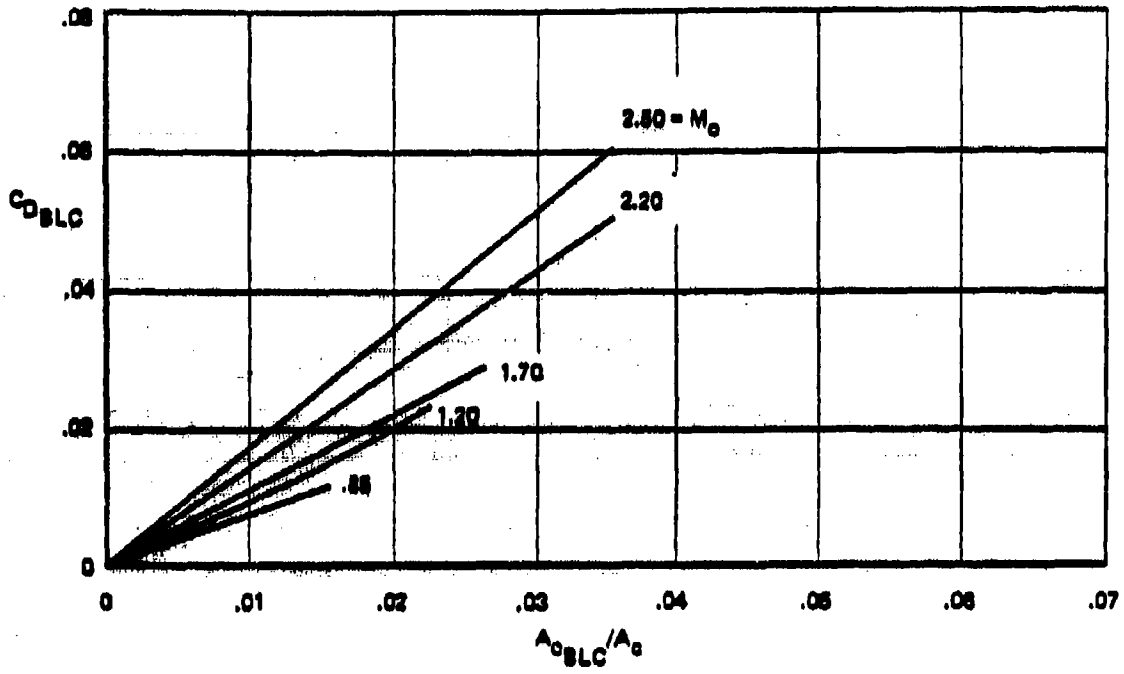

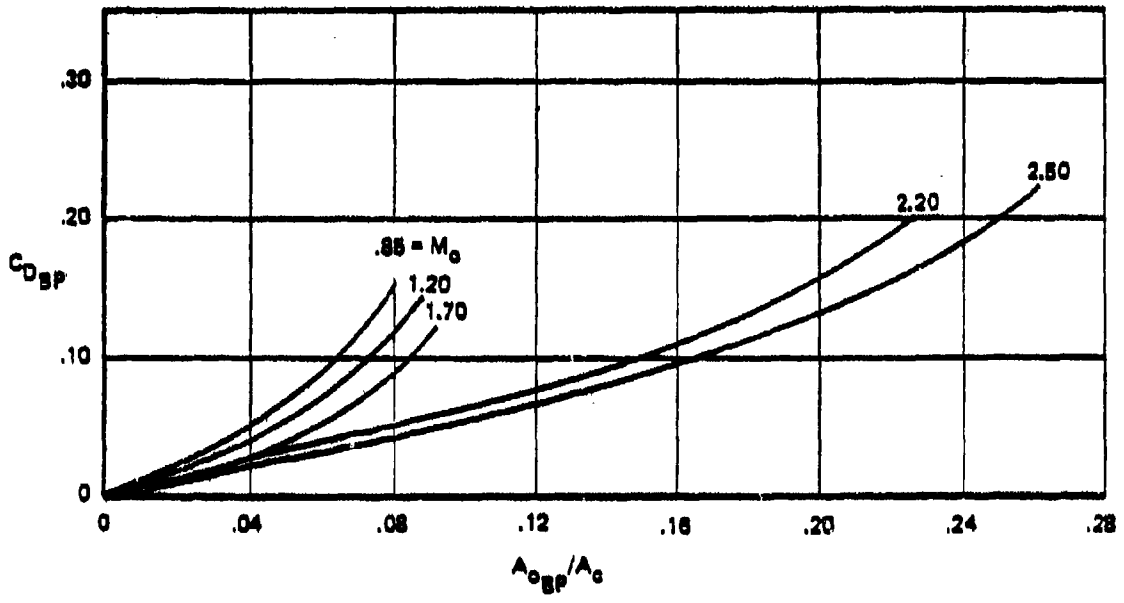

Figure 21. Performance Characteristics for Inlet Configuration #3 (continued)

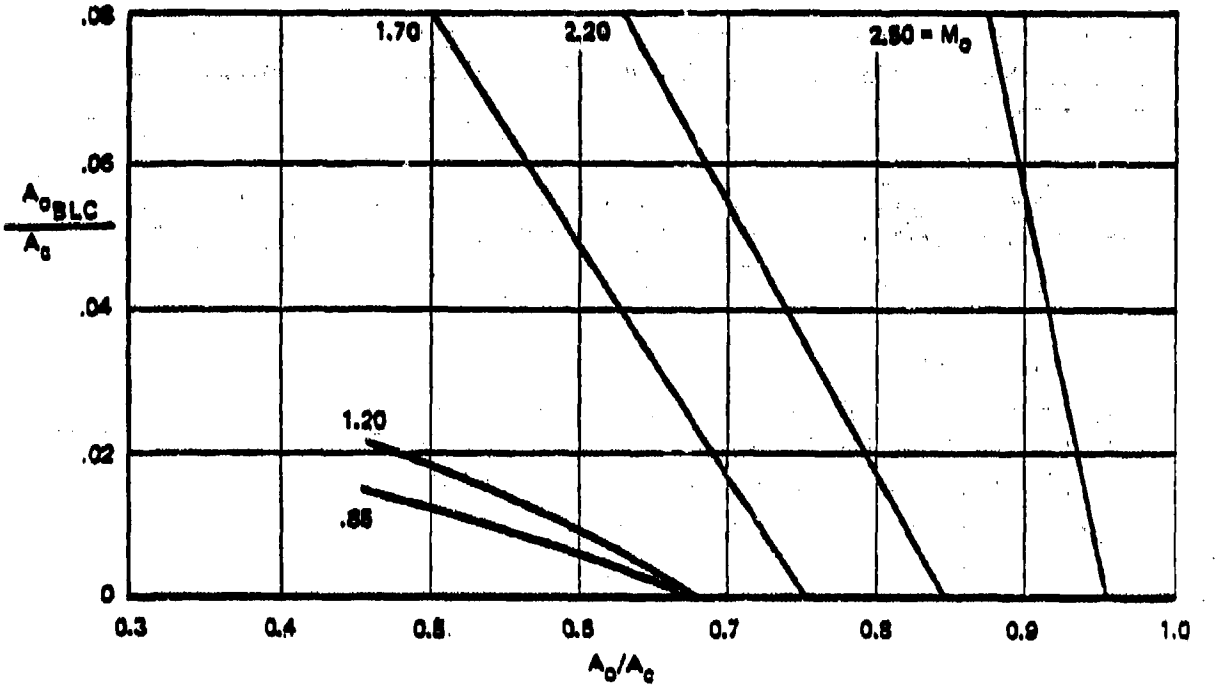

Figure 21. Performance Characteristics for Inlet Configuration #9 (concluded)

2.1.10 Inlet Configuration #10 - Half-Round, External Compression, Translating-Spike Inlet

The side mounted half-round inlets have translating 25 degrees half-angle cone centerbodies. The movable centerbody is used to provide a large throat area for low speed operation and, by translating forward, can also provide shock-on-lip for high recovery, low drag supersonic operation at Mach 1.60.

A moderately blunted, fixed cowl lip and large blow-in doors are used to achieve high total pressure recovery and low distortion at static and low-speed conditions.

No boundary layer bleed or bypass are used. In the normal process of developing an inlet of this type, wind tunnel tests would be conducted to optimize the inlet configuration. If these tests show that the addition of internal boundary layer bleed is necessary, no more than 1 - 2% of inlet air would be required for bleed. The addition of this bleed would not significantly change the configuration.

The inlet performance characteristics of this configuration are based on engineering analysis. The inlet configuration is shown in Figure 22 and the inlet performance characteristics are presented in Figure 23.

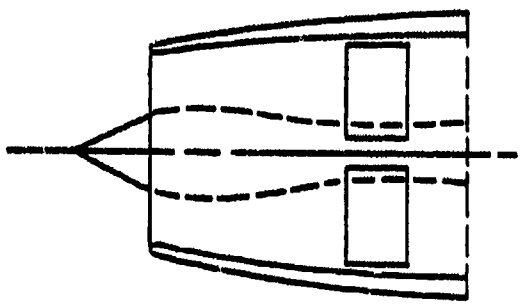

Figure 22. Supersonic (M_0=1.60) Half-Round Inlet

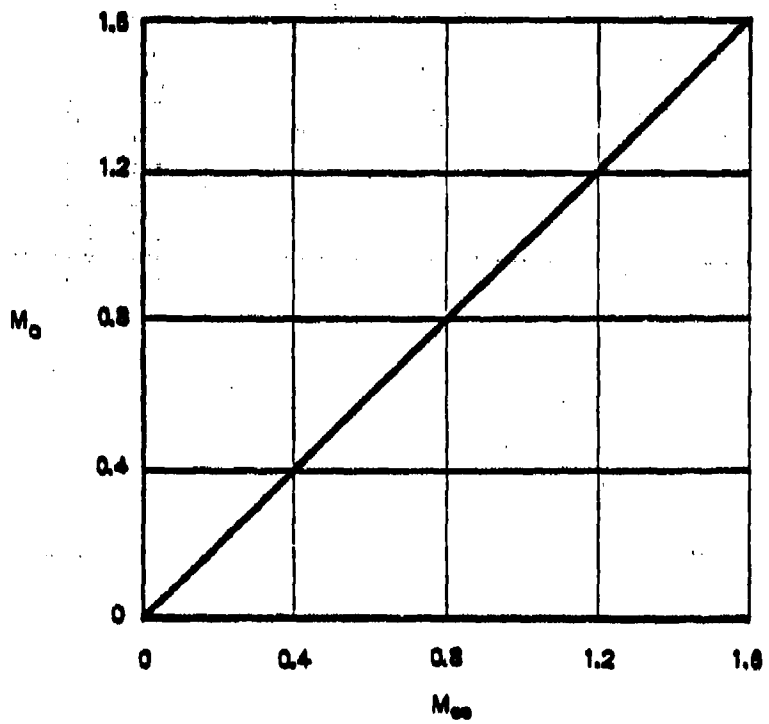

Figure 23. Performance Characteristics for Inlet Configuration #10

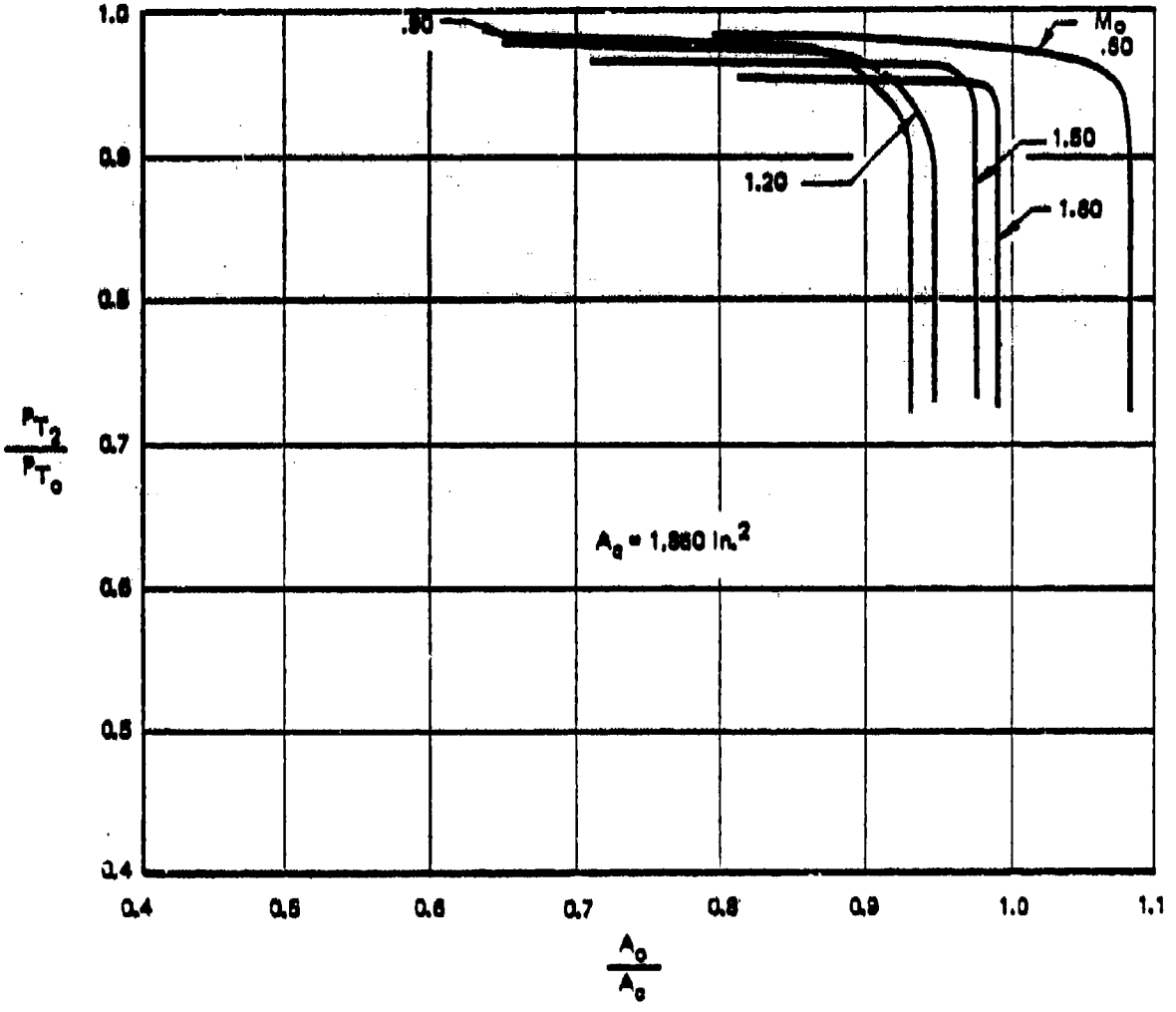

Figure 23. Performance Characteristics for Inlet Configuration #10 (continued)

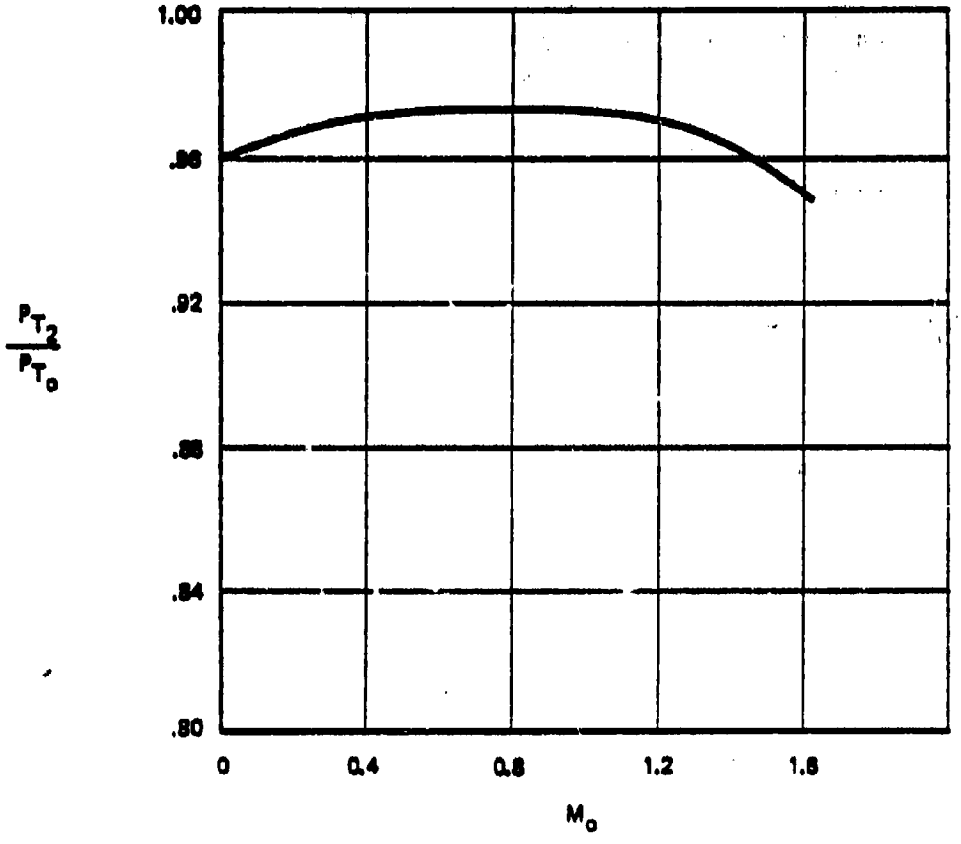

Figure 23. Performance Characteristics for Inlet Configuration #10 (continued)

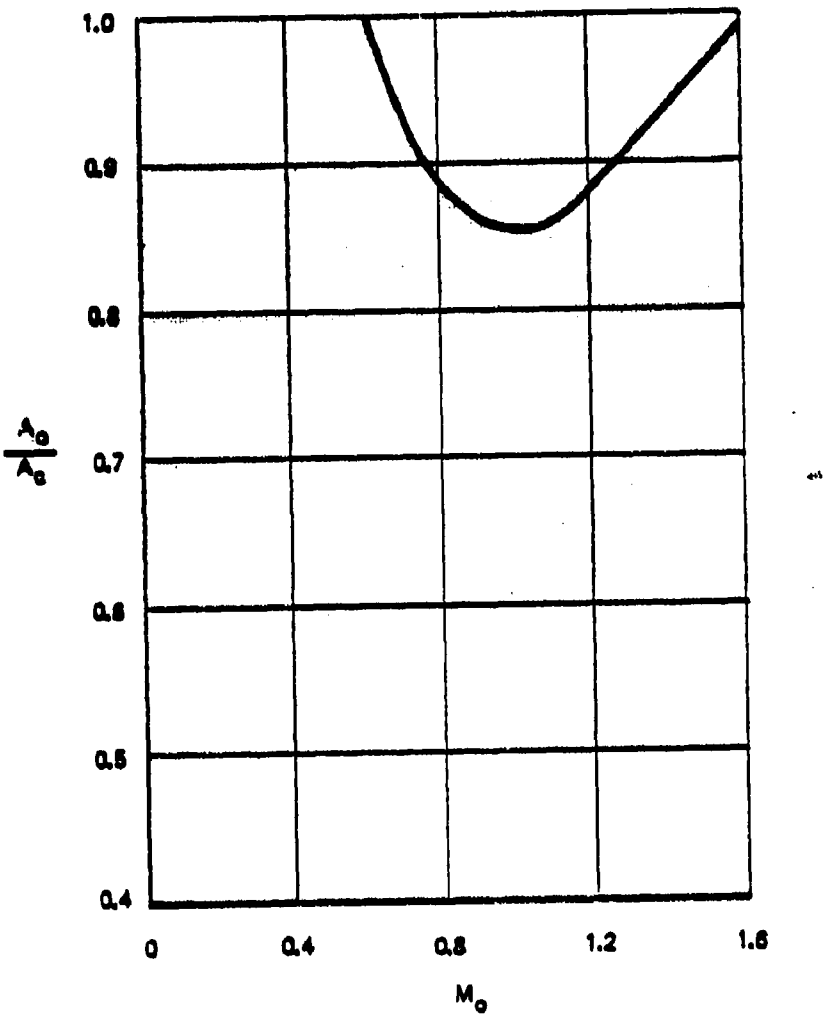

Figure 23. Performance Characteristics for Inlet Configuration #10 (continued)

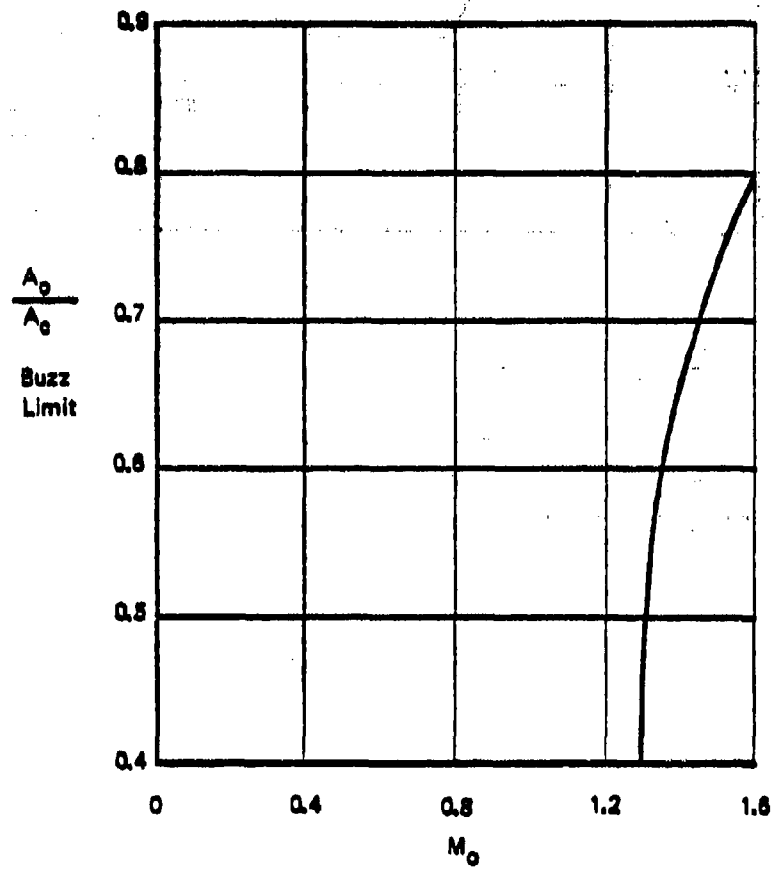

Figure 23. Performance Characteristics for Inlet Configuration #10 (continued)

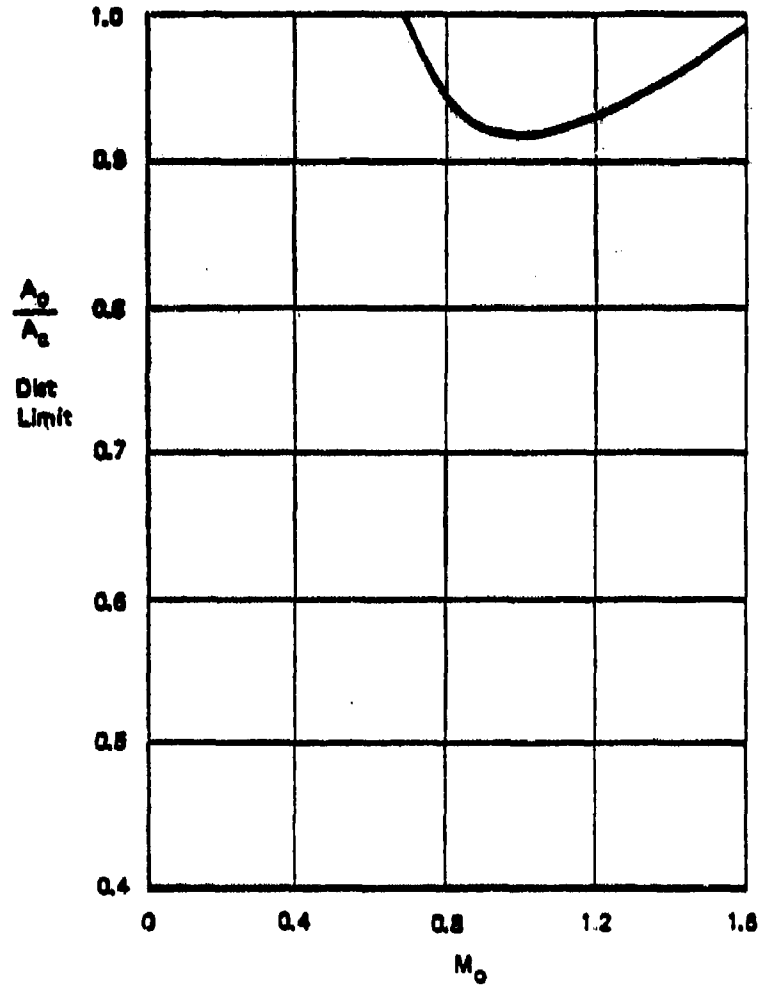

Figure 23. Performance Characteristics for Inlet Configuration #10 (continued)

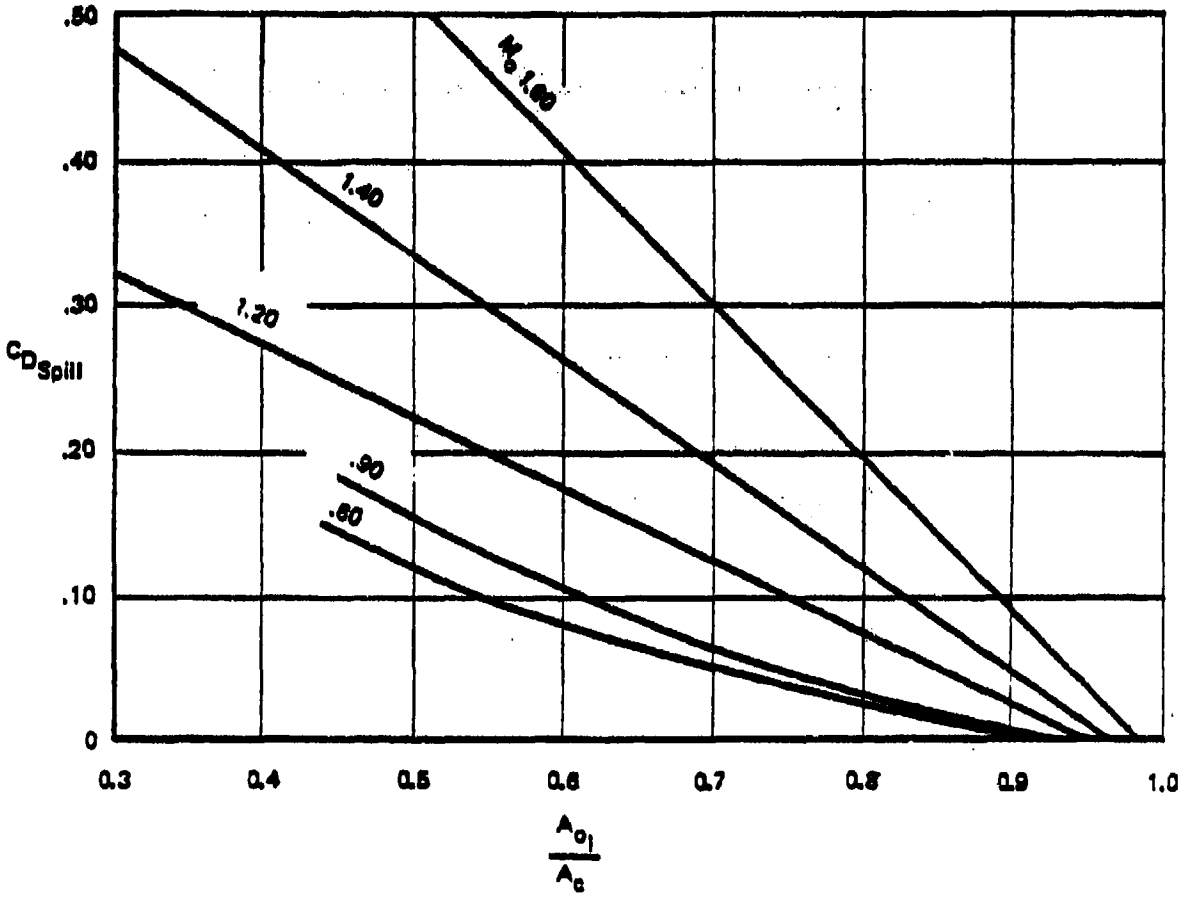

Figure 22. Performance Characteristics for Inlet Configuration #10 (continued)

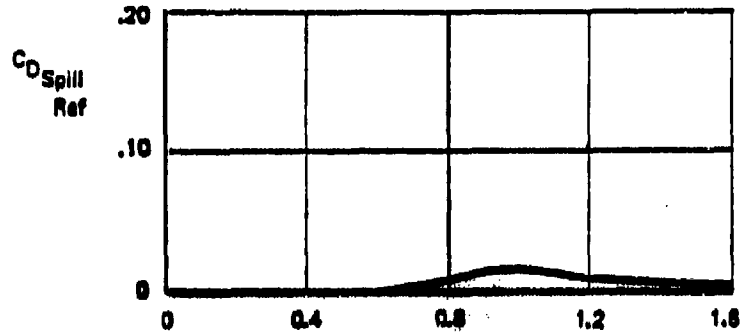

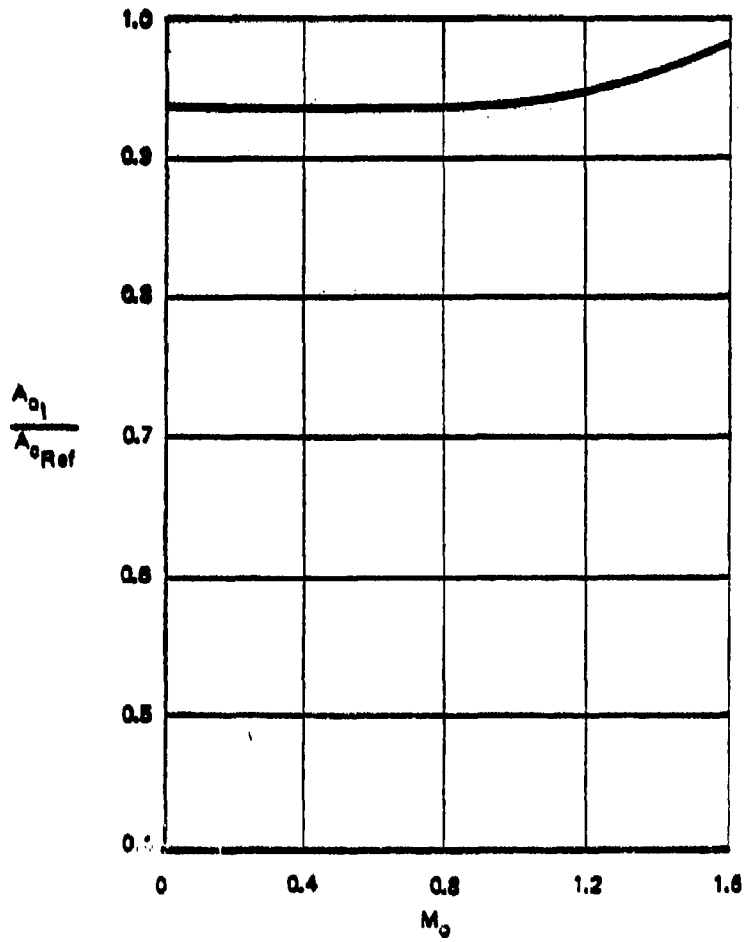

Figure 23. Performance Characteristics for Inlet Configuration #10 (concluded)

2.1.11 Inlet Configuration #11 - Half-Round, Expanding-Centerbody, Three-Shock, External Compression Inlet

This inlet uses an expanding second cone to achieve changes in compression surface angle and throat area. Boundary layer bleed is provided in the form of porosity on the second cone and a throat slot.

The inlet performance characteristics are based on the results of engineering analysis. The geometric features of the inlet are shown in Figure 24. The inlet performance characteristics are presented in Figure 25.

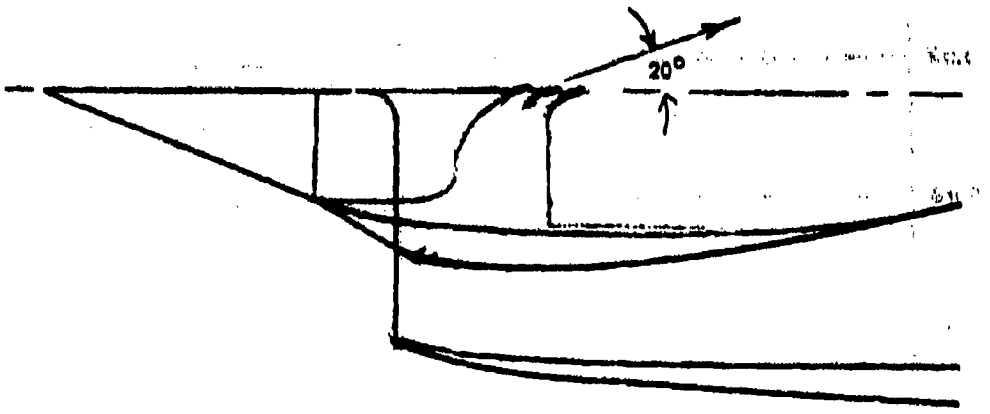

Figure 24. Half Round External Compression Mach 2.0 Inlet

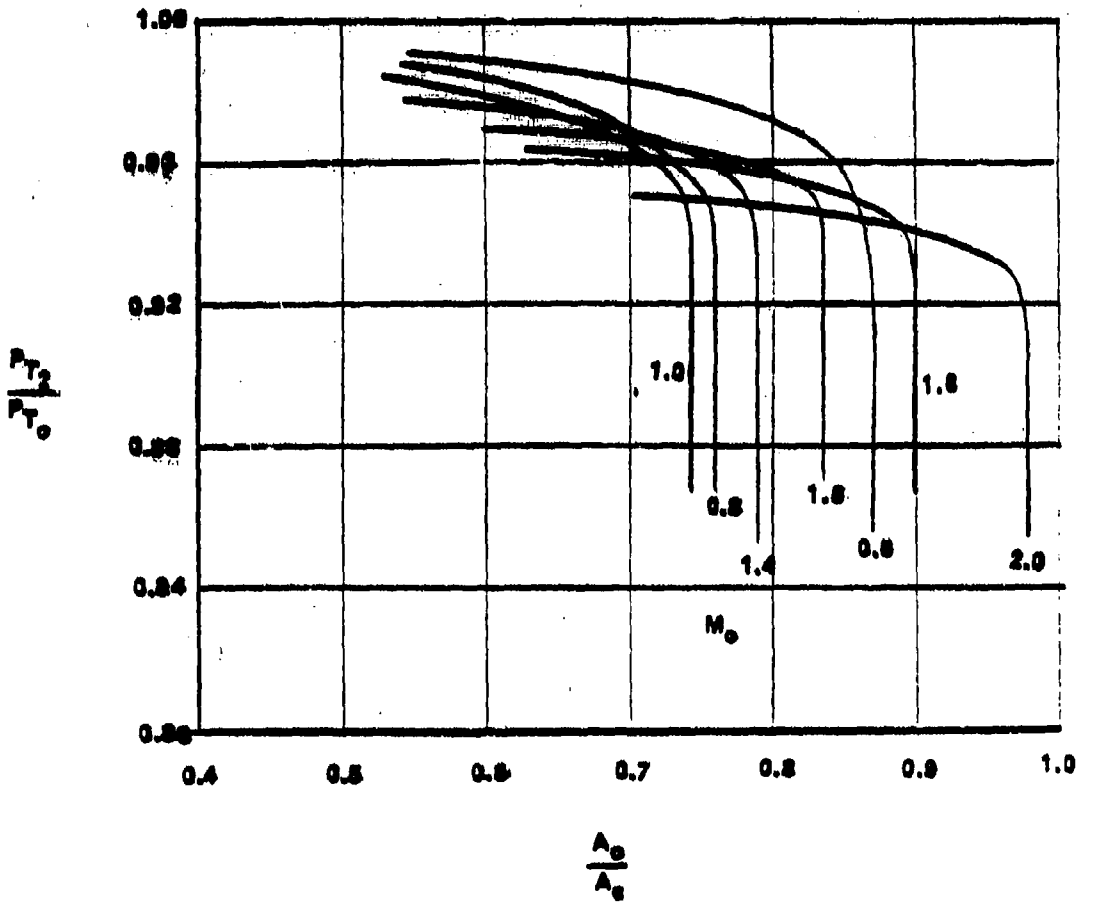

Figure 25. Performance Characteristics for Inlet Configuration #11

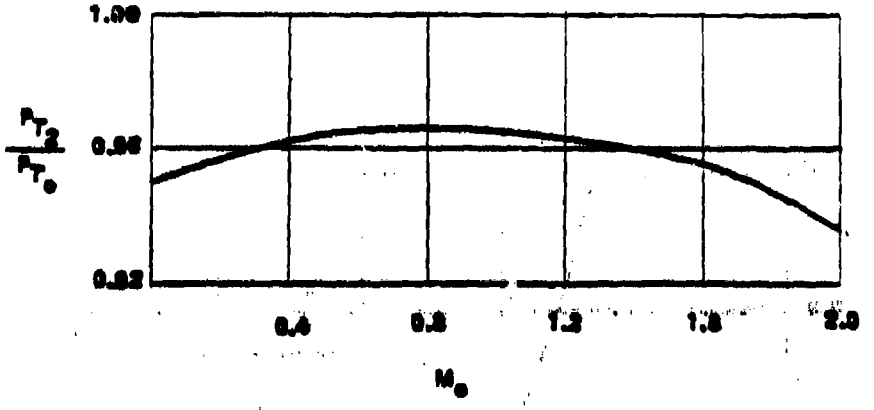

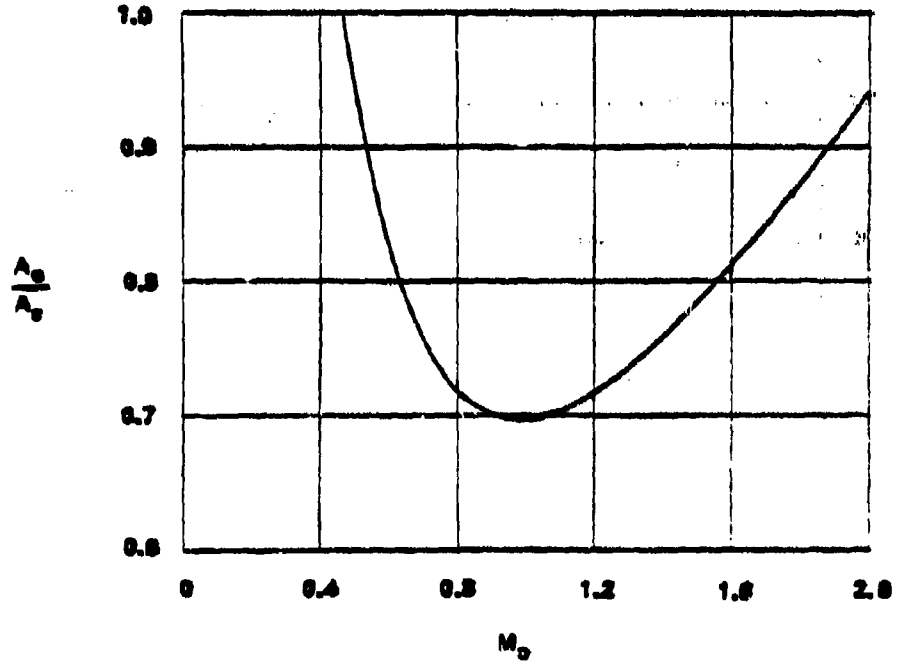

Figure 25. Performance Characteristics for Inlet Configuration #11 (continued)

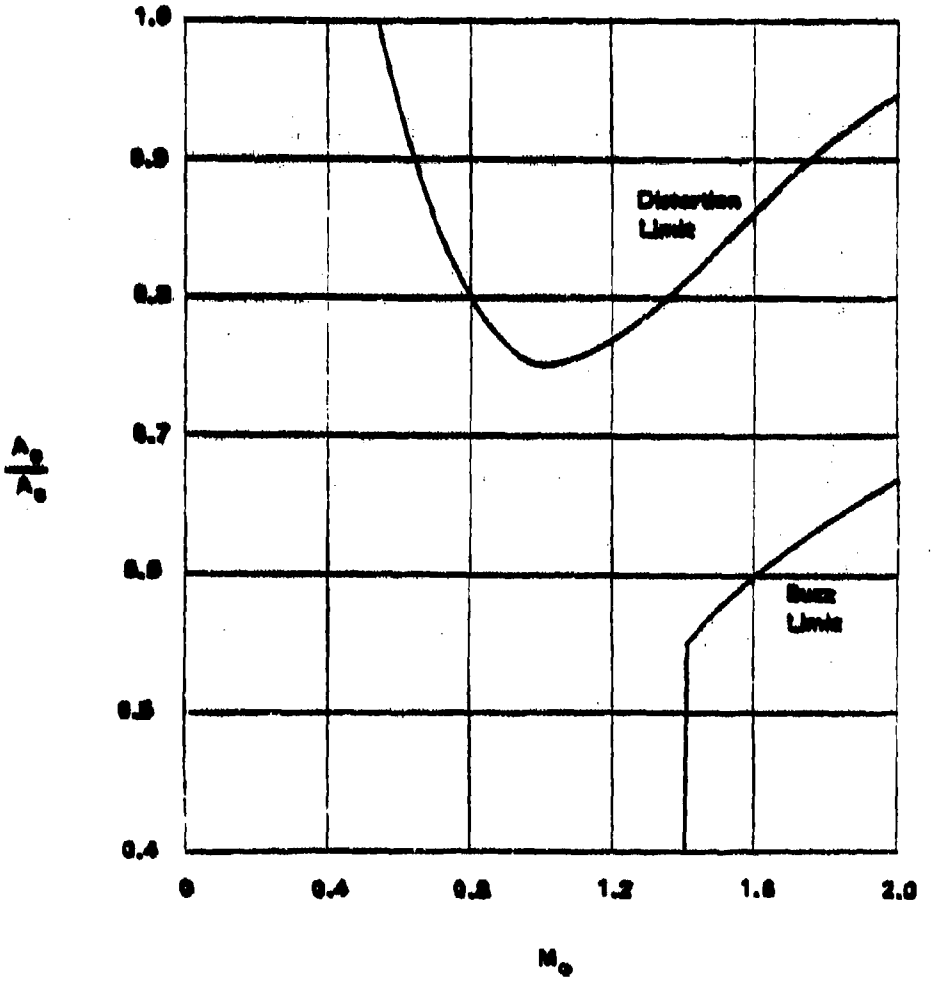

Figure 29. Performance Characteristics for Inlet Configuration #11 (continued)

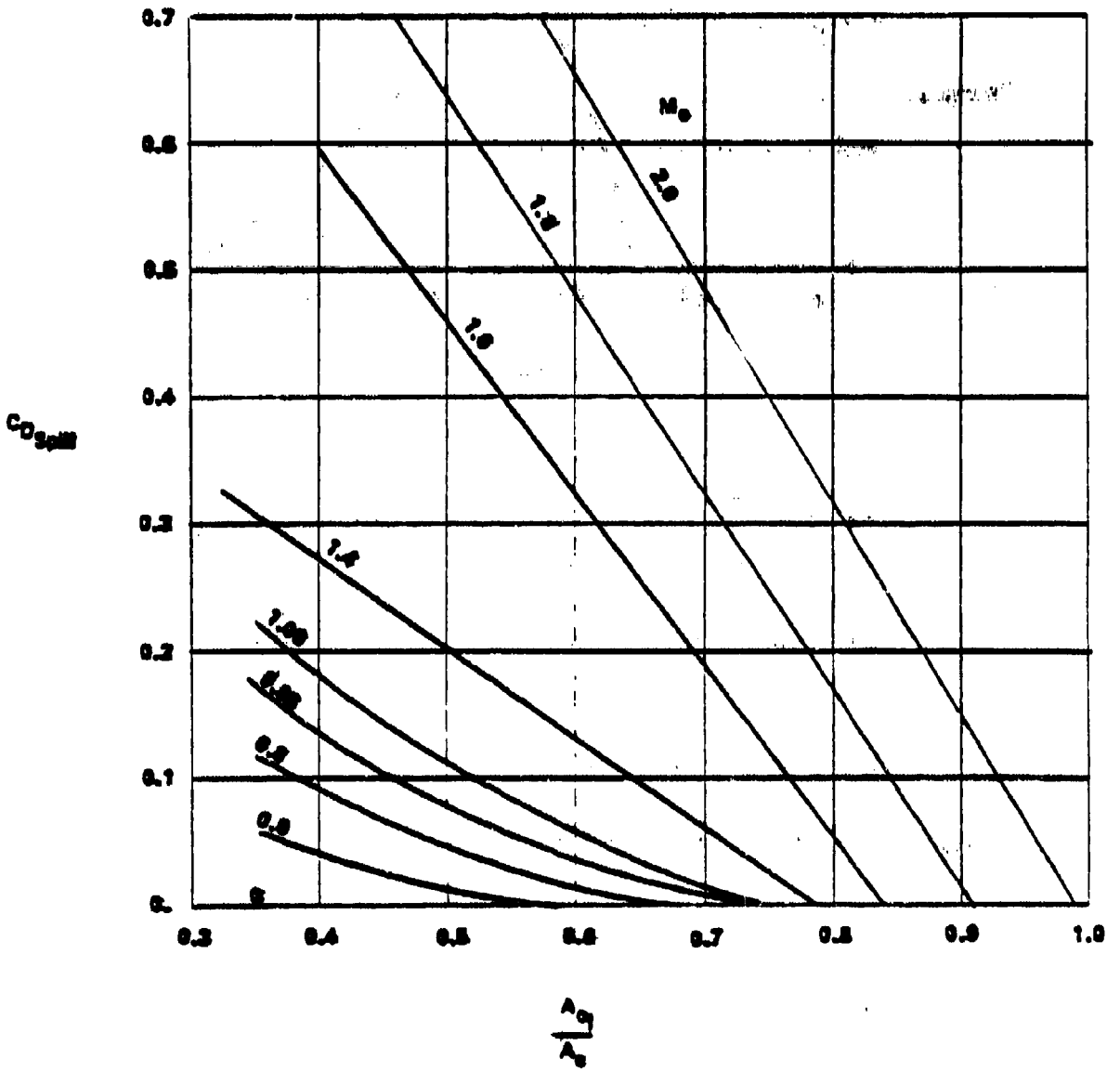

Figure 25. Performance Characteristics for Inlet Configuration #11 (continued)

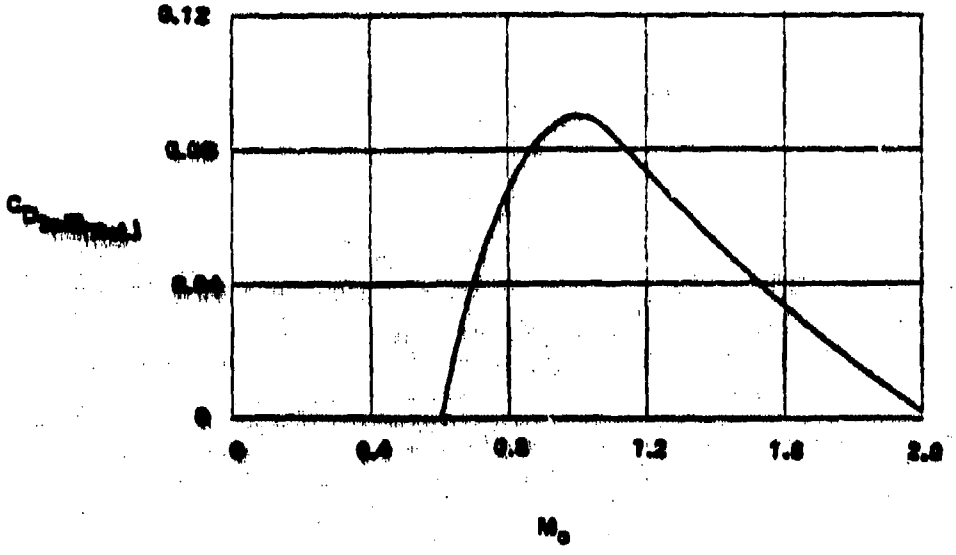

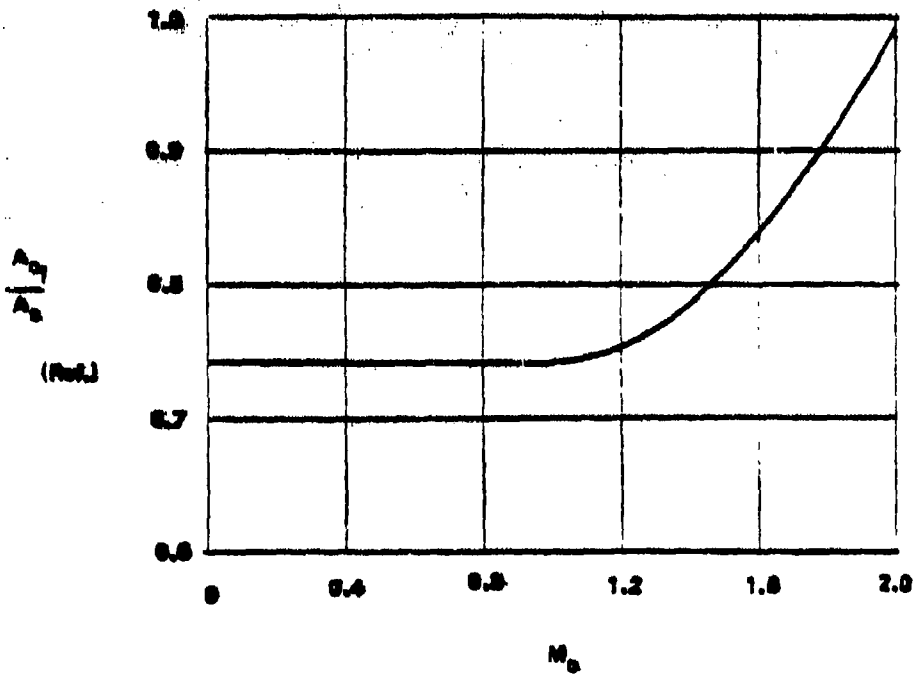

Figure 25. Performance Characteristics for Inlet Configuration #11 (continued)

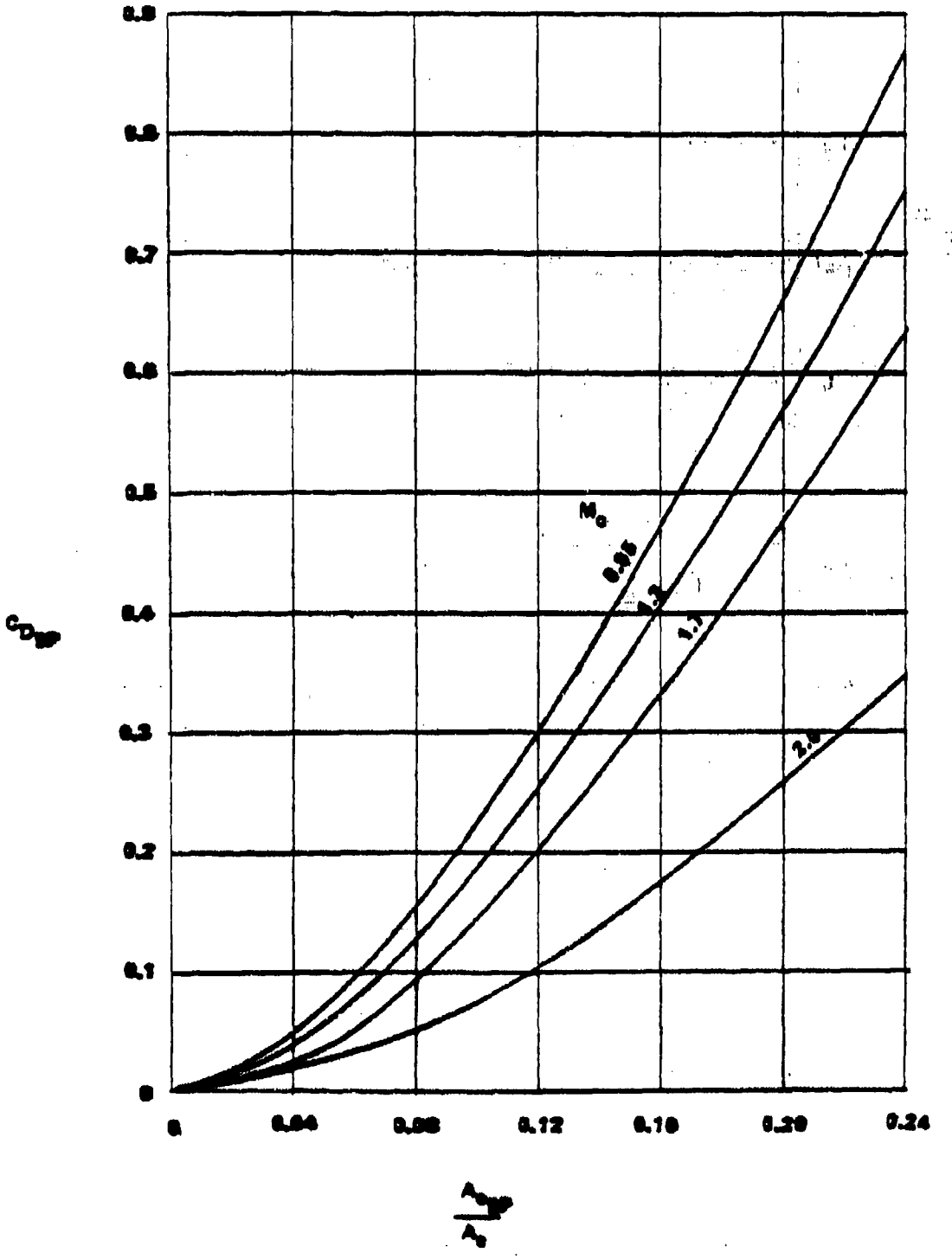

Figure 25. Performance Characteristics for Inlet Configuration #11 (continued)

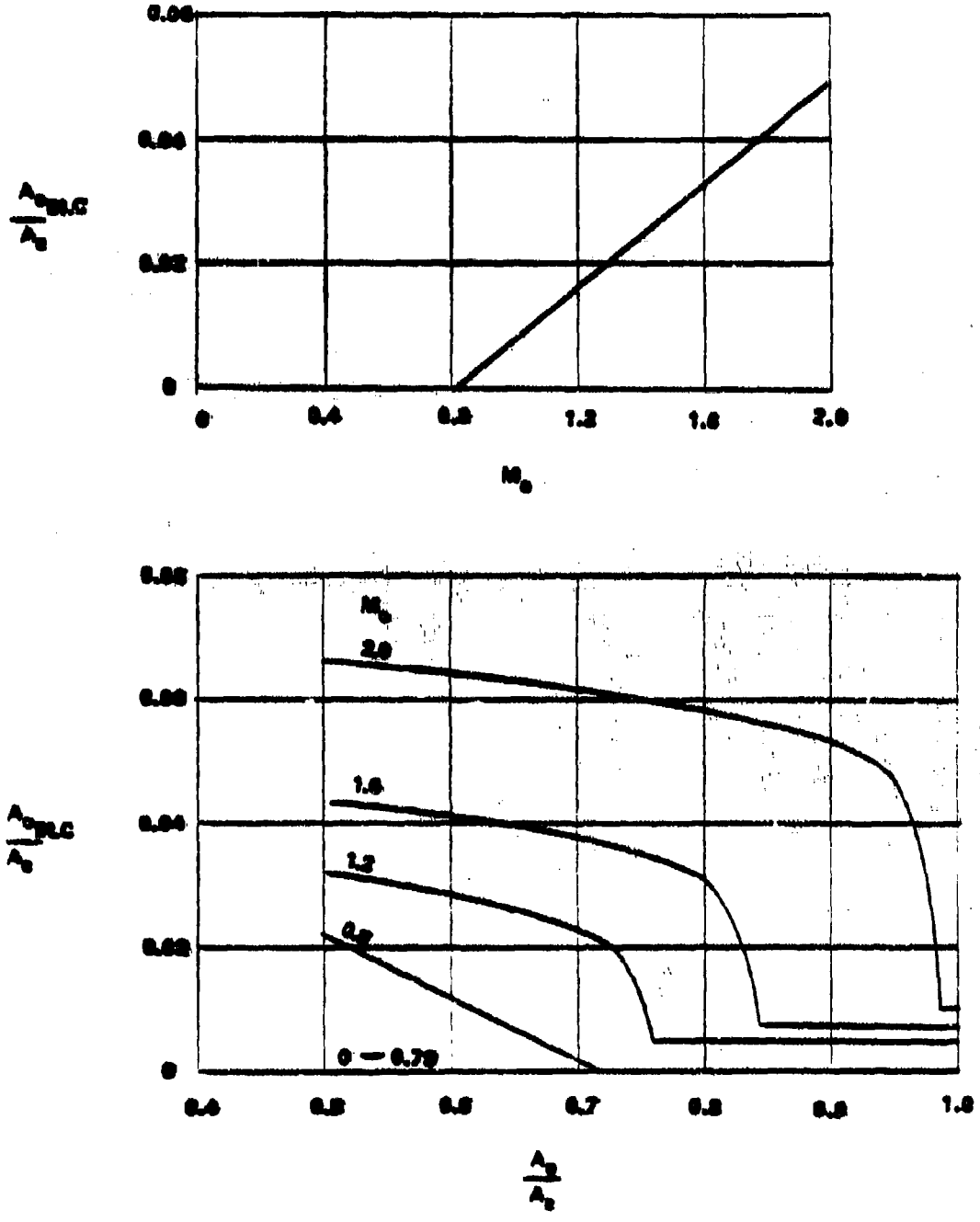

Figure 25. Performance Characteristics for Inlet Configuration #11 (continued)

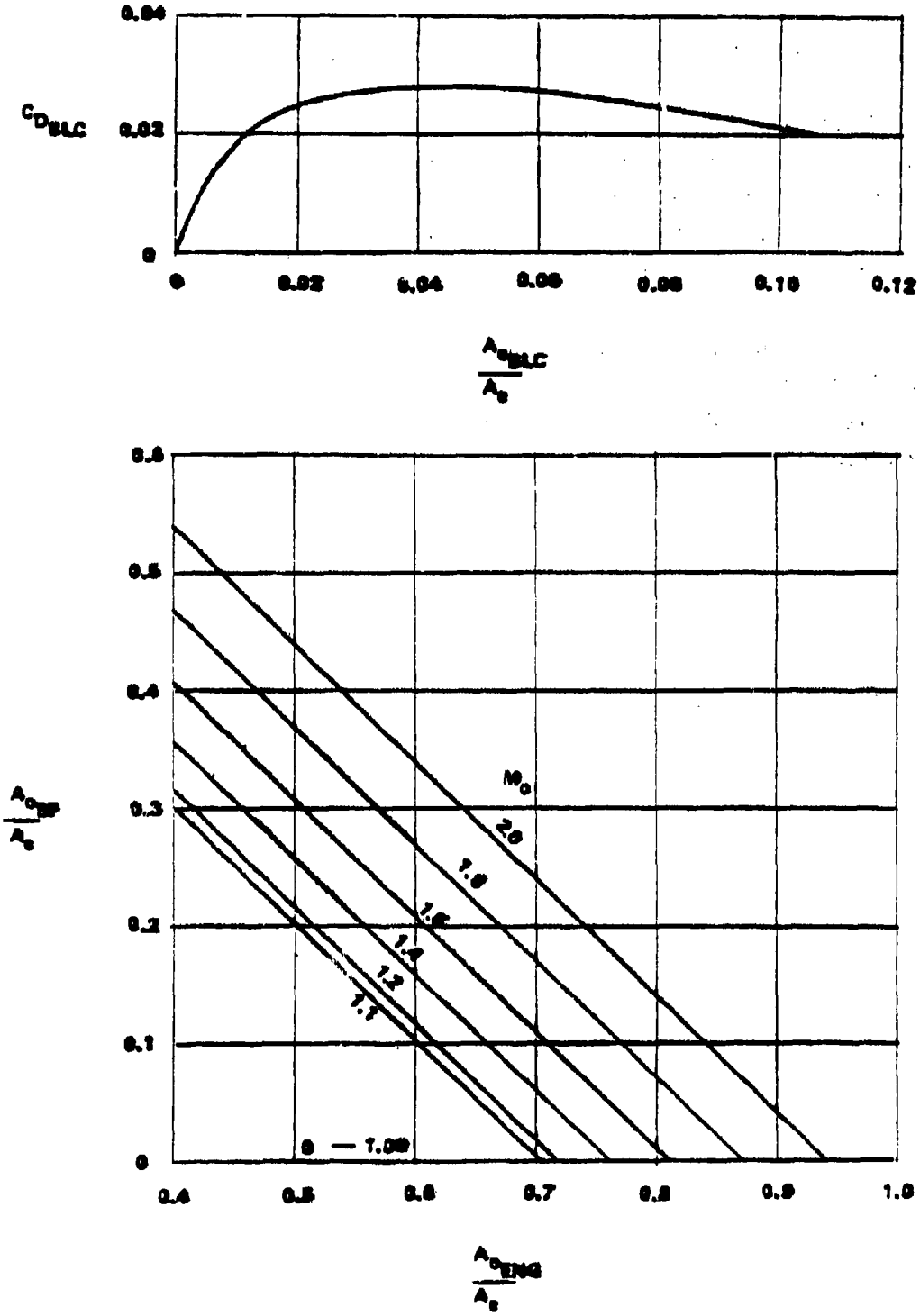

Figure 25. Performance Characteristics for Inlet Configuration #11 (concluded)

2.1.12 Inlet Configuration #12 - Half-Round, Three-Shock, External Compression, Variable Cone Inlet

This inlet has a fixed 18^{o} first cone angle and a variable second cone angle. Porous plate boundary layer bleed is provided on the second cone in the region of the design terminal shock location. The boundary layer bleed flow is routed aft and exits through low angle louvers or a door well aft of the cowl lip. Design throat Mach number is 0.7.

The inlet performance characteristics of this configuration are based on data from Reference 7 and engineering analysis. The geometry of the inlet is shown in Figure 26 and the inlet performance characteristics are presented in Figure 27.

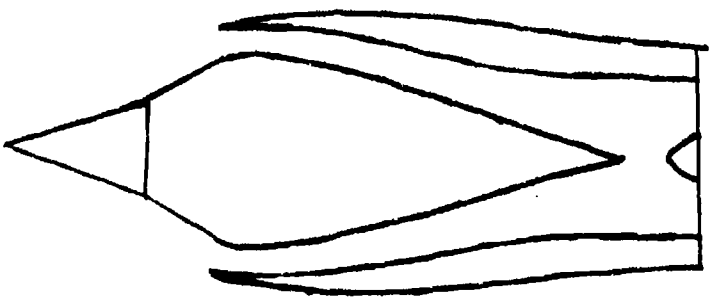

Figure 26. Half-Round External-Compression Inlet for Mach 2.5

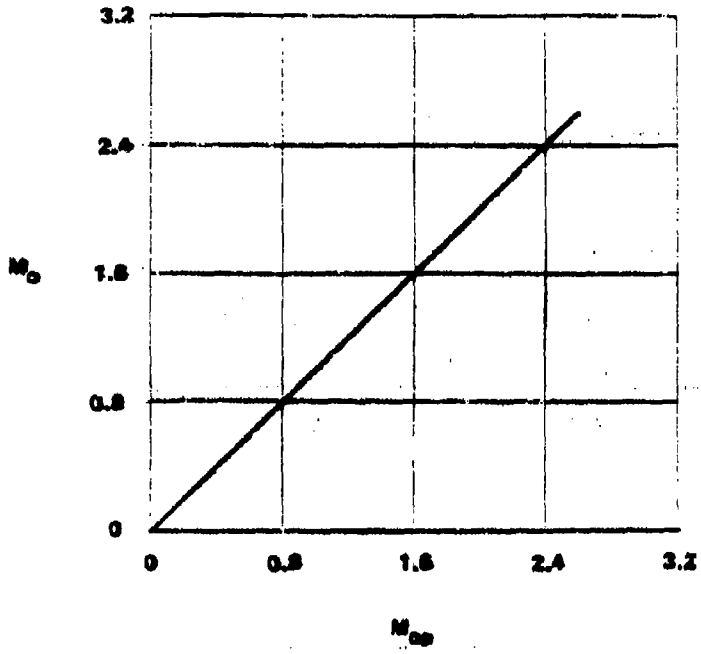

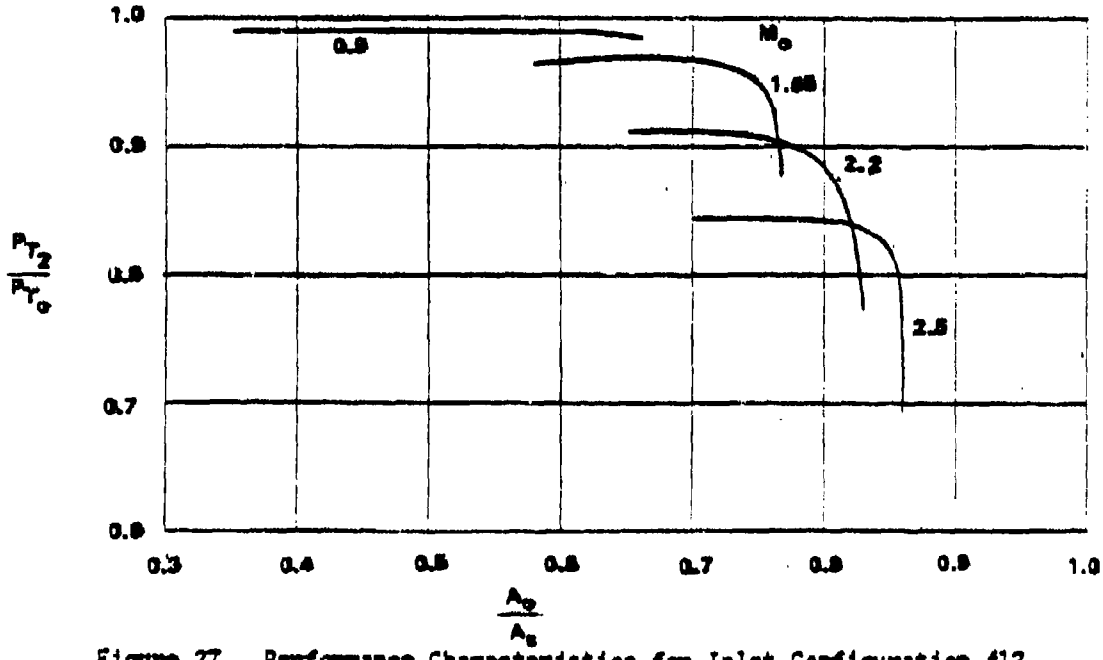

Figure 27. Performance Characteristics for Inlet Configuration #12

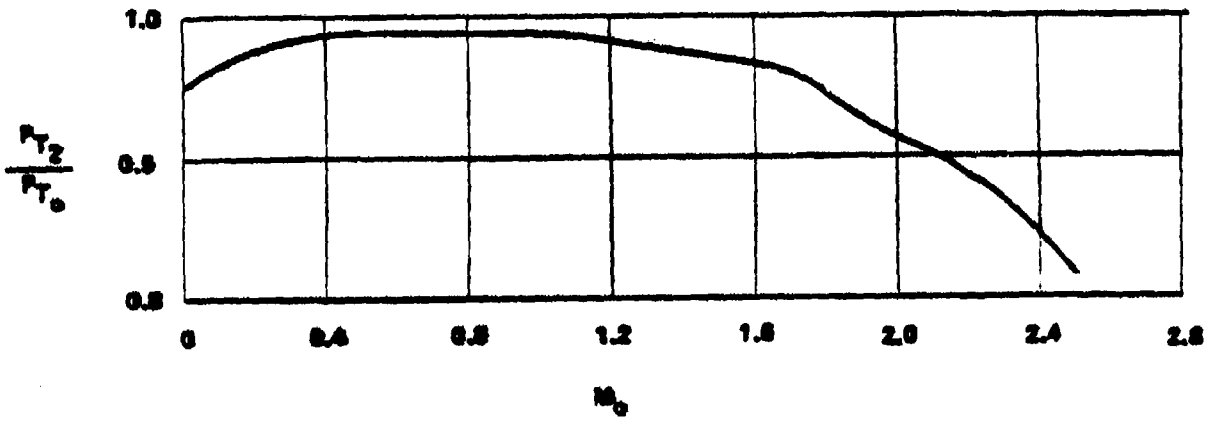

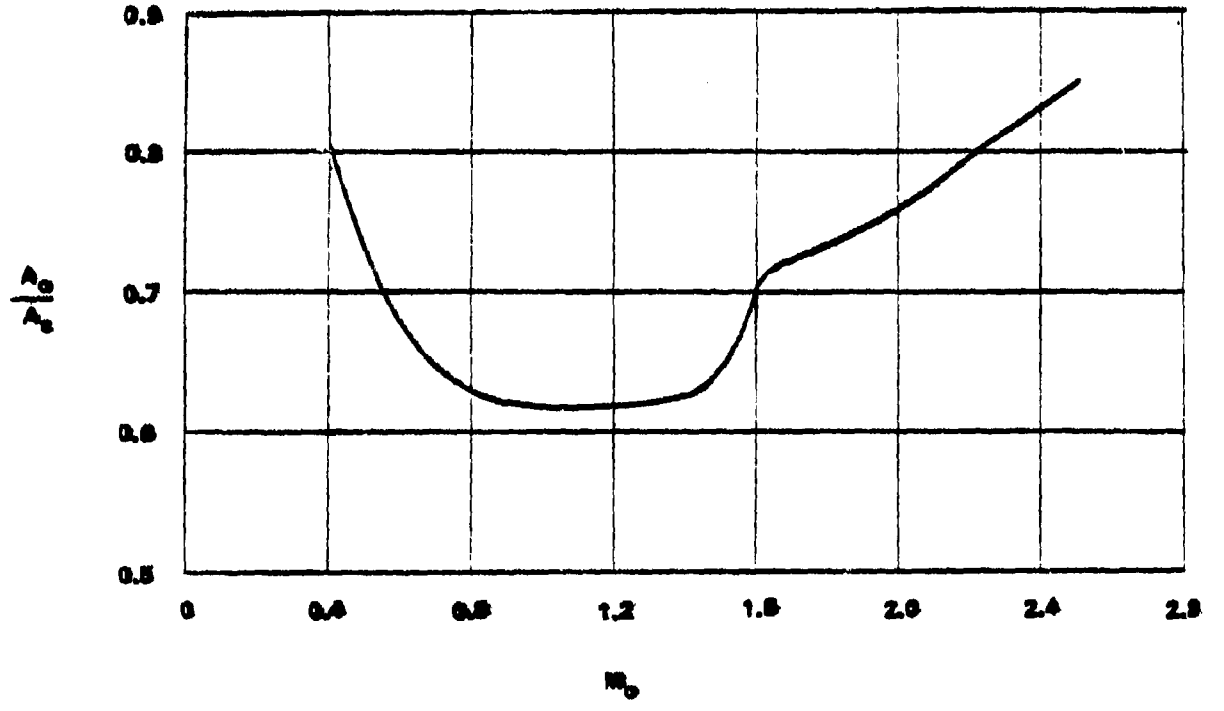

Figure 27. Performance Characteristics for Inlet Configuration #12 (continued)

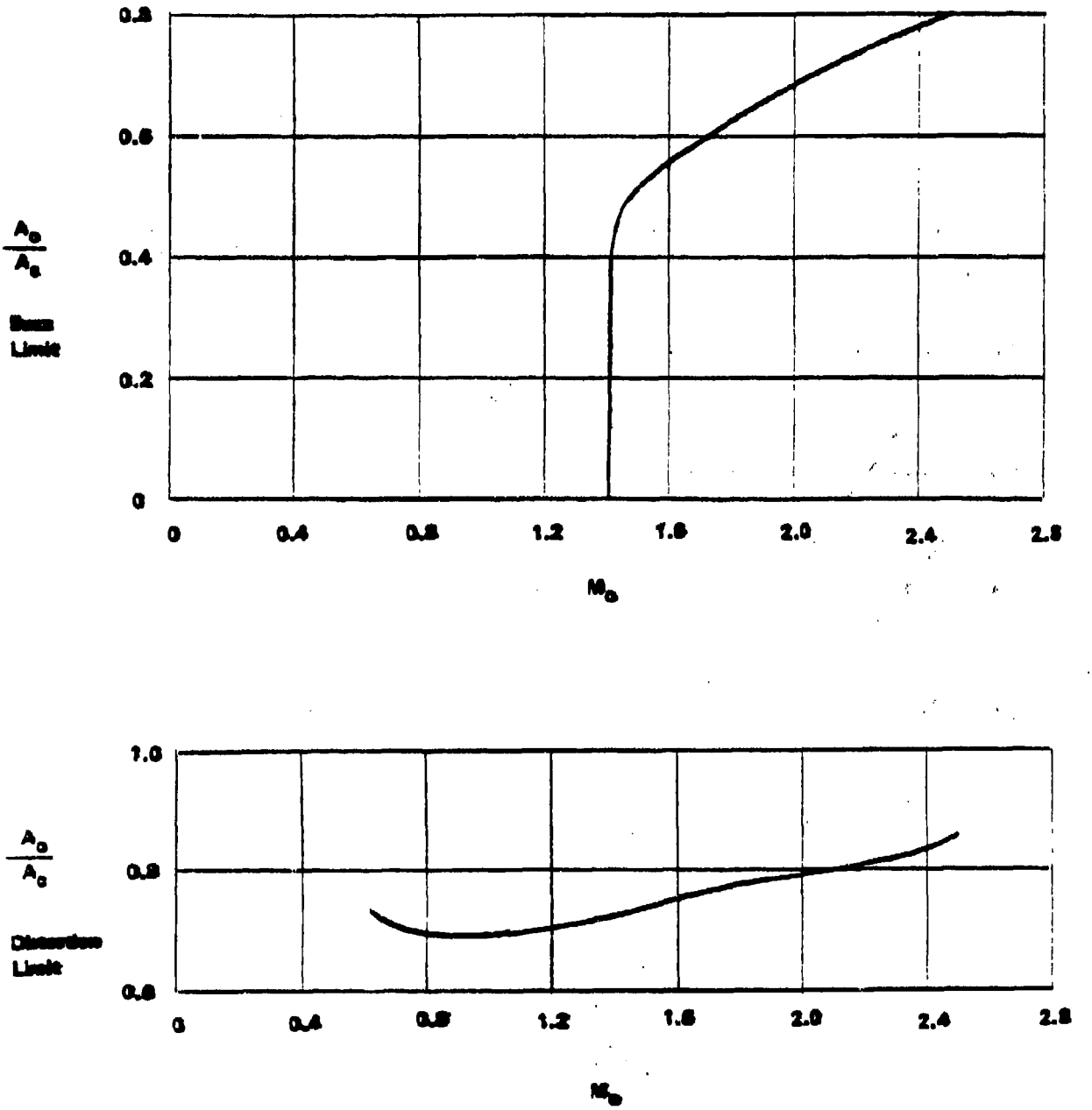

Figure 27. Performance Characteristics for Inlet Configuration #12 (continued)

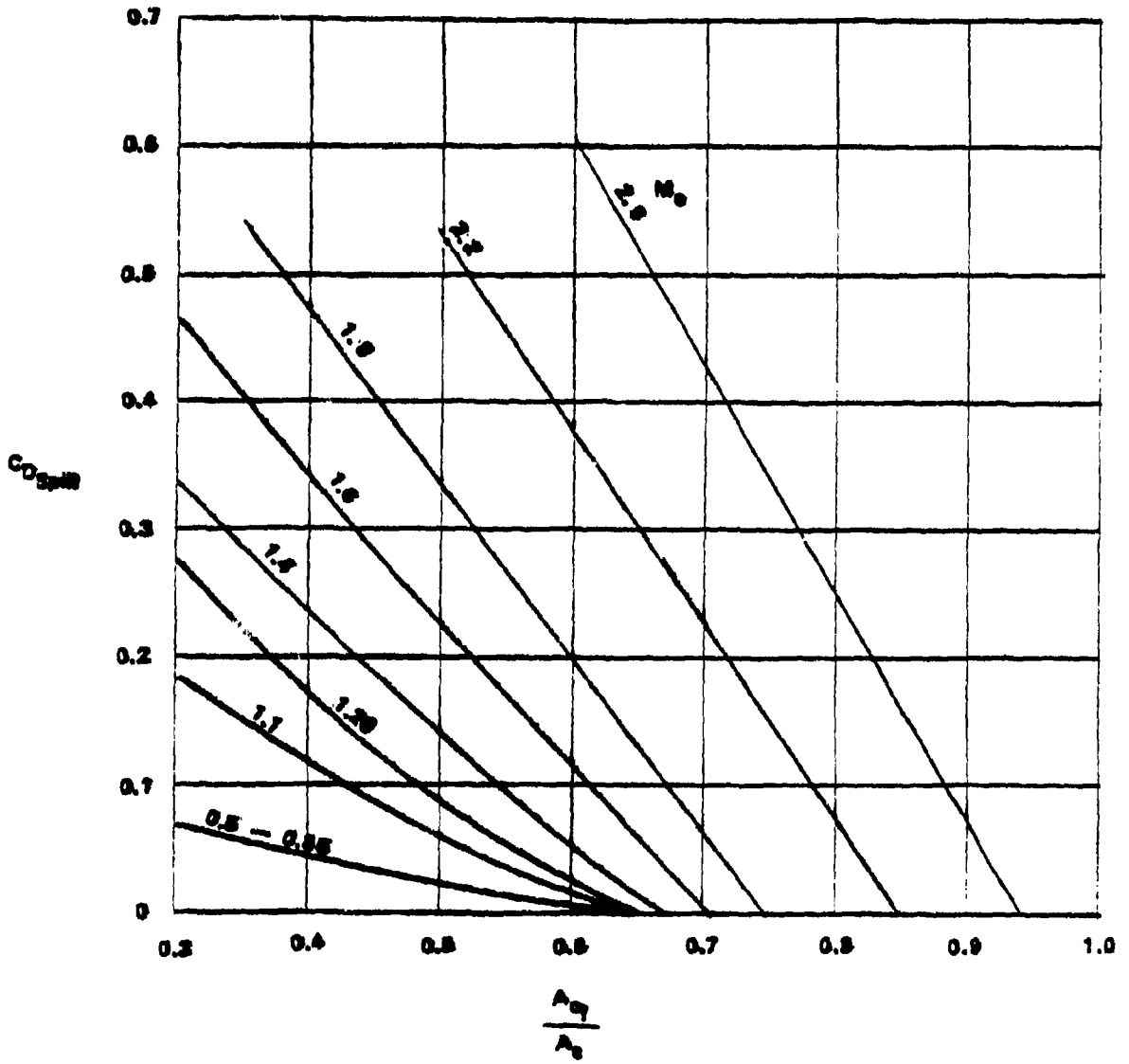

Figure 27. Performance Characteristics for Inlet Configuration #12 (continued)

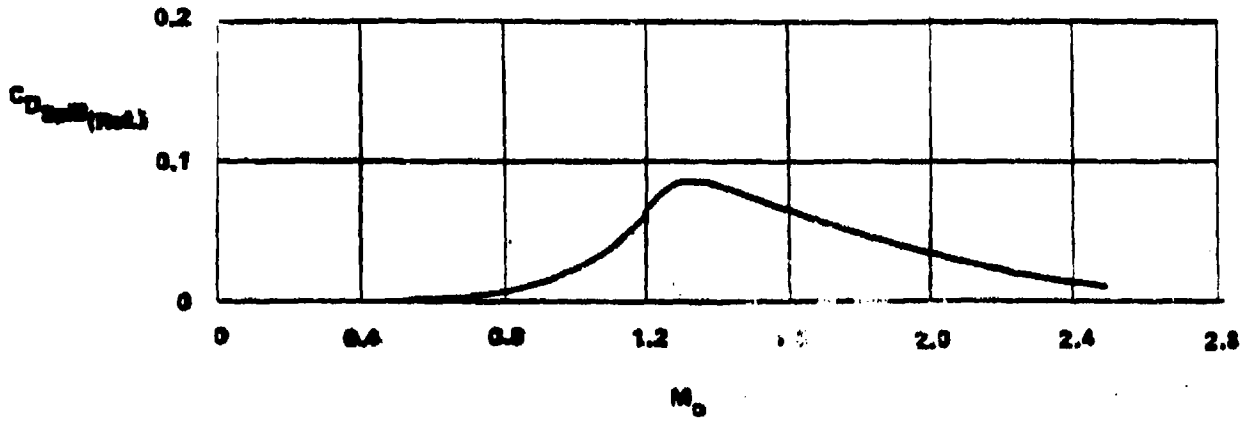

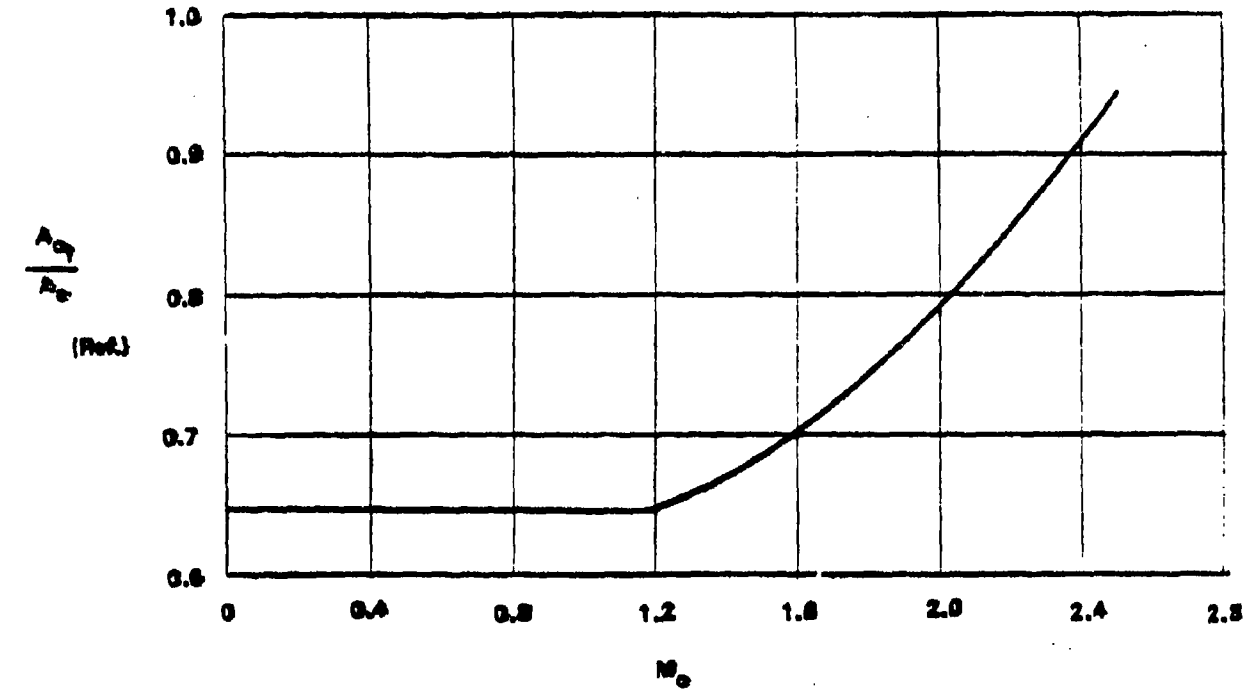

Figure 27. Performance Characteristics for Inlet Configuration #12 (continued)

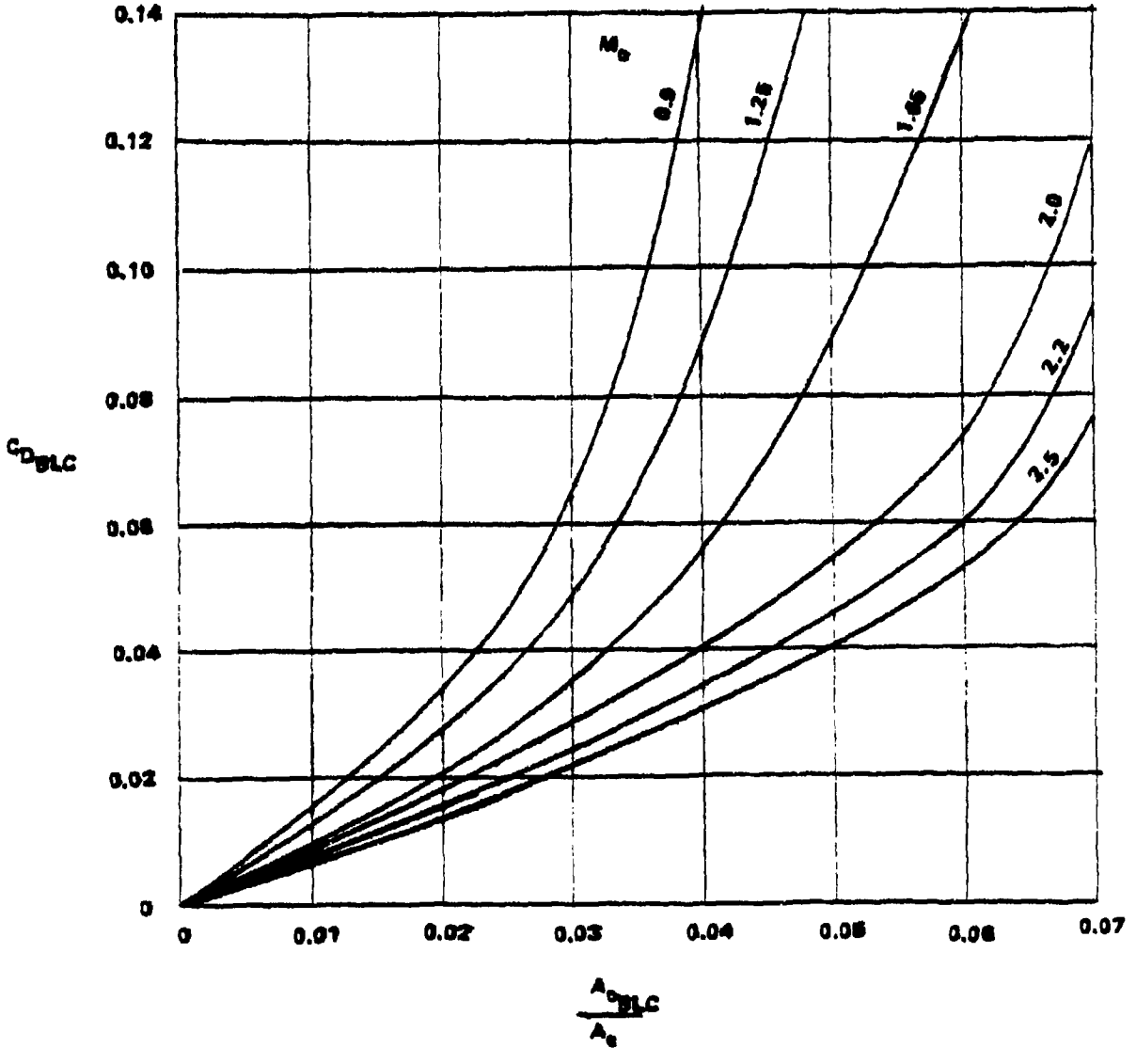

Figure 27. Performance Characteristics for Inlet Configuration #12 (continued)

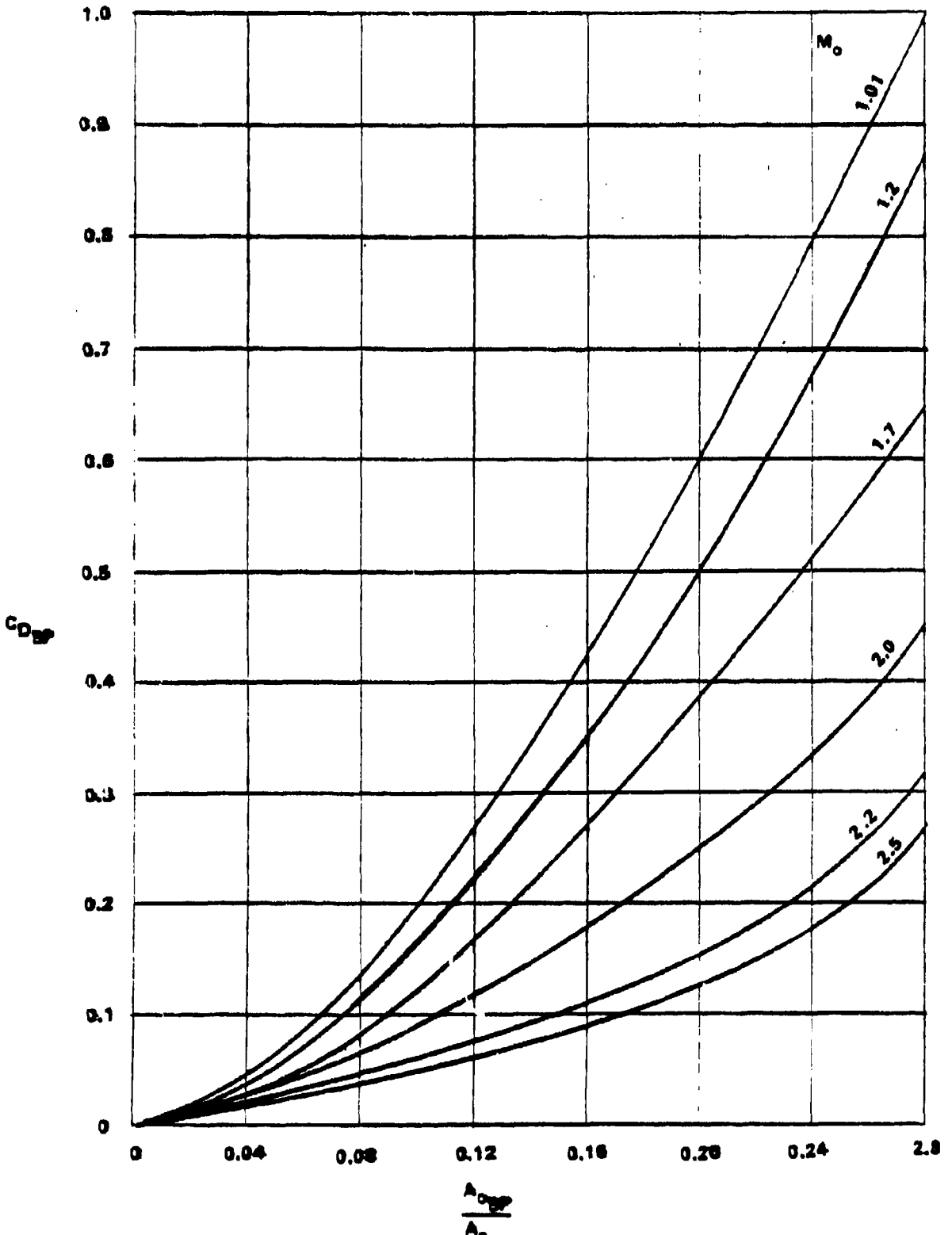

Figure 27. Performance Characteristics for Inlet Configuration #12 (continued)

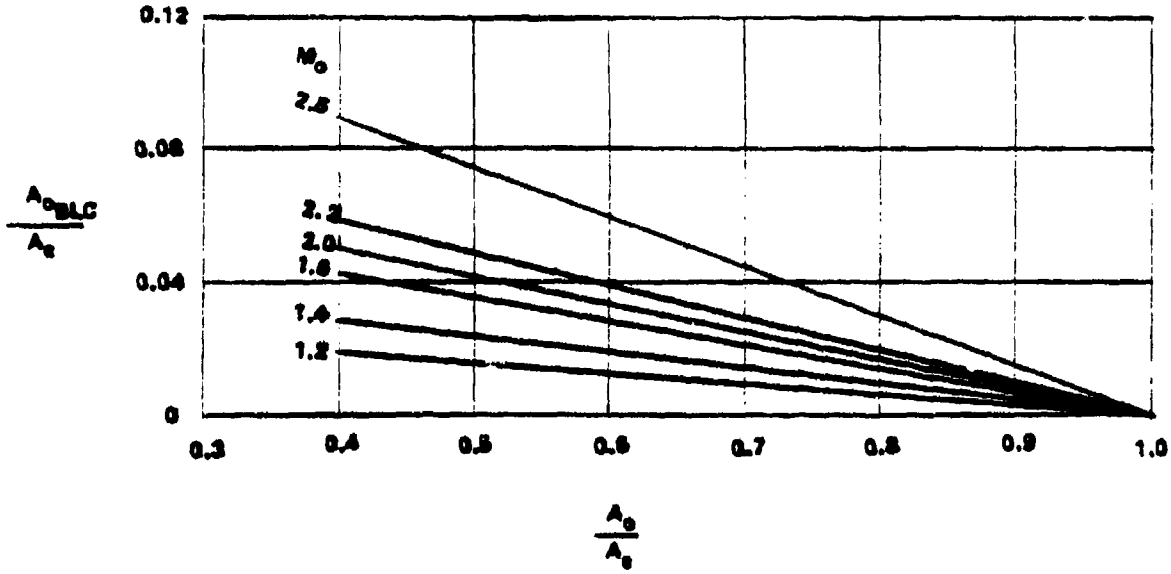

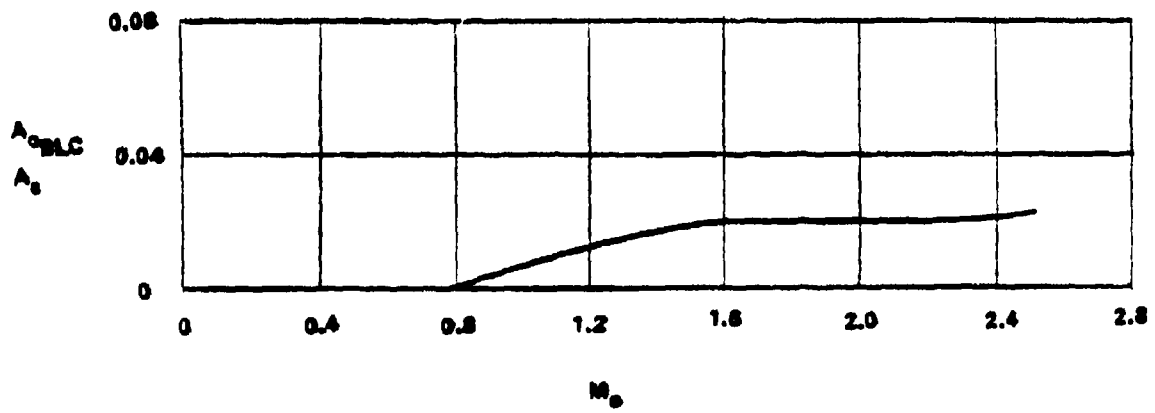

Figure 27. Performance Characteristics for Inlet Configuration #12 (continued)

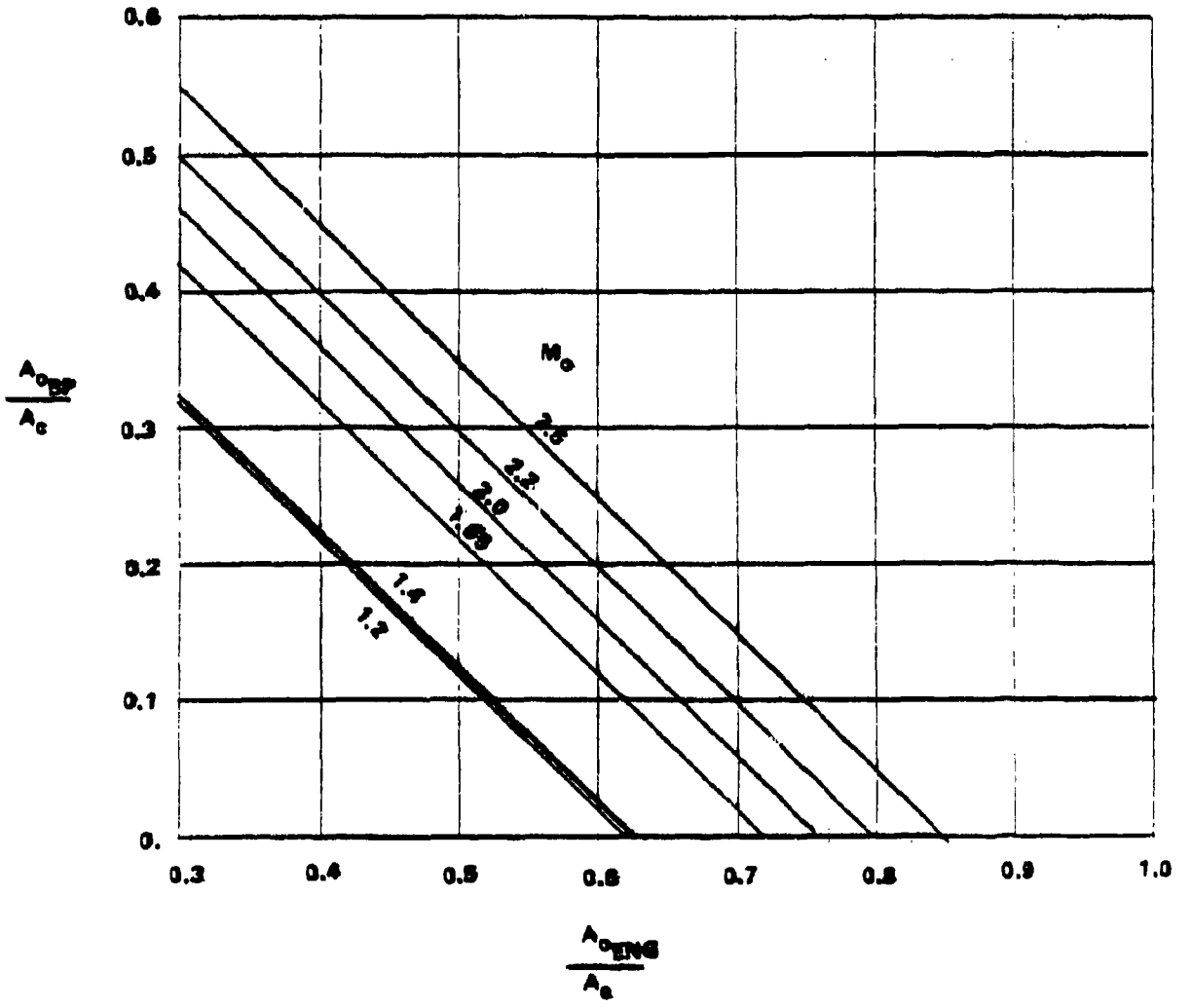

Figure 27. Performance Characteristics for Inlet Configuration #12 (concluded)

2.1.13 Inlet Configuration #13 - Mixed Compression, Two-Dimensional, Variable-Geometry Inlet

The mixed compression inlet is a suitable candidate for the fighter/bomber mission instead of an external compression inlet because it offers the potential for higher pressure recovery, lower drag, and better matching characteristics for the sustained Mach 2.5 high speed flight condition. Also, it does not have to meet the same requirements for extremely high maneuverability (high angles-of-attack), which would be difficult to control for the mixed compression inlet.

Boundary layer bleed is accomplished by use of porous ramps, cowl, and side-plates. Bleed air is collected in divided plenum chambers behind the porous walls and is then dumped overboard through choked convergent nozzles as near the plenum chamber as possible. Divided plenums are used to provide optimum bleed capability at lowest drag penalty. Movable ramp and throat panels are used to achieve the best inlet geometry over a wide range of flight Mach numbers.

A bypass system is also used to dump excess inlet air overboard and maintain the terminal shock in its design location just downstream of the geometric throat during started operation and just forward of the lip during external compression operation ($M < 2.0$). Bypass doors are assumed to be variable geometry C-D nozzles.

For takeoff and low speed operation, the ramp system is collapsed to provide a maximum throat area equal to $0.765A_C$. Takeoff doors having a throat area equal to $.12\ A_C$ per engine will also be required. These should be located near the aft end of the subsonic diffuser near the engine.

The ramp geometry was selected to provide shock on lip operation at Mach 2.60. This provides a small margin for angle-of-attack transients and overspeed at Mach 2.50.

The inlet performance characteristics are based largely on the results of a study documented in Reference 8. The inlet geometry is shown in Figure 28 and the inlet performance characteristics are presented in Figure 29.

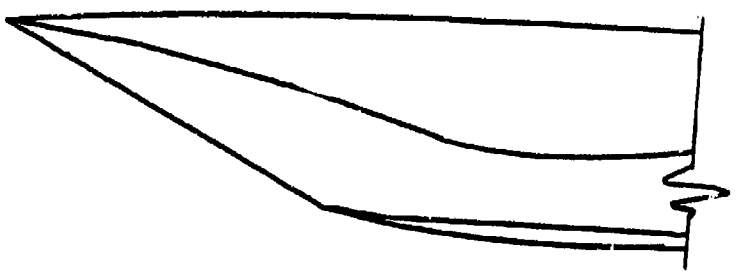

Figure 28. Mach 2.5 Mixed-Compression Two-Dimensional Inlet

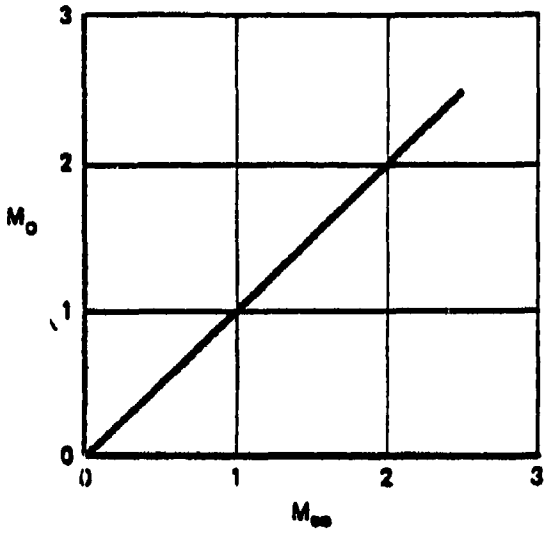

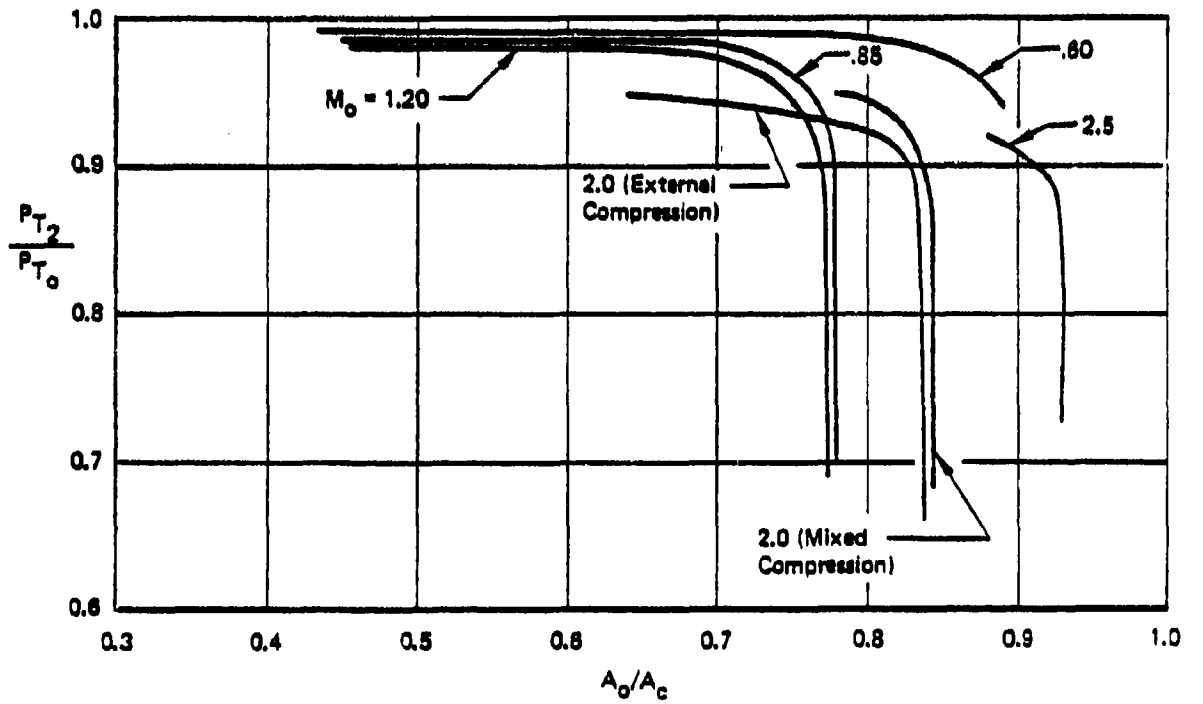

Figure 29. Performance Characteristics for Inlet Configuration #13

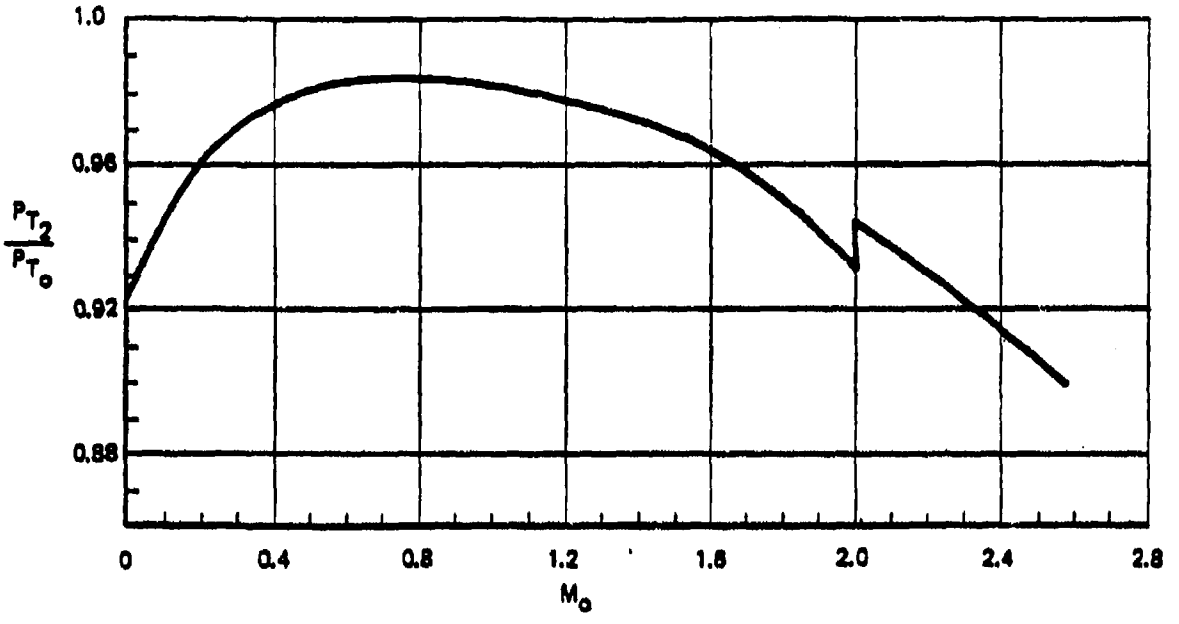

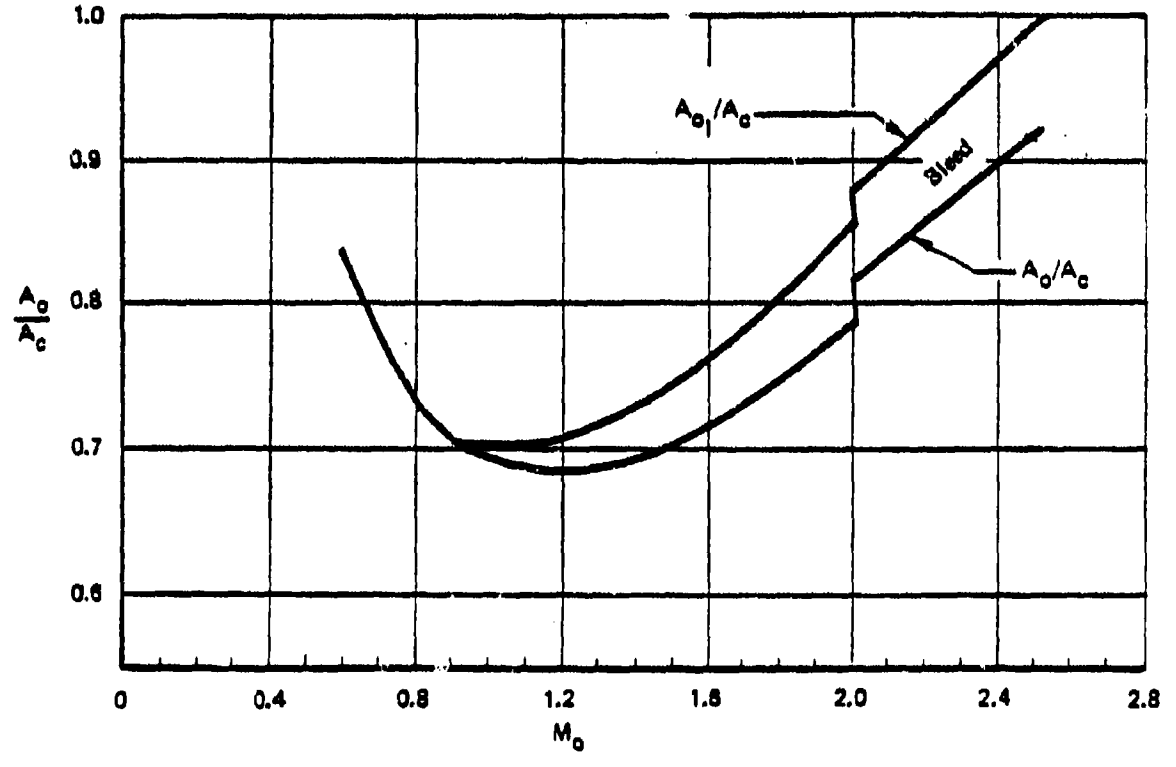

Figure 29. Performance Characteristics for Inlet Configuration #13 (continued)

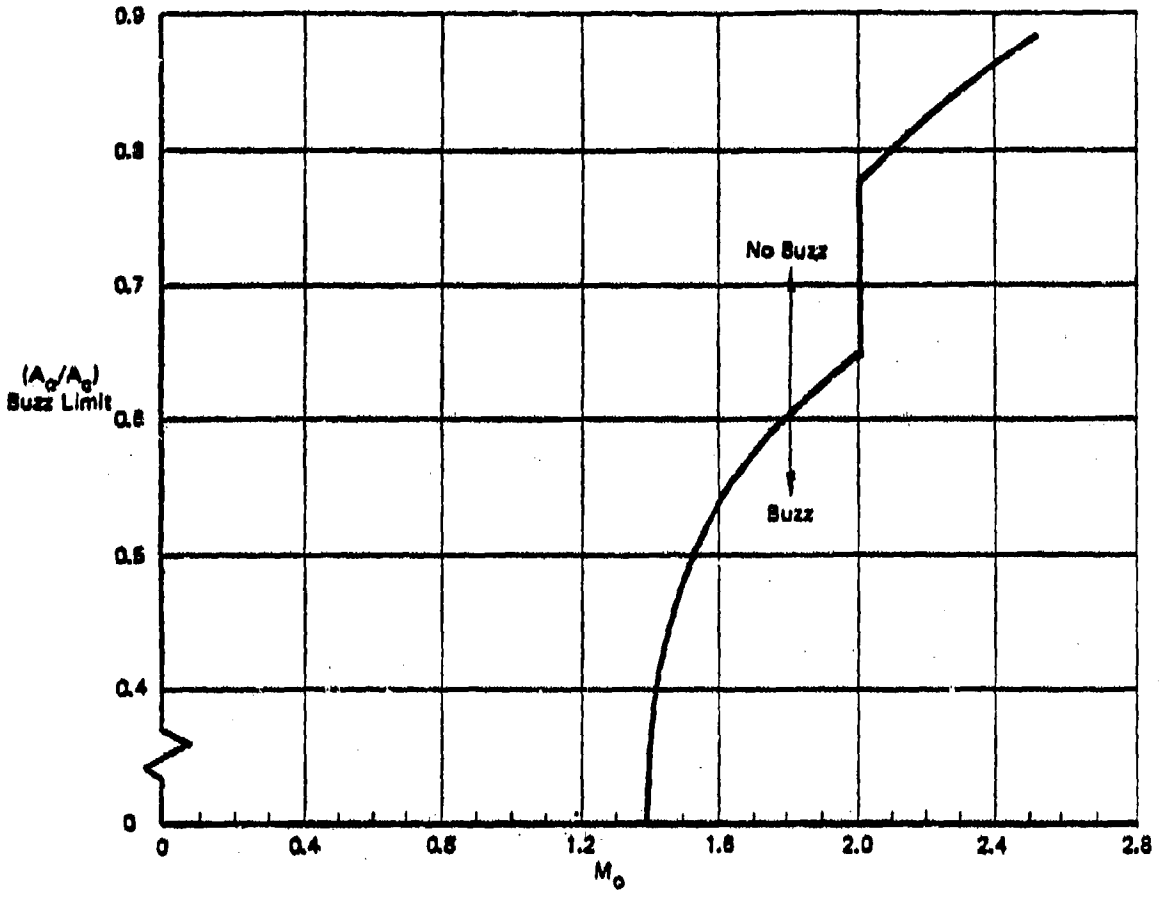

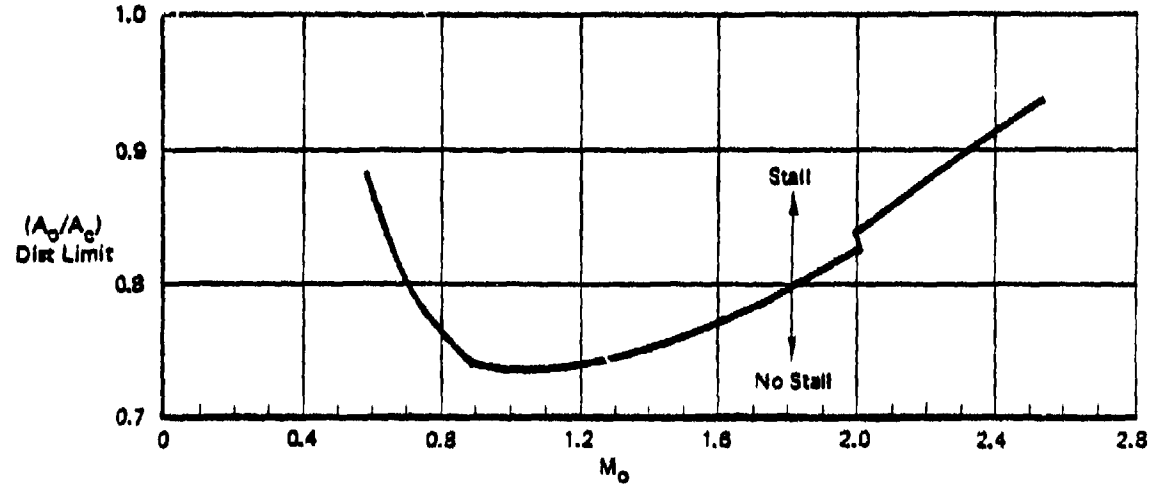

Figure 29. Performance Characteristics for Inlet Configuration #13 (continued)

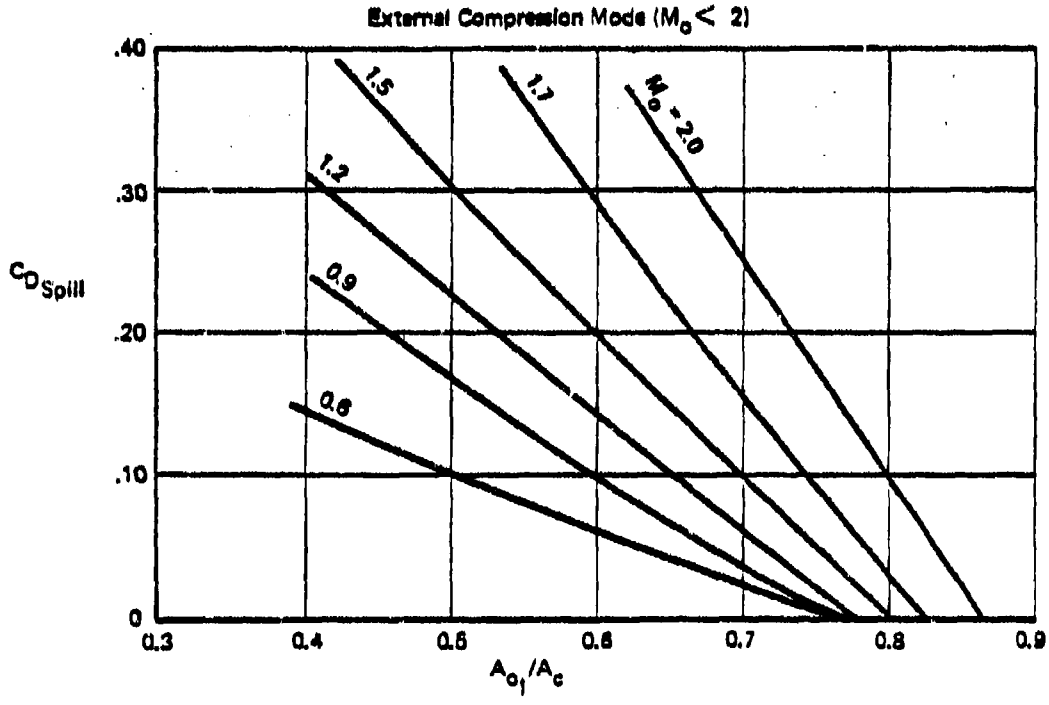

Figure 29. Performance Characteristics for Inlet Configuration #13 (continued)

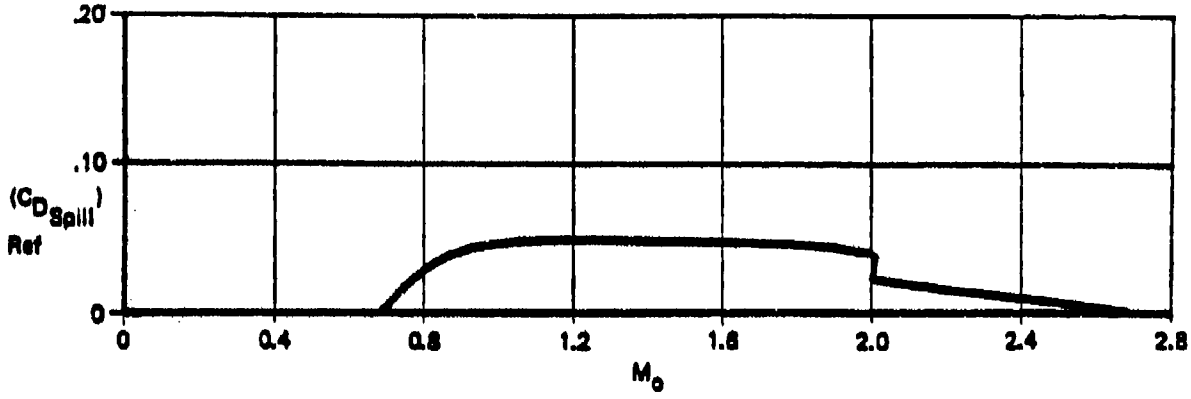

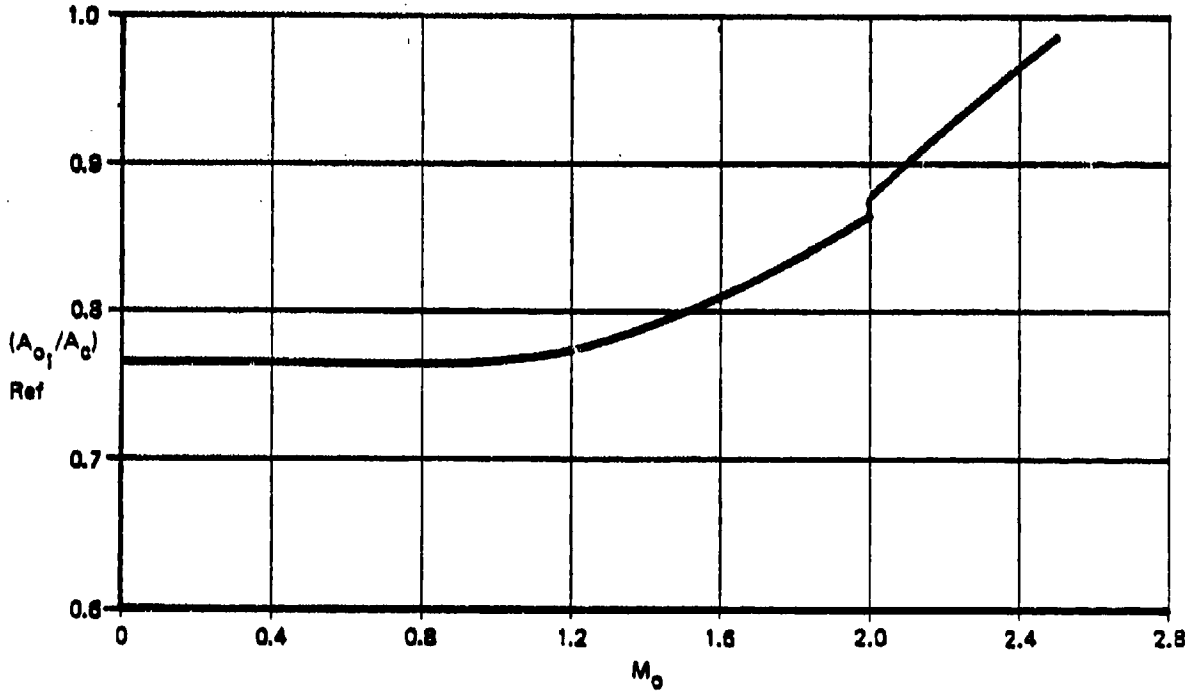

Figure 29. Performance Characteristics for Inlet Configuration #13 (continued)

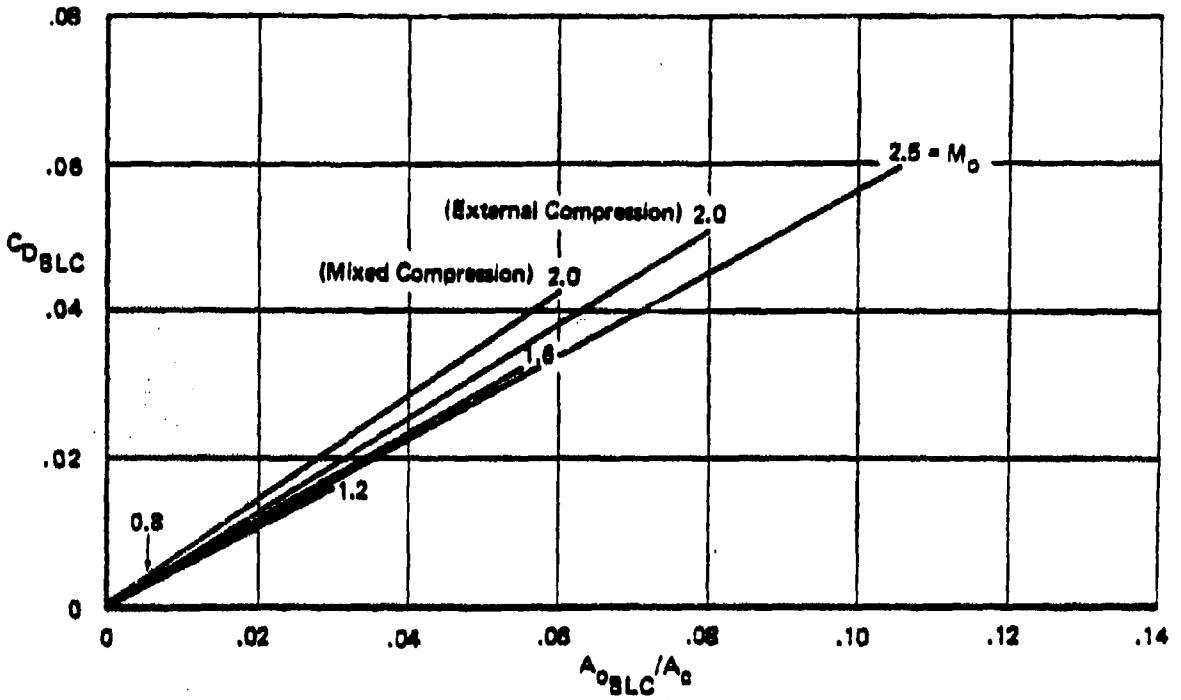

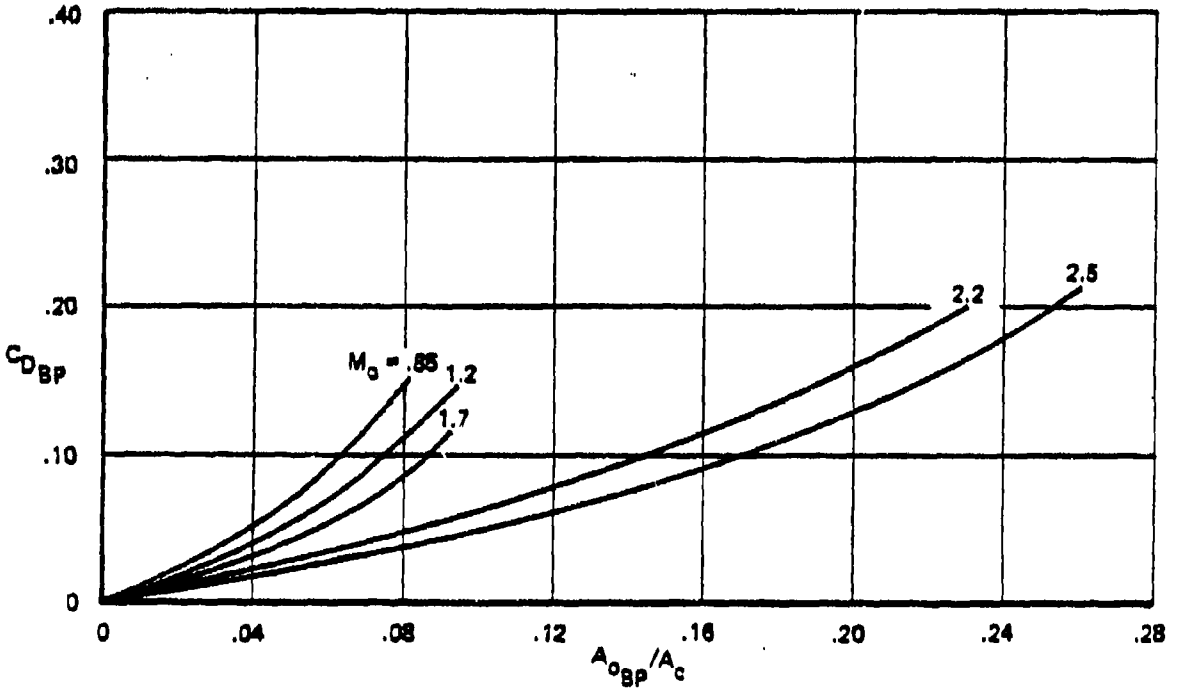

Figure 29. Performance Characteristics for Inlet Configuration #13 (continued)

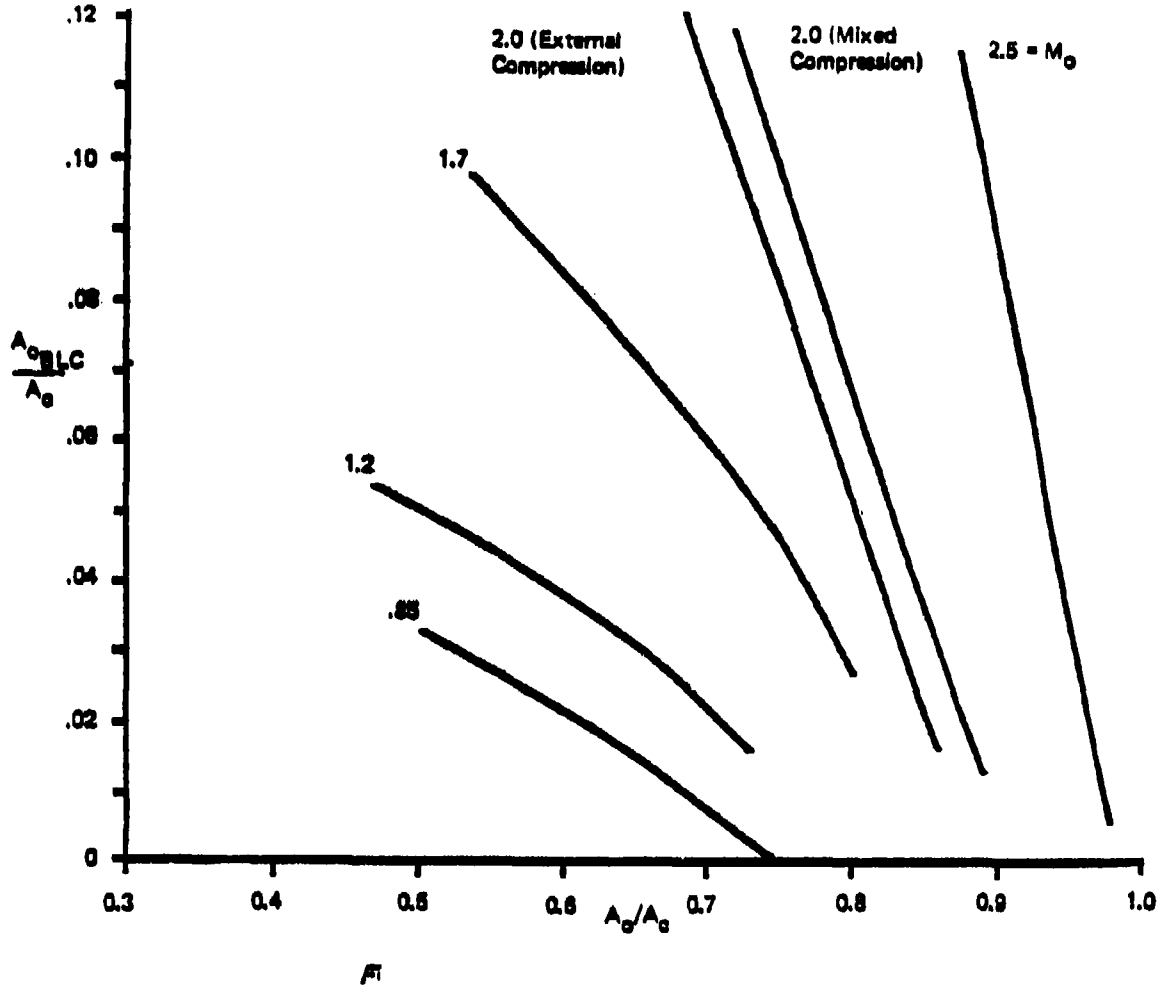

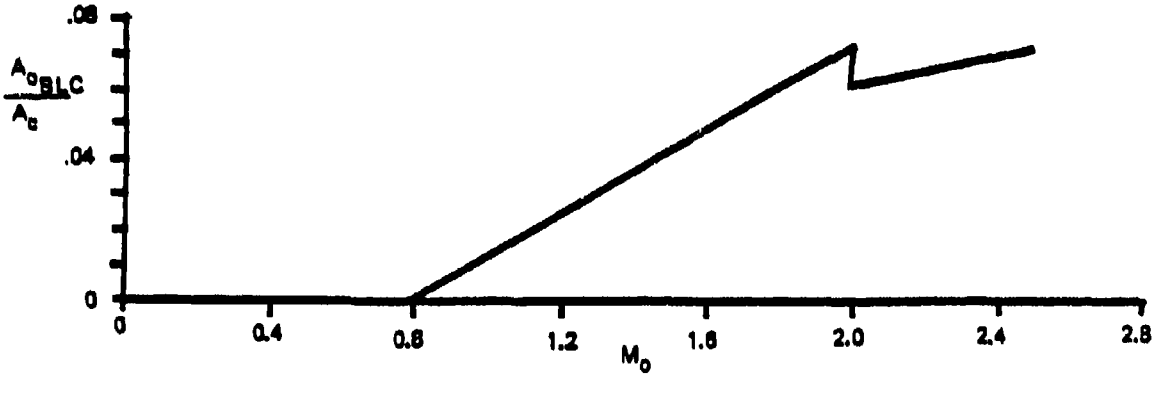

Figure 29. Performance Characteristics for Inlet Configuration #13 (continued)

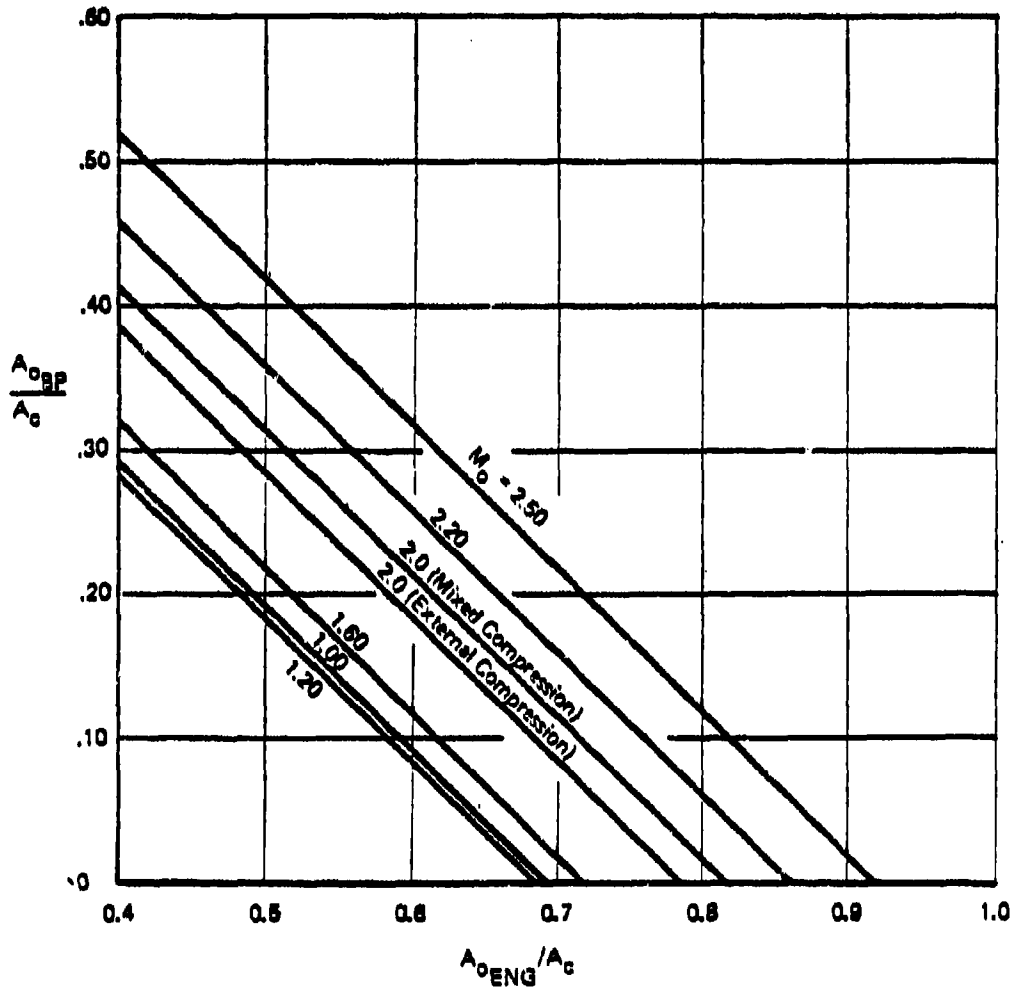

Figure 29. Performance Characteristics for Inlet Configuration #13 (concluded)

2.1.14 Inlet Configuration #14 - Mixed Compression, Variable-Geometry, Two-Dimensional Inlet

The inlet is a mixed-compression type, with inlet "starting" occurring at Mach 2.0. Below Mach 2.0, the inlet operates in the external compression mode. Extensive boundary layer bleed is used on the inlet internal ramps, sideplates, and cowl to avoid problems with shock-boundary layer interactions. Three separate plenum chambers are used for collecting the boundary layer bleed air before it is exited overboard through choked convergent exit nozzles. The use of three separate plenums makes it possible to operate with a relatively high plenum pressure and hence, less drag.

The inlet ramp system is designed to provide shock-on-lip operation at Mach 3.0. Approximately 1% supersonic spillage is allowed to help insure that shocks are not ingested at inadvertent overspeed conditions or transient angle-of-attack maneuvers. Full sideplates are provided to minimize sideplate spillage.

A variable bypass sytem is provided ahead of the engine to bypass excess inlet airflow and help restart the inlet. The maximum bypass door throat area is 0.50 A_C. It is assumed that a maximum inlet throat area equal to at least 0.70 A_C can be achieved by retracting the ramps. The requirement for takeoff doors to provide good recovery and low distortion during takeoff can be examined when engine airflow demand characteristics are known.

The total pressure recovery versus mass flow plots have been estimated by using the test results from XB-70, (Reference 9), SST, Boeing in-house studies and tests, and theory. The inlet geometry is shown in Figure 30 and the inlet performance characteristics are presented in Figure 31.

Figure 30. Mach 3.0 Mixed-Compression Two-Dimensional Inlet

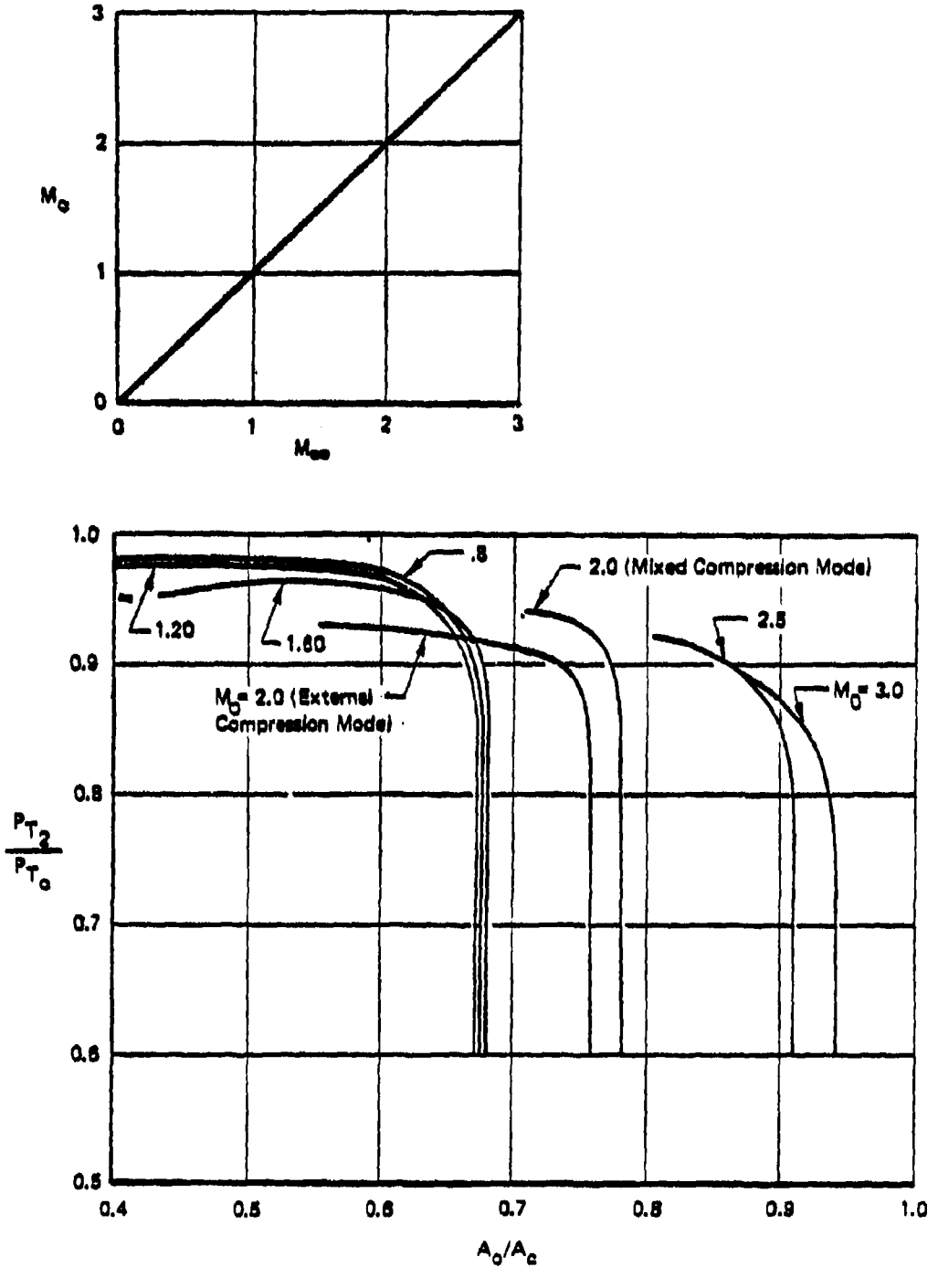

Figure 31. Performance Characteristics for Inlet Configuration #14

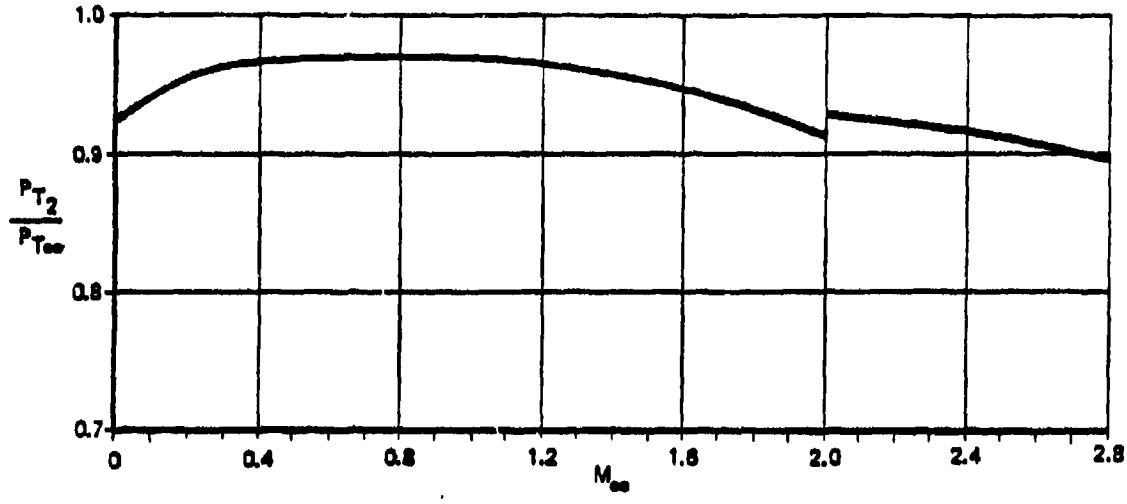

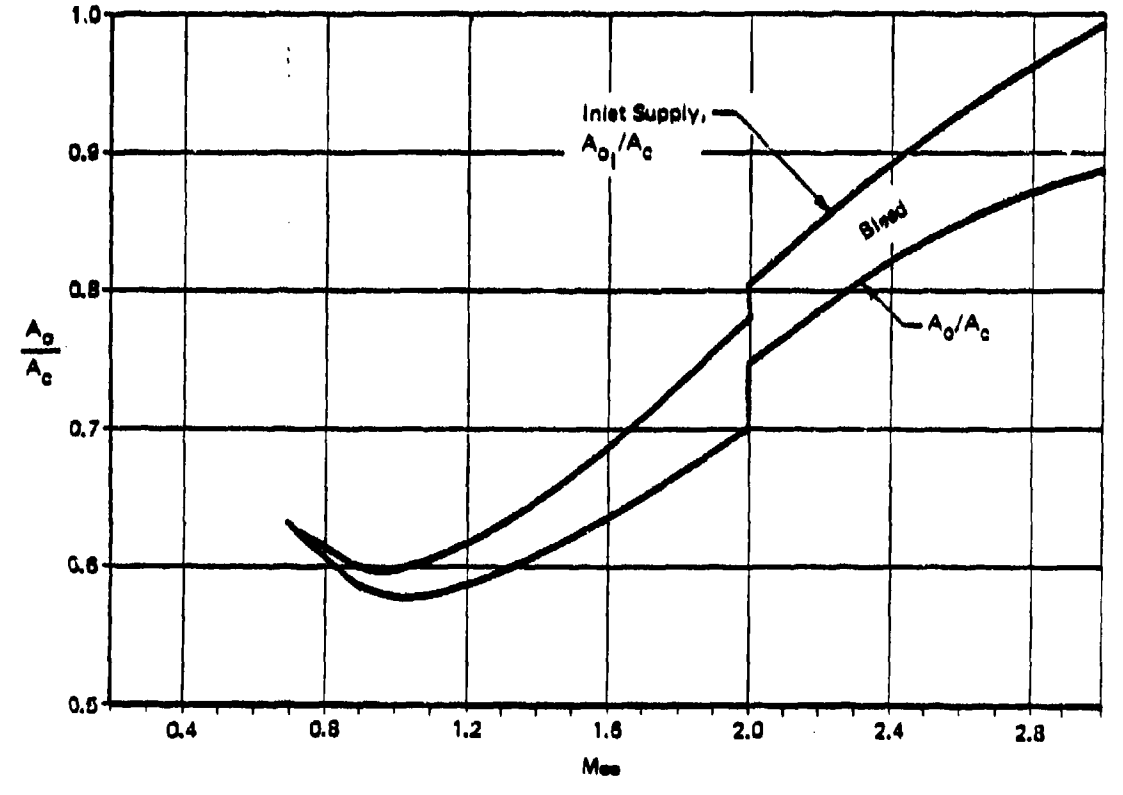

Figure 31. Performance Characteristics for Inlet Configuration #14 (continued)

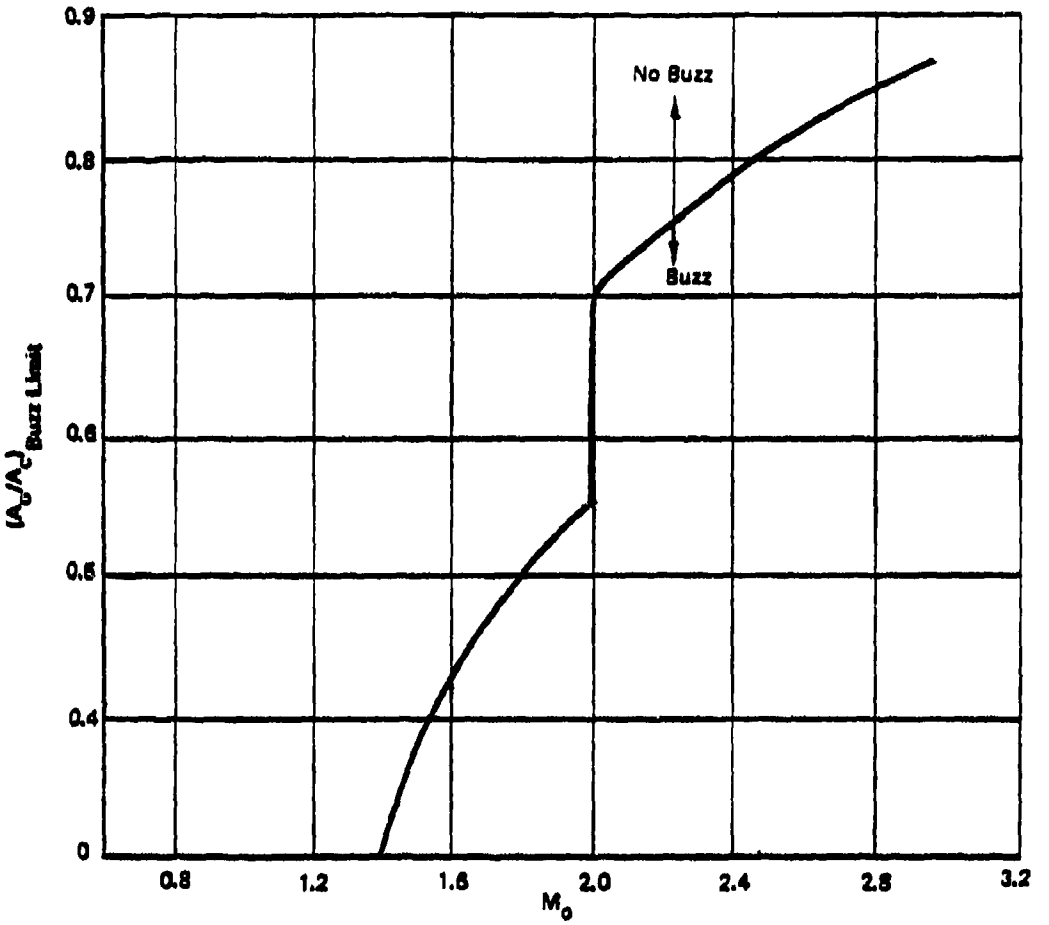

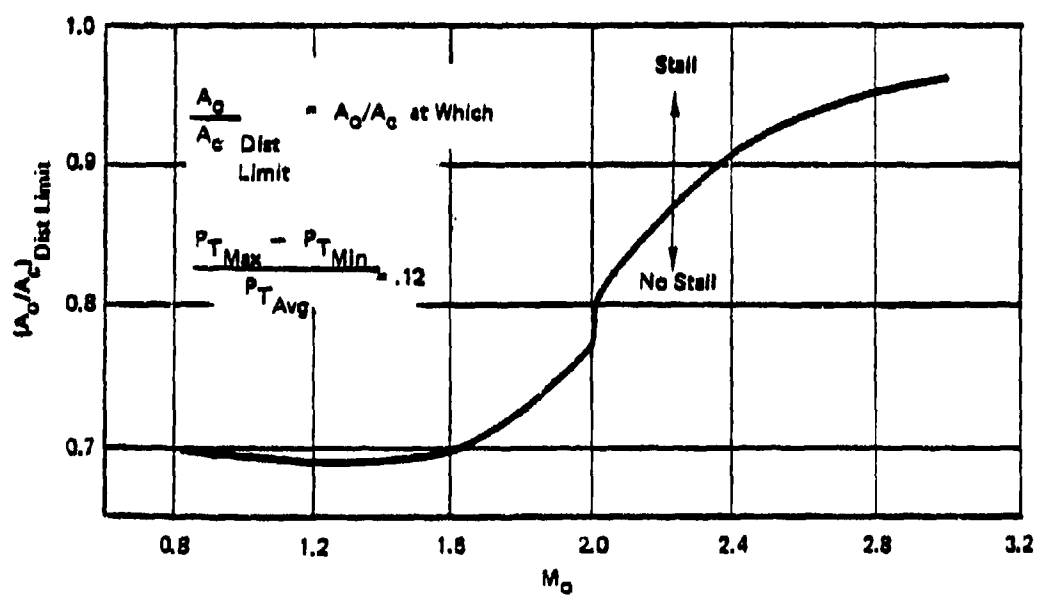

Figure 31. Performance Characteristics for Inlet Configuration #14 (continued)

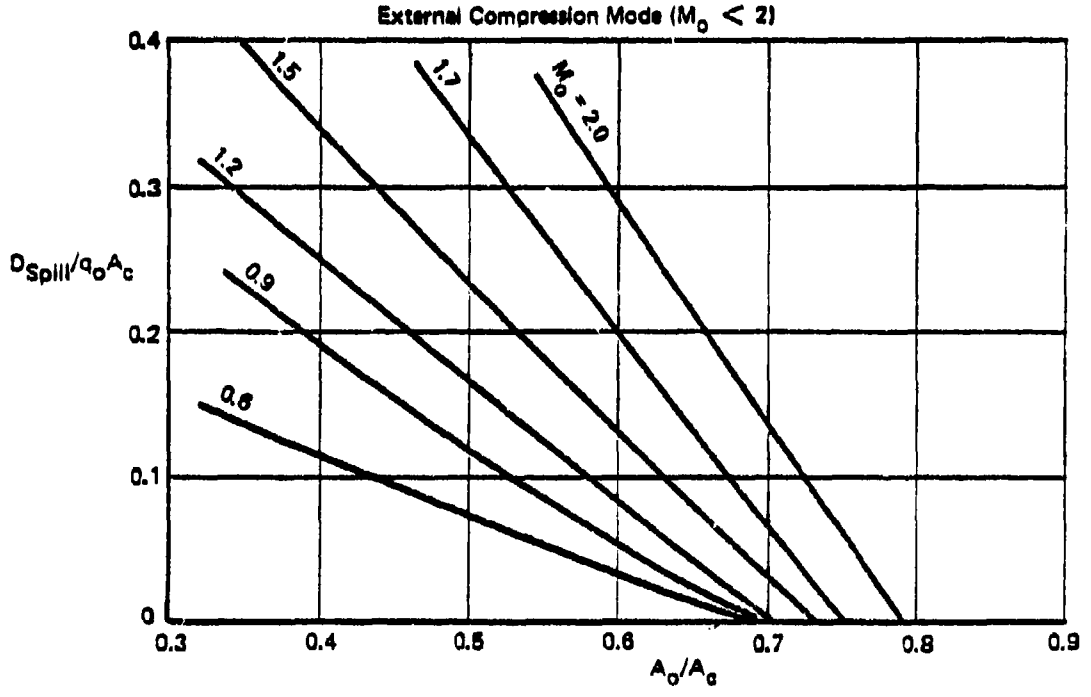

Figure 31. Performance Characteristics for Inlet Configuration #14 (continued)

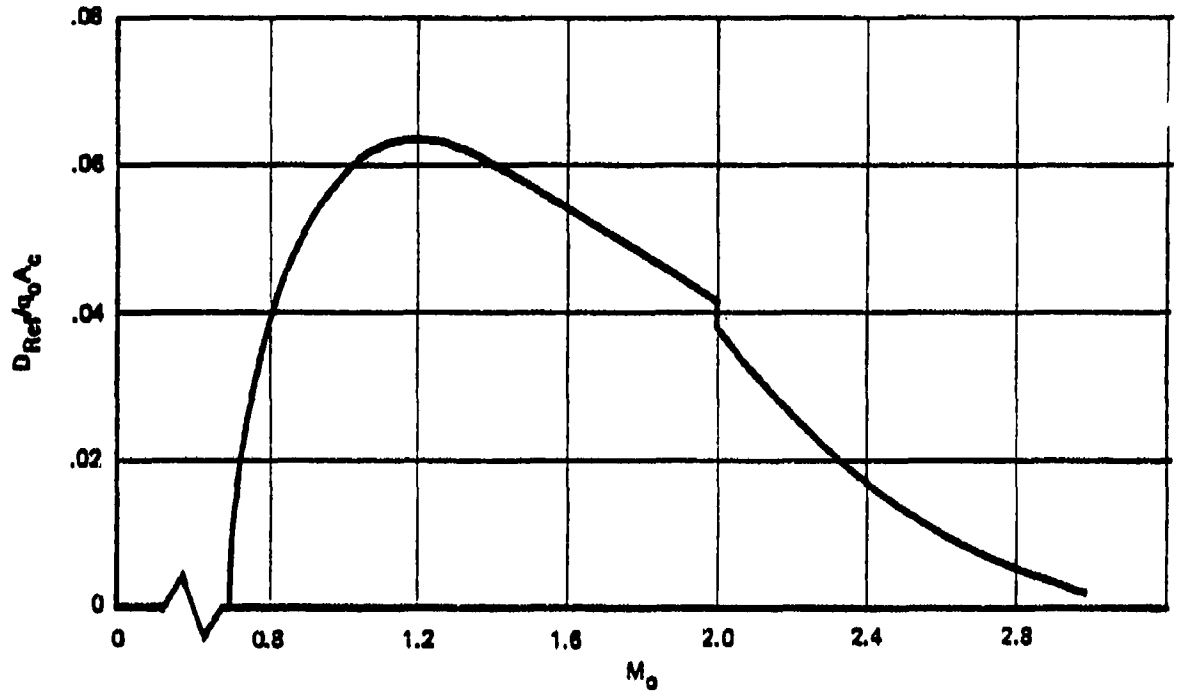

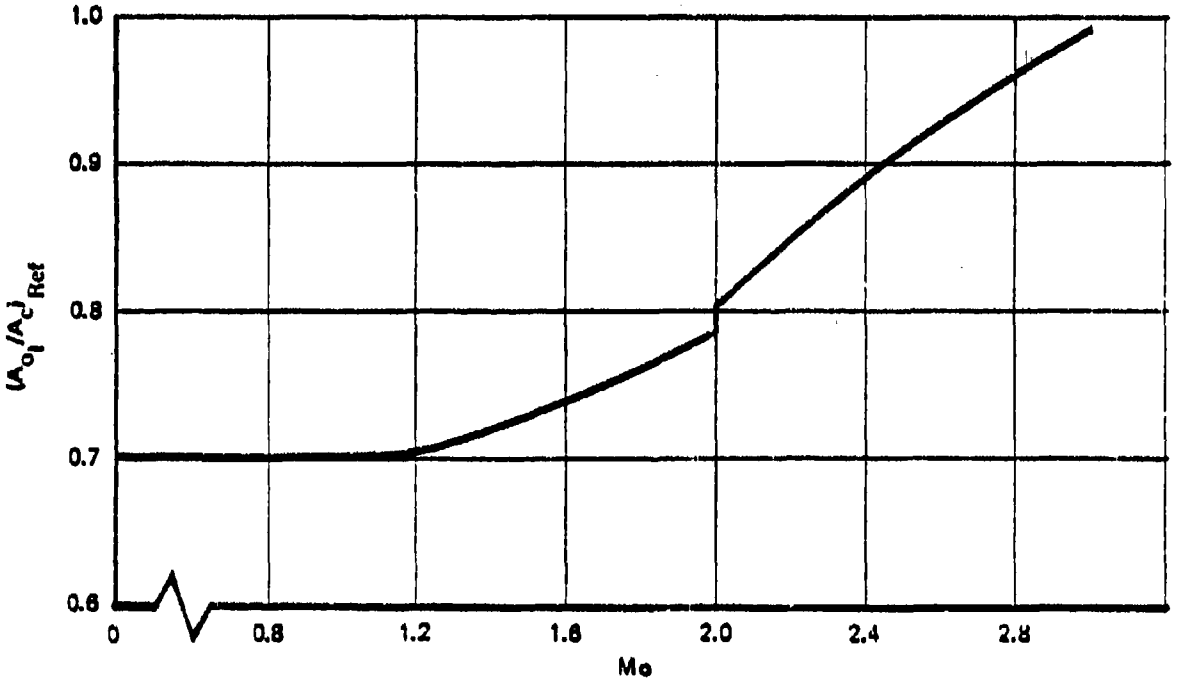

Figure 31. Performance Characteristics for Inlet Configuration #14 (continued)

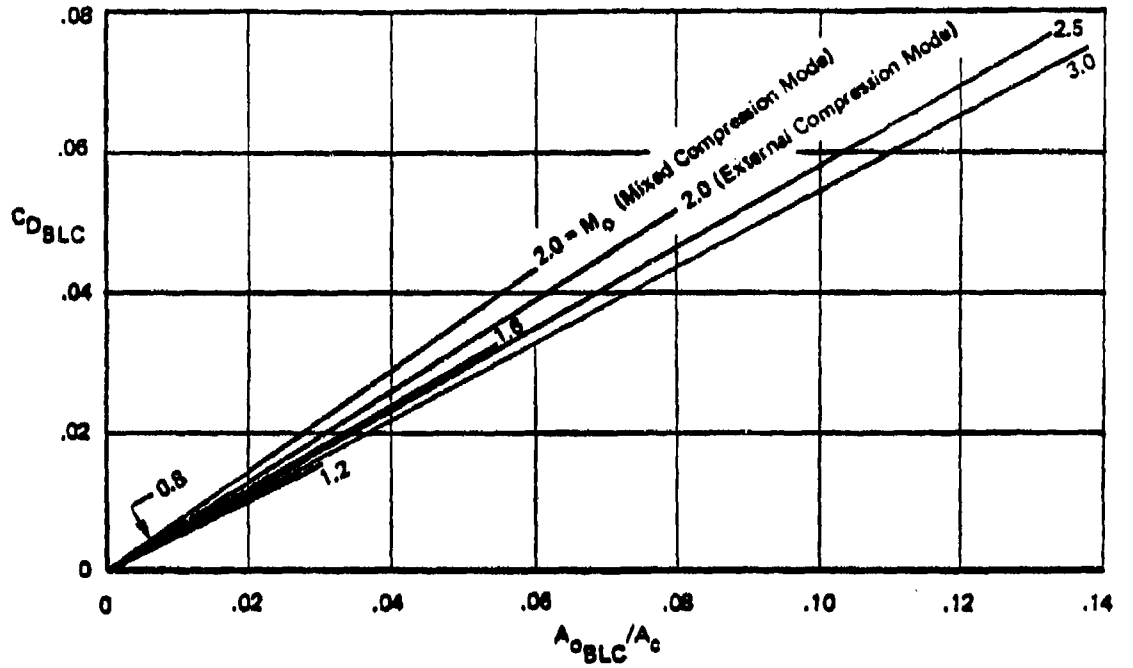

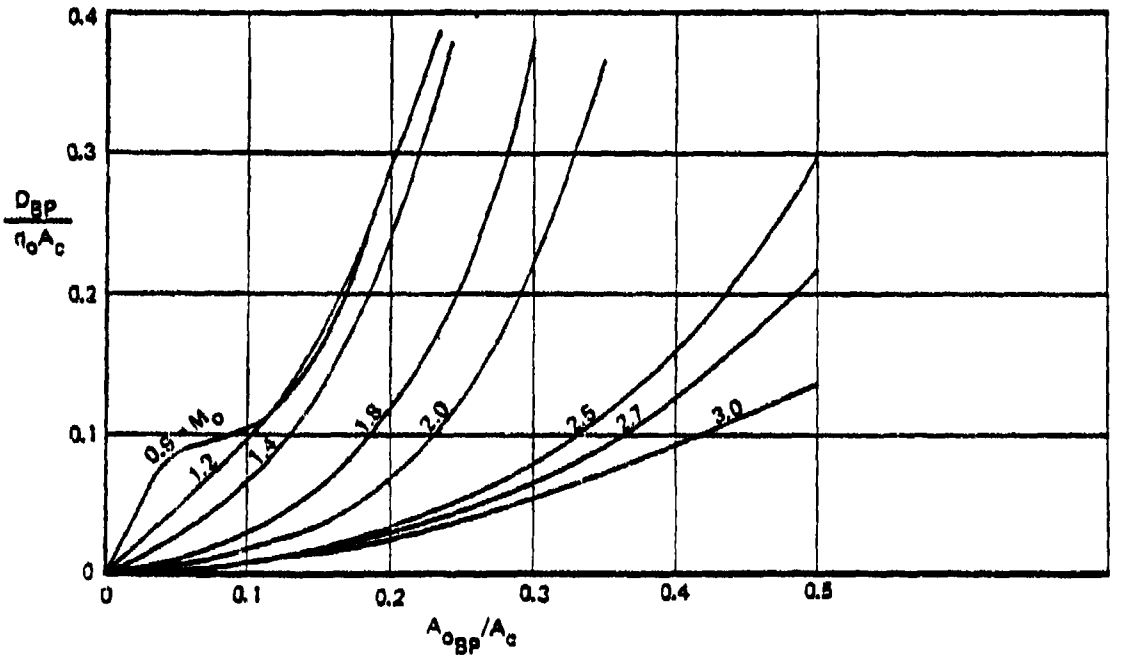

Figure 31. Performance Characteristics for Inlet Configuration #14 (continued)

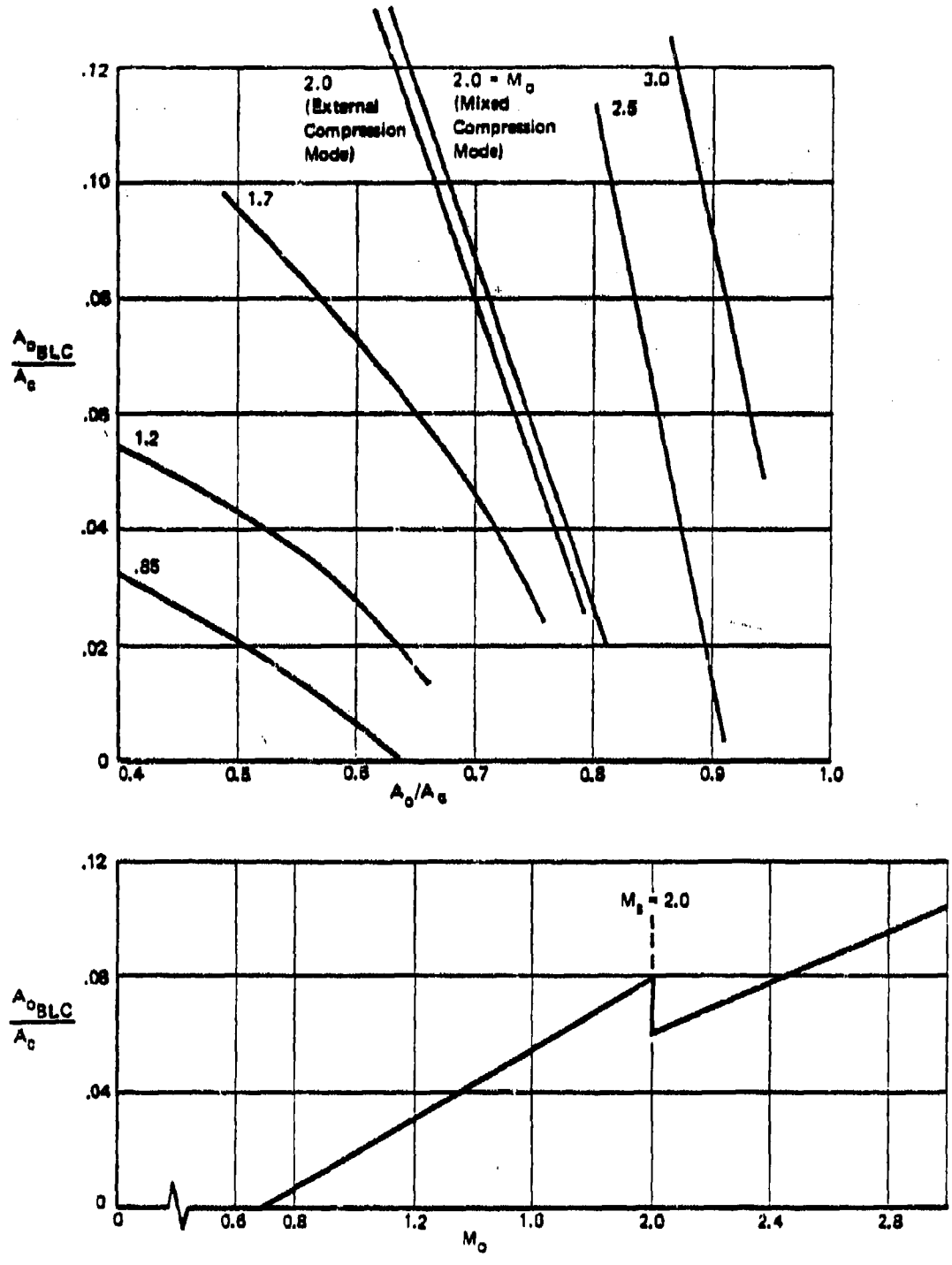

Figure 31. Performance Characteristics for Inlet Configuration #14 (continued)

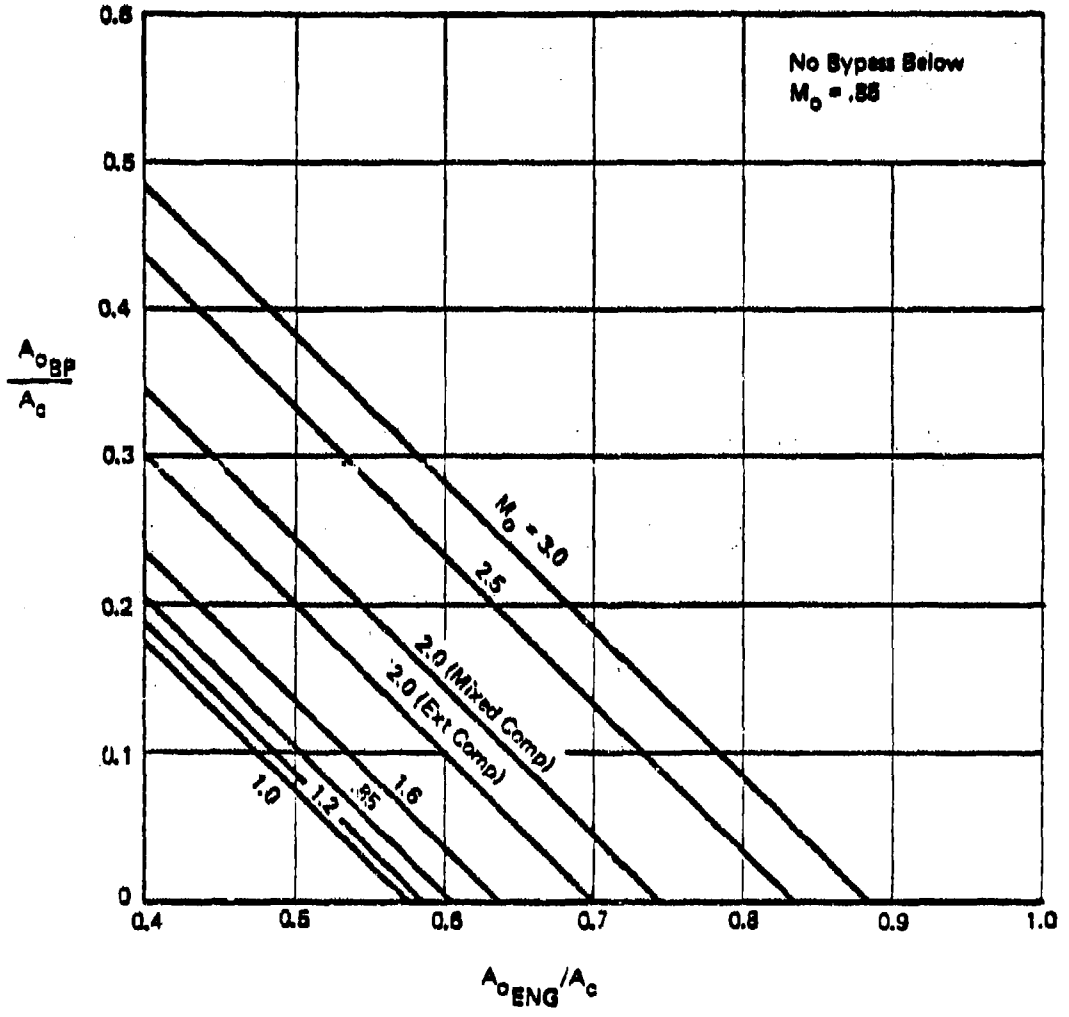

Figure 31. Performance Characteristics for Inlet Configuration #14 (concluded)

2.1.15 Inlet Configuration #15 - Mixed Compression, Variable-Geometry, Two-Dimensional Inlet

The initial ramp surface angle is fixed at 7^{o}. Boundary layer bleed is collected in three divided plenum chambers.

The inlet performance characteristics for this configuration are based on the data contained in Reference 10 and engineering analysis. The geometry of the inlet is shown in Figure 32 and the inlet performance characteristics are presented in Figure 33.

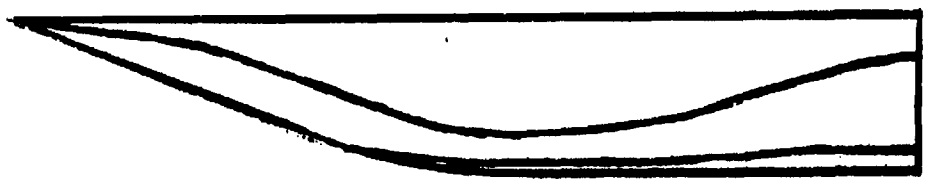

Figure 32. Mach 3.5 Two-Dimensional Mixed-Compression Inlet

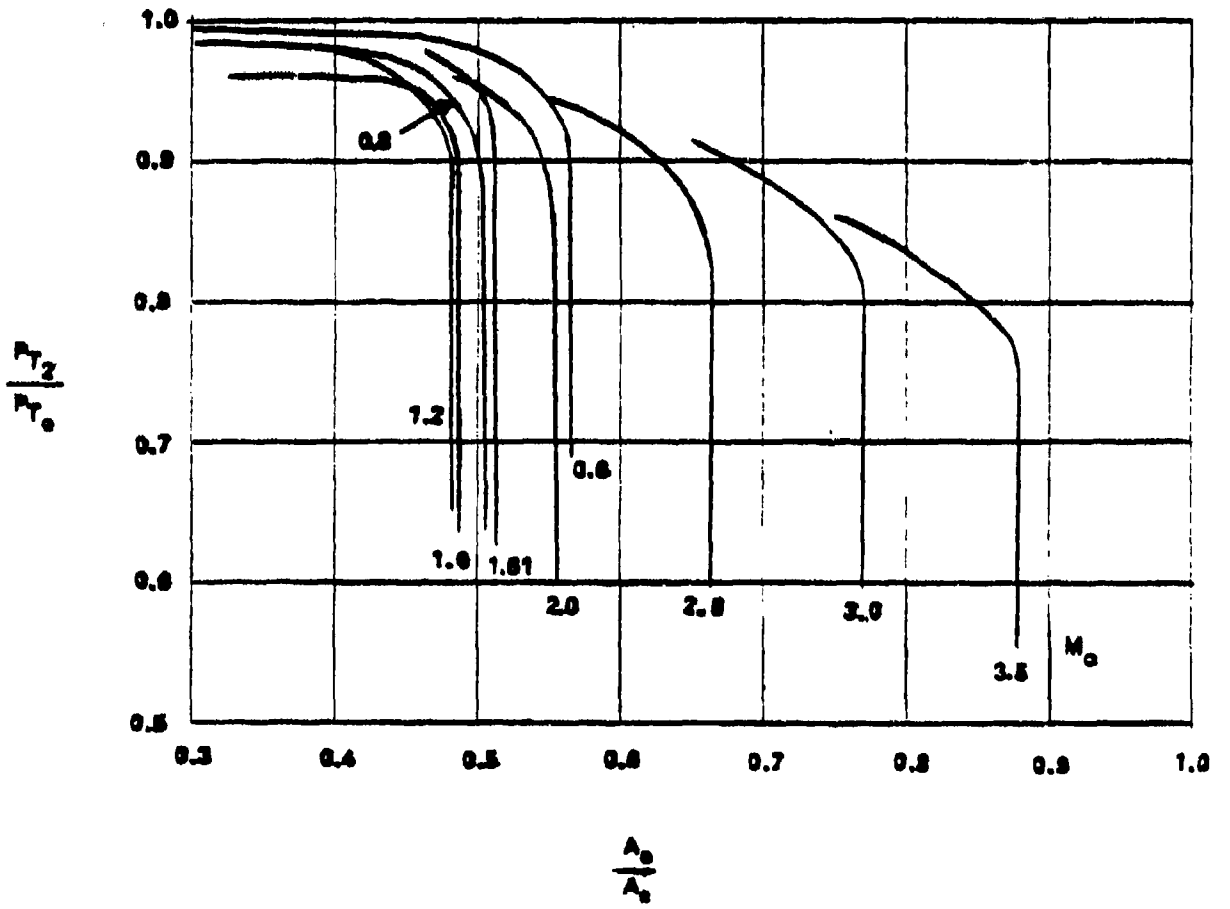

Figure 33. Performance Characteristics for Inlet Configuration #15

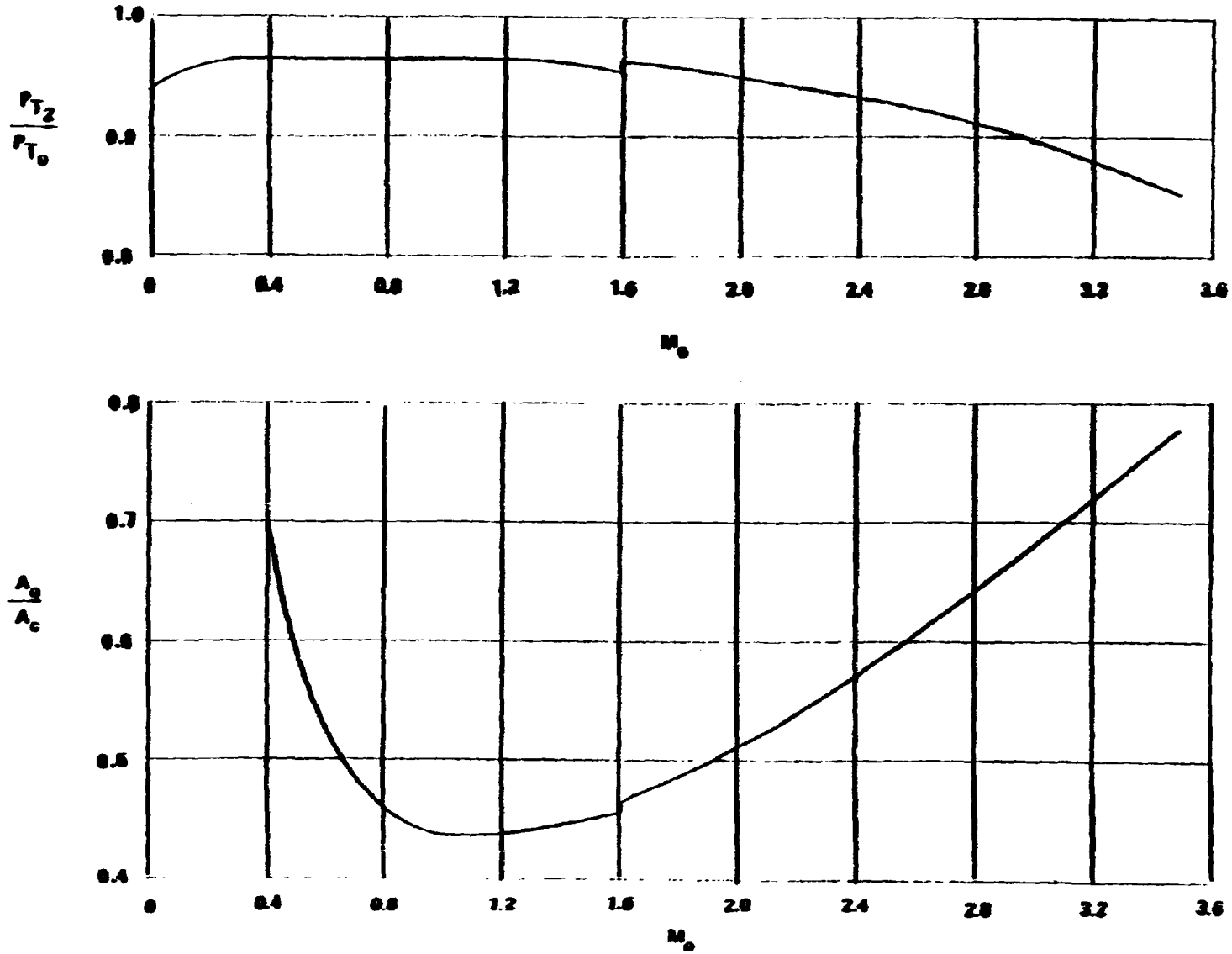

Figure 33. Performance Characteristics for Inlet Configuration #15 (continued)

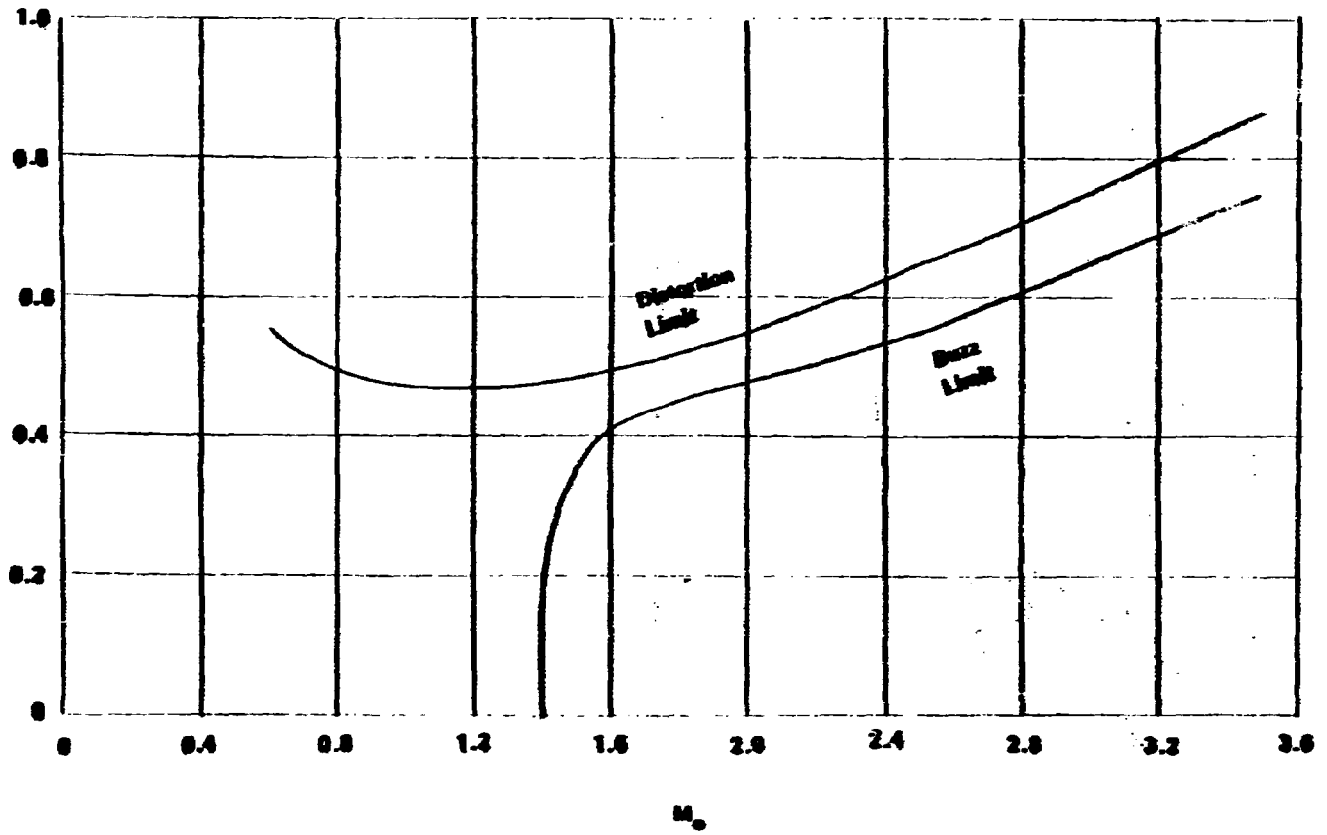

Figure 33. Performance Characteristics for Inlet Configuration #15 (continued)

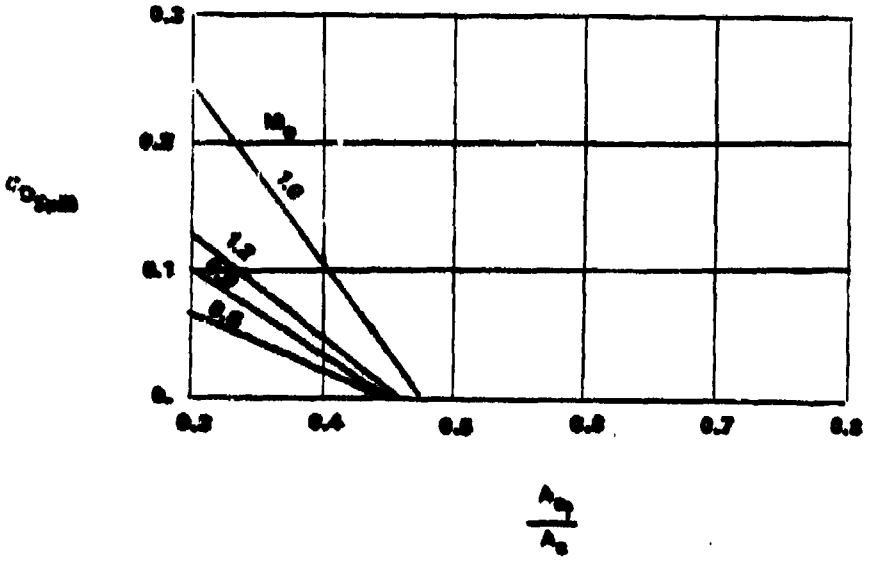

Figure 33. Performance Characteristics for Inlet Configuration #15 (continued)

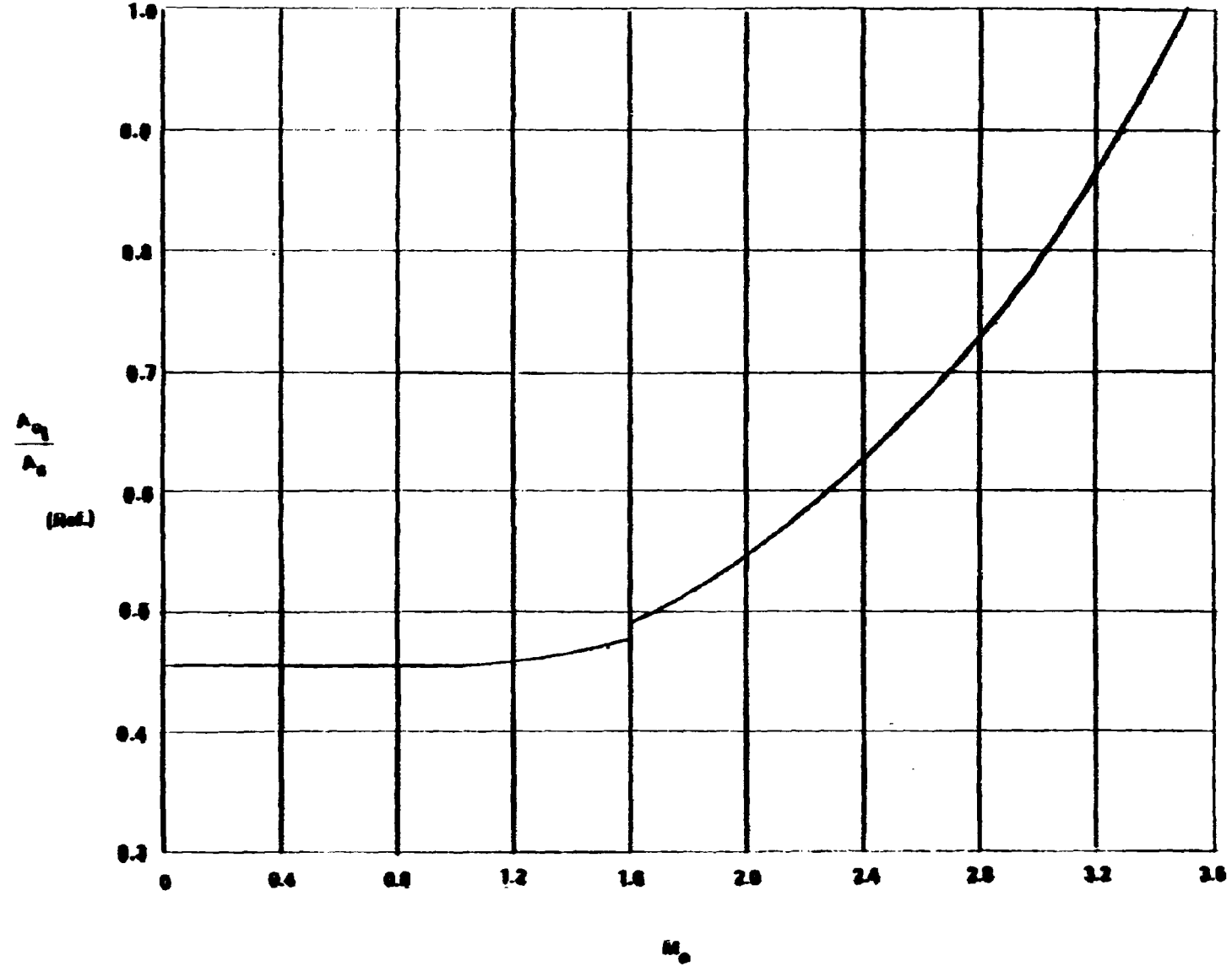

Figure 33. Performance Characteristics for Inlet Configuration #15 (continued)

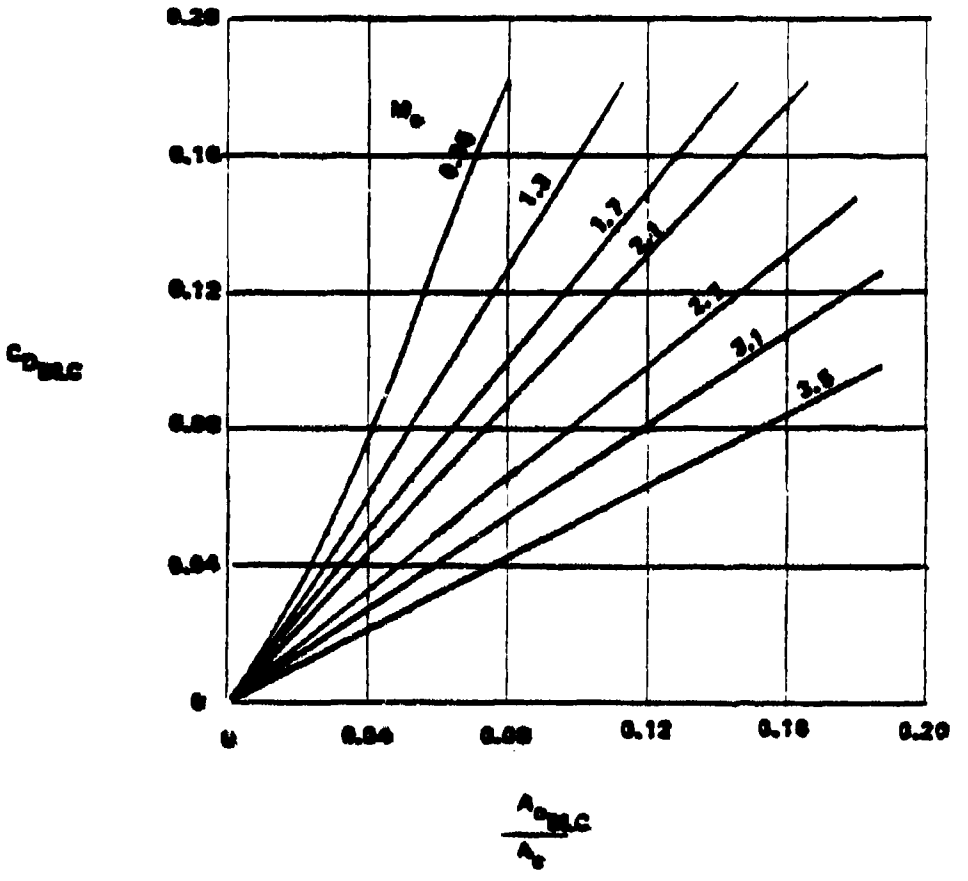

Figure 33. Performance Characteristics for Inlet Configuration #15 (continued)

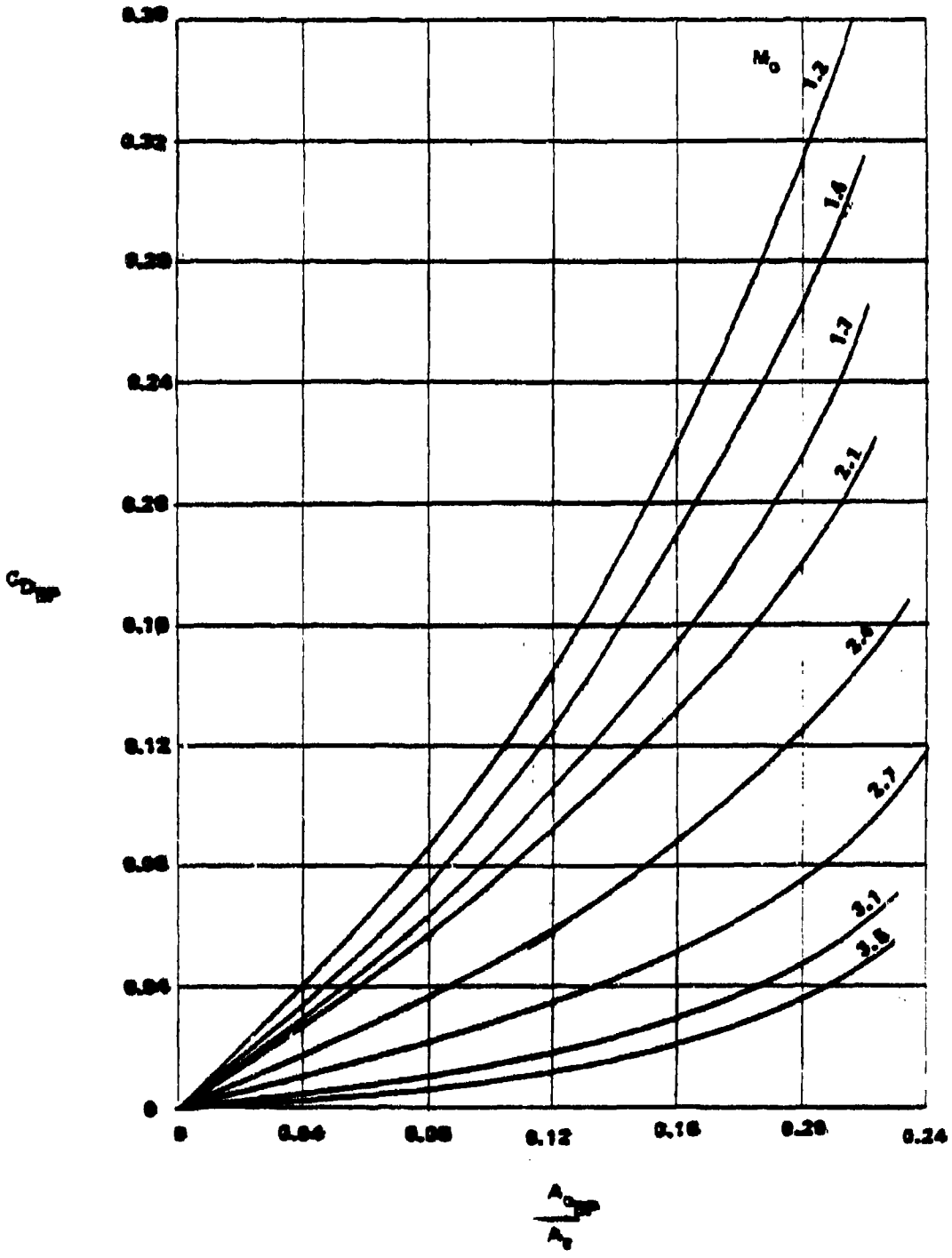

Figure 33. Performance Characteristics for Inlet Configuration #15 (continued)

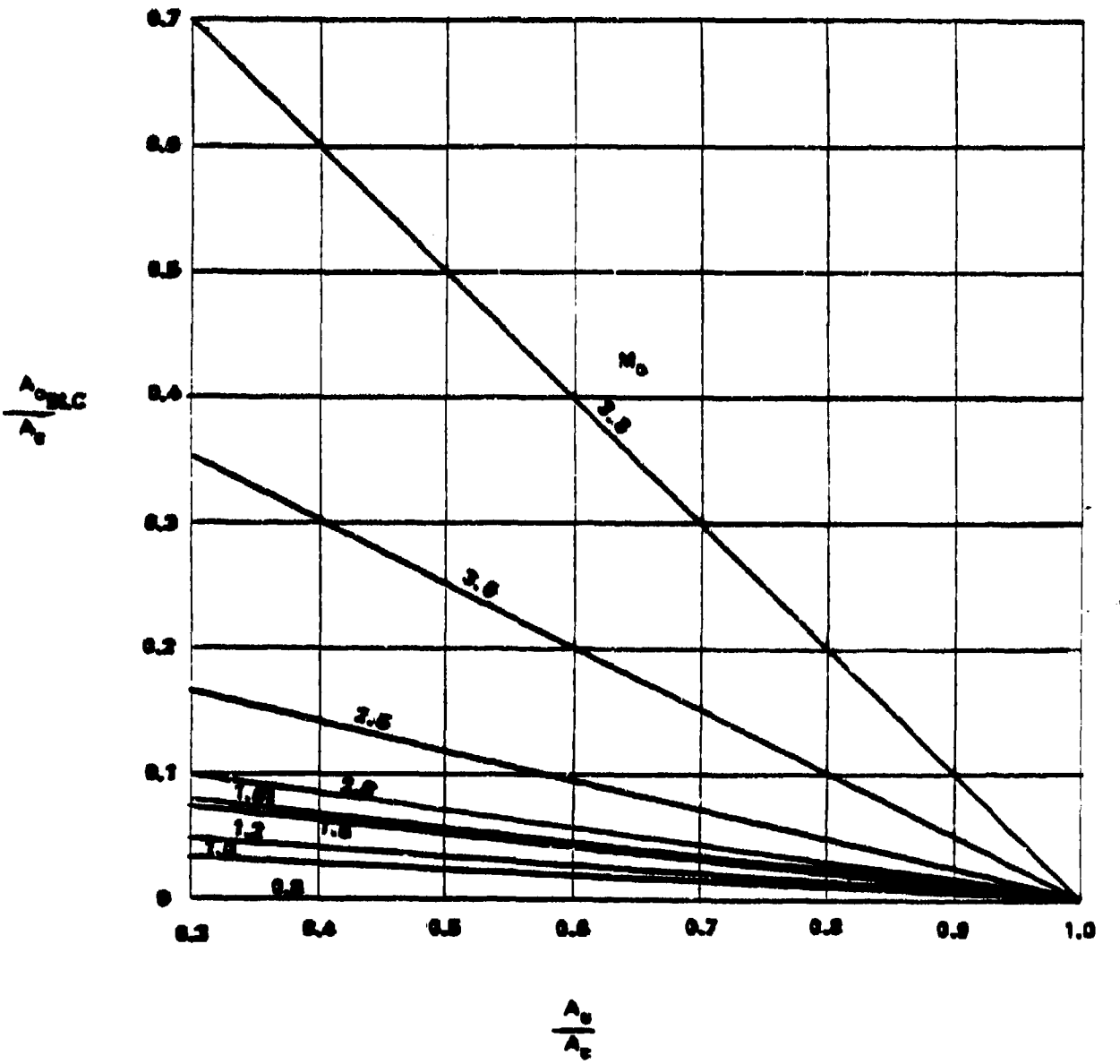

Figure 33. Performance Characteristics for Inlet Configuration #15 (continued)

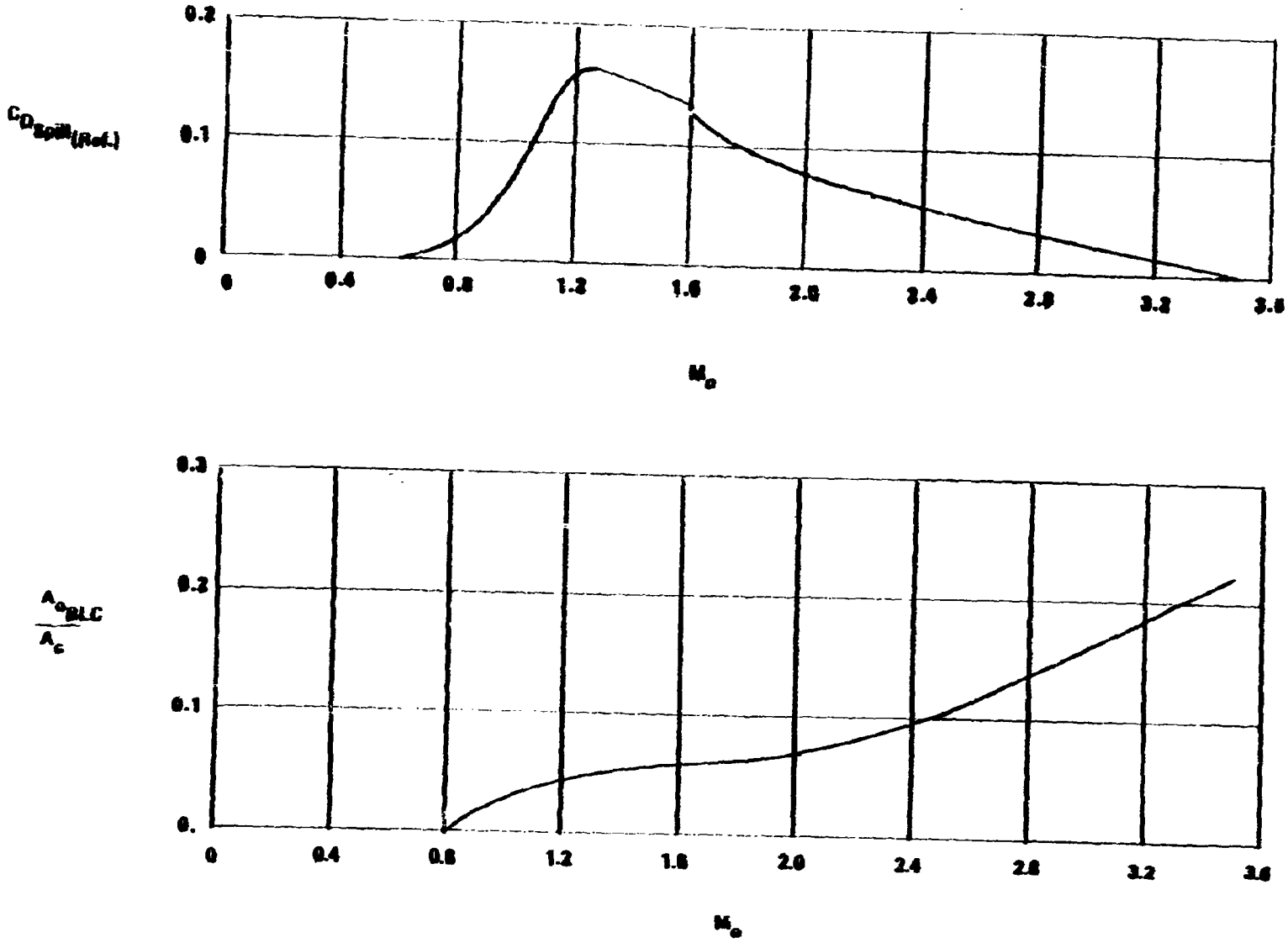

Figure 33. Performance Characteristics for Inlet Configuration #15 (continued)

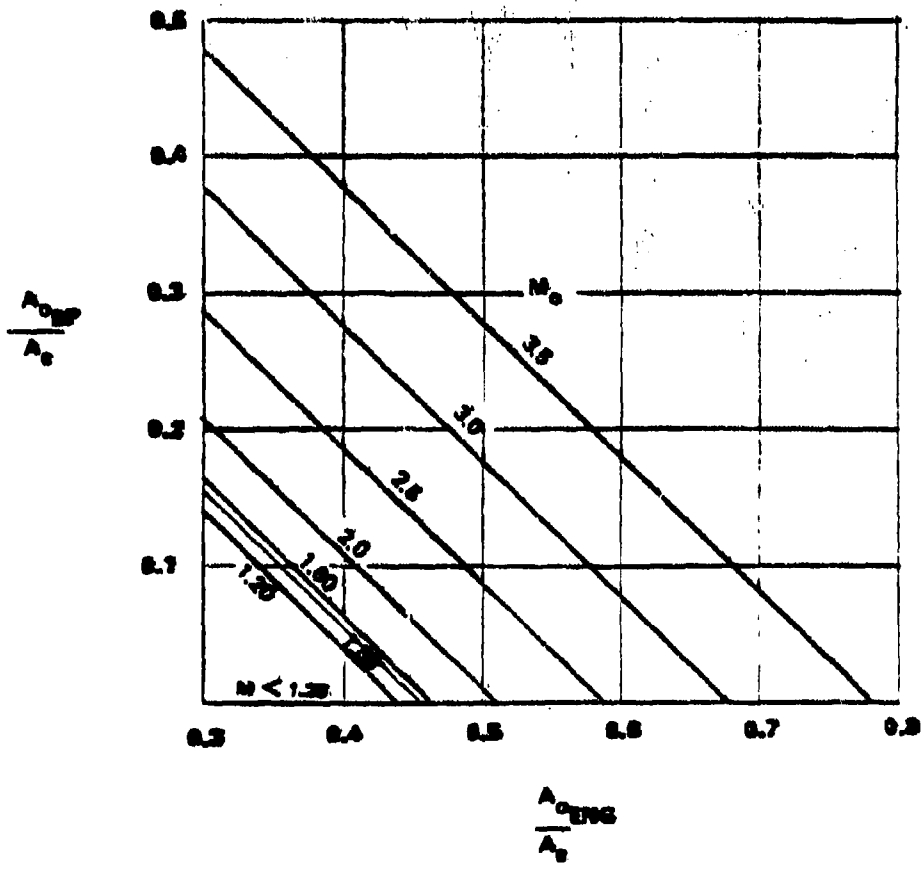

Figure 33. Performance Characteristics for Inlet Configuration #15 (concluded)

2.1.16 Inlet Configuration #16 - Mixed-Compression, Axisymmetric, Translating-Centerbody Inlet

This inlet configuration utilizes a sophisticated boundary layer control bleed system developed using the analytical techniques described in Reference 11. The inlet starting Mach number is 1.60.

The inlet performance characteristics of this configuration were obtained from information contained in Reference 12 and engineering analysis. The geometry of the inlet is shown in Figure 34 and the performance characteristics are presented in Figure 35.

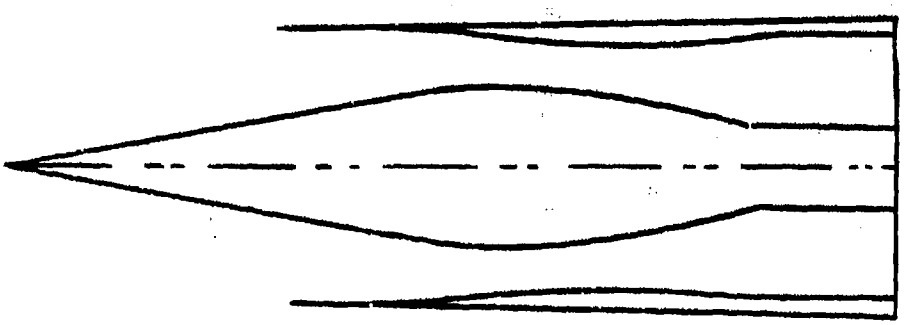

Figure 34. Mach 2.35 Mixed-Compression Axisymmetric Inlet

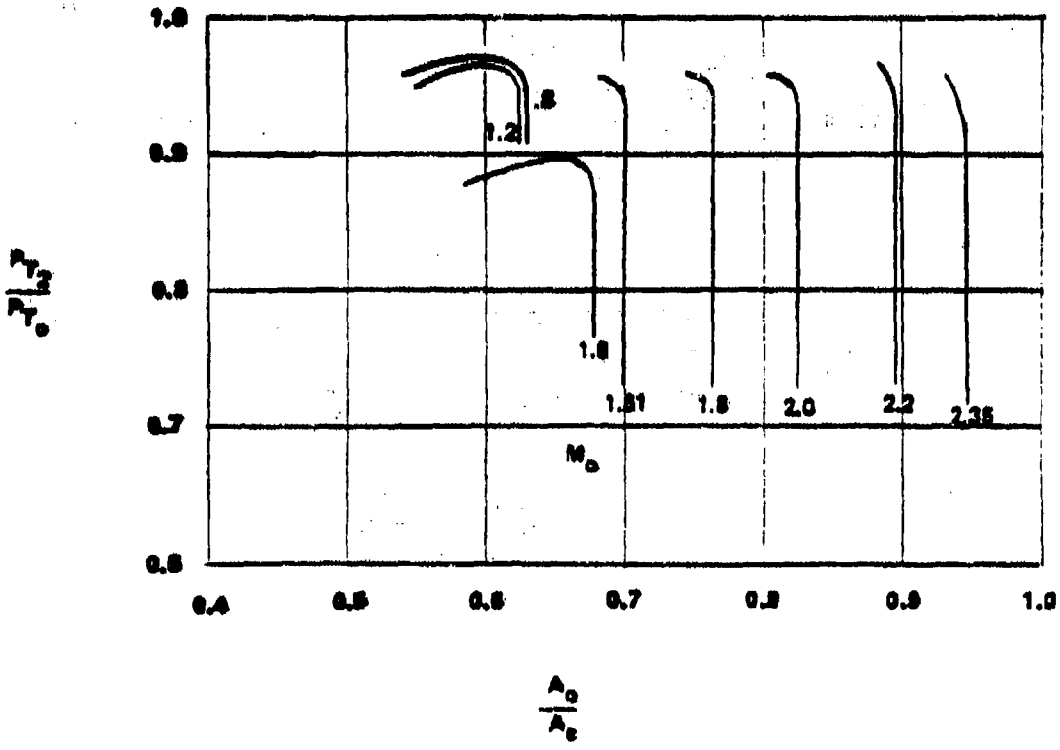

Figure 35. Performance Characteristics for Inlet Configuration #16

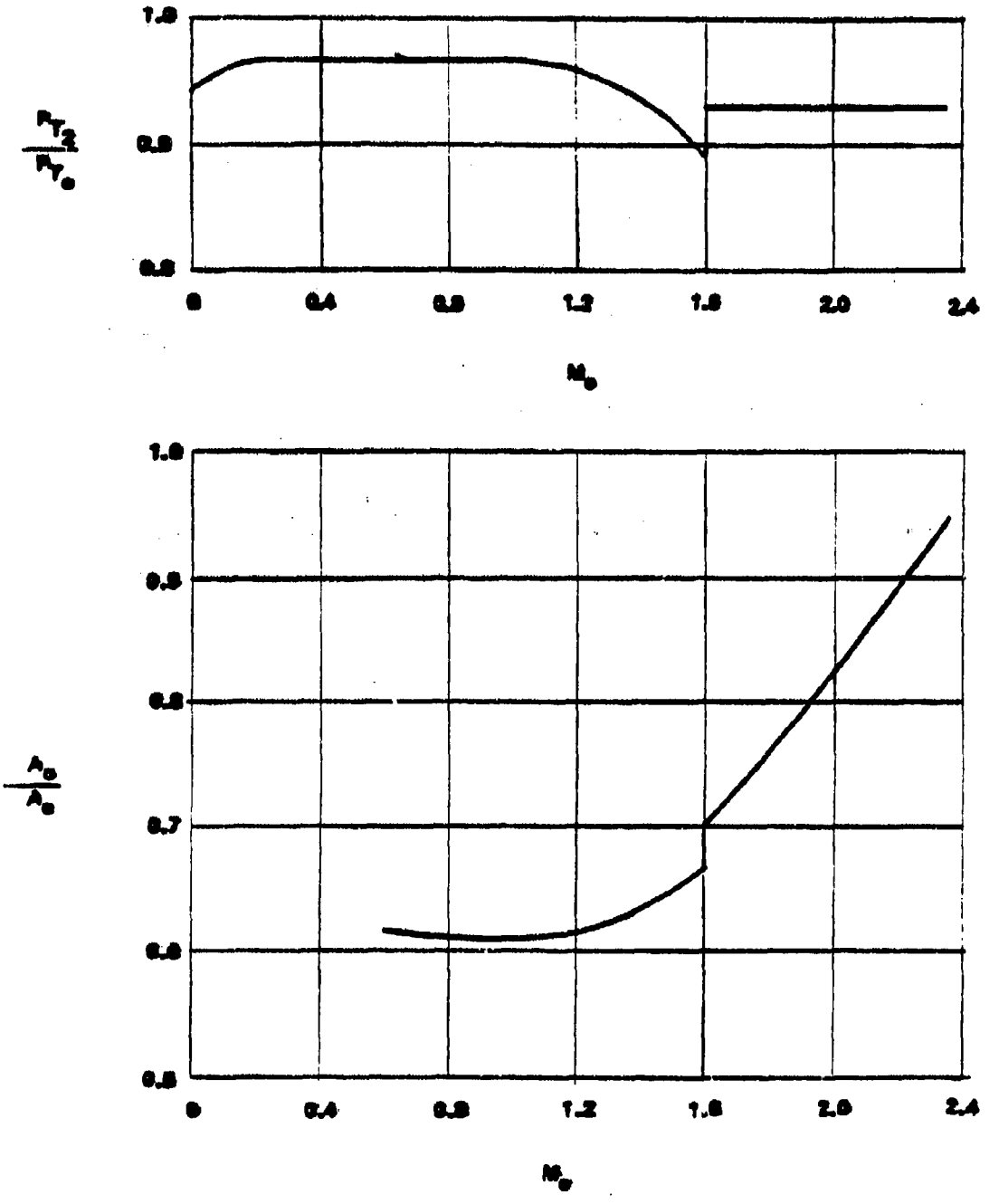

Figure 35. Performance Characteristics for Inlet Configuration #16 (continued)

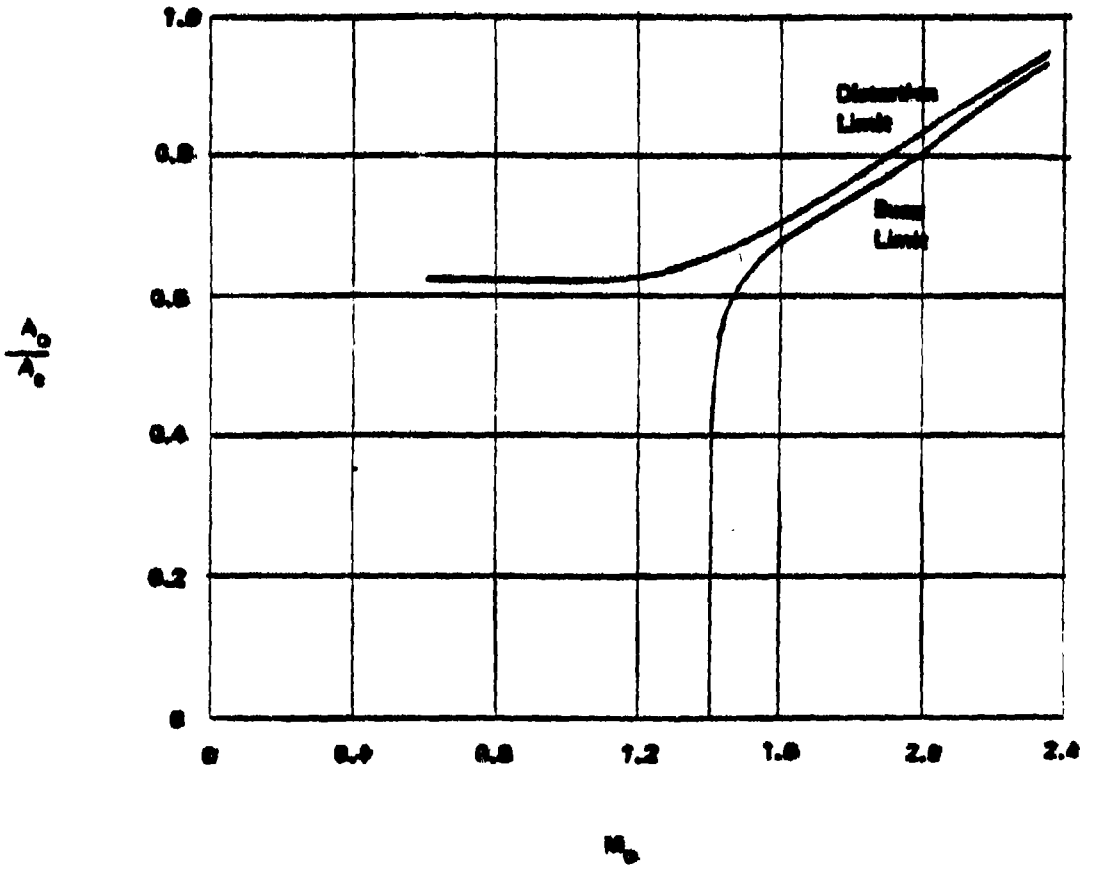

Figure 35. Performance Characteristics for Inlet Configuration #16 (continued)

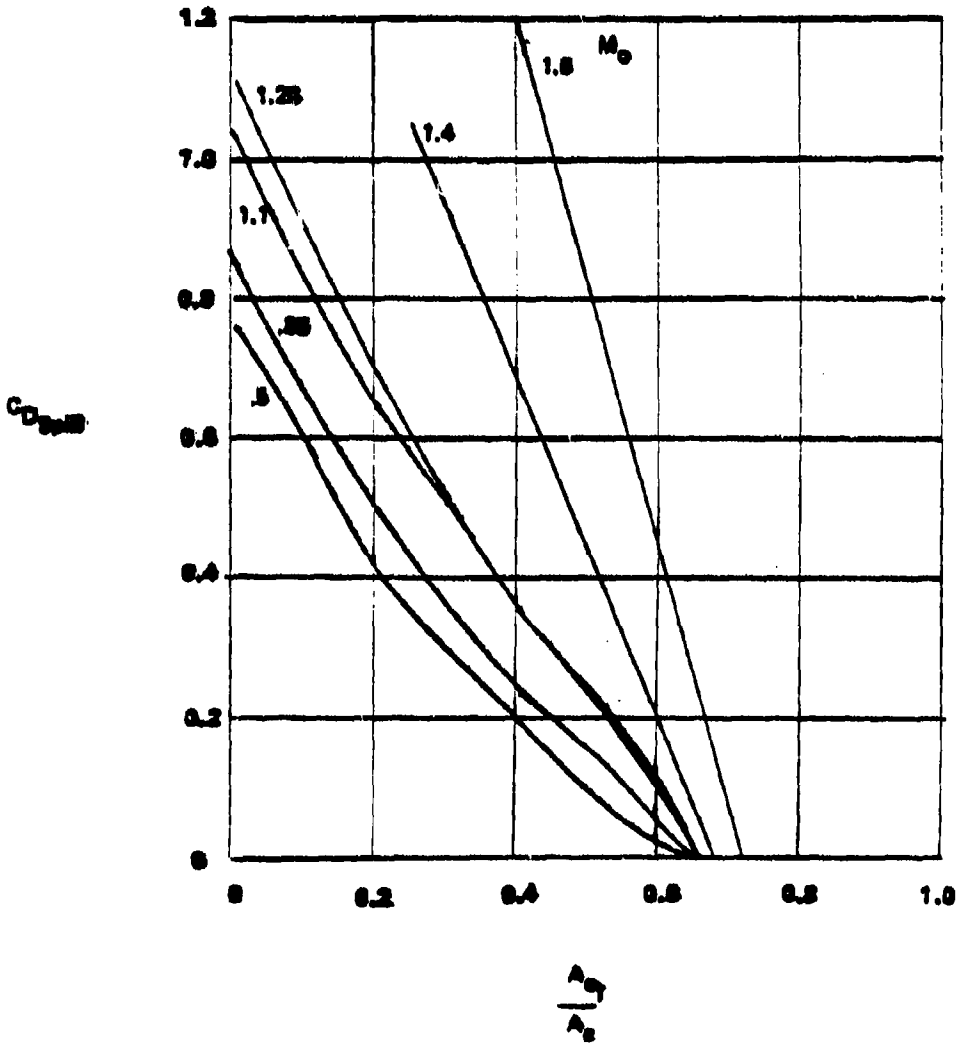

Figure 35. Performance Characteristics for Inlet Configuration #16 (continued)

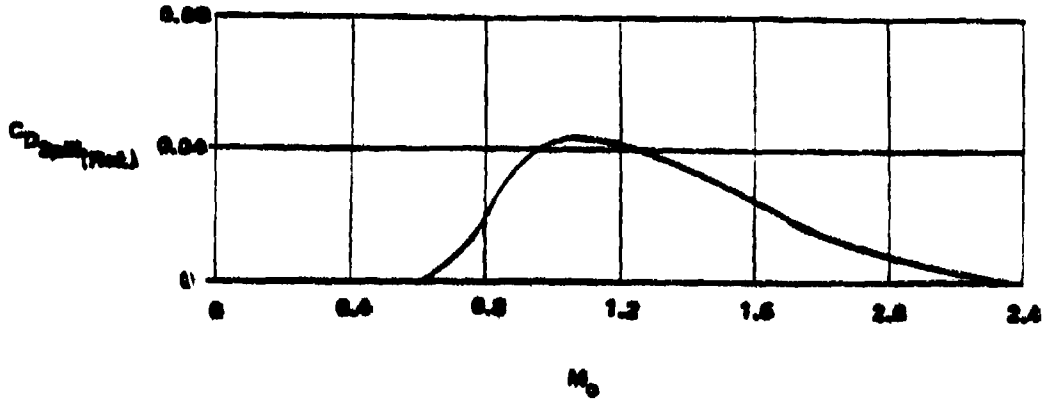

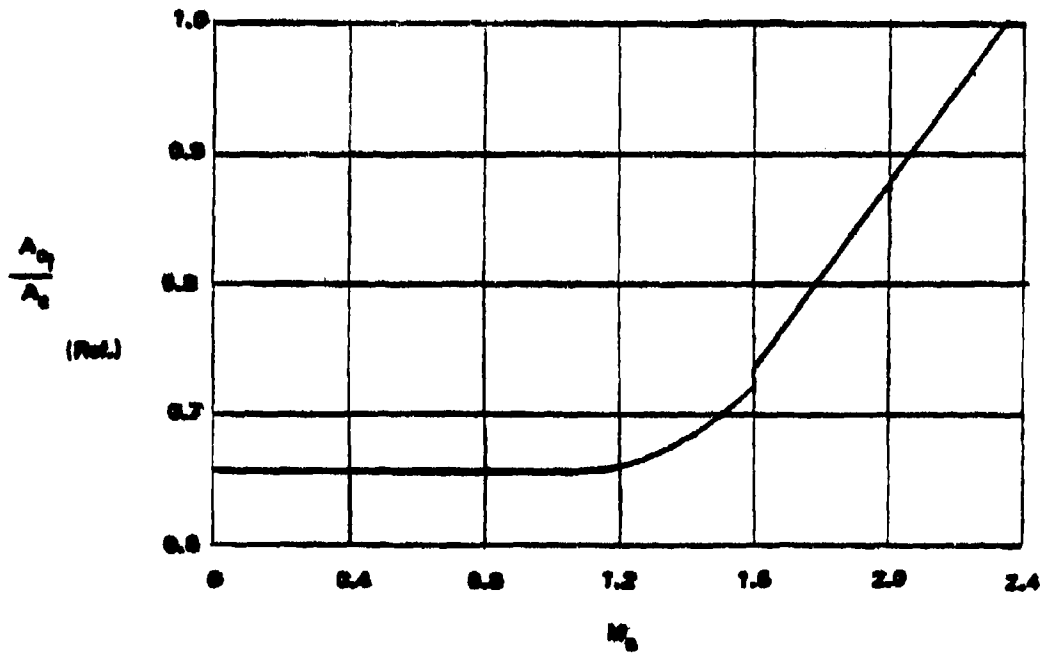

Figure 35. Performance Characteristics for Inlet Configuration #16 (continued)

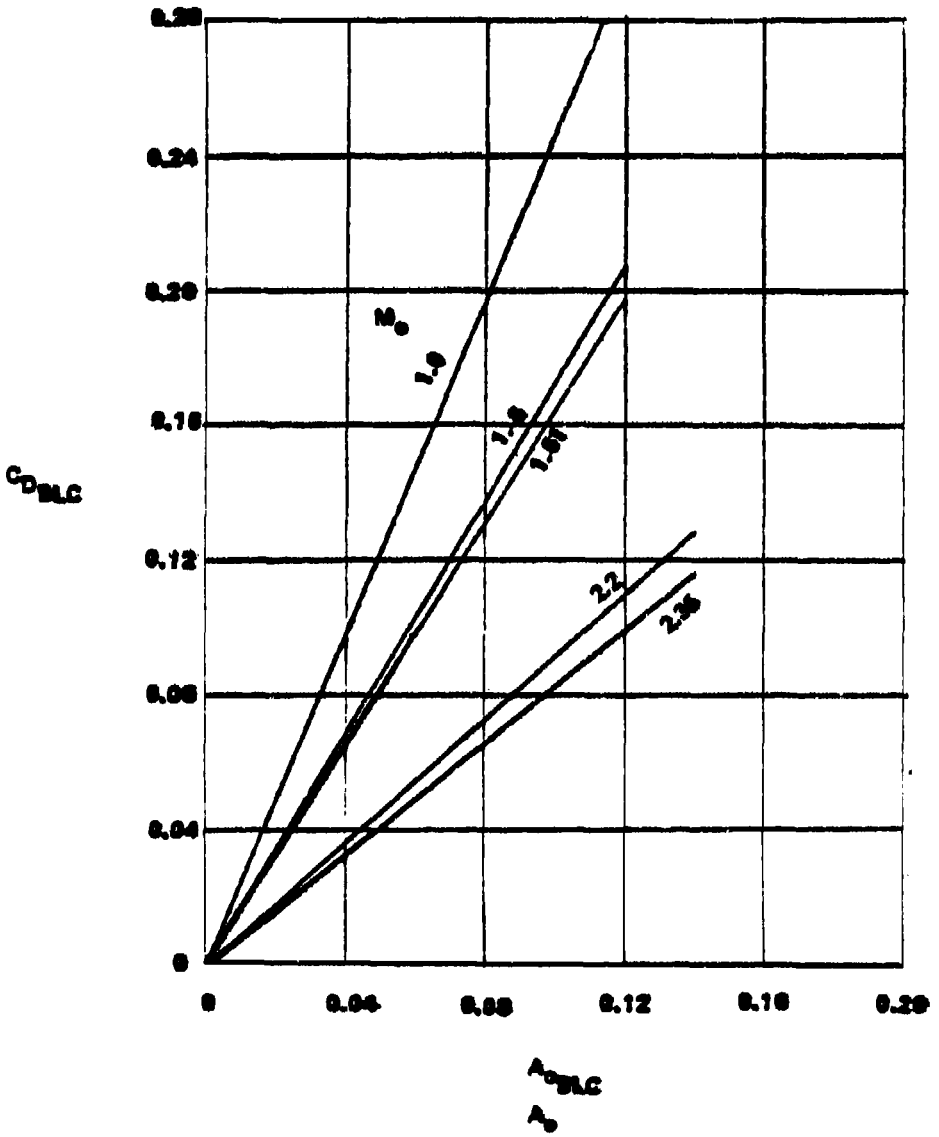

Figure 35. Performance Characteristics for Inlet Configuration #16 (continued)

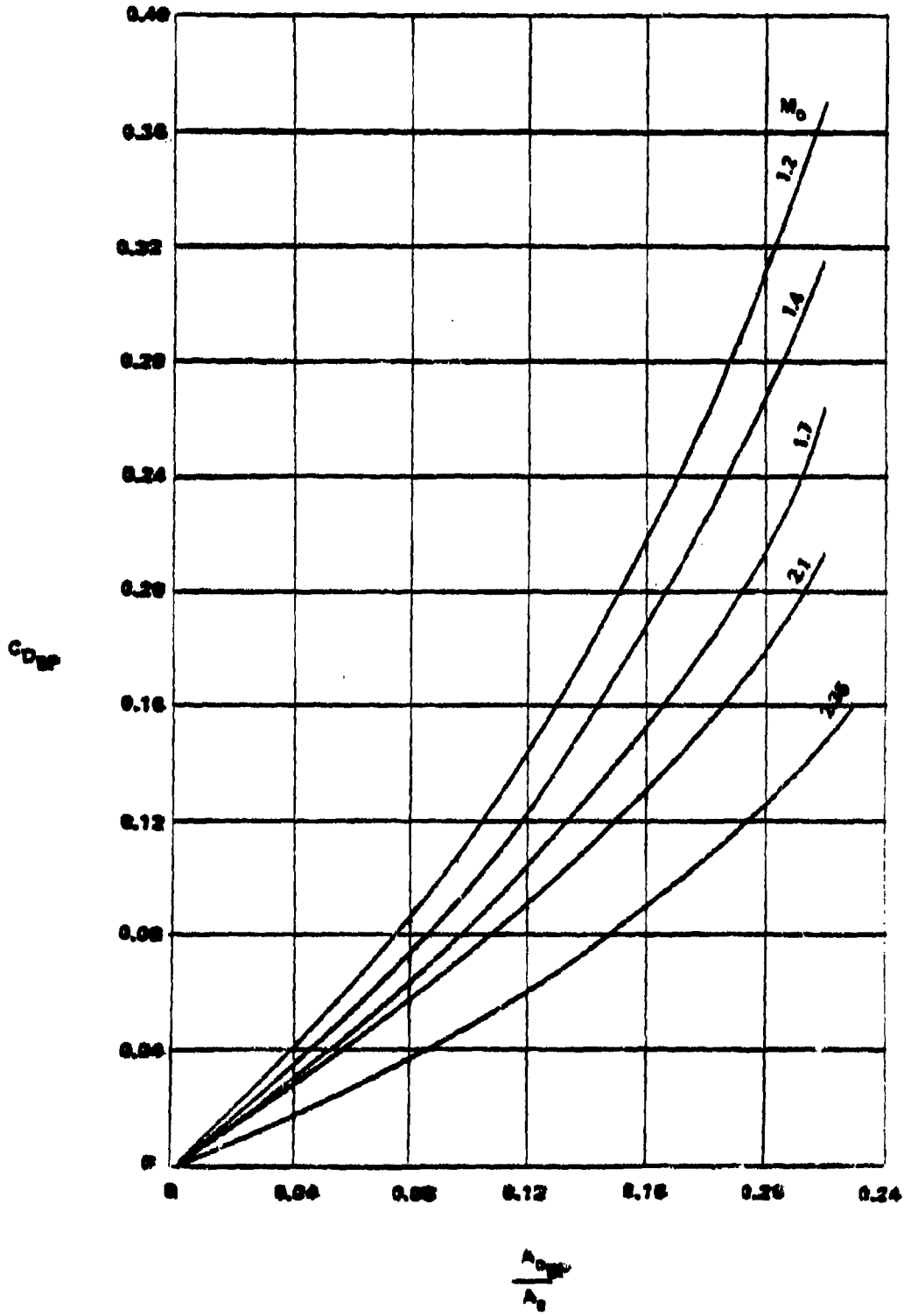

Figure 35. Performance Characteristics for Inlet Configuration #16 (continued)

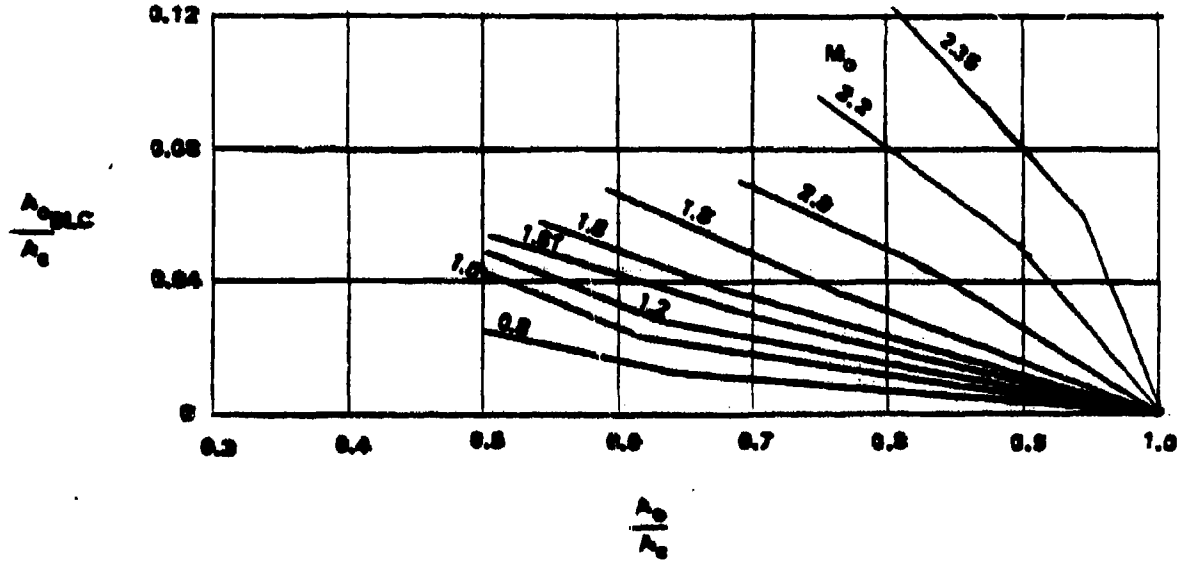

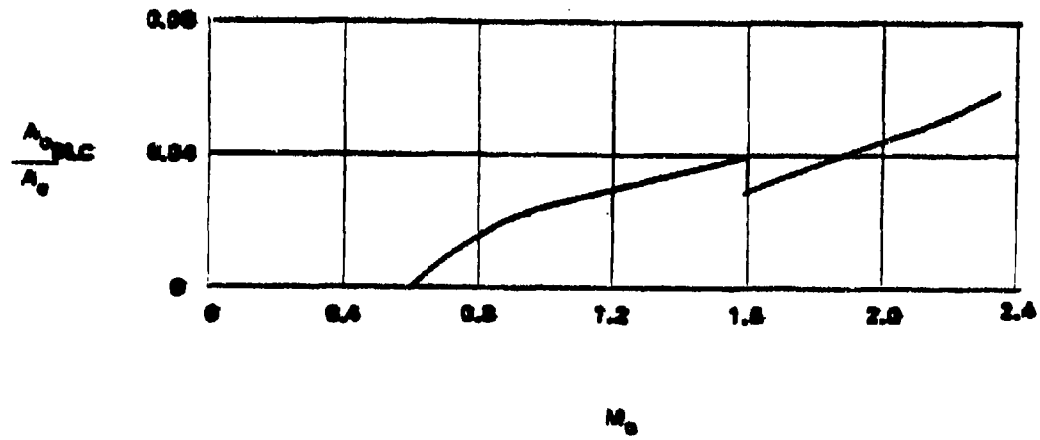

Figure 35. Performance Characteristics for Inlet Configuration #16 (continued)

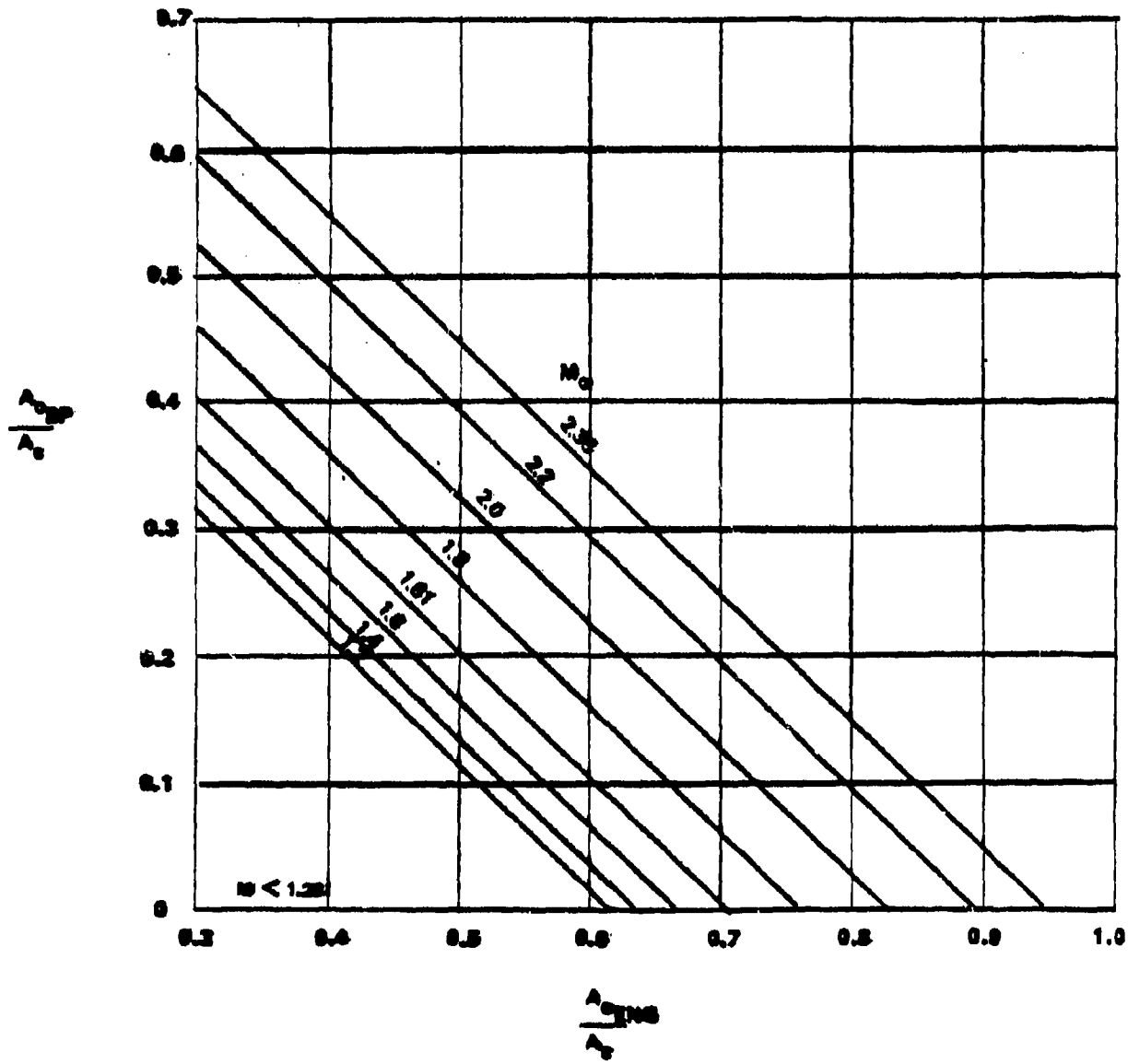

Figure 35. Performance Characteristics for Inlet Configuration #16 (concluded)

2.1.17 Inlet Configuration #17 - Mixed-Compression, Axisymmetric, Translating Centerbody Inlet

The design Mach number for this inlet is 3.0. The initial cone angle is 10°. Boundary layer control bleed flow is removed through porous bleed holes on cowl and centerbody surfaces. Four individual bleed zones were provided.

The performance characteristics of this inlet are based on the design studies and data reported in Reference 13 and engineering analysis. The inlet geometry is shown in Figure 36 and the inlet performance characteristics are presented in Figure 37.

Figure 36. Mach 3.0 Axisymmetric Mixed-Compression Inlet

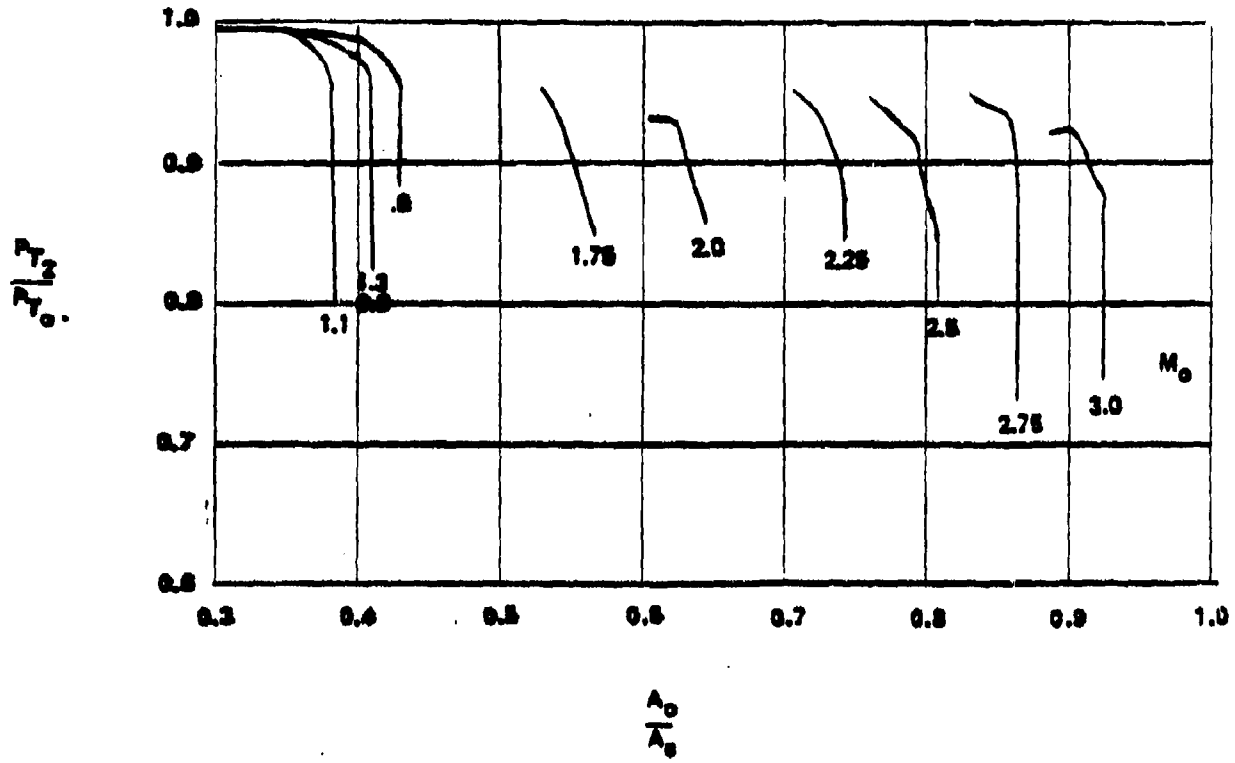

Figure 37. Performance Characteristics for Inlet Configuration #17

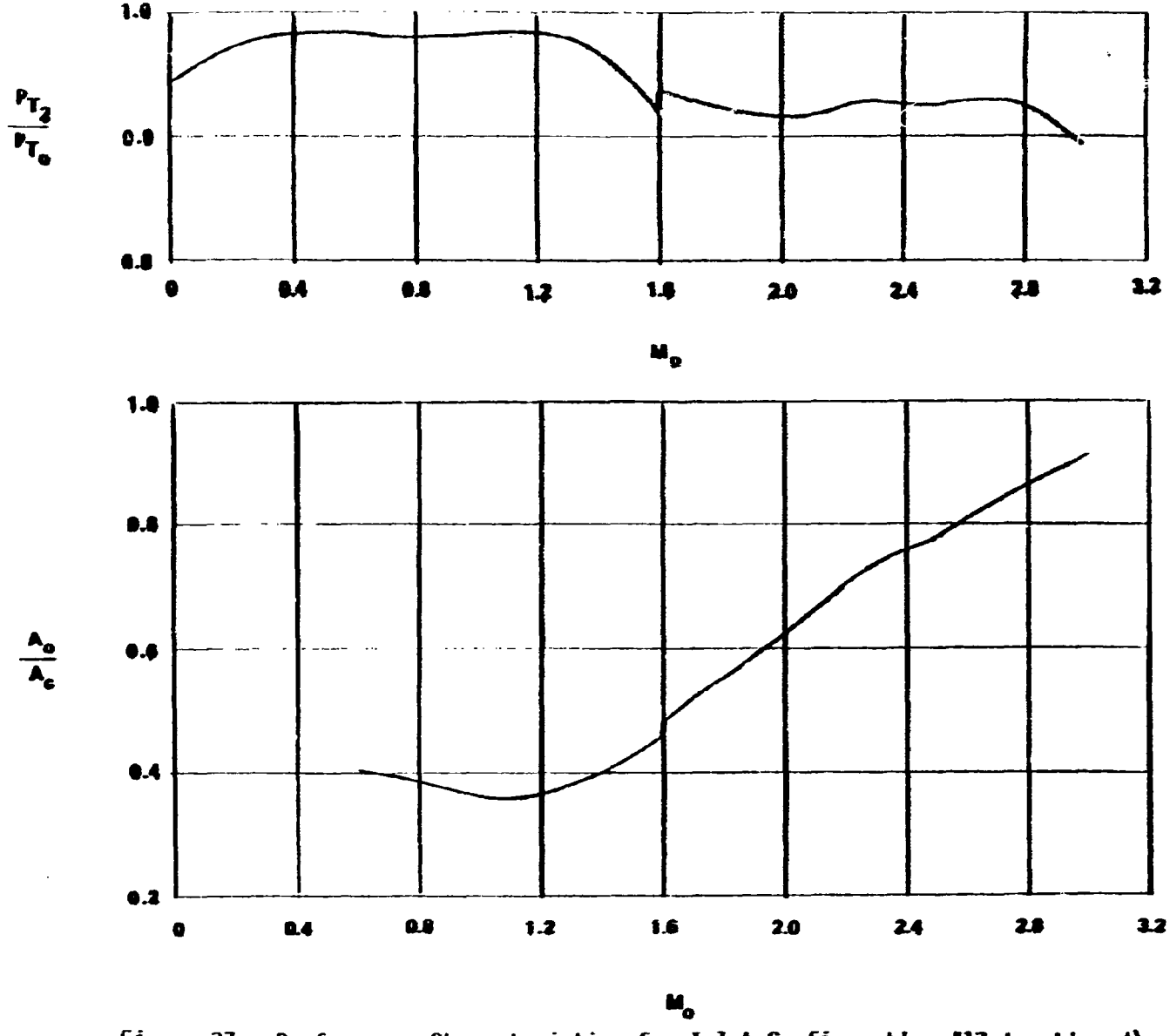

Figure 37. Performance Characteristics for Inlet Configuration #17 (continued)

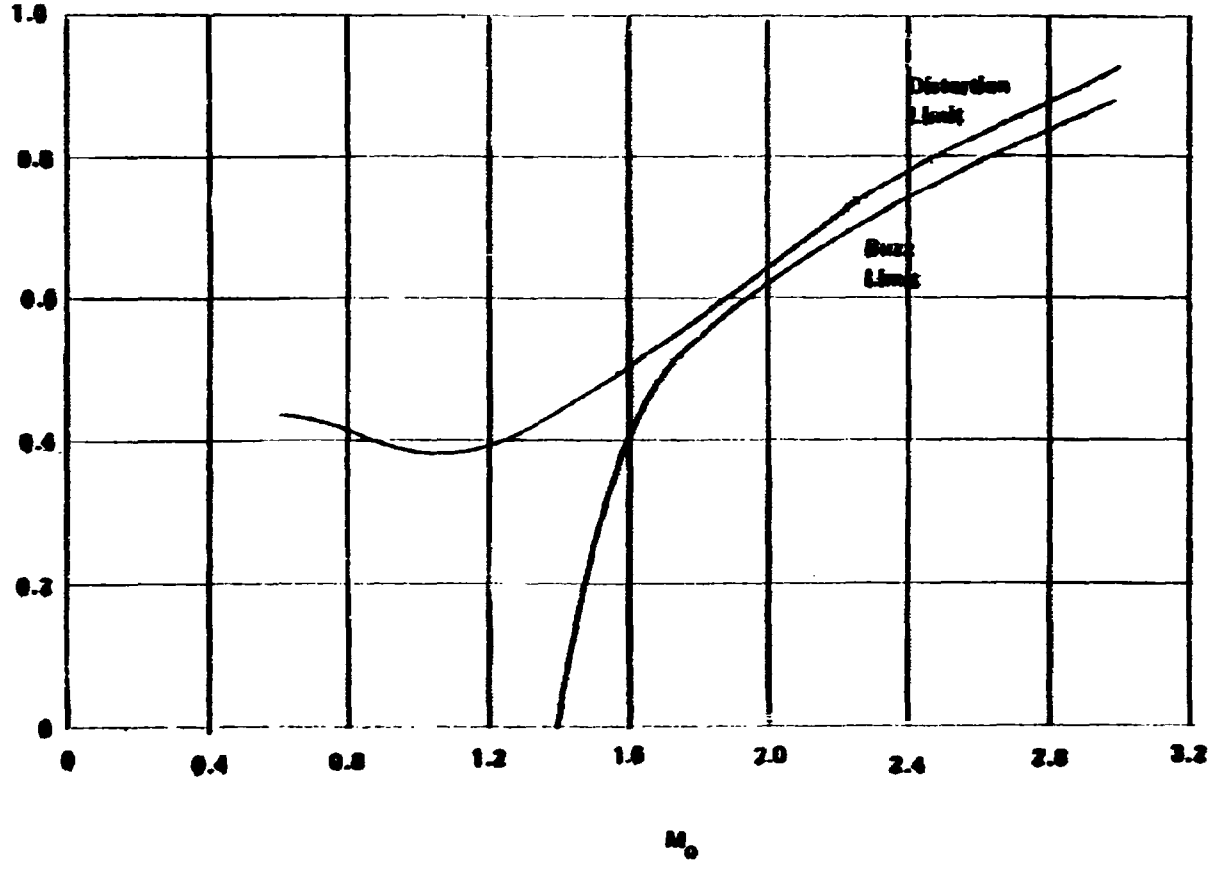

Figure 37. Performance Characteristics for Inlet Configuration #17 (continued)

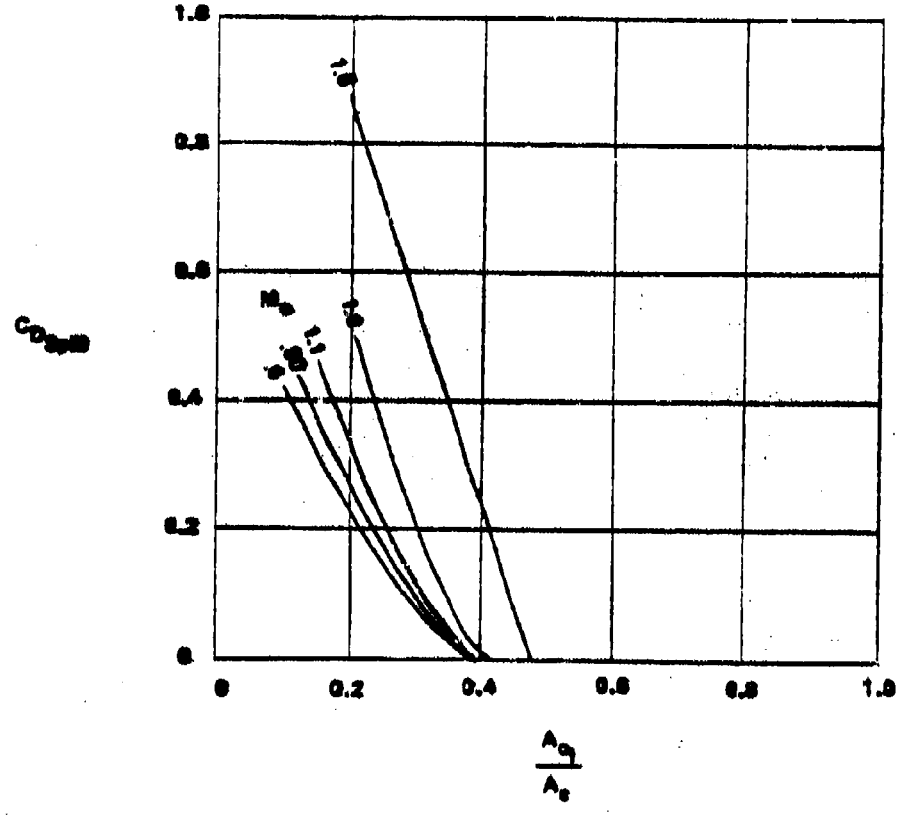

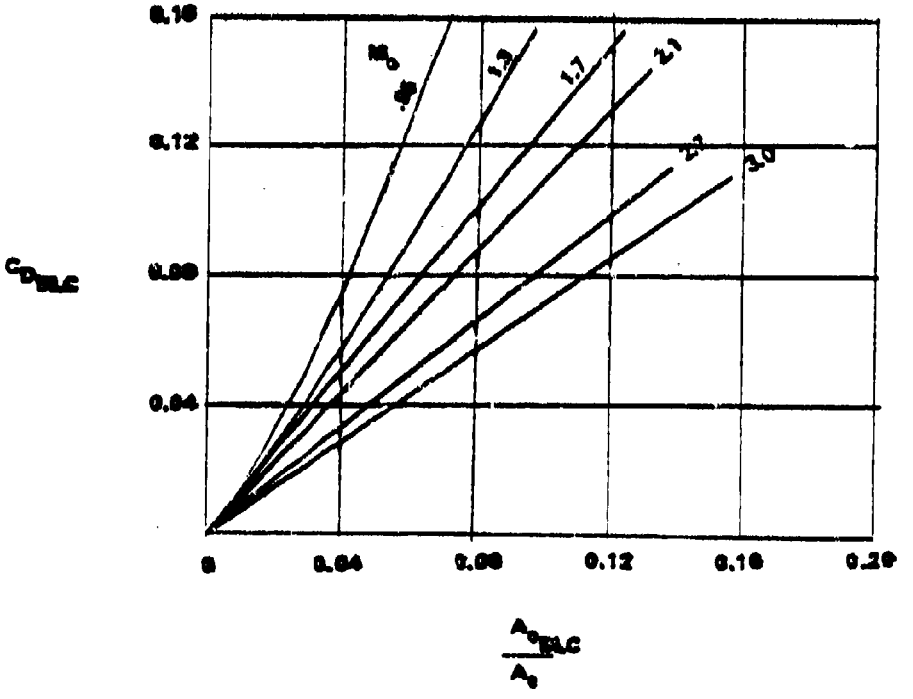

Figure 37. Performance Characteristics for Inlet Configuration #17 (continued)

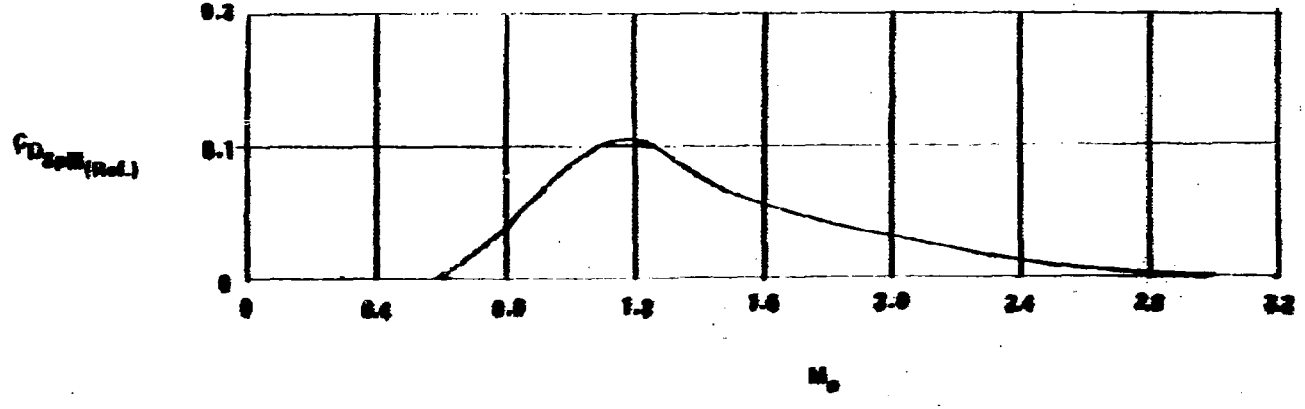

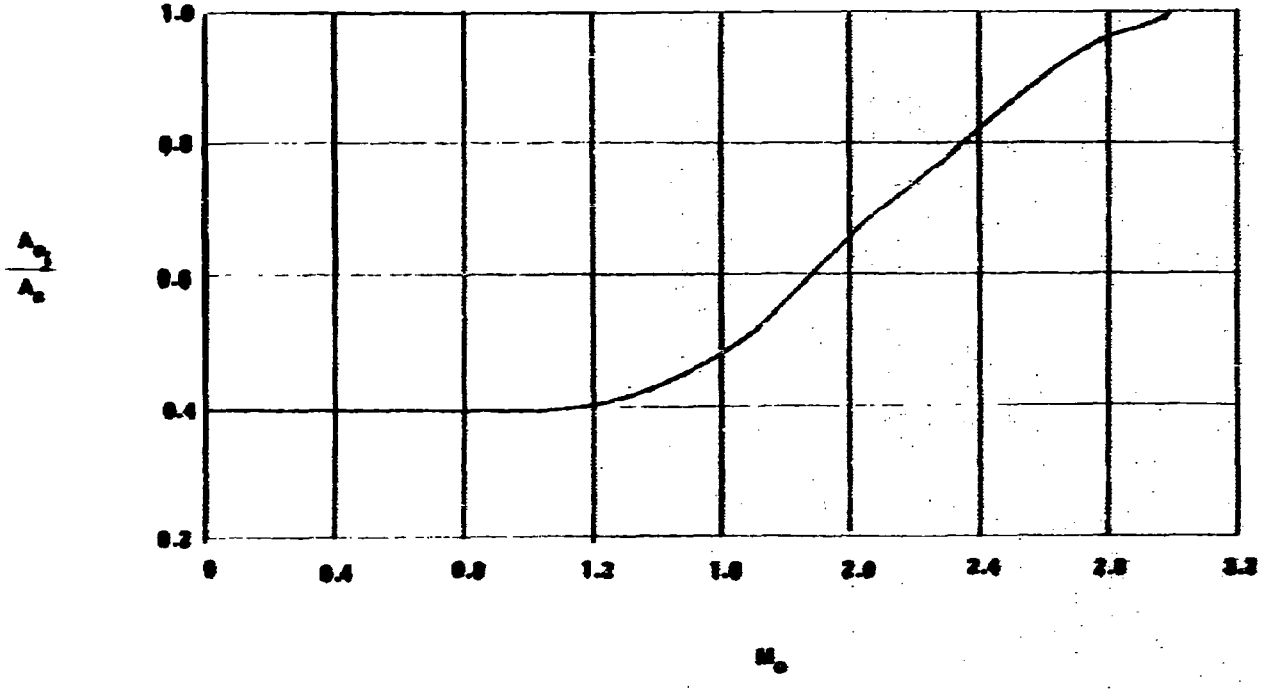

Figure 37. Performance Characteristics for Inlet Configuration #17 (continued)

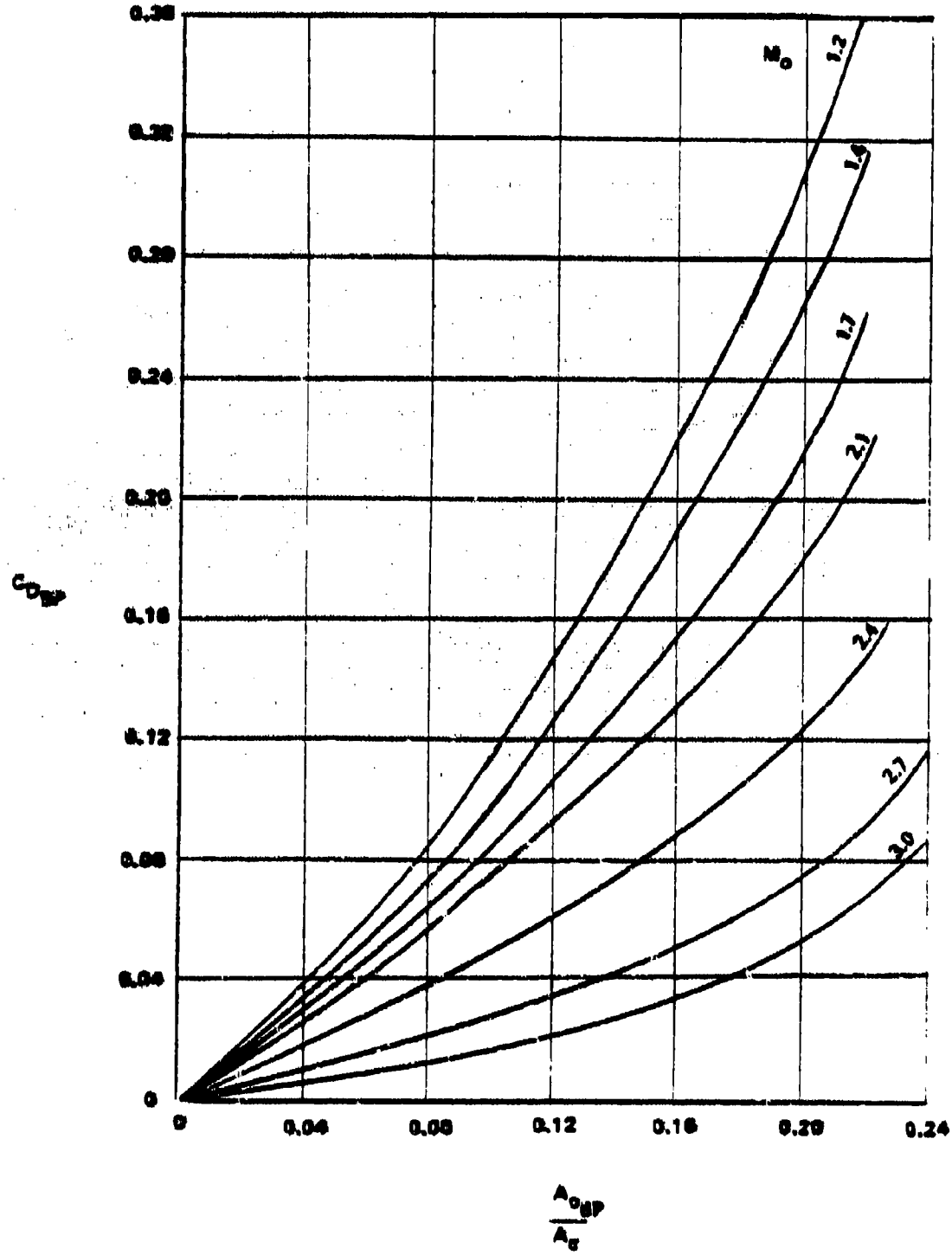

Figure 37. Performance Characteristics for Inlet Configuration #17 (continued)

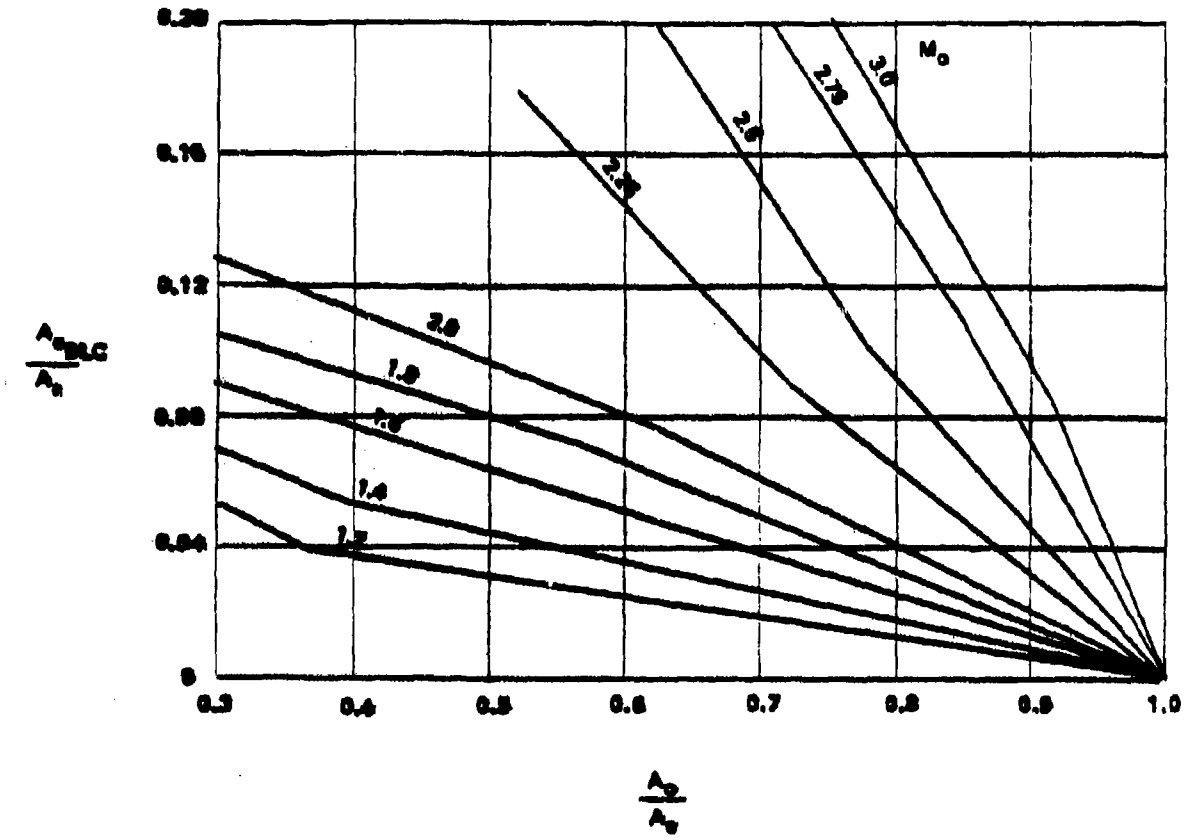

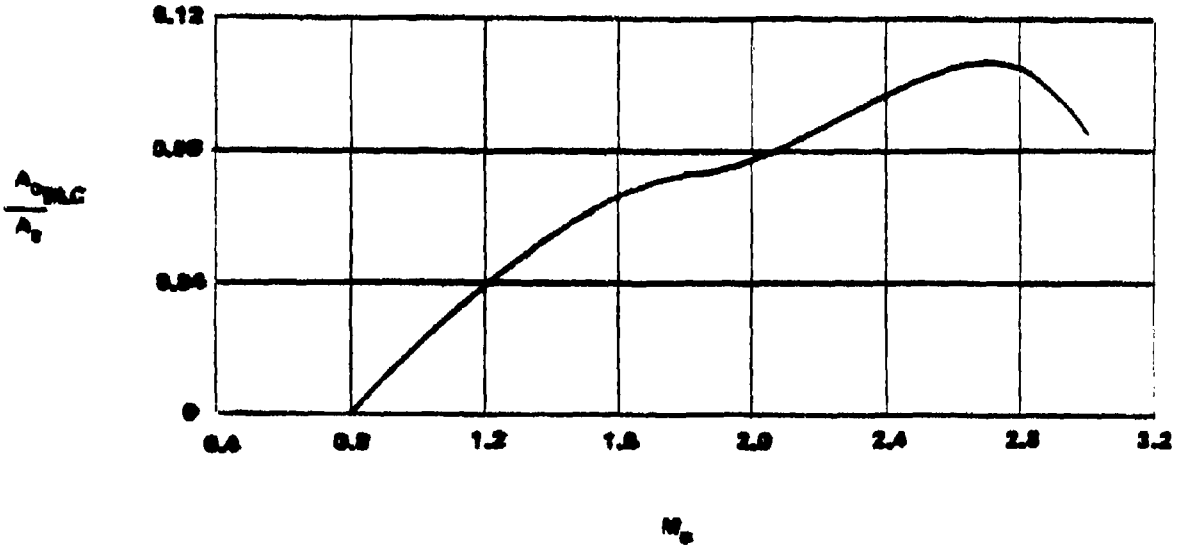

Figure 37. Performance Characteristics for Inlet Configuration #17 (continued)

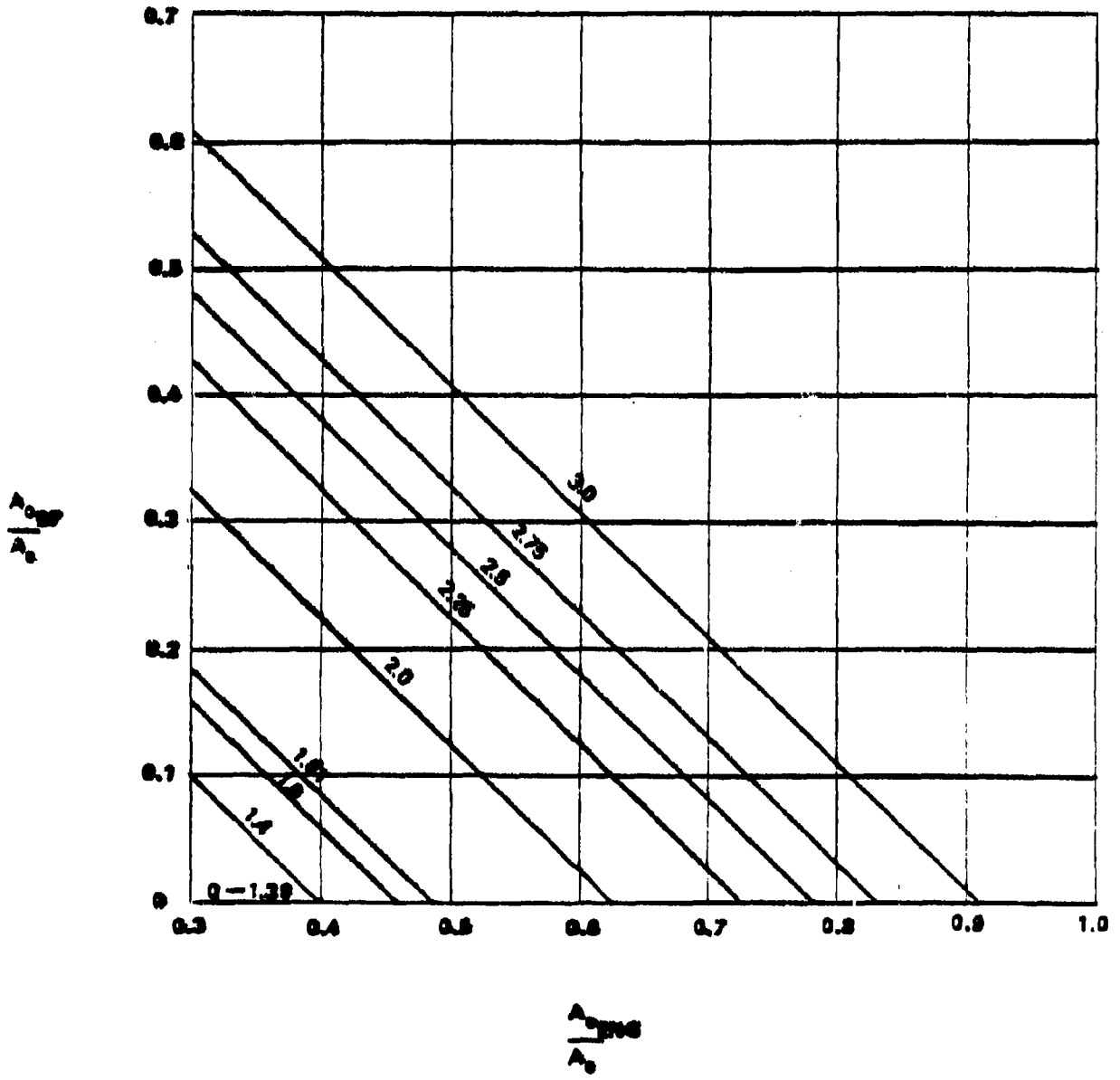

Figure 37. Performance Characteristics for Inlet Configuration #17 (concluded)

2.1.18 Inlet Configuration #18 - Mixed-Compression, Axisymmetric, Translating Centerbody Inlet

The mixed-compression inlet was designed for a Mach number of 3.5. A sophisticated boundary layer control bleed system was provided based on the results of detailed analyses. The cowl bleed system included four separate bleed plenums with separate overboard exits for each plenum. The centerbody includes 12 bleed plenums in a "traveling" bleed arrangement. Excess inlet airflow can be exited through bypass doors.

The inlet performance characteristics of this configuration are based on the data and design in Reference 14, supplemented with additional engineering analyses. The inlet geometry is shown in Figure 38 and the performance characteristics are presented in Figure 39.

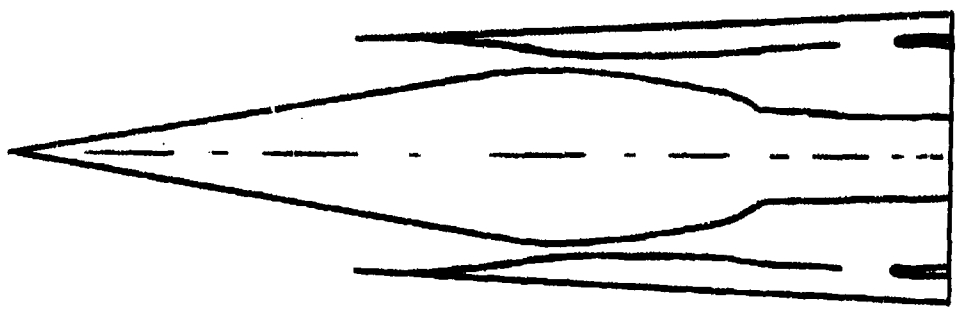

Figure 38. Mach 3.5 Axisymmetric Mixed-Compression Inlet

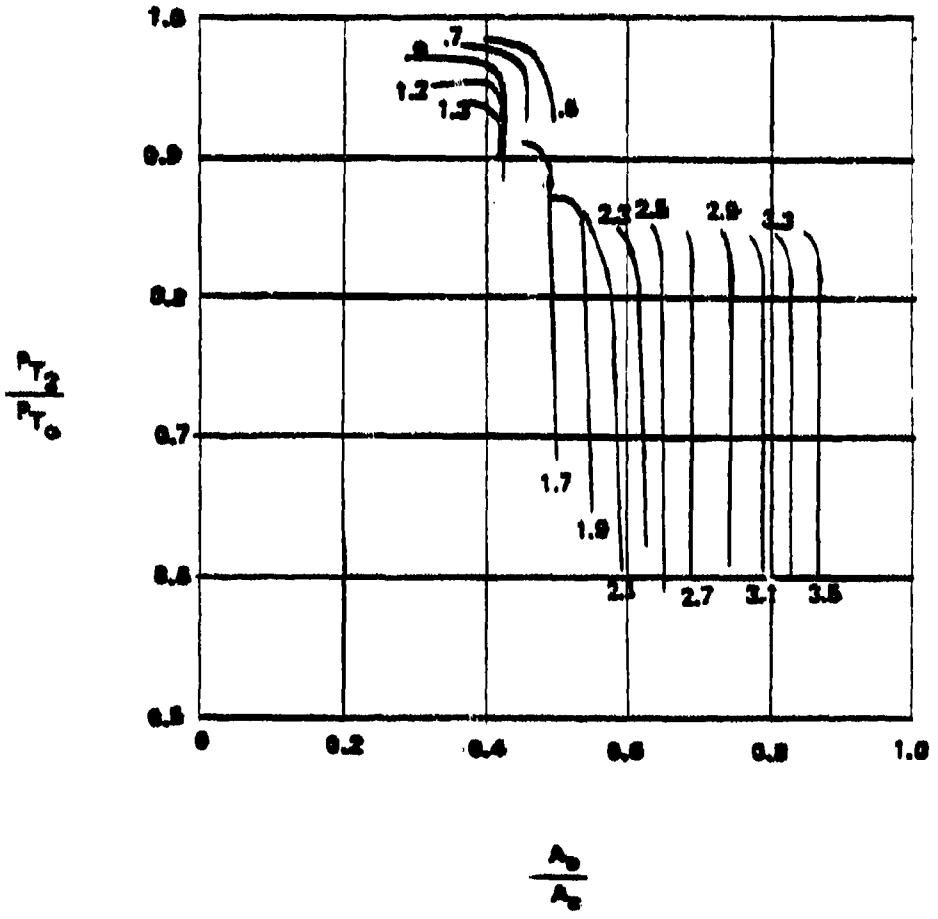

Figure 39. Performance Characteristics for Inlet Configuration #18

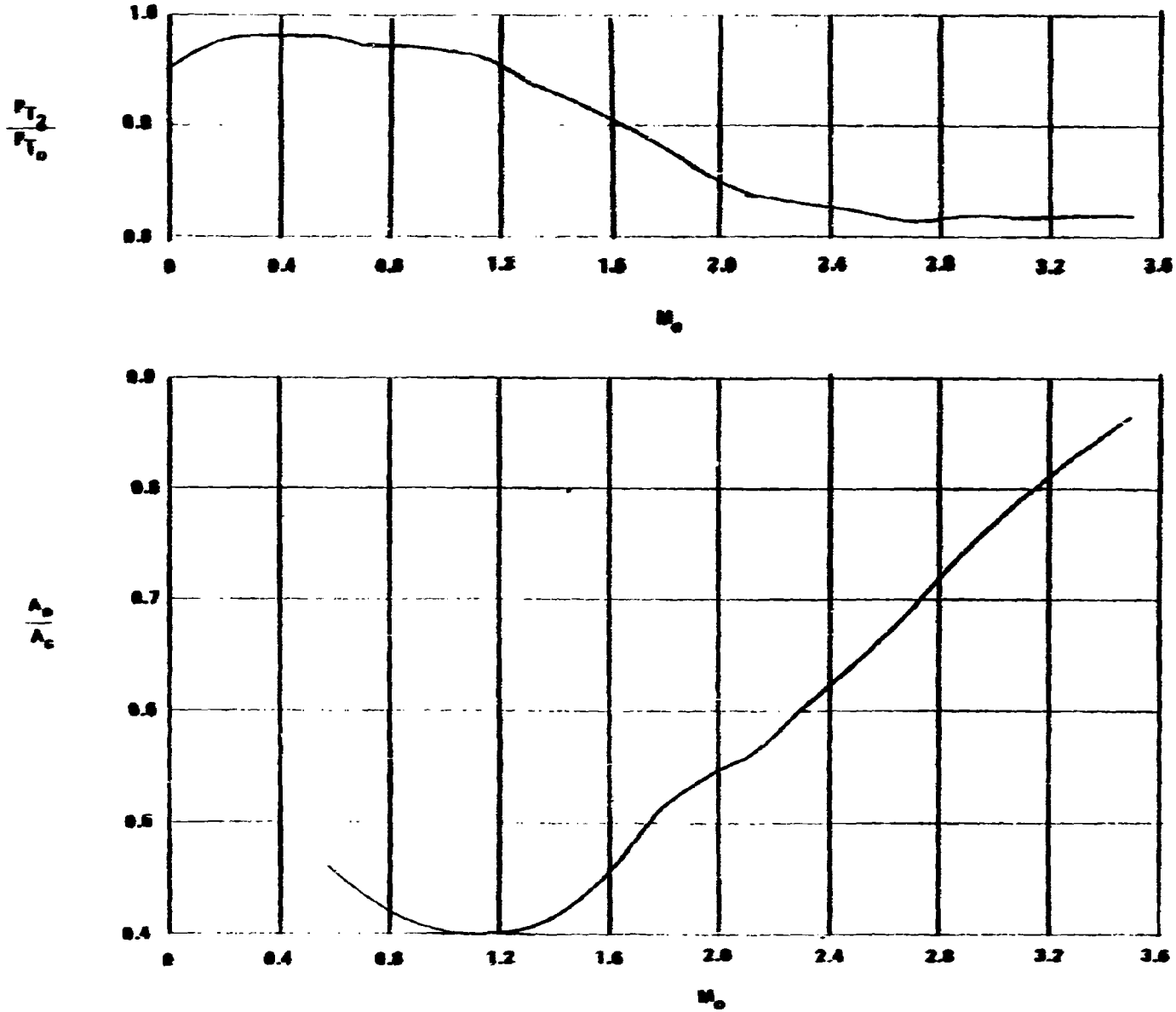

Figure 39. Performance Characteristics for Inlet Configuration #18 (continued)

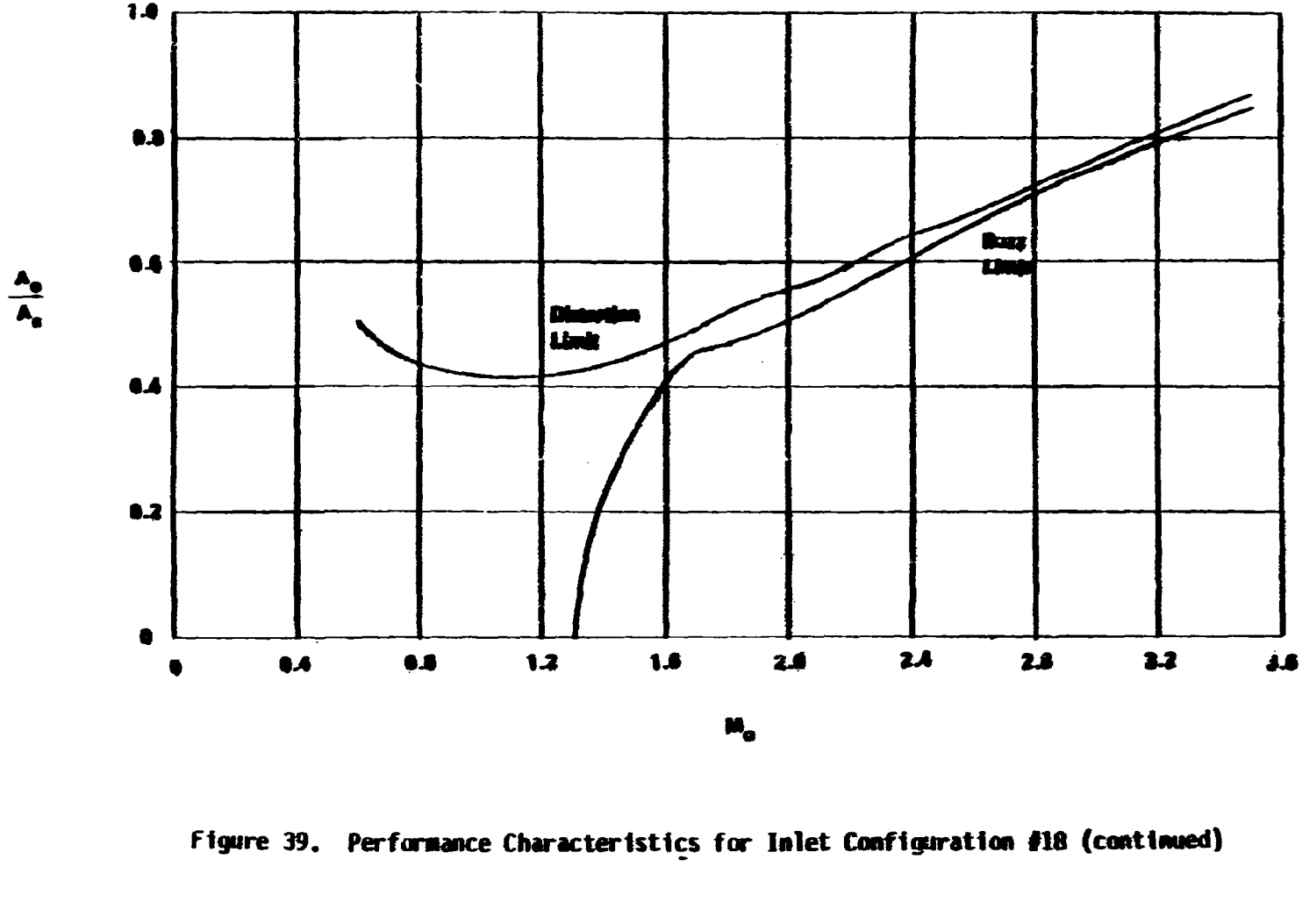

Figure 39. Performance Characteristics for Inlet Configuration #18 (continued)

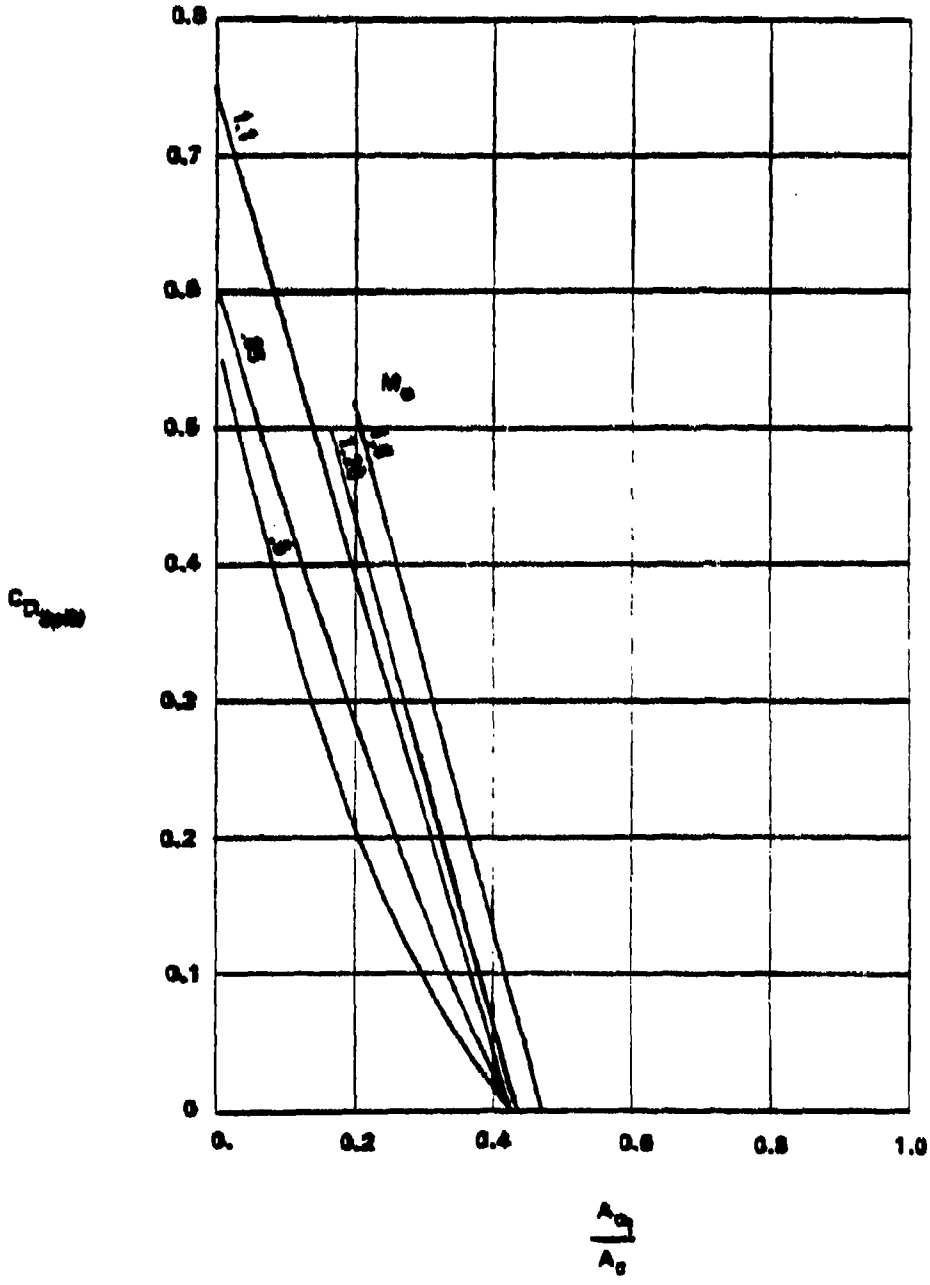

Figure 39. Performance Characteristics for Inlet Configuration #18 (continued)

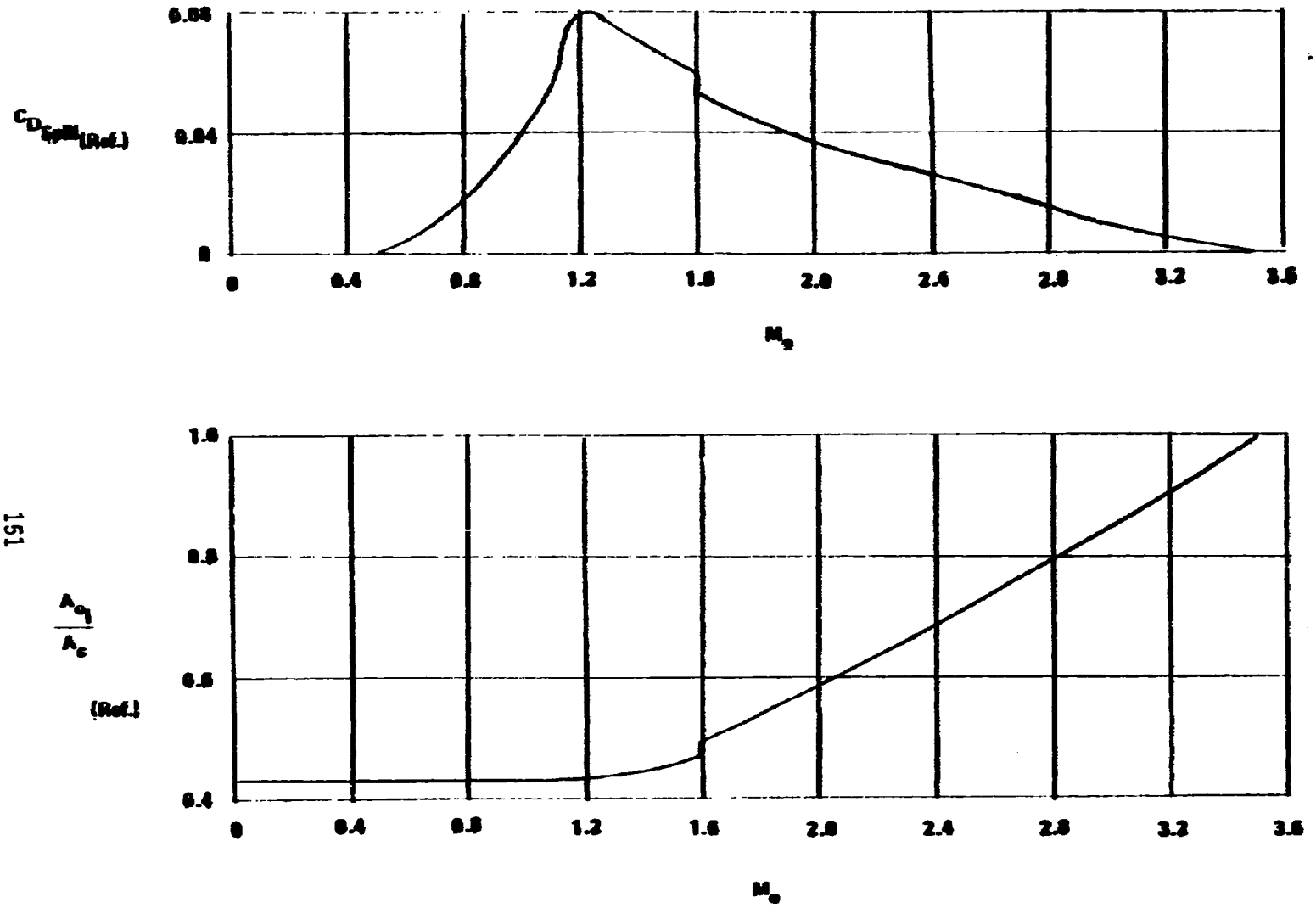

Figure 39. Performance Characteristics for Inlet Configuration #18 (continued)

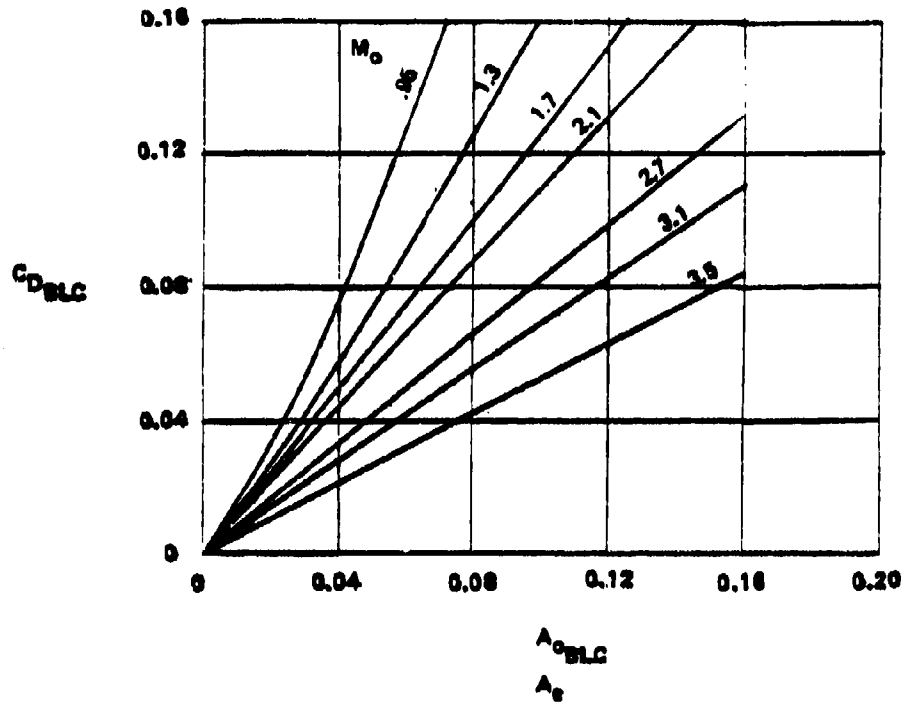

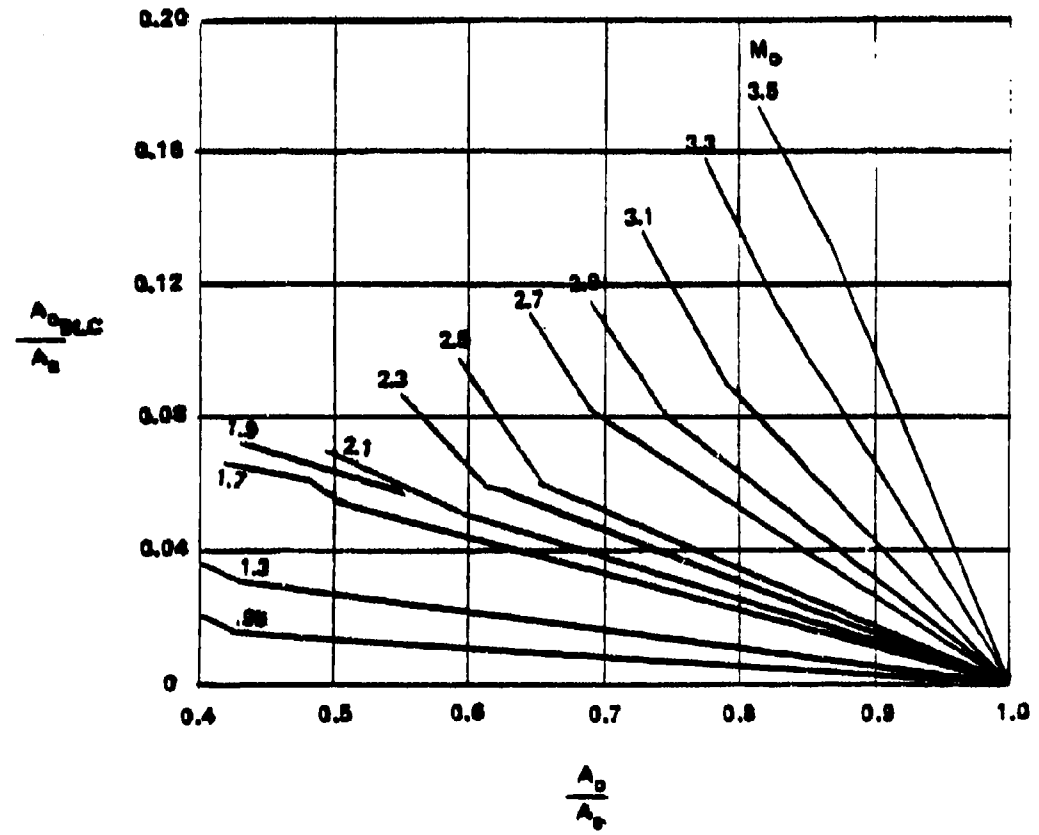

Figure 39. Performance Characteristics for Inlet Configuration #18 (continued)

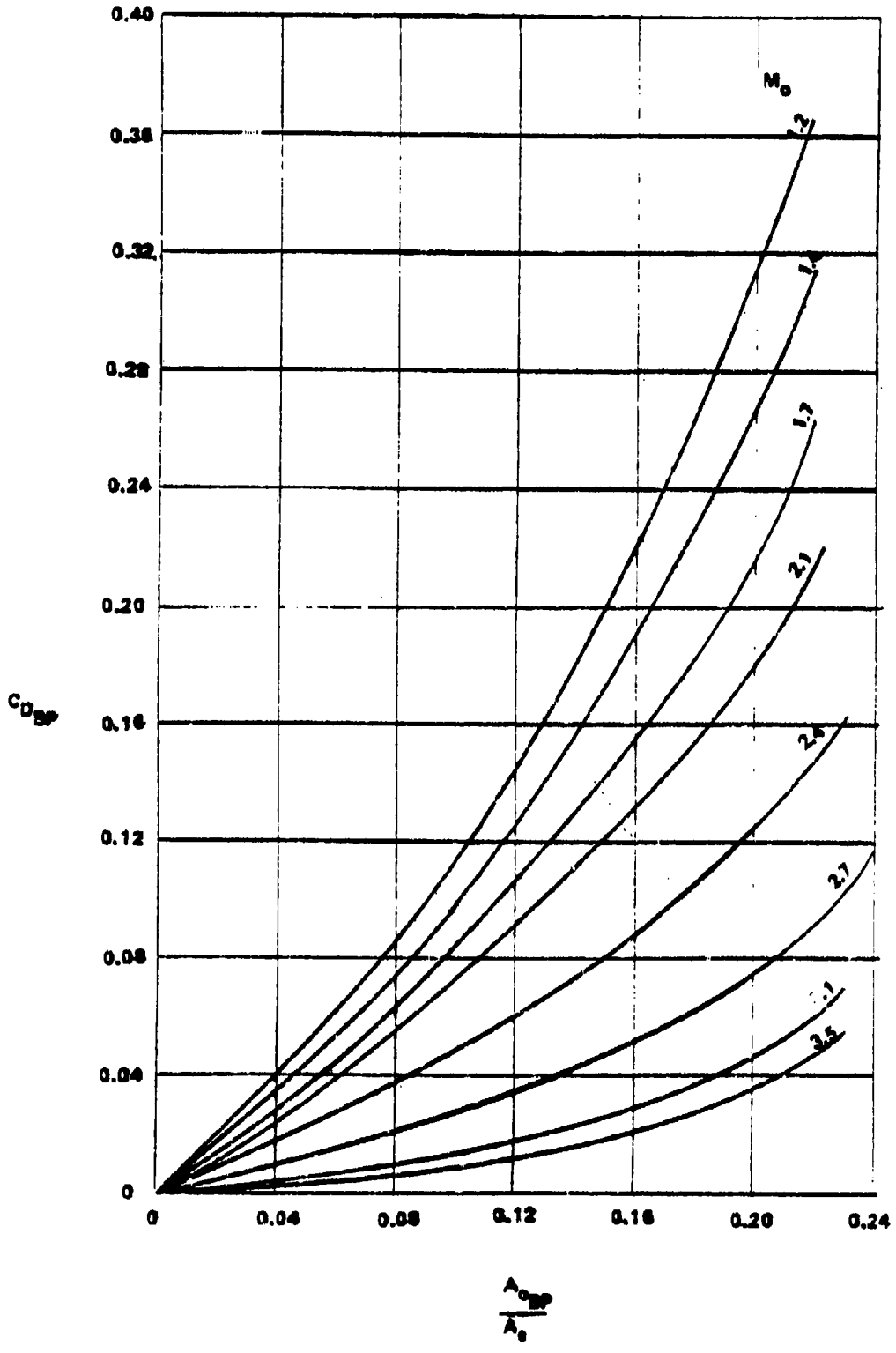

Figure 39. Performance Characteristics for Inlet Configuration #18 (continued)

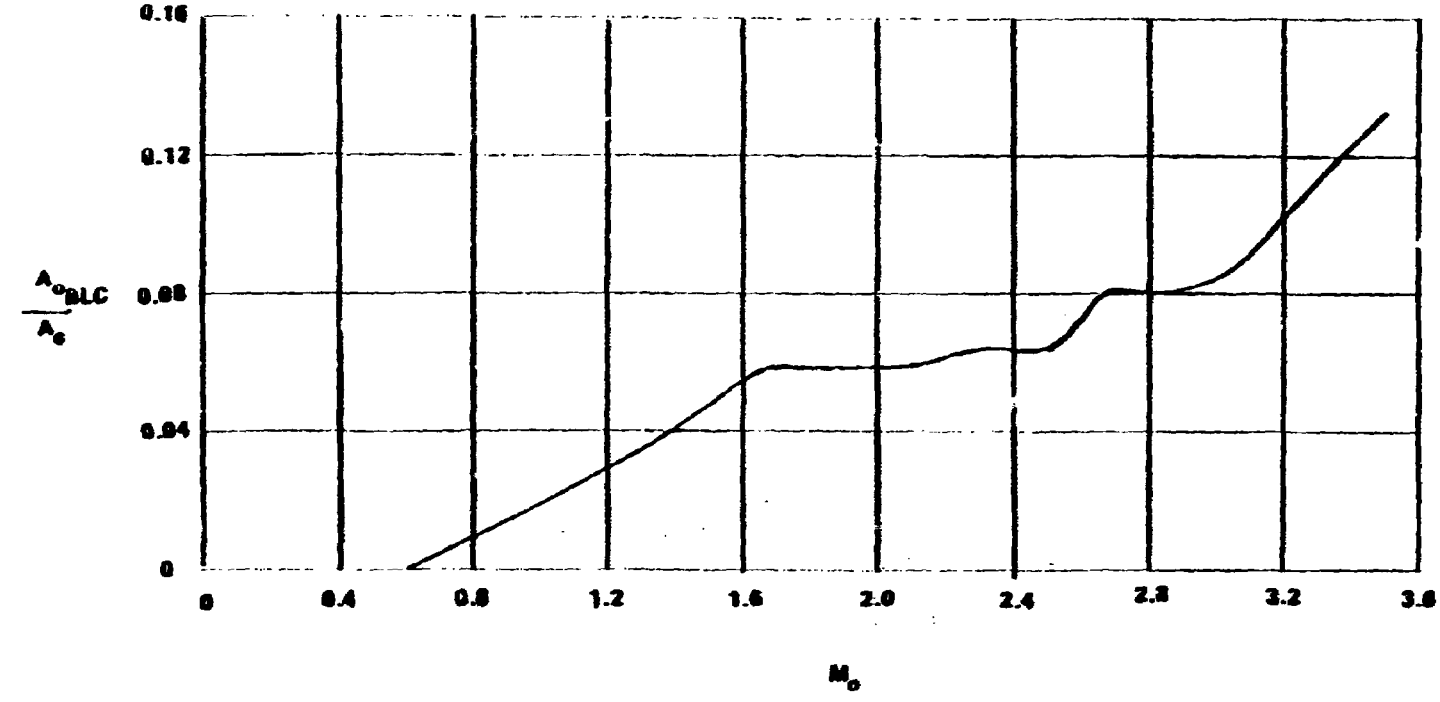

Figure 39. Performance Characteristics for Inlet Configuration #18 (continued)

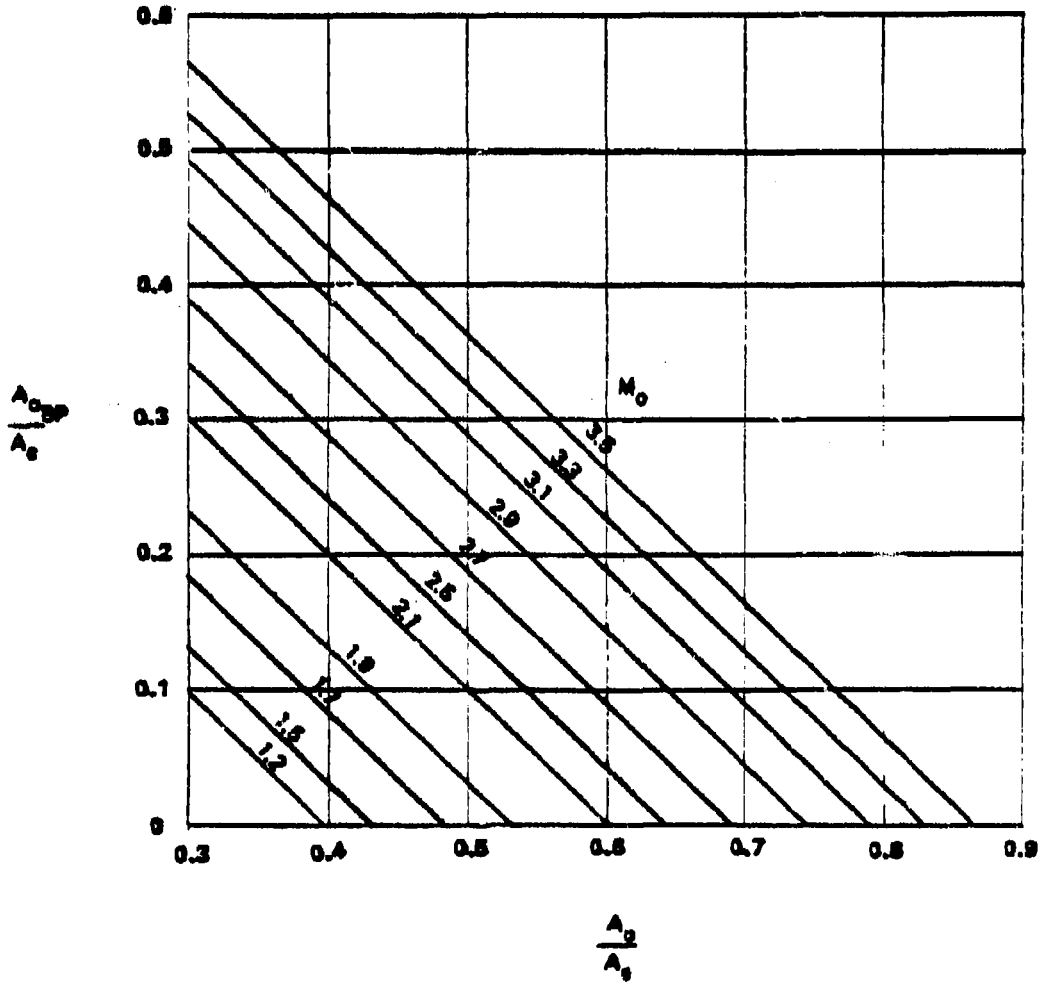

Figure 39. Performance Characteristics for Inlet Configuration #18 (concluded)

SECTION III
NOZZLE/AFTBODY CONFIGURATIONS AND PERFORMANCE CHARACTERISTICS

Eight different nozzle/aftbody configuration concepts were selected to use for generating a library of aftbody drag characteristics. The types of aftbodies selected are shown in Figure 40, together with the four basic nozzle types used to generate nozzle C_{F_G} maps.

As shown in Figure 40, each of the aftbodies has a configuration number associated with it and a computer file name that represents the aftbody drag map data in tabulated form. Figure 41 presents a summary of each of the aftbody configurations and sources of the aftbody drag maps.

Following Figure 41, each of the nozzle/aftbody configuration area distributions is presented along with the predicted drag map for that configuration. The drag maps shown are for the fully-expanded ($P_9/P_0 = 1.0$) condition.

The derivative parameters for each of the baseline aftbody configurations consist of the following items:

1) A "baseline" area distribution that consists of a table of coordinates of body cross-sectional area versus fuselage station

2) A "baseline" radial tail orientation angle. (The program is structured to accept an input table of incremental drag coefficient as a function of free-stream Mach number and radial tail attachment angle. Insufficient data are available at present, however, to complete the data tables; therefore, the incremental drag correction is zero for all configurations.)

3) A "baseline" fore-and-aft tail position, $(X - X_9)/(X_{10} - X_9)$

4) A "baseline" base area ratio, A_B/A_{10}

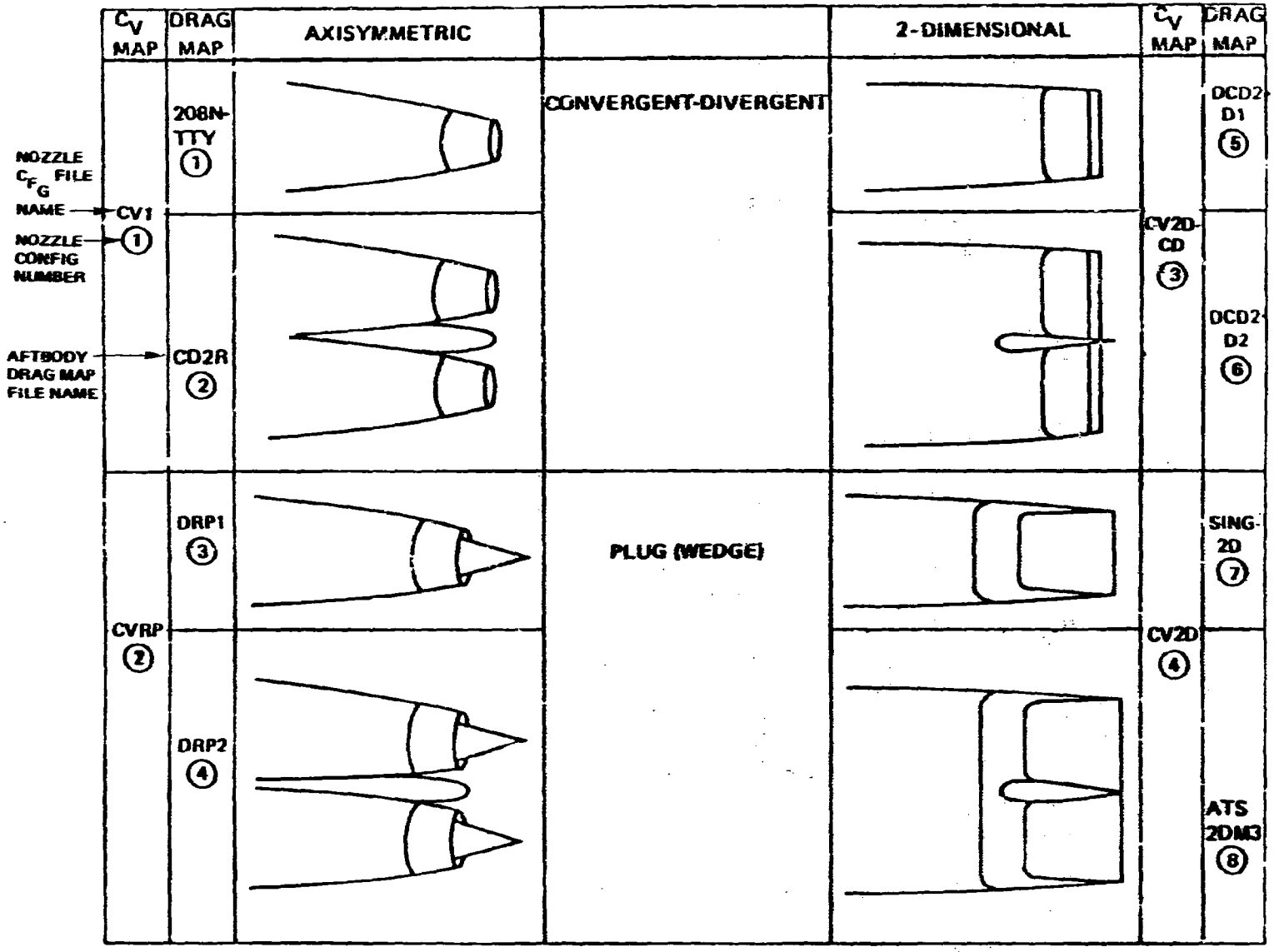

Figure 40. Nozzle/Aftbody Files

CONFIG. NO.	DESCRIPTION	FILE NAME	SOURCE OF DRAG MAP DATA
1	Single axisymmetric convergent-divergent nozzle installation based on Boeing LWF configuration	208NTTY	Predicted from parametric data relating drag as a function of R/D_M, β, P_9/P_0, and D_9/D_{10}, checked by single nozzle experimental data and IMS method.
2	Twin axisymmetric convergent-divergent nozzles in a closely-spaced aftbody installation based on Boeing ATS studies	CD2R	Calculated IMS_T parameters from area distribution; Drag correlations vs. IMS_T from ESIP contract test results.
3.	Single axisymmetric plug nozzle installation based on using a plug nozzle installed on the same aftbody as in Configuration #1 above	DRP1	Calculated IMS_T parameters from area distribution; Drag correlations vs. IMS_T from plug nozzle test data.
4.	Twin axisymmetric plug nozzle installation based on using a twin plug nozzle installed on the same aftbody as in Configuration #2 above	DRP2	Calculated IMS_T parameters from area distributions; Drag correlations vs. IMS_T from plug nozzle test data
5.	Single two-dimensional convergent-divergent nozzle in an ATS-type aftbody configuration	DCD2D1	Calculated IMS_T parameters from area distributions; Drag correlations vs. IMS_T were same as 2-D wedge nozzle correlations
6.	Twin two-dimensional convergent-divergent nozzles in an ATS-type closely-spaced aftbody configuration	DCD2D2	Calculated IMS_T parameters from area dsitributions; Drag correlations vs. IMS_T were same as 2-D wedge nozzle correlations
7.	Single two-dimensional wedge nozzle installed in a supercruiser aftbody	SING2D	Calculated IMS_T parameters from area distributions; Drag correlations vs. IMS_T from two-dimensional nozzle test data
8.	Twin two-dimensional wedge nozzles installed in closely-spaced ATS-type configuration aftbody	ATS2DM3	Calculated IMS_T parameters from area distributions. Drag correlations vs. IMS_T from two-dimensional nozzle test data

Figure 41. Summary of Aftbody Configurations and Drag Maps

The baseline area distributions are presented in this section for each of the library aftbody configurations. As discussed above, radial tail location effects data maps are not available due to insufficient data. Baseline fore-and-aft tail locations for each configuration are shown in the figures that accompany each area distribution plot. Each of the baseline nozzle/aftbody configurations has no base area; therefore the "baseline" base area ratios, A_B/A_{10} for all configurations is zero. The nozzle/aftbody configurations and their associated drag maps are presented in Figure 42 through 57.

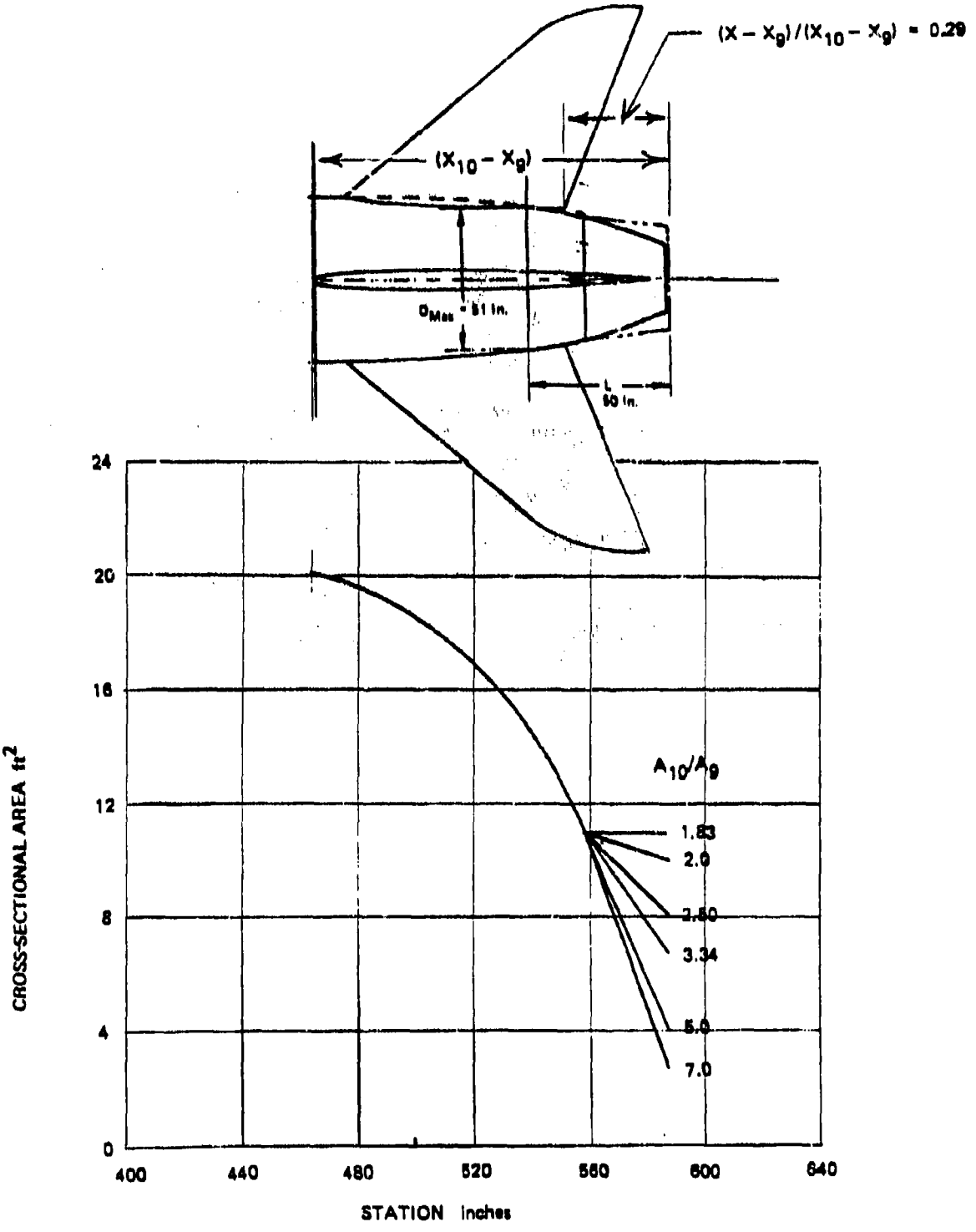

Figure 42. Nozzle/Aftbody Area Distribution for a Single Round C-D Nozzle Installation

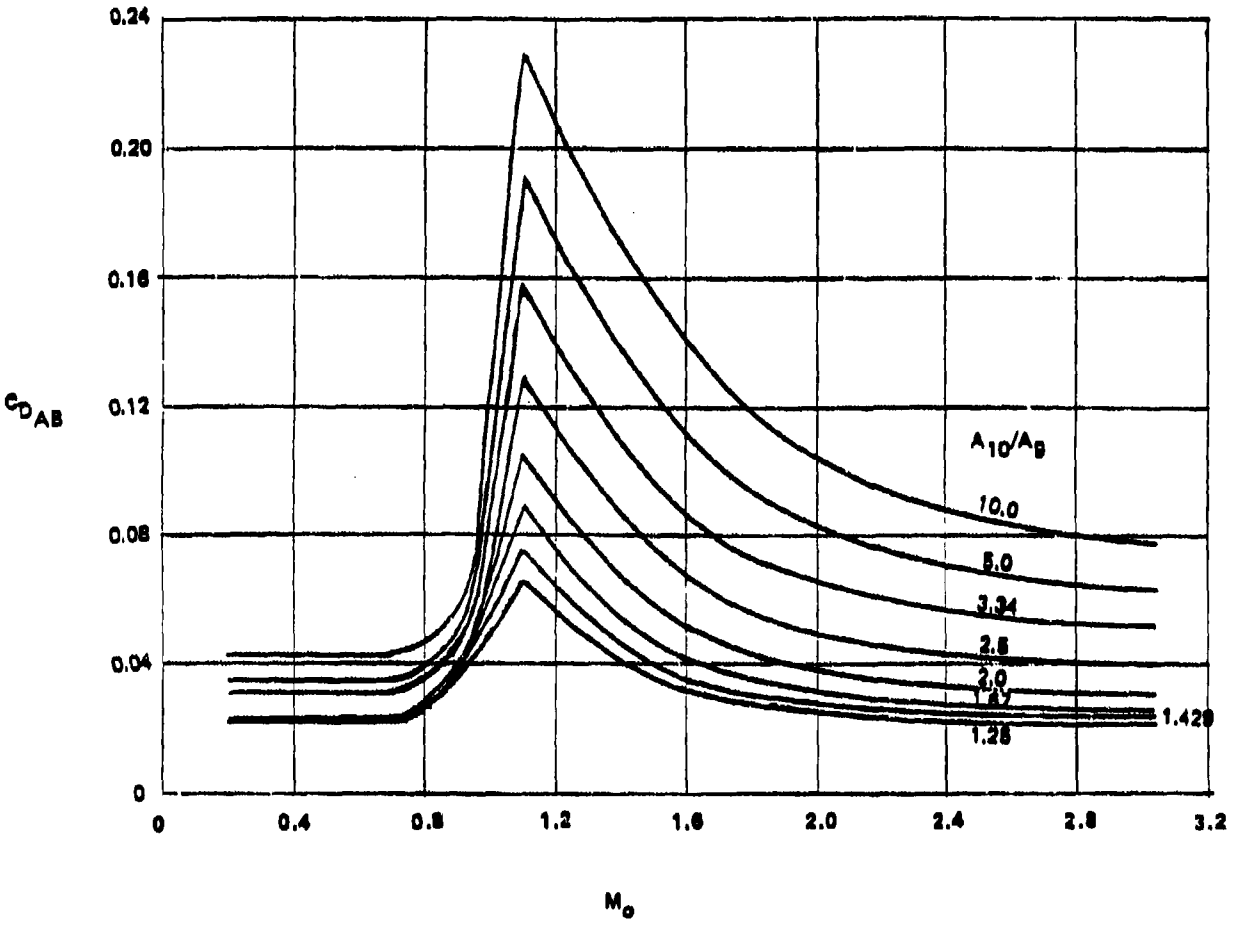

Figure 43. Drag for a Single Round C-D Nozzle Installation

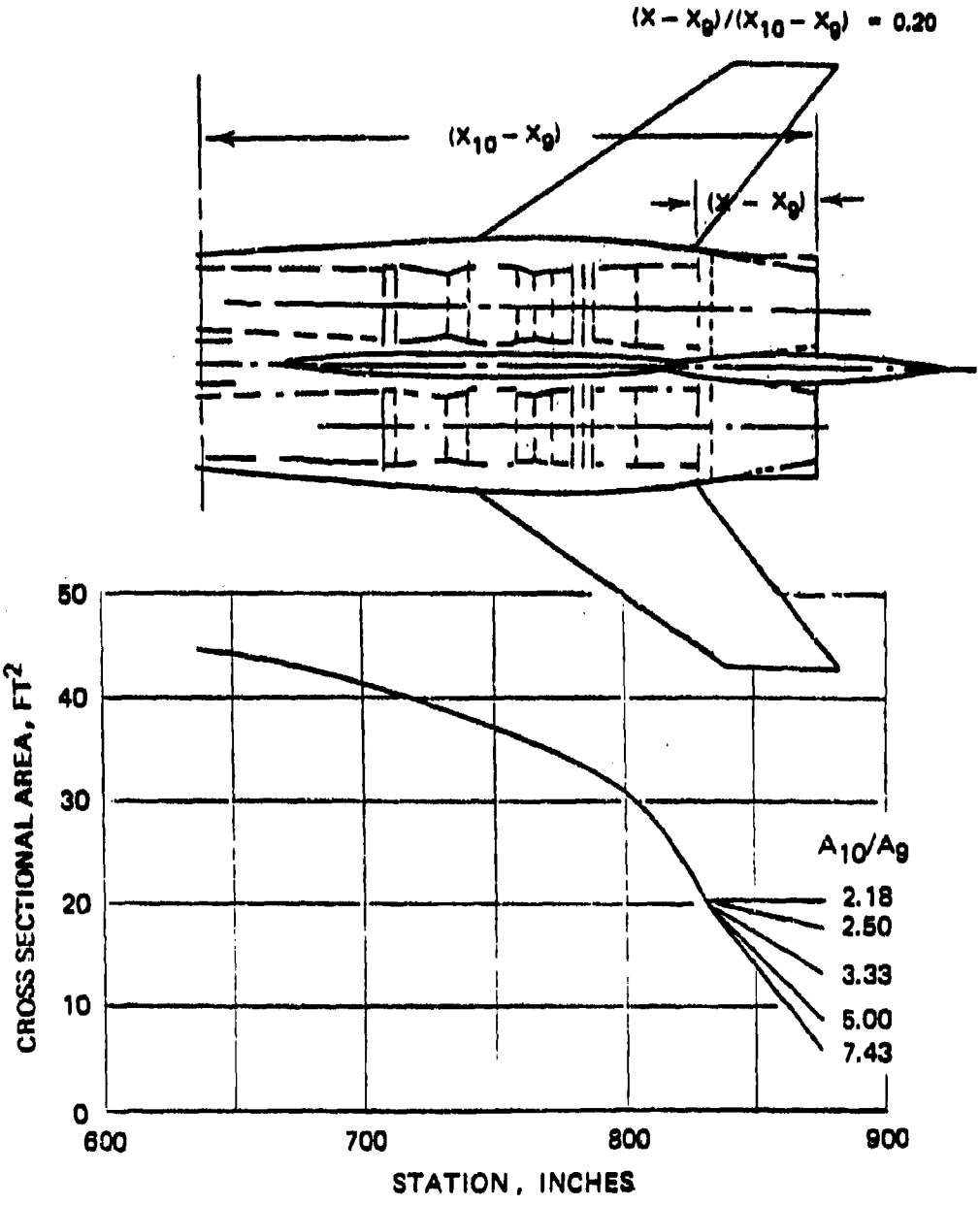

Figure 44 Nozzle/Aftbody Area Distribution for a Twin Round Nozzle Configuration

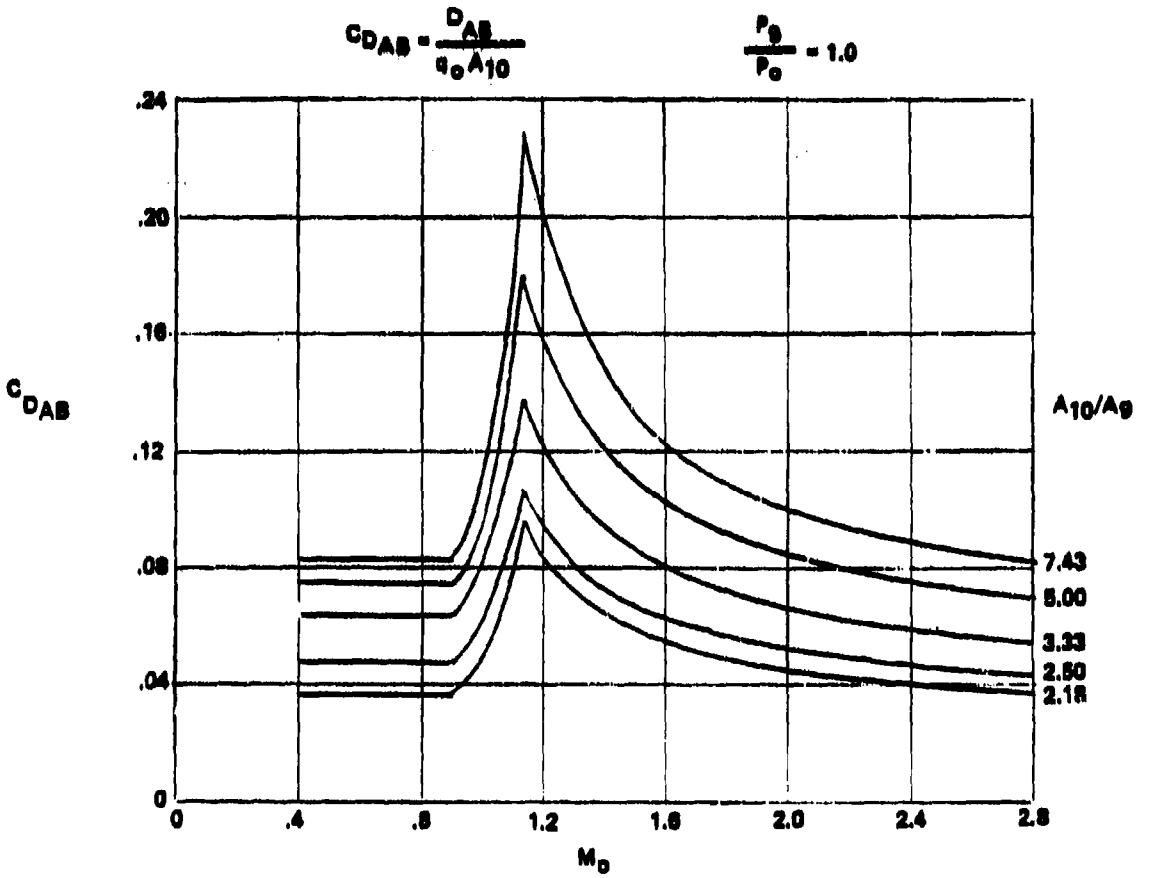

Figure 45. Drag for a Twin Round C-D Nozzle Installation

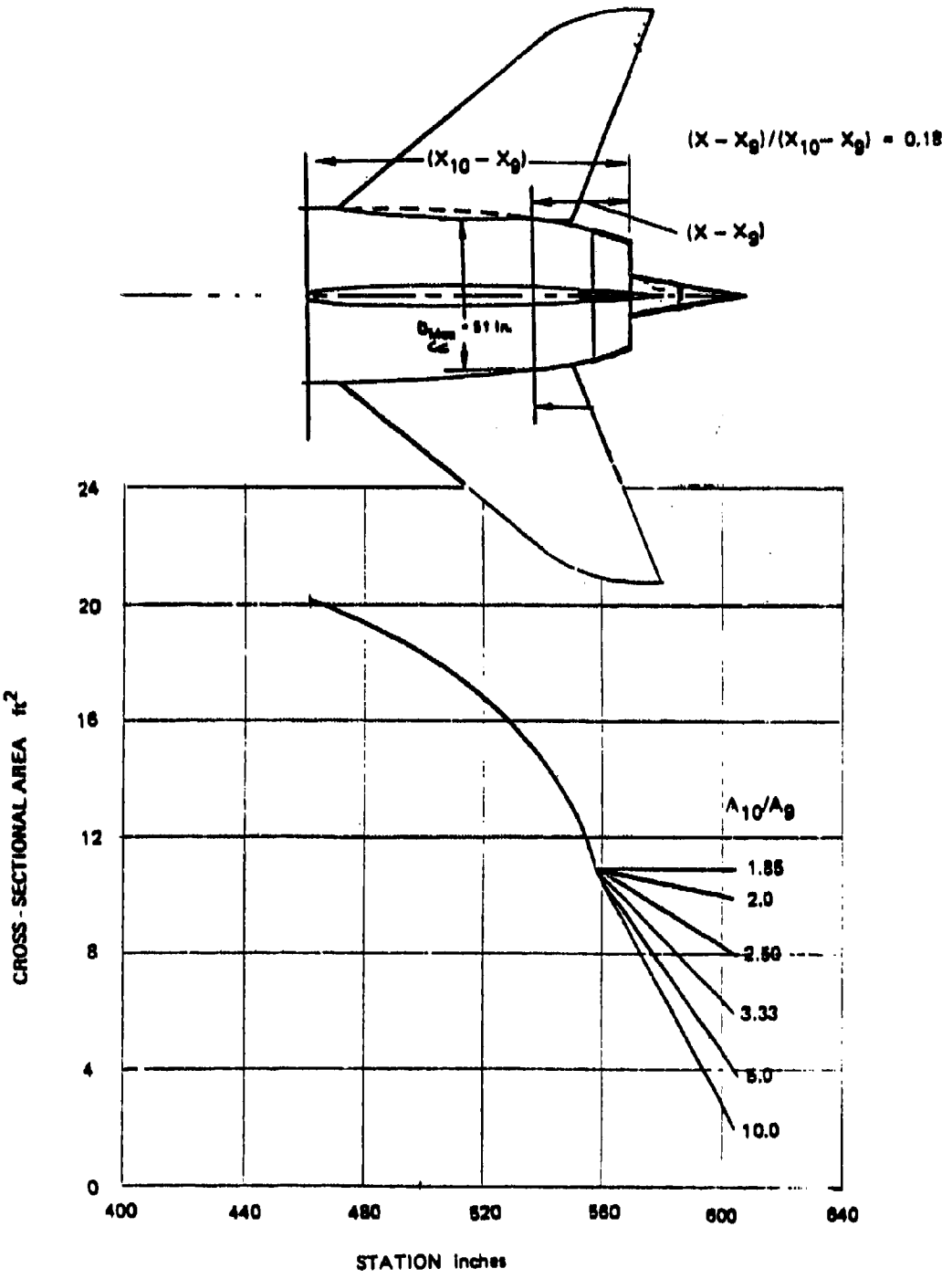

Figure 46. Nozzle/Aftbody Area Distribution for a Single Round Plug Nozzle Installation

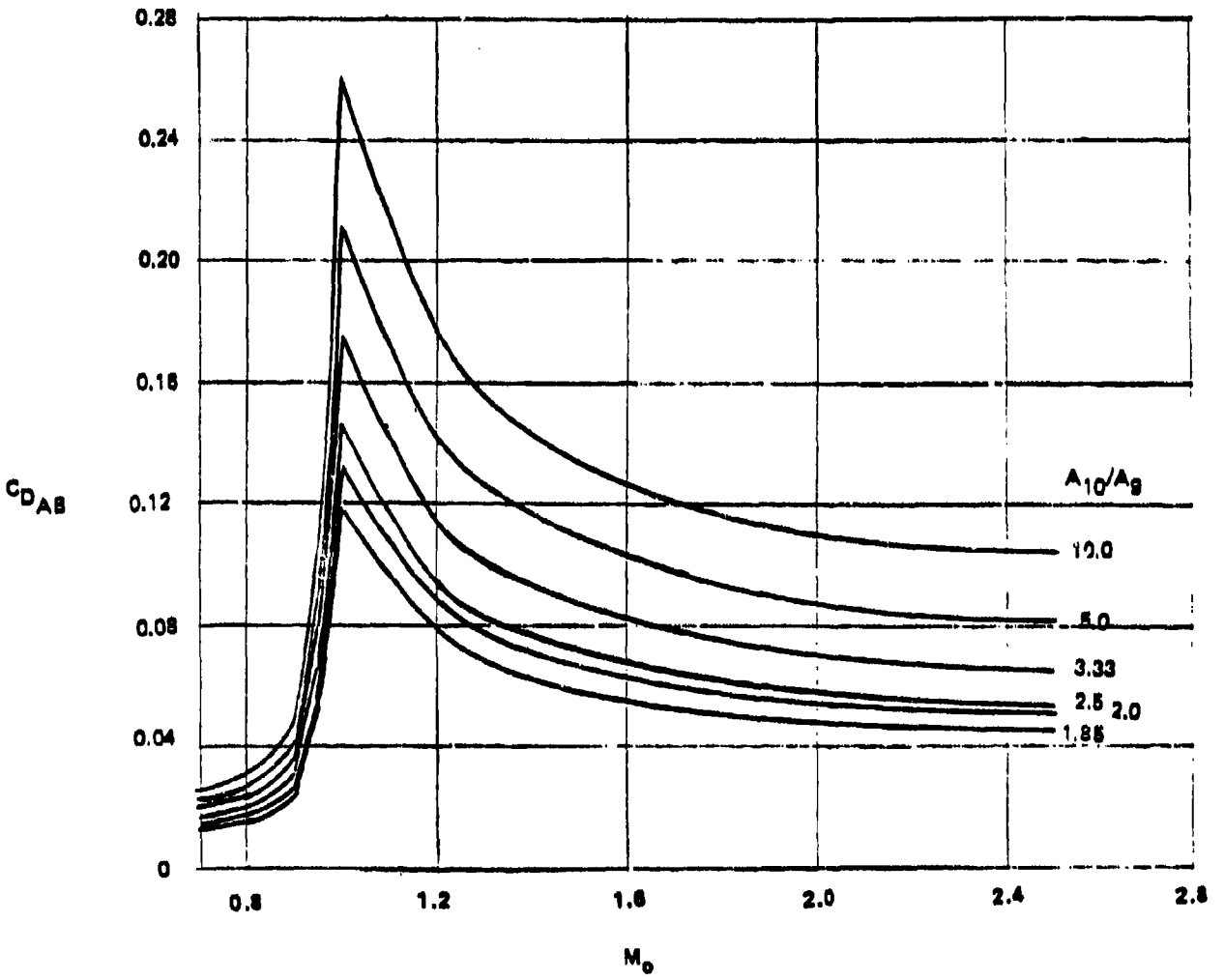

Figure 47. Drag for a Single Round Plug Nozzle Installation

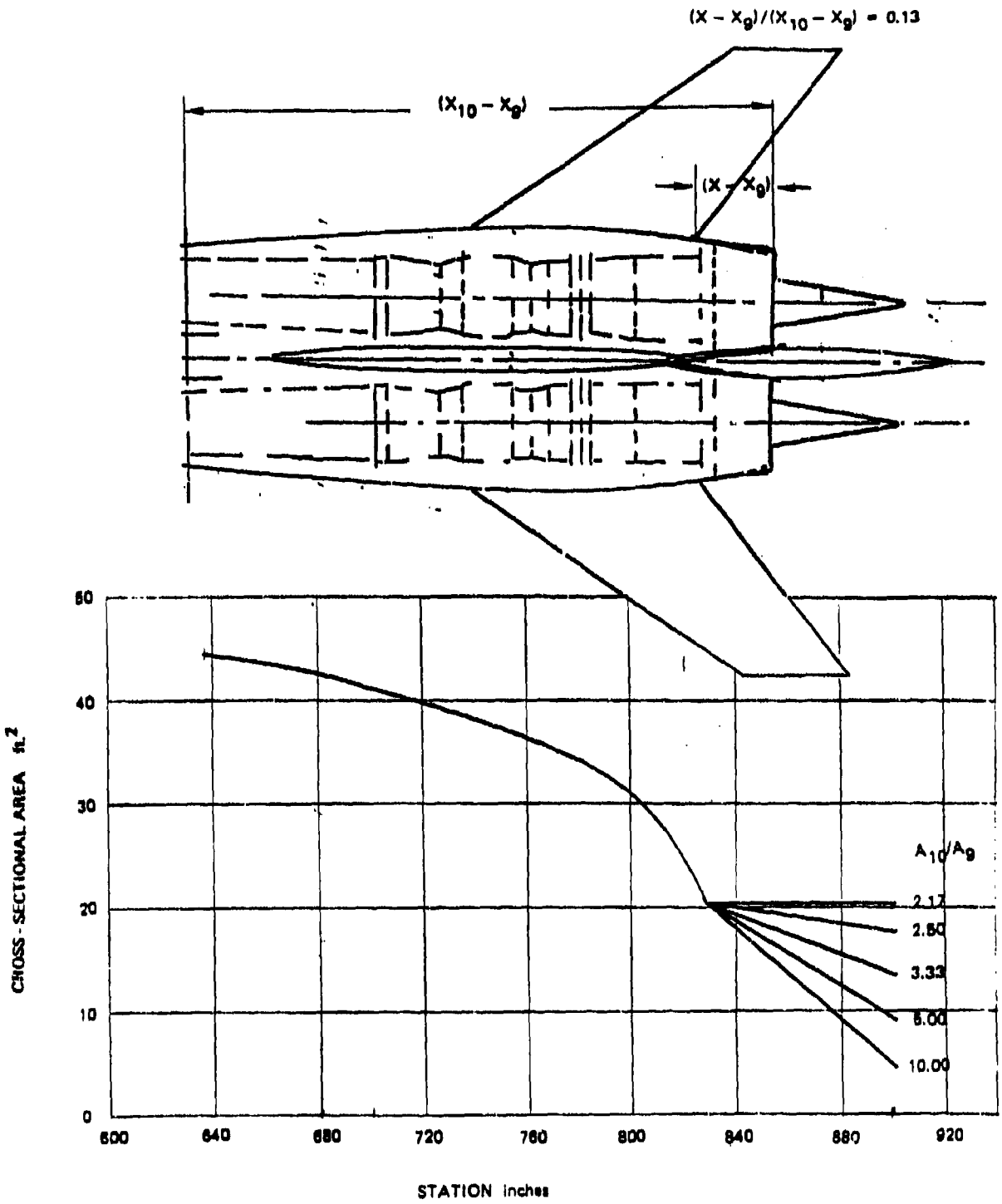

Figure 48. Nozzle/Aftbody area Distribution for a Twin Round Plug Nozzle Installation

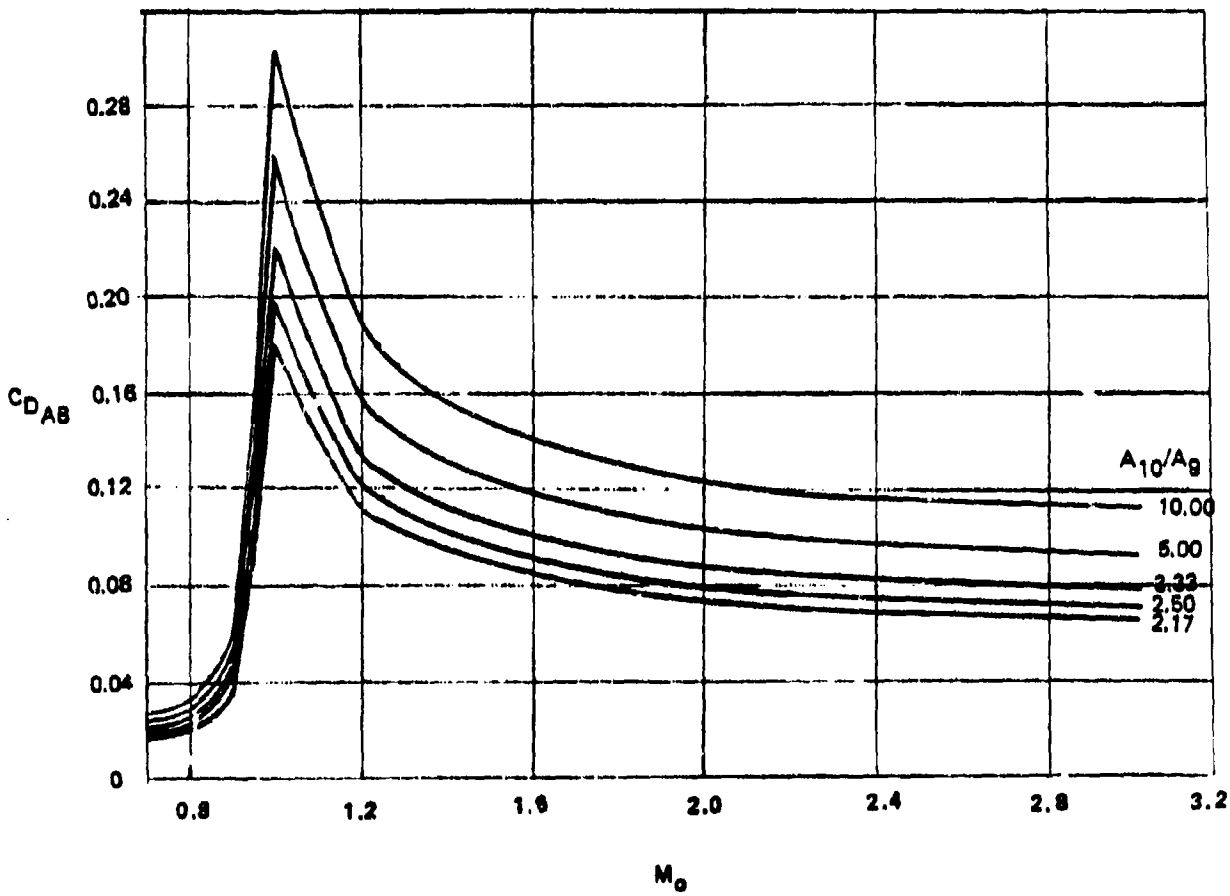

Figure 49. Drag for a Twin-Round Plug Nozzle Installation

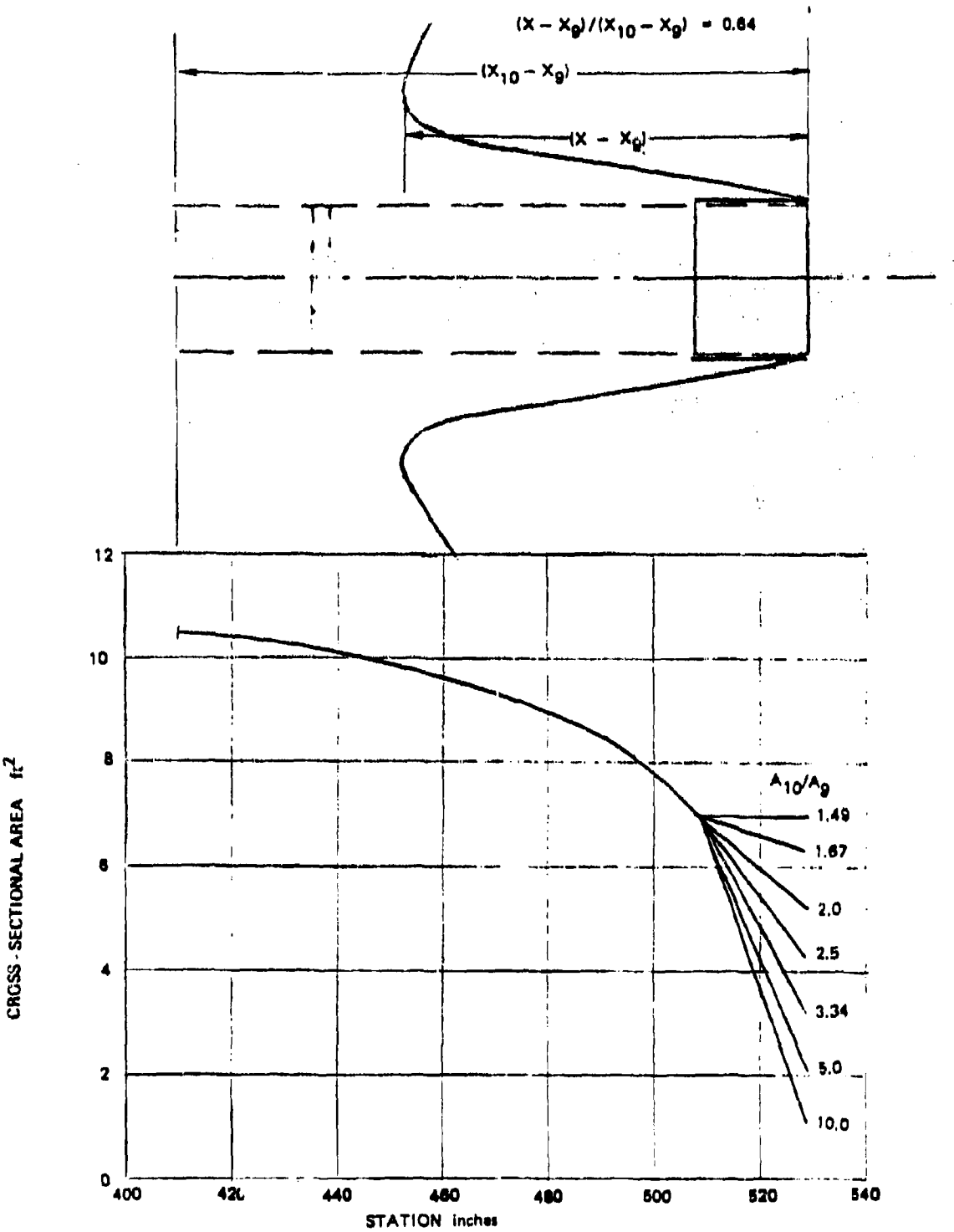

Figure 50. Nozzle/Aftbody Area Distribution for a Single 2-D C-D Nozzle Installation

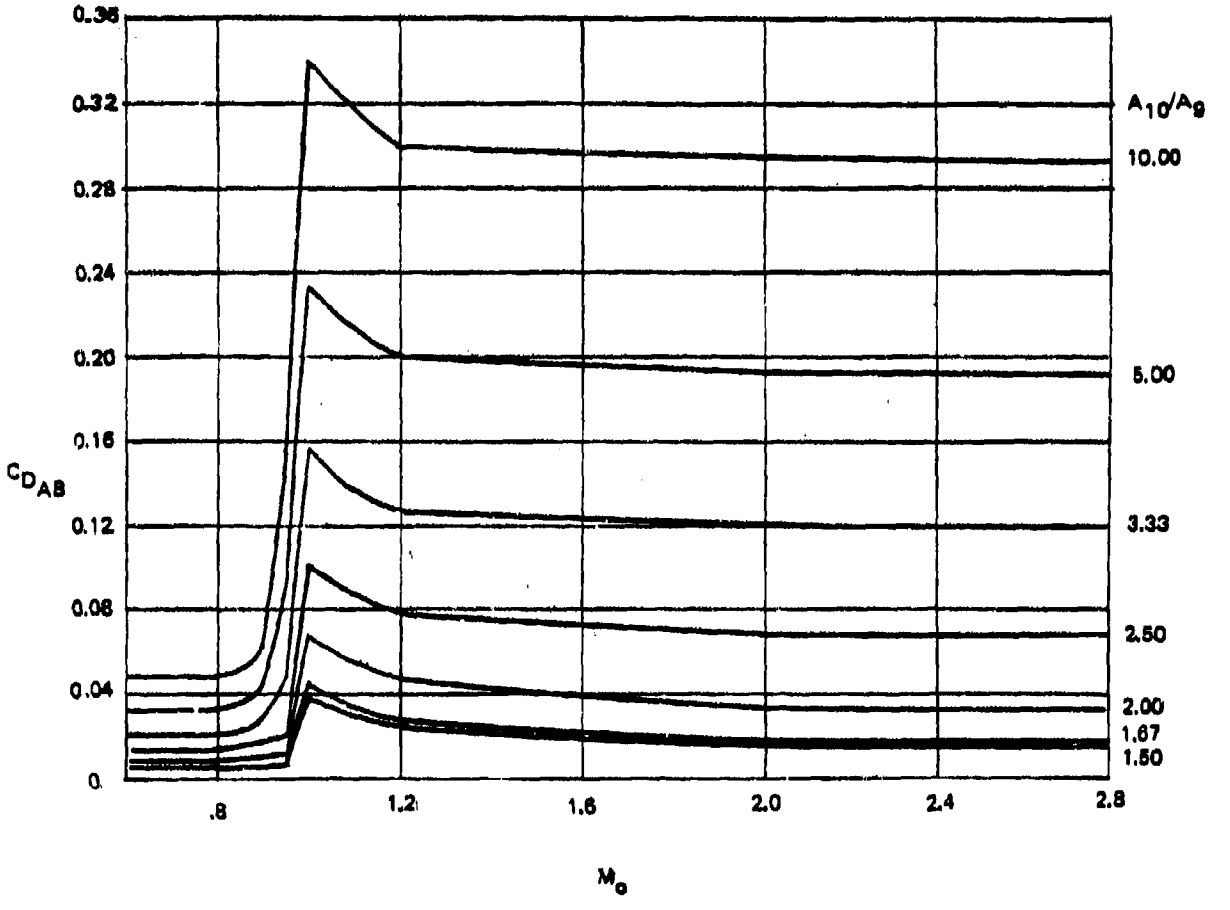

Figure 51. Drag for a Single 2-D C-D Nozzle/Aftbody Installation

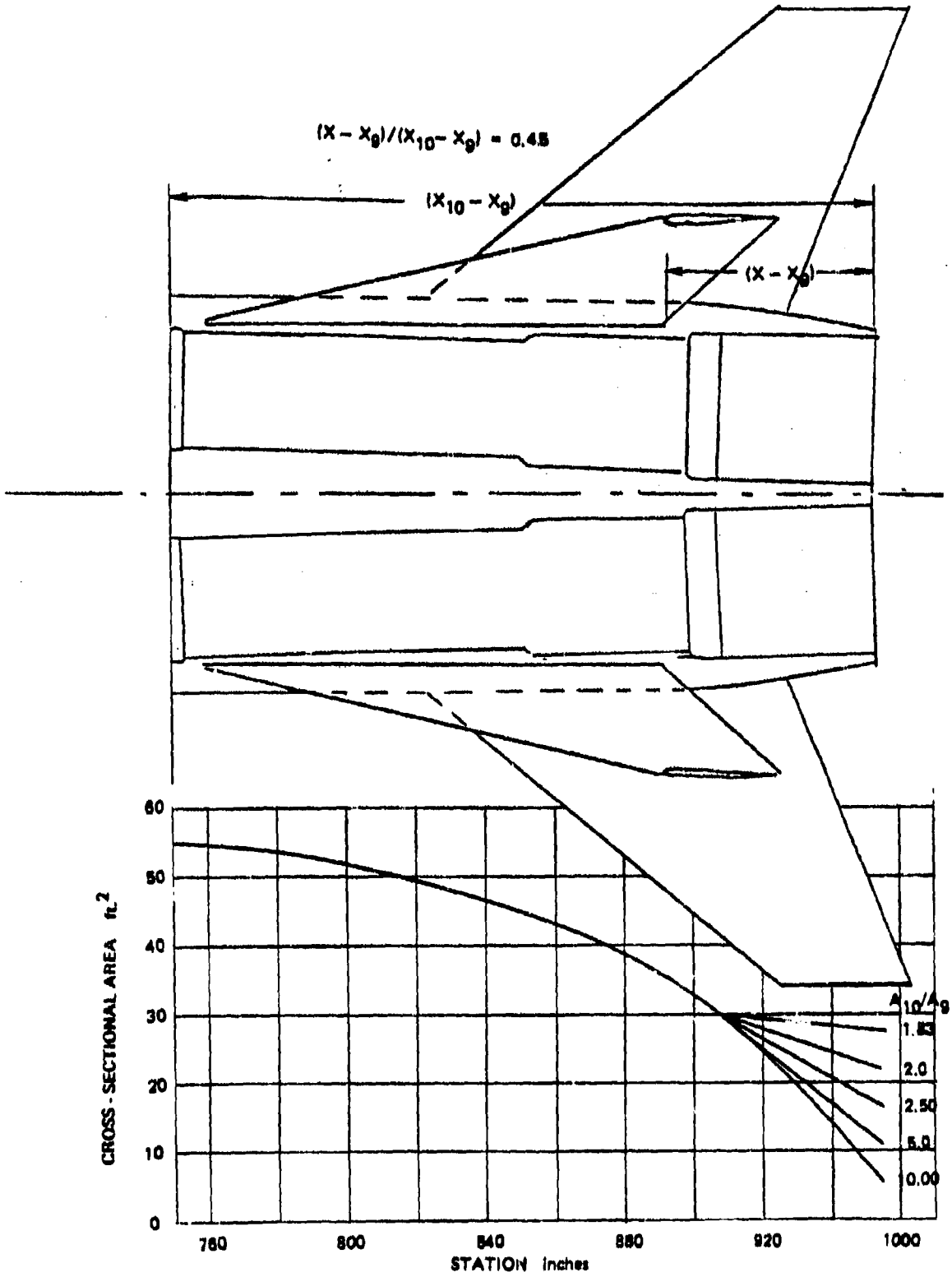

Figure 52. Nozzle/Aftbody Area Distribution for a Twin 2-D C-D Nozzle Installation

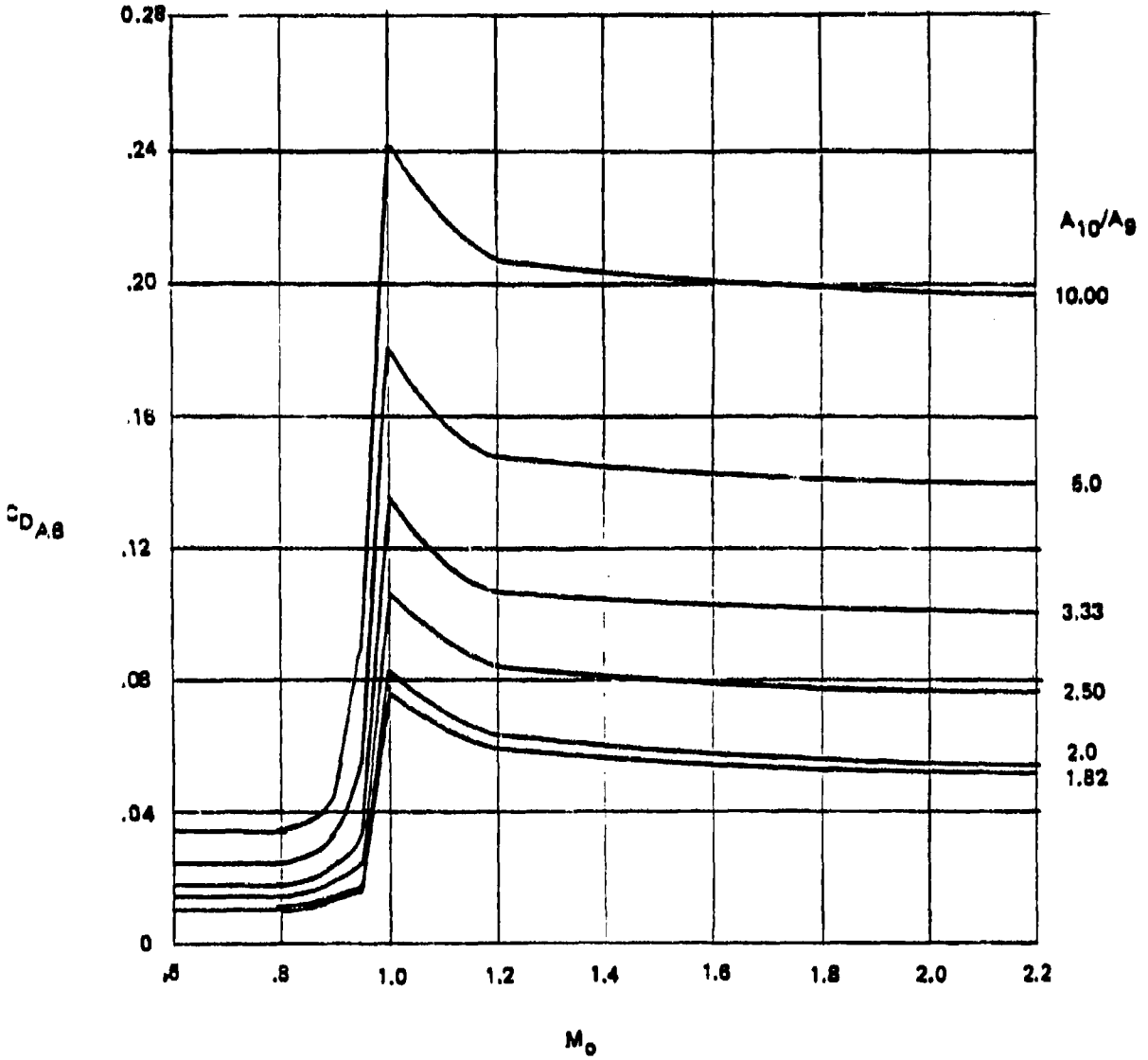

Figure 53. Drag for a Twin 2-D C-D Nozzle Installation

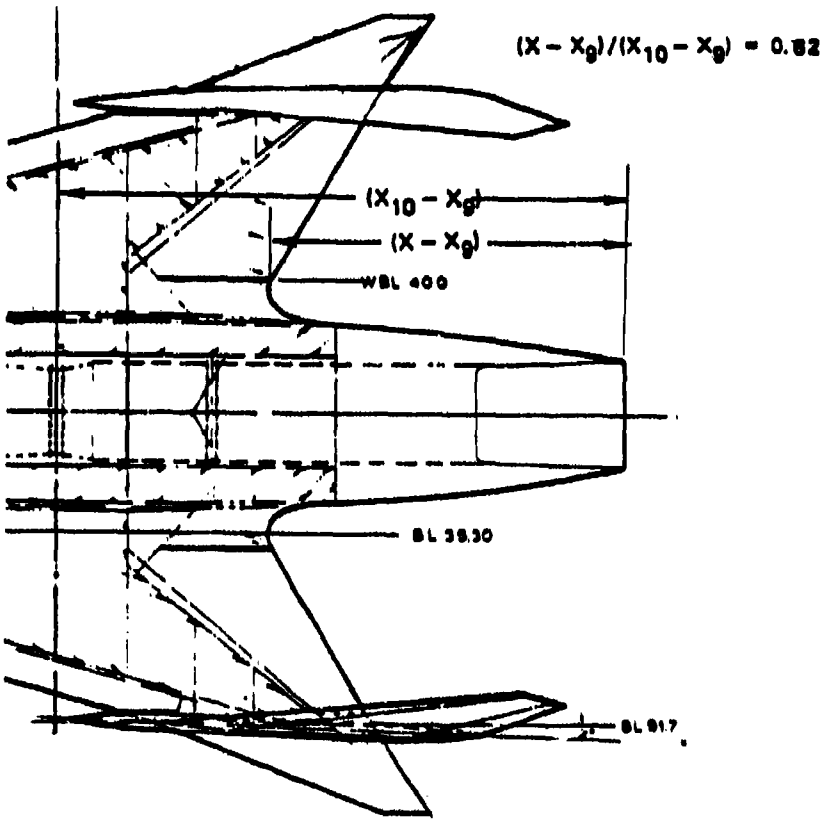

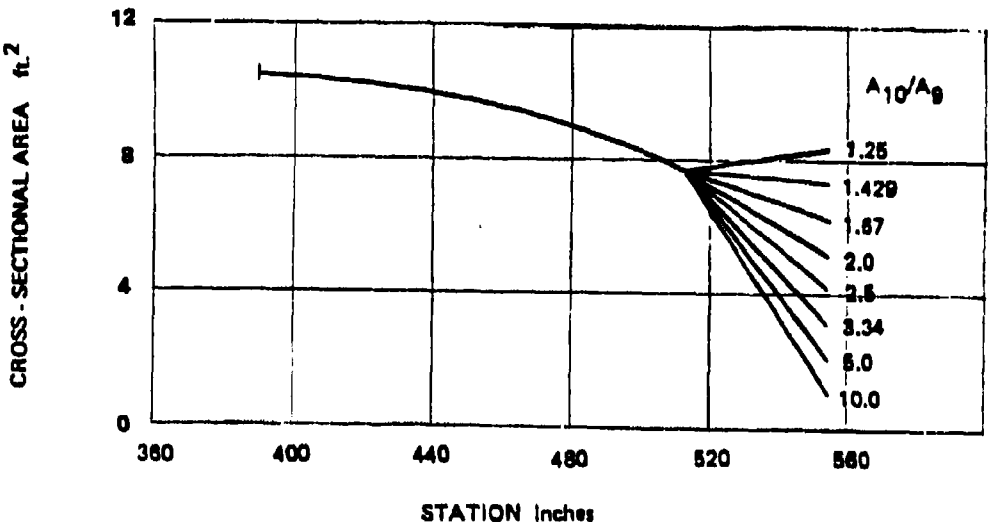

Figure 54. Nozzle Aftbody Area Distributon for a Single 2-D Wedge Nozzle Installation

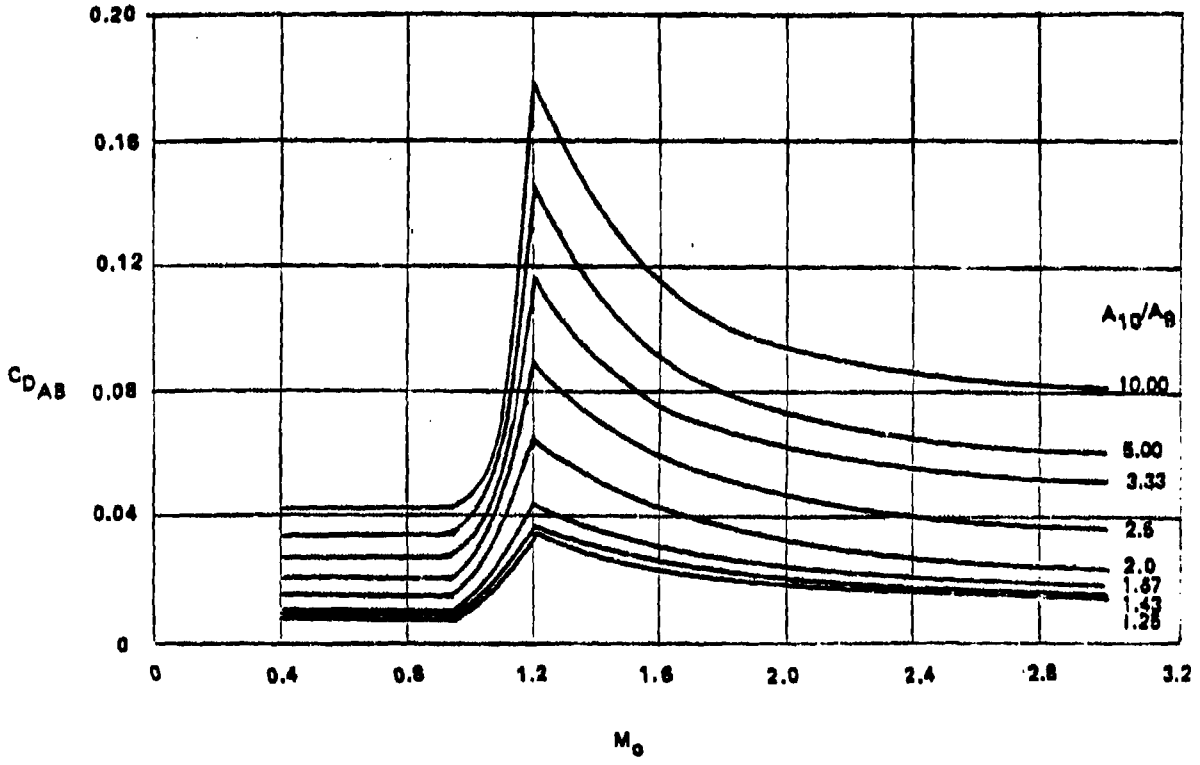

Figure 55. Drag for a Single 2-D Wedge Nozzle/Aftbody Installation

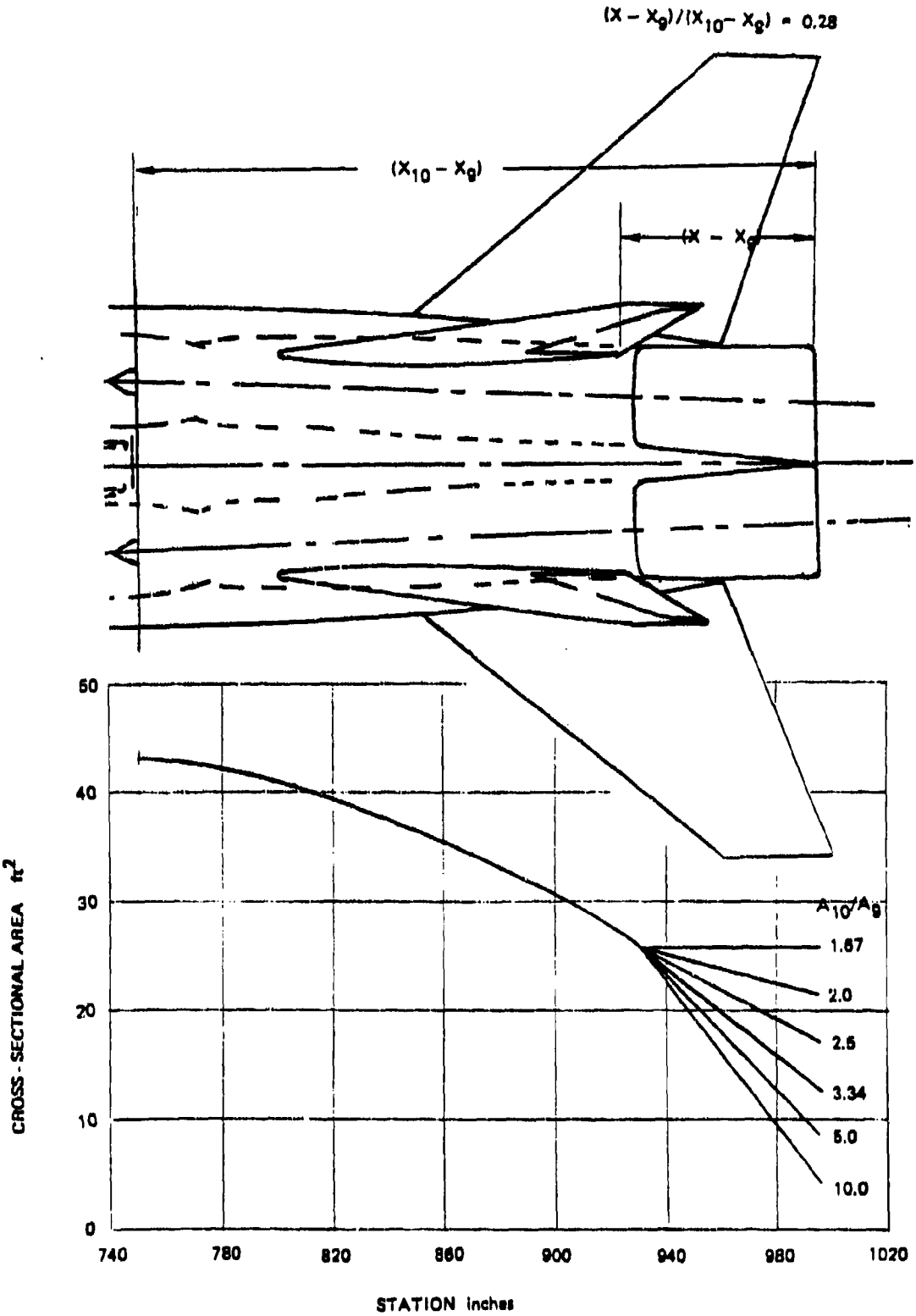

Figure 56. Nozzle/Aftbody Area Distribution for a Twin 2-D Wedge Nozzle Installation

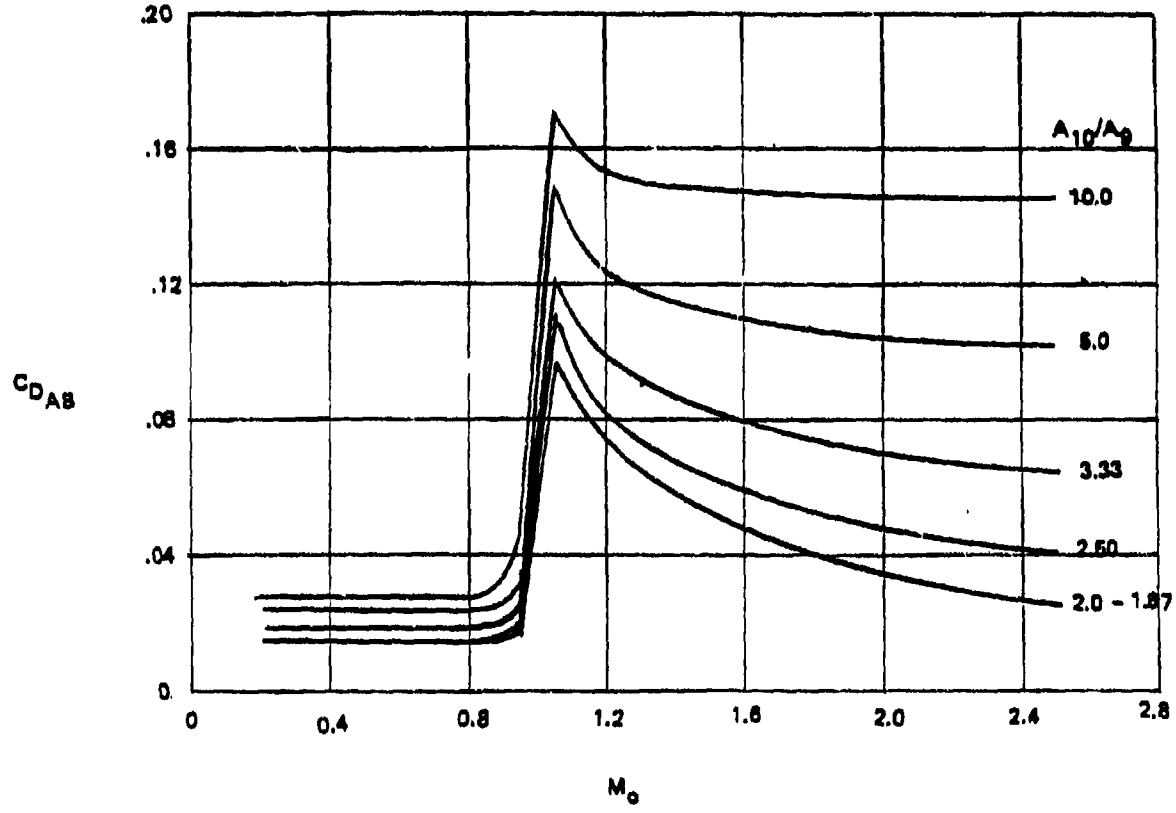

Figure 57. Drag for a Twin 2-D Wedge Nozzle Configuration

SECTION IV
NOZZLE INTERNAL CONFIGURATIONS AND C_{F_G} MAPS

Four different nozzle internal configurations were selected and utilized to provide a library of typical nozzle internal performance characteristics. These nozzles included:

1) Axisymmetric convergent-divergent nozzle
2) Axisymmetric plug nozzle
3) Two-dimensional convergent-divergent nozzle
4) Two-dimensional wedge nozzle

4.1 NOZZLE GEOMETRIES AND C_{F_G} MAPS

Each of the nozzle configurations is described in this section of the report, followed by plotted data showing the variation of nozzle gross thrust coefficient, C_{F_G}, as a function of nozzle total pressure ratio P_{T8}/P_0.

4.1.1 Nozzle Configuration #1 - Axisymmetric, Convergent-Divergent Nozzle

Axisymmetric convergent-divergent nozzles can vary in complexity from a lightweight fixed geometry to a relatively heavy fully variable exit area and throat area design. The configuration selected for this study is a simple variation of the fixed geometry design utilization mechanically slaved nozzle exit area and throat area to obtain variable internal expansion as a function of powersetting (throat area). This type of design is currently used on the J101/F404 and F100 turbofan engines. The baseline nozzle internal divergence half-angle (θ_{DIV}) for this configuration is 11.48^{o} which occurs at a nozzle area ratio of 1.60. The geometry of the nozzle and the nozzle performance map are shown in Figure 58.

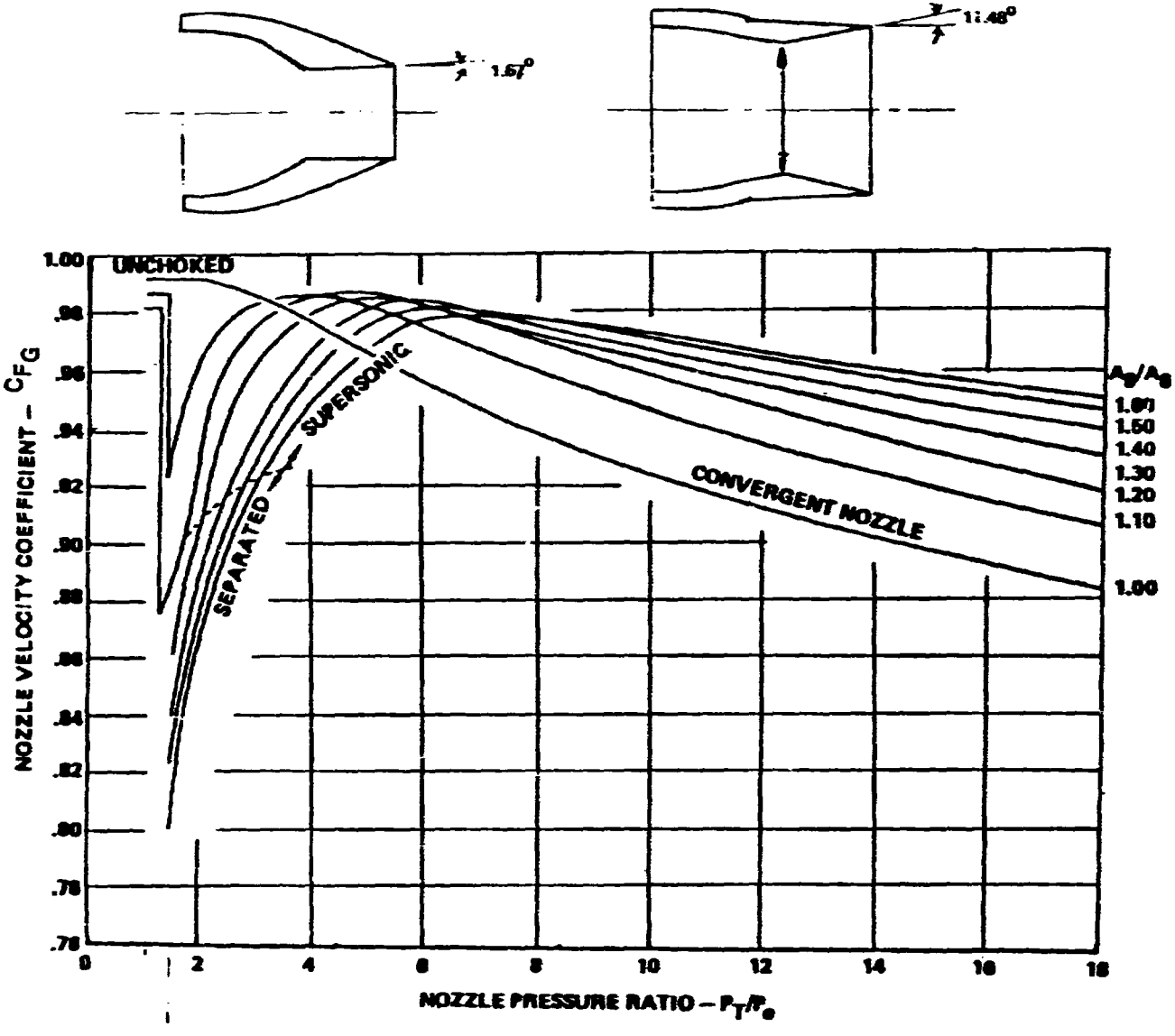

Figure 58. Gross Thrust Coefficient for a Round C-D Nozzle

4.1.2 Nozzle Configuration #2 - Axisymmetric Plug Nozzle

Important design variables of axisymmetric plug nozzles include the plug angle, cowl internal angle, cowl exit to throat area ratio, throat inclination angle, and cowl boattail angle. Various methods can be applied to achieve plug nozzle throat area variation. The selected plug configuration shown above utilizes variable plug and cowl geometry to achieve throat area and expansion area ratio control at dry and A/B powersetting. The baseline plug half-angle, θ_p, for this configuration is 10^0. The nozzle geometry and performance characteristics are shown in Figure 59.

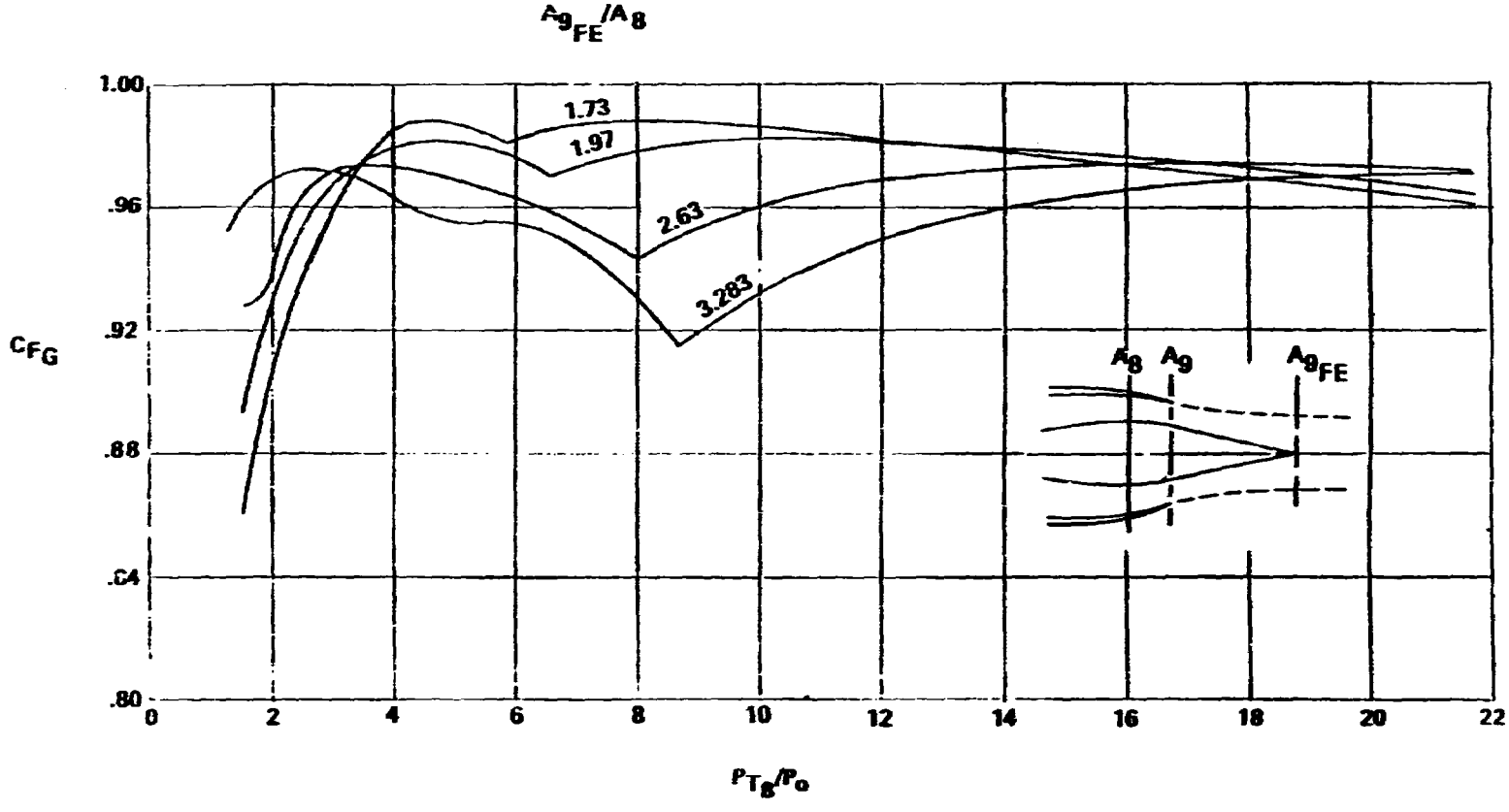

Figure 59 Gross Thrust Coefficient for Axisymmetric Plug Nozzles

4.1.3 Nozzle Configuration #3 - Two-Dimensional Convergent-Divergent Nozzle

The non-axisymmetric C-D nozzle configuration is based on concepts studied under the AFFDL Non-Axisymmetric Nozzle program (ITESC). The concept allows independent actuation to control throat area and exit area. The design employs divergent flaps to achieve a maximum internal area ratio of 1.6. The sidewalls are cut back to reduce weight and cooling requirements. The baseline aspect ratio for this configuration is 1.0. The baseline divergence half-angle, θ_{DIV}, is 22^{o} at a nozzle area ratio A_9/A_8 of 1.6. The geometry of the nozzle and the performance characteristics are shown in Figure 60.

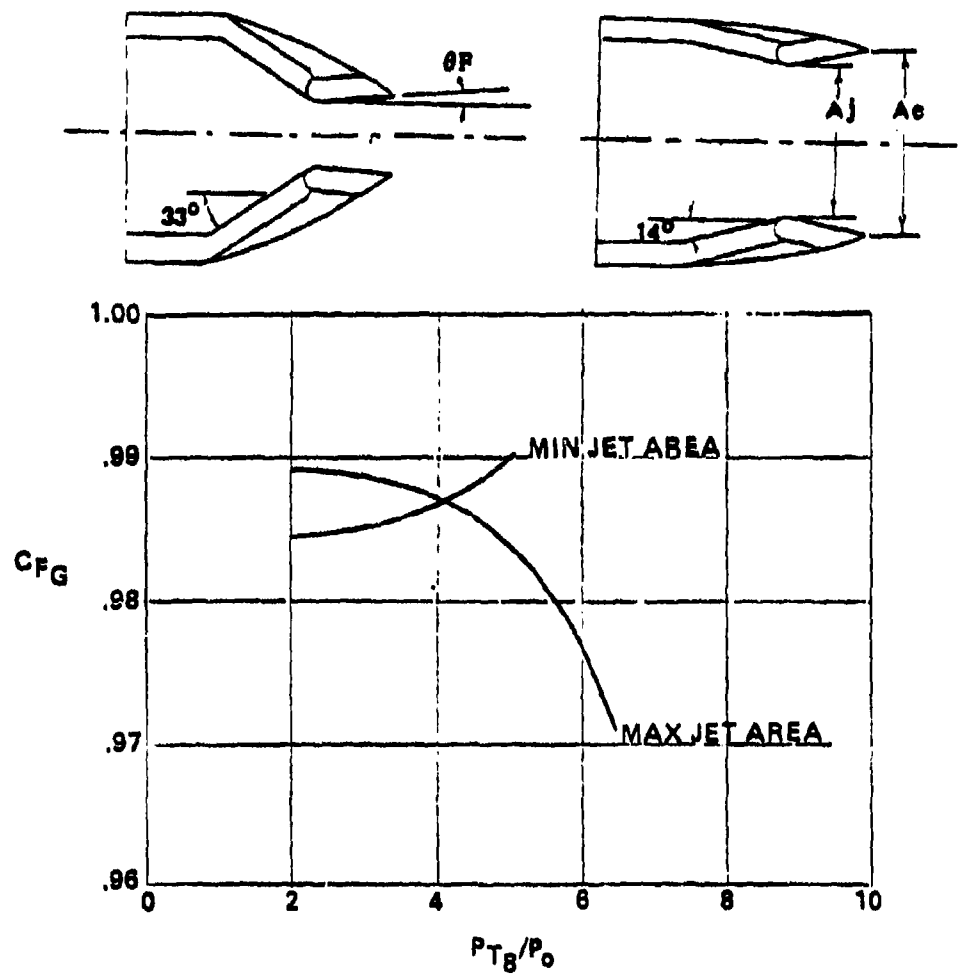

Figure 60 Gross Thrust Coefftctent for a 2-D/C-D Nozzle

4.1.4 Nozzle Configuration #4 - Two-Dimensional Wedge Nozzle

The non-axisymmetric wedge nozzle configuration is the Boeing 2-D Airframe Integrated Nozzle concept featuring airframe/nozzle structural and aerodynamic integration. A variable geometry centerbody wedge provides independent throat and exit area control allowing optimization of thrust/drag performance over a wide range of dry and A/B powersetting. The cowl geometry is fixed. The baseline aspect ratio for this configuration is 1.0 and the baseline wedge half-angle, θ_p, is 10^o. The nozzle geometry and performance characteristics are presented in Figure 61.

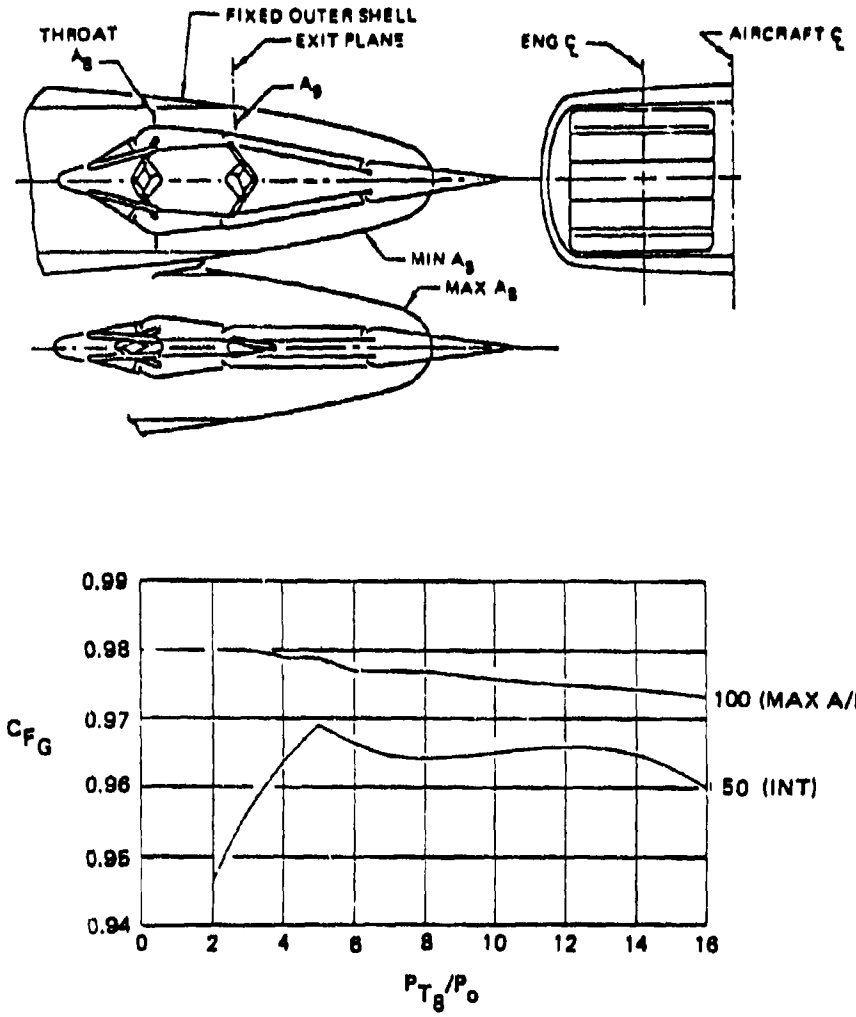

Figure 61 Gross Thrust Coefficient for a 2-D Wedge Nozzle

REFERENCES

1. Ball, W. H., Propulsion System Installation Corrections, AFFDL-TR-72-147-Volumes I-IV, Air Force Flight Dynamics Laboratory, December 1972.

2. Weirich, R. L., "A Summary of the Angle-of-Attack Performance Characteristics at Supersonic and Subsonic Mach Numbers of Several Air Induction Systems which are Applicable to Fighter-Type Aircraft, Langley Working Paper No. LWP-481, NASA Langley Research Center, 1963.

3. Landgraf, C. W., "Performance Comparison-Blow-in-Door and Fixed Lip Inlets", Coordination Sheet No. ME-747P-3302, March 14, 1972, The Boeing Company 747 Propulsion Staff.

4. Randall, L. M., et al, Experimental Investigation to Determine the Effect of Several Design Variables on the Performance of the F-100 Duct Inlet, NA-53-26, North American Aviation, Inc., 7 January 1953.

5. Ross, P. A., and Ball, W. H., "Propulsion System Development for Lightweight Fighter-Inlet Design and Performance, D180-14475-1TN, The Boeing Company, August 1, 1974.

6. Jonnson, T. J., and Huff, J. H., "Propulsion System Integration and Test Program (Steady State), Part IV. Inlet Drag Tests", AFAPL-TR-69-44, Air Force Aero Propulsion Laboratory, June 1969.

7. Cawthon, J. A., et al, Supersonic Inlet Design and Airframe-Inlet Integration Program (Project Tailor-Mate), Volume\III, Composite Inlet Investigation, AFFDL-TR-71-124, Vol. III, Air Force Flight Dynamics Laboratory, WPAFB, Ohio, May 1973.

8. Young, L. C., "Internal Aerodynamics Lecture Course Presentation at Wright-Patterson Air Force Base, Dayton, Ohio, Chapter 2.5: Internal Compression Inlets; and Chapter 2.6: Internal Compression Inlet Design", September 25, 1967.

9. Randall, L. M., The XB-70A Air Induction System, AIAA Paper No. 66-634, AIAA Second Propulsion Joint Specialist Conference, Colorado Springs, Colorado, 13-17 June 1966.

10. Anderson, W. E., and Wong, N. D., "A Two-Dimensional, Mixed-Compression Inlet System Designed to Self-Restart at a Mach Number of 3.5", Journal of Aircraft, Vol. 7, No. 5, Sept-Oct 1970.

11. Paynter, G. C., Shock and Ramp Induced Incipient Separation of a Turbulent Boundary Layer, D6-11847, The Boeing Company, November 3, 1967.

12. Syberg, J., "Analytic Design of AST Inlet", Boeing Company Document D180-20551-1, The Boeing Company, Seattle, Washington, March 8, 1977.

13. Smeltzer, D. B., and Sorensen, N. E., "Investigation of a Nearly Isentropic Mixed-Compression Axisymmetric Inlet System at Mach Numbers 0.6 to 3.2, NASA TN D-4557, NASA Ames Research Center, Moffett Field, CA, May 1968.

14. Syberg, J., and Koncsek, J. L., "Experimental Evaluation of a Mach 3.5 Axisymmetric Inlet", NASA CR-2563, Prepared by Boeing Commercial Airplane Company for NASA Ames Research Center, July 1975.

*U.S.Government Printing Office: 1978 — 657-002/161